AD-A109 848 FLUIDYNE ENGINEERING CORP MINNEAPOLIS MINN F/G 14/2
AERODYNAMIC AND ACOUSTIC TESTS OF A 1/15 SCALE MODEL DRY COOLED--ETC(U)
OCT 75 J L GRUNNET, I L VER, G GETTER N62467-74-C-0490

UNCLASSIFIED NL

1 OF 4
AD A
109848

A

84

LEVEL 4

AD

DISTRIBUTION STATEMENT

Approved for public release;

Distribution Unlimited

DTIC FILE COPY

FluiDyne

ENGINEERING CORP.

FLUIDYNE ENGINEERING CORPORATION

AERODYNAMIC AND ACOUSTIC TESTS OF A 1/15 SCALE MODEL DRY COOLED JET AIRCRAFT RUNUP NOISE SUPPRESSION SYSTEM

by
James L. Grunnet
FluiDyne Engineering Corporation

and
Dr. István L. Vér
Bolt, Beranek and Newman, Incorporated

with report coordination by
Gustav Getter
Gustav Getter Associates, P.C.

Conducted for
The United States Navy
Southern Division
Naval Facilities Engineering Command
Charleston, South Carolina

Navy Contract N62467-74-C-0490
(Model Study of a Dry Jet Engine Noise Suppression System)
FluiDyne Project 1019
BB&N Project #11856
October 1975

Approved: Owen P. Lamb
Owen P. Lamb
Vice President

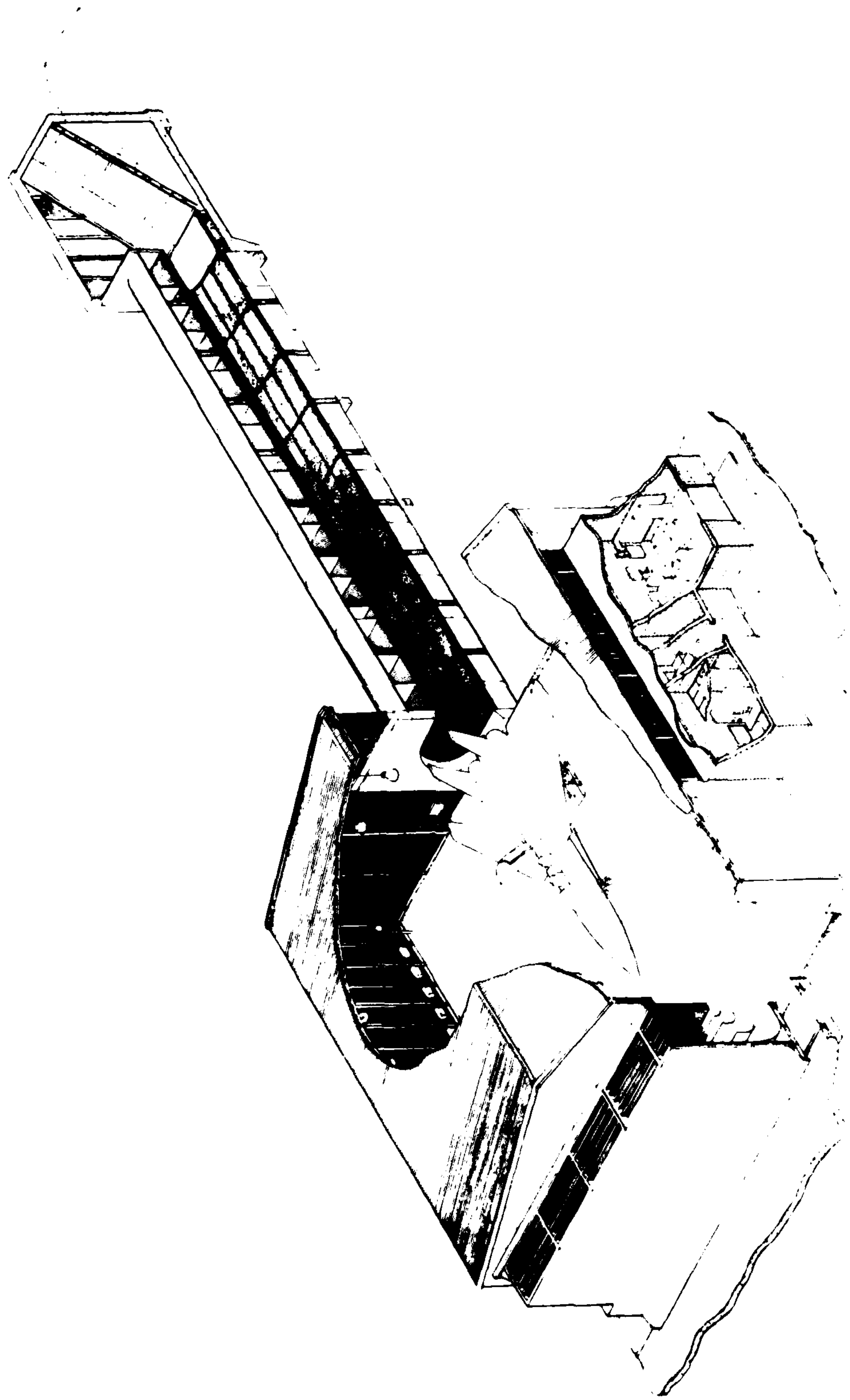

CUTAWAY OF NAS MIRAMAR HUSH HOUSE

ABSTRACT

This report presents the results of 1/15 scale model tests conducted a) to verify the acoustical and cooling air pumping performance of a full-scale, in aircraft, Hush House type of dry sound suppressor designed for the F-14 aircraft, and b) to provide additional design information usable for future Hush House suppressor designs. The model was fabricated and tested by FluiDyne Engineering ~~Corporation~~ Minneapolis, Minnesota for the United States Navy under Navy Contract N62467-74-C-490. Testing took place in FluiDyne's Medicine Lake Laboratory, utilizing an arrangement of two reverberant rooms for sound power level, PWL, measurements; one representing the Hush House interior, and the other representing the out-of-doors. The design of the reverberant rooms, the design of the model scale sound absorbing surfaces, and the measurement and analysis of noise data were carried out by personnel from Bolt, Beranek and Newman, Waltham, Massachusetts. Coordination in putting together the final report was provided by Gustav Getter Associates, P. C., New Rochelle, New York.

The test program was divided into four parts: a jet survey, aero-acoustic testing, aero-thermal testing, and acoustic testing. During the jet survey, the noise and free jet mixing characteristics of the 1/15 scale model F-14A afterburning nozzle configuration were measured at nozzle pressure ratios of 2 and 3 and at jet stagnation temperatures of nominally 0, 2000 and 3000°F. The prime purpose of the aero-acoustic testing was to obtain augmenter secondary air pumping performance data with different augmenter diameters, as well as information regarding aero-acoustic noise reduction in what is essentially an ejector configuration. During the aero-thermal test program, the jet nozzle was moved and deflected laterally and vertically from the centerline of an acoustically lined obround augmenter whose cross-section simulated at 1/15 scale the NAS Miramar sound suppressor. The principal measurements taken were augmenter wall temperatures, as well as noise data from which the influence of nozzle position and deflection on noise reduction could be determined. The effect of the variables on augmenter pumping was also determined.

The acoustic testing was mainly concerned with (1) the noise reduction achievable for different lengths of lined augmenter with and without a 45° absorptive exit ramp, (2) the noise reduction with different augmenter liner designs, (3) the acoustic performance of a one-foot length of lined augmenter at various axial locations in a length of hard-walled augmenter, and (4) the acoustical performance of a configuration made up of a hard-walled obround augmenter, subsonic diffuser, and stack with sound-absorbing baffles which was tested for comparison with the Miramar suppressor configuration. Additional information was also obtained regarding pumping performance and wall temperature.

Test results indicate that adequate cooling air pumping is not a problem, per se, but an off-center, deflected jet corresponding to the F-14 configuration results in high augmenter wall temperatures. Noise measurements on the full length acoustically lined augmenter model indicate that, with the F-14A, the full-scale NAS Miramar suppressor will meet 85 dBA at 250 feet from the engine exhaust with the possible exception of a small region axially downstream of the ramp. The noise reduction afforded by stack and baffles configuration was poorer than that provided by the full length acoustically lined augmenter especially at low frequencies.

In addition to the customary analysis of the test data, the basic data have been correlated and condensed in a separate report section as a design tool for future Hush Houses. The graphs associated with this section permit augmenter sizing which will result in acceptable augmenter wall temperatures and noise levels.

TABLE OF CONTENTS

LIST OF FIGURES

1. Figures Describing the Basic Test Set-up and Models and Presenting Aerodynamic/Thermodynamic Test Results

LIST OF TABLES

DEFINITION OF AERODYNAMIC/THERMODYNAMIC SYMBOLS

(Symbols in parentheses correspond to computer printout of data contained in the Data Appendix)

A	Area
A^*	Choked throat area (M = 1.0)
A_A	Augmenter cross-sectional area
A_{AM}	Primary burner air meter throat area
A_D	Subsonic diffuser exit area
A_{NT}	Jet nozzle throat area
A_{PM}	Pilot burner air meter throat area
A_{SM}	Secondary air meter throat area
A/R	Aspect ratio of augmenter cross-section
ARP	Augmentation ratio parameter (see eqn. 6.2.2 page 109)
D	Diameter
D_A	Augmenter cross-sectional diameter
D_{AM}	Effective diameter of obround augmenter = $\sqrt{4\ A_A/\pi}$
D_N	Jet nozzle exit diameter
D_{NT}	Jet nozzle throat diameter
L	Length
L_A	Augmenter Length
L_D	Subsonic diffuser length
mw	Molecular weight
mw_{air}	Molecular weight of air
mw_N	Jet exhaust molecular weight
P	Absolute pressure
P_{amb}	(PA) Static pressure outside of Hush House
P_{bar}	(BARO) Local barometric pressure during model tests
P_{BE}	(PSEC) Burner enclosure interior pressure during model tests corresponding to Hush House interior pressure
P_{EE}	(PAMB) Exhaust enclosure pressure during model tests corresponding to Hush House outside ambient pressure
P_{inlet}	Hush House air inlet static pressure
$P_{interior}$	Hush House interior static pressure

P_{NB}	Jet nozzle base pressure
P_{NB_p}	Jet nozzle base pressure parameter (see eqn. 6.3.3 and 6.3.4, page 111)
P_p	Pressure parameter (see eqn. 6.3.2, page 111)
P_{shell}	Augmenter shell static pressure
P_{SM}	(PSSM) Secondary air meter throat static pressure
P_{wall}	Augmenter wall static pressure
P_T	Total Pressure (absolute pressure)
$P_{T_{AM}}$	(PTAM) Primary burner air meter total pressure
$P_{T_{exit}}$	Augmenter plus ramp or augmenter plus diffuser exit total pressure (usually equal to $P_{ambient}$)
$P_{T_{flow}}$	Hush House interior flow total pressure
P_{T_N}	(PTN) Jet nozzle inlet total pressure
$P_{T_{PM}}$	(PTPM) Pilot burner air meter inlet total pressure
$P_{T_{ramp}}$	Ramp exit total pressure
$P_{T_{sec}}$	(PSEC) Secondary (pumped) air flow total pressure
$P_{T_{SM}}$	(PTSM) Secondary air meter inlet total pressure
r	Radius
r_{NT}	Jet nozzle throat radius
T	Absolute temperature
T_{amb}	Hush House external ambient temperature
T_{BE}	(TAMB) Burner enclosure air temperature during model tests corresponding to Hush House external ambient temperature
T_{EE}	Exhaust enclosure air temperature during model tests (used in the analysis of acoustical data)
T_{mix}	Average mixed temperature of jet and pumped flows
T_{mix_p}	Average mixed temperature parameter
T_{ramp}	Ramp surface temperature
T_{wall}	Augmenter wall temperature
T_{wall_p}	Augmenter wall temperature parameter (see eqn. 6.4.4, page 112)
T_T	Total temperature

$T_{T_{AM}}$	(TTAM) Primary burner air meter inlet total temperature
T_{T_N}	(TTN) Jet nozzle total temperature
$T_{T_{PM}}$	Pilot burner air meter inlet total temperature
$T_{T_{SM}}$	(TTSM) Secondary air meter inlet total temperature
V	Velocity
V_{jet}	Ideal jet velocity expanded from P_{T_N} to P_{amb}
$V_{mix\ avg}$	Average mixed velocity in augmenter
$V_{mix\ max}$	Maximum measured core velocity some distance from jet nozzle exit
W	Mass flow rate
$\dot{W}_{aircraft}$	Aircraft engine exhaust mass flow rate
$\dot{W}_{air\ meters}$	Sum of primary and pilot air meter mass flow rates during model tests
$\dot{W}_{fuel}$	Fuel mass flow rate during model tests
$\dot{W}_{inlet}$	Total Hush House inlet mass flow rate
$\dot{W}_N$	(WN) Jet nozzle mass flow rate from model tests corresponding to aircraft engine exhaust mass flow rate
$\dot{W}_{pumped}$	(WS) Secondary (pumped) air mass flow rate
X	Axial location
X_A	Axial location in augmenter
X_N	Axial distance between jet nozzle exit and augmenter entrance
Y	Lateral distance from jet nozzle centerline at nozzle exit to nearest augmenter wall
Y_{CTR}	Lateral distance from augmenter center to augmenter wall
Y_P	Nozzle centerline lateral position parameter = $\dfrac{Y - r_{NT}}{Y_{CTR} - r_{NT}}$
Z	Vertical distance from jet nozzle centerline at nozzle exit to nearest augmenter wall
Z_{CTR}	Vertical distance from augmenter center to augmenter wall
Z_P	Nozzle centerline vertical position parameter = $\dfrac{Z - r_{NT}}{Z_{CTR} - r_{NT}}$
α	Angle
α_S	Angle of lateral (sidewise) jet deflection
α_V	Angle of vertical jet deflection
λ_N	Jet nozzle pressure ratio (see eqn 6.1.1, page 105)

DEFINITION OF ACOUSTIC SYMBOLS

α	Sound absorption coefficient
ρ_{EXIT}	Density of jet exhaust gas at exit plane
ρ_{AMB}	Density of ambient temperature air
δ	Boundary layer thickness
dB	Decibel
dBA	A-weighted sound level
DI	Directivity correction in dB for sound propagation parallel to the ground
f	Frequency of sound
f_F	Full-scale frequency
f_M	Model-scale frequency
f_p	Frequency at which a spectrum of sound power level peaks
Hz	Hertz, unit of frequency
ΔL_{NF}	No-flow attenuation of lined augmenter measured with loudspeaker excitation
ΔL	Total attenuation of jet noise by the lined augmenter, dB
λ_N	Jet nozzle pressure ratio
n	Scale factor (full-scale dimension : model-scale dimension)
ϕ	Directivity angle: 0° in downstream direction along centerline of exhaust stack
NR	Noise reduction for sound propagating from one room into an adjacent room, dB

PWL	Sound power level, dB re 10^{-12} watt
PWL_{AJ}	Attenuated sound power level of the jet
PWL_{free}	Unattenuated sound power level of the free jet
PWL_{F}	Sound power level of a full-scale jet
PWL_{M}	Measured sound power level of a model jet
PWL_{NF}	Normalized sound power level of a full-scale jet
PWL_{NM}	Normalized sound power level of a model jet
PWL_{outlet}	Sound power level exiting from downstream end of augmenter (with ramp)
PWL_{SN}	Sound power level of self-generated noise of augmenter (i.e., noise generated by flow of air; not primary jet noise)
ΔPWL	Measured difference between total free jet sound power level PWL_{free} and sound power level at the augmenter exit PWL_{outlet}, dB
ΔPWL_0	Baseline ΔPWL in dB for the condition [illegible]=4 in.; nozzle at F-14 position (Y_P=0.45); 72-in. [illegible] lined obround augmenter with lined 45° exit ramp; effective obround augmenter diameter of 12 in.; T_{TN} =520, 2300, and 3300°R; and λ_N=2 and 3.
ΔPWL_S	Shift of sound power level spectrum as derived in Eq. 2.3.1
ΔPWL_1	Correction to ΔPWL in dB for length of lined augmenter different from 72 in. (model-scale)
ΔPWL_2	Correction to ΔPWL in dB for effective diameter of obround augmenter different from 12 in. (model-scale)
ΔPWL_3	Correction to ΔPWL in dB for center position of jet nozzle
ΔPWL_4	Correction to ΔPWL in dB for radial or lateral position of the nozzle different from the F-14 position (Y_P=0.45, or model-scale nozzle 3.6 in. right of the centerline)

ΔPWL_5	Correction to ΔPWL in dB for angular alignments
R	Distance from augmenter exit, ft
S	Strouhal number = $\frac{fD_N}{U_j}$
S_p	Peak Strouhal number = $\frac{f_p D_N}{U_j}$
SPL	Sound pressure level, dB re 0.0002 dyne/cm^2
$\overline{SPL}$	Room-average SPL
$\overline{SPL'}$	Room-average SPL produced by the reference sound source
T_{T_N}	Total jet nozzle temperature in ° Rankine
T_{60}	Reverberation time; time in seconds for SPL in a room to decay 60 dB
U_{eff}	Effective ramp flow velocity
U_j	Jet exit velocity
V	Velocity
V_0	Arbitrary reference velocity
V_{EX}	Velocity of flow from augmenter exit
$V_{mix\ max}$	Maximum velocity of mixed jet flow at exit
V_j	Jet velocity
Vol	Room volume, m^3
W	Acoustic power, watts
W_{AJ}	Acoustic power of attenuated jet noise at augmenter exit
W_{EXH}	Acoustic power at augmenter exit $= W_{AJ} + W_{SN}$
W_{SN}	Acoustic power of self-generated noise at augmenter exit

1.0 INTRODUCTION

1.1 Historical Background

In the United States, ground run-up sound suppressor installations for jet aircraft or isolated engines having afterburners have been primarily of the wet-cooling type and mostly jet engine (out-of-airframe) test cells and portable sound suppressors or semi-enclosures for in-airframe run-up (for an early example of a dry-cooled semi-enclosure, see Reference A/T-1). These approaches have a number of disadvantages. With wet-cooling, the suppressor exhaust includes water vapor, raw fuel and free carbon when the afterburner is fired, because the water spray quenches the flame. Thus, an unsightly vapor cloud is presented and pollutants may deposit on parked cars and buildings. This sooty vapor has a deleterious effect on some types of acoustical treatment.

Portable in-airframe run-up sound suppressors or semi-enclosures have problems apart from those created by wet-cooling, and the noise reduction affordable by such installations is limited. These suppressors are designed to seal around one aircraft type and are not adaptable. The requirement for acoustical sealing creates a requirement for accurate positioning of the aircraft relative to the suppressor. Even with careful positioning, some of the jet noise and inlet noise leaks through the seals between the aircraft and the exhaust sound suppressor and inlet sound suppressor. Furthermore, a large portion of the aircraft is not enclosed, so casing noise is usually unattenuated.

In about 1966 the Swedish firm, Granges Nyby, designed a complete aircraft acoustical enclosure, or Hush House, for the SAAB Draken aircraft. This enclosure employed an acoustically-treated augmenter tube which was sized so that the momentum flux of the aircraft's exhaust jet would pump enough outside air through the enclosure to cool the exhaust gases and eliminate the need for water spray. More recently, this same firm has provided similar Hush Houses for the SAAB Viggen and F-4K Phantom airplanes. These enclosures or Hush Houses have had good acceptance by their users. Positioning of the aircraft is not difficult; both outside and inside sound levels are acceptable; the aircraft enclosures provide a lighted, all-weather, 24 hour-a-day place to work on the aircraft; and the installations have exhibited a good service life. Furthermore, this dry-cooled Hush House concept can be designed so as to be adaptable to several aircraft types. This comes about because there is no need for close alignment, close axial spacing or sealing between the nozzle exit and the much larger augmenter entrance. Consequently, if one designs a Hush House for the largest in a series of aircraft, simple mechanical contrivances (nose wheel elevator, for example) can be used to adapt to smaller aircraft which will fit in the enclosure.

The Hush House approach is not inexpensive. However, if one adds up the advantages of adaptability, usefulness as an all-weather, 24 hour-a-day enclosure for the aircraft for secondary tasks other than run-up, acceptability of the interior environment for making adjustments to the engines while operating in the aircraft, potential low maintenance, etc., these enclosures may be more cost effective than less expensive sound suppressor concepts. The substitution of dry-cooling for water spray cooling ameliorates a growing confrontation in the area of pollution control and is certainly more cost effective than the more sophisticated wet-cooled systems having scrubbers and their associated water treatment facilities. The United States Navy has recognized these Hush House advantages (see Reference A/T-2) and for several years has shown an interest in pursuing this approach by on-site inspection and evaluation of the European Hush Houses and by support of cost studies such as the one by Gustav Getter Associates reported in Reference A/T-3. That study provided cost estimates for portable in-aircraft sound suppressors and semi-enclosures, as well as complete aircraft enclosures both dry and wet. For complete Hush House enclosures, the results indicated a lower long-term cost for the dry suppressor approach. In addition, a dry suppressor using an acoustically lined augmenter appeared to be less expensive than one which employed a hard-walled augmenter with sound absorptive baffles in a vertical exhaust stack. The Gustav Getter Associates study report also recommended that a model study be performed to provide acoustical and aerodynamic/thermodynamic data usable in designing Hush Houses and their sound suppressors.

1.2 Parallel Model Test and Full-Scale Hush House Construction Programs

Subsequent to the publication of the Gustav Getter Associates study report, two things have transpired: 1) a full-scale Hush House for the F-14 has been designed by Gustav Getter Associates and constructed at NAS Miramar, California, with checkout taking place during August and September, 1975 (see Figure 1.2-1). This Hush House was designed with no model test results or in-house experience for guidance. 2) A 1/15 scale model test program has been funded by the United States Navy and carried out by FluiDyne Engineering Corporation, Minneapolis, Minnesota, with support from Bolt, Beranek and Newman, Waltham, Massachusetts, and Gustav Getter Associates P.C., New Rochelle, New York. The results of the model study are the principal subject of this report. Both the full-scale F-14 Hush House and the related model test program envisioned the following Hush House attributes:

1. convenience of use (aircraft easily installed and completely protected from the weather; adequately lighted working area);

2. multi-aircraft use capability (including the F-14 having nine feet between engine exhaust centerlines and a one degree lateral inclination of each engine's thrust axis; $y_p = 0.45$, $\alpha_s = 1°$);

3. all air-cooled (even with an engine operating in maximum afterburning mode);

4. low maintenance (structural and acoustical material out of the direct jet blast and, as much as possible, out of the hot mixed core flow);

5. significant outdoor noise reduction (85 dBA permitted at 250 ft. from the aircraft exhaust);

FLUIDYNE ENGINEERING CORPORATION

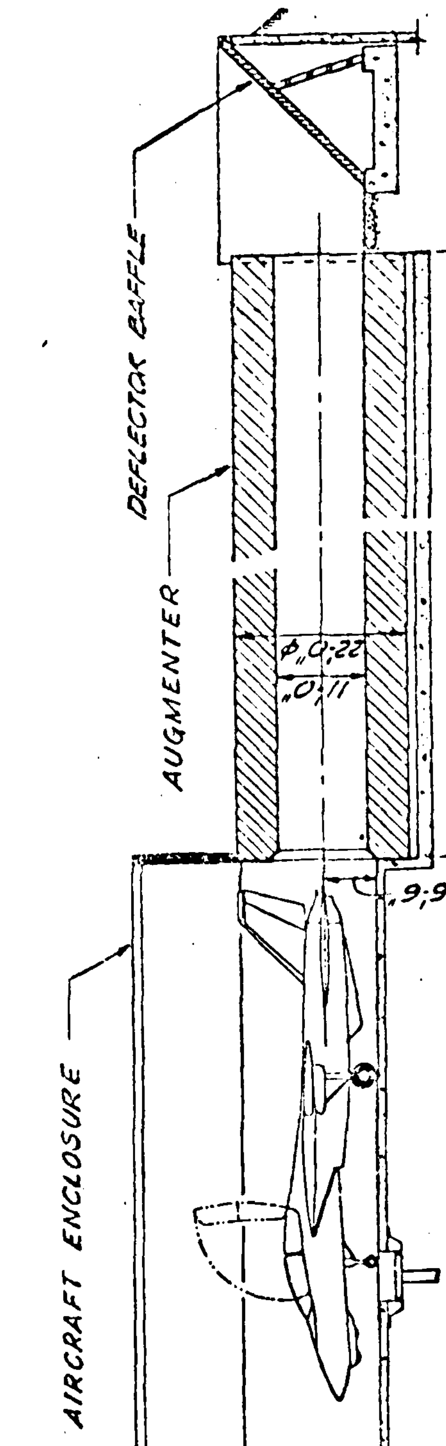

FIGURE 1.2-1 SIDE VIEW OF F-14 HUSH HOUSE AT NAS MIRAMAR

6. interior noise acceptable for working around the aircraft during run-up with only normal ear protection (interior noise level no greater than 2 dBA above the corresponding aircraft free field noise).

The model test program reported herein was not a general research program, but was designed to provide data directly correlatable with the full-scale NAS Miramar Hush House. Enough variables were run, however, so that information is available not only for correlation with the performance of the Miramar Hush House, but also for more effective design of future Hush Houses and for guiding modifications to the present Miramar F-14A design, which might be required to bring its performance up to specification.

In addition to the FluiDyne employees who ran the tests and Mr. Douglas Andersen of Bolt, Beranek & Newman who set up, calibrated and operated the sound pressure level recording apparatus during the entire test program, the following people connected with this program or the Miramar Hush House project were among those who observed the test equipment and witnessed one or more runs.

Mr. Robert E. Foster, United States Navy, Charleston, South Carolina (Project Design Engineer)

Mr. Meyer Lepor, United States Navy, San Diego, California

Dr. Wayne Sule, United States Navy, Lakehurst, New Jersey

Dr. István L. Vér of Bolt, Beranek & Newman, Waltham, Massachusetts (Chief Acoustician)

Mr. Gustav Getter of Gustav Getter Associates, P. C. New Rochelle, New York (Report and Data Coordinator)

2.0 BRIEF TEST PROGRAM DESCRIPTION, DESIGN DATA SUMMARY AND PREDICTION OF FULL SCALE HUSH HOUSE PERFORMANCE

For the test program, the aircraft jet exhaust was simulated by a propane air burner with 3000°F maximum combustion temperature and a jet nozzle having throat diameter, D_{NT}, and exit diameter, D_N, sized at 1/15 of the afterburning F-14A nozzle configuration (D_{NT} = 2.50", D_N = 2.74" on the model). The testing was carried out using two reverberant rooms separated by a sound insulating wall, as shown in Figure 2.0-1 below, to facilitate sound power level measurements. One room, referred to here

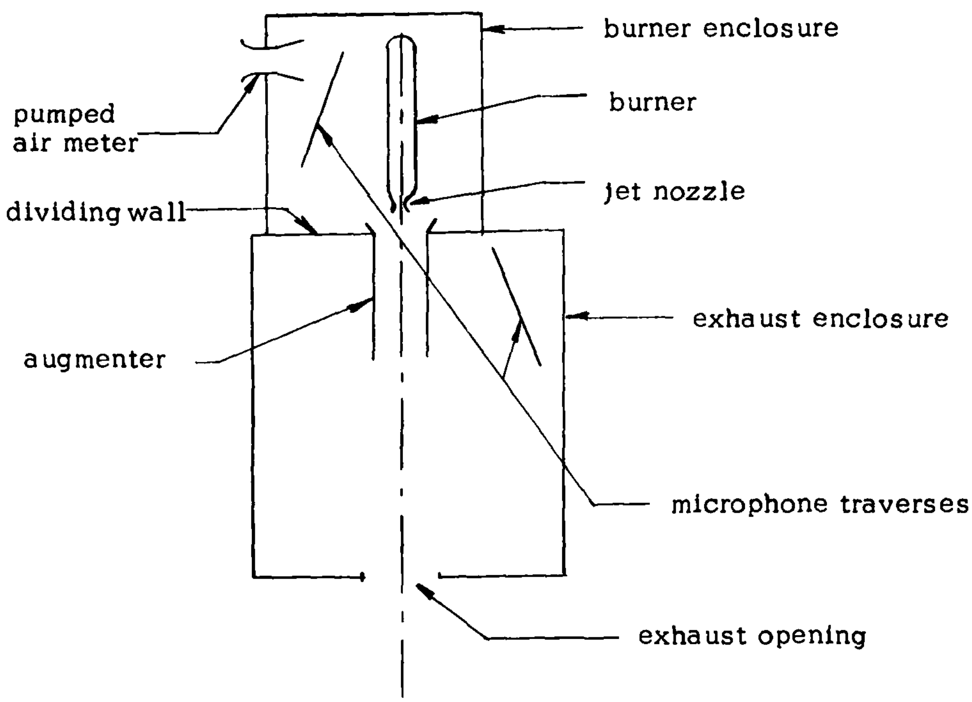

Figure 2.0-1. Arrangement of the Reverberant Rooms

as the burner enclosure, corresponds to the Hush House interior. The other room, the exhaust enclosure, corresponds to the out-of-doors. Space-time-average sound pressure level data were recorded in both enclosures for essentially every test run in the program using traversing microphones. With the rooms suitably calibrated acoustically using a standard noise source, the space-average sound pressure level data were converted into sound power levels. The burner enclosure is equipped with a venturi meter air inlet to measure the pumped air flow and the exhaust enclosure is provided with suitable ports for the flow to exit.

The test program was designed to provide information in three principal areas which are interrelated and have direct applicability to dry sound suppressor design, namely: augmenter pumping (augmentation ratio); jet impingement and augmenter wall temperature; and sound absorptive augmenter noise reduction performance. Consequently, the test program was divided into four parts, each with its own primary emphasis:

1. jet survey testing,
2. aero-acoustic testing,
3. aero-thermal testing, and
4. acoustic testing.

2.0.1 Jet Survey Testing (Test Series 1 through 3)

The jet survey tests emphasized noise measurements on the free model scale exhaust jet. The resulting model scale noise corresponded to the free-field aircraft exhaust noise. Total pressure and temperature surveys of the mixing free jet were also made, as illustrated in Figure 2.0-2 below.

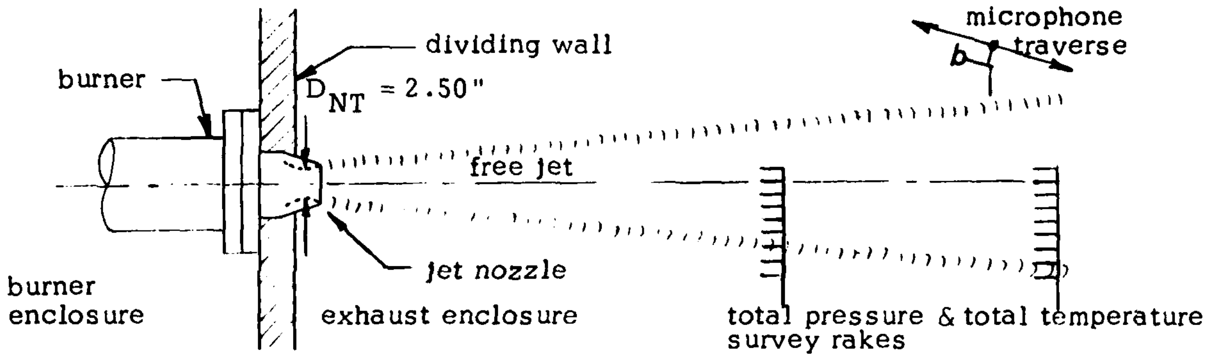

Figure 2.0-2. Experimental Arrangement for the Jet Survey Tests

2.0.2 Aero-Acoustic Testing (Test Series 4 through 12)

The aero-acoustic tests, as illustrated in Figure 2.0-3, primarily emphasized augmenter pumping performance and secondarily, noise reduction for round hard-walled ejector environments. Variables included augmenter diameter (from 8" to 17.5"), augmenter length (from 36" to 120"), jet nozzle exit to augmenter entrance spacing and a subsonic diffuser. Different augmenter entrance configurations were also tested.

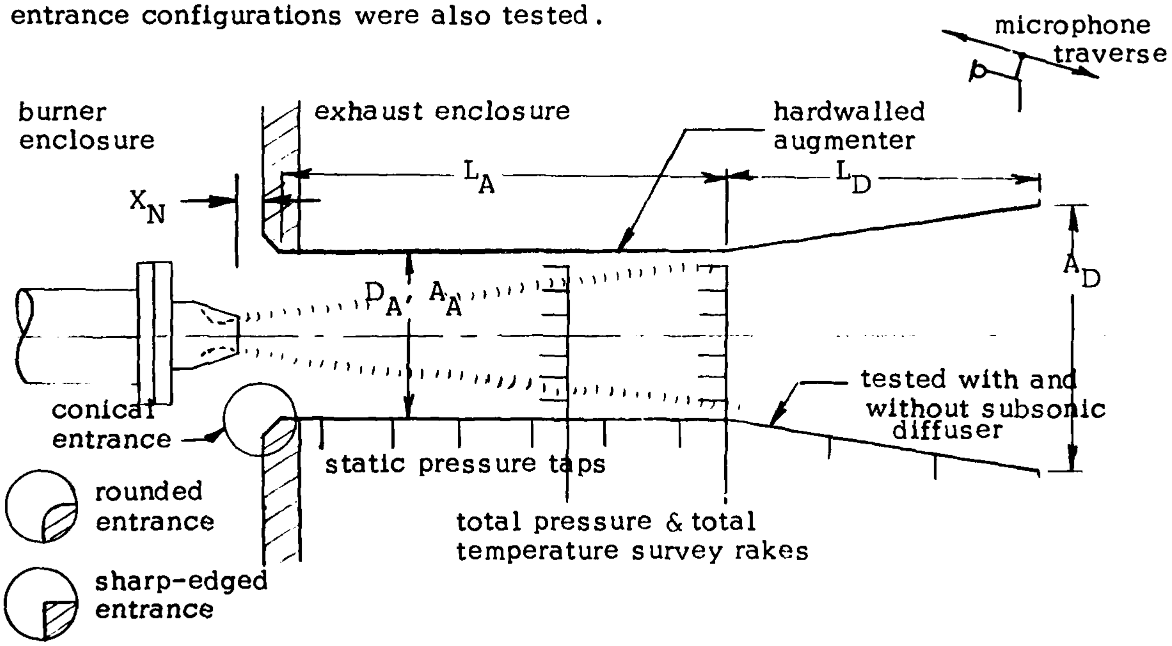

Figure 2.0-3. Experimental Arrangement for the Aero-Acoustic Tests

2.0.3 Aero-Thermal Testing (Test Series 13 through 16)

The aero-thermal testing, Figure 2.0-4, concentrated on jet impingement and resulting wall temperatures when the jet axis was translated or deflected either vertically or horizontally from the centered, aligned position in a sound absorbing obround augmenter modelling the Miramar configuration at 1/15 scale. An important secondary requirement was the determination of the effect of jet offset and inclination on the noise reduction afforded by the sound absorbing liner. Lateral jet position, Y_p, vertical jet position, Z_p, and vertical and lateral jet deflection, α_v and α_s were the geometric variables in these tests. The definitions of Y_p and Z_p are given with Figure 2.0-4 below.

$$Y_p = \frac{Y - r_{NT}}{Y_{ctr} - r_{NT}}, \quad Z_p = \frac{Z - r_{NT}}{Z_{ctr} - r_{NT}}$$

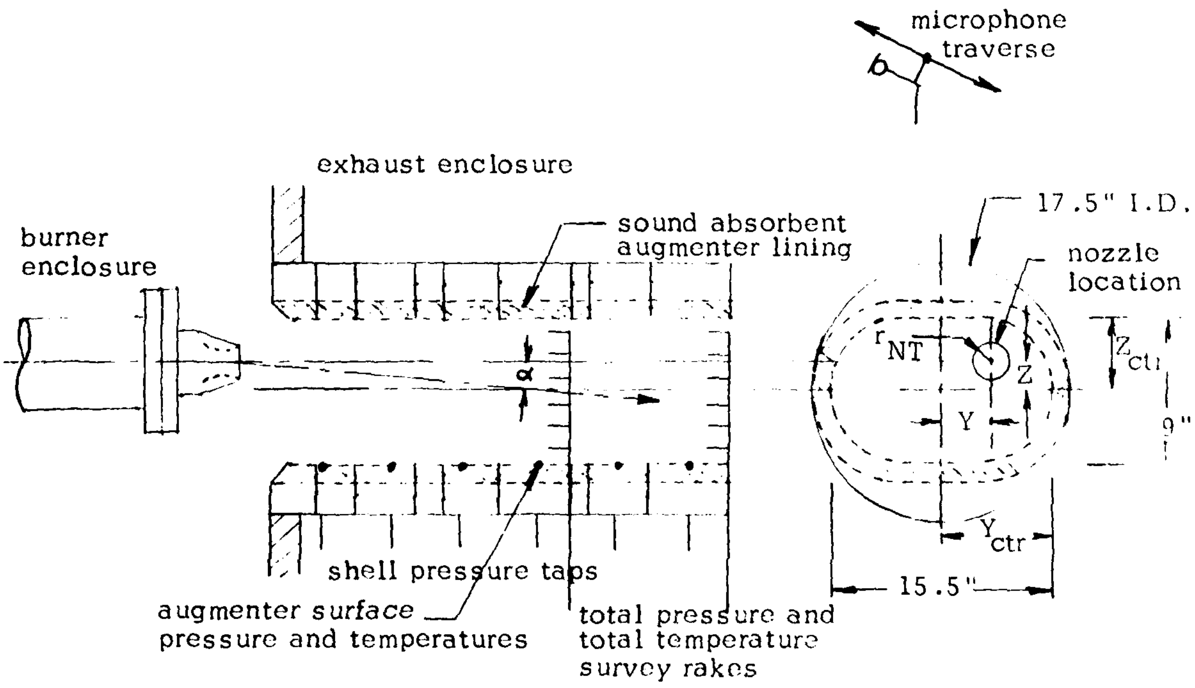

Figure 2.0-4. Experimental Arrangement for Aero-Thermal Testing

2.0.4 Acoustic Testing (Test Series 17 through 26)

The aim of the acoustic testing was to obtain the reduction in sound power level of various lined augmenter configurations, as illustrated in Figure 2.0-5. The reduction in sound power level, ΔPWL, is defined as the difference in sound power level in the exhaust enclosure measured with the free jet and with the lined augmenter configuration, respectively. The exhaust configurations investigated included:

1. the two different absorbing liner designs of Figure 2.0-5, one of them simulating the full-scale Miramar augmenter liner and the other an alternative design;

2. different lengths of lined augmenter up to 96 in. with and without a sound absorbing 45° deflector ramp;

3. a one-foot length of absorptive augmenter placed at different downstream positions in an otherwise hard-walled augmenter tube; and

4. the hard-walled augmenter with subsonic diffuser, turning vanes and stack filled with parallel sound absorbing baffles configuration, as shown in Figure 2.0-6. This configuration represented an alternative concept to the lined augmenter configuration.

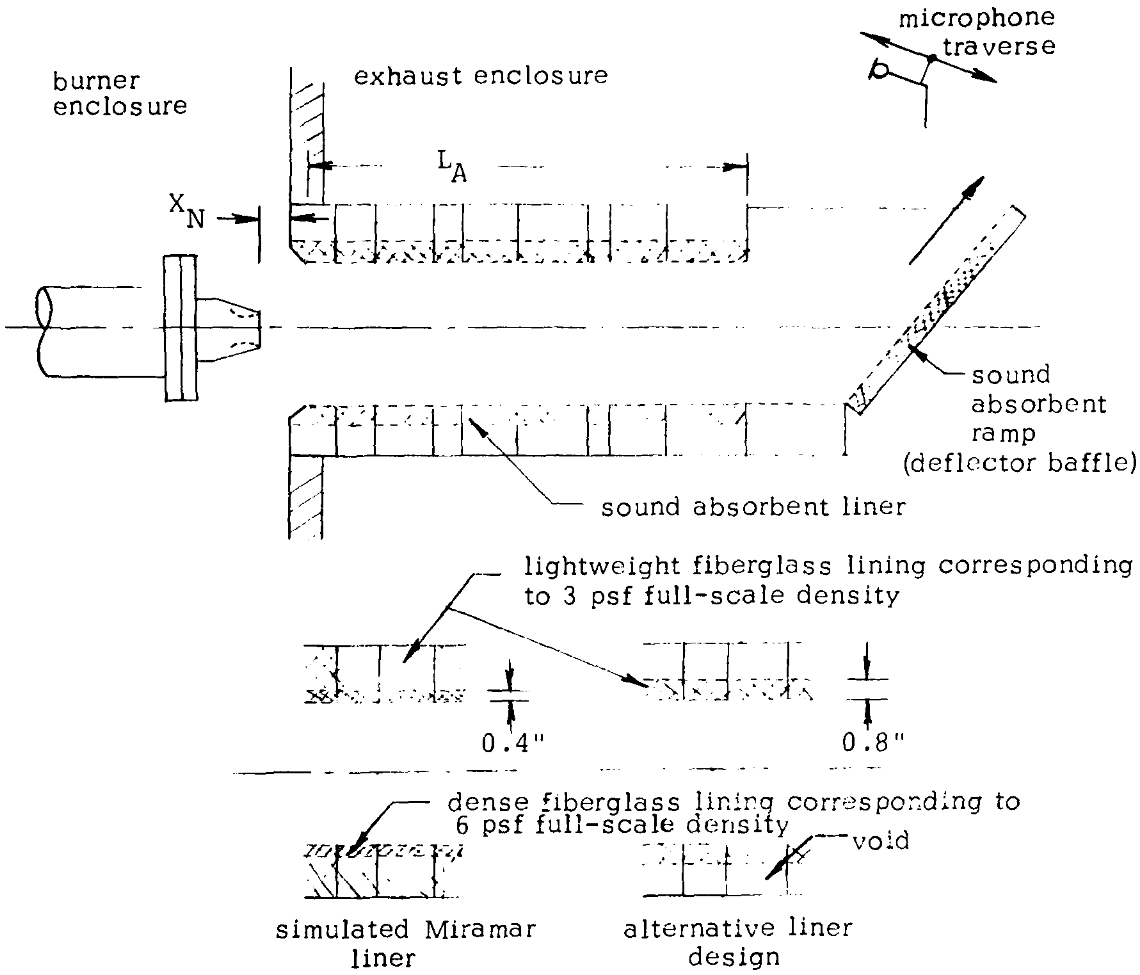

Figure 2.0-5. Experimental Arrangement for the Acoustic Tests with the Lined Augmenter Tube

The majority of the test variables are shown schematically in Figure 2.0-5 above. It should be noted that all of the acoustical tests were run with the obround augmenter and the jet in the F-14A lateral position (i.e., $Y_p = 0.45$) but undeflected.

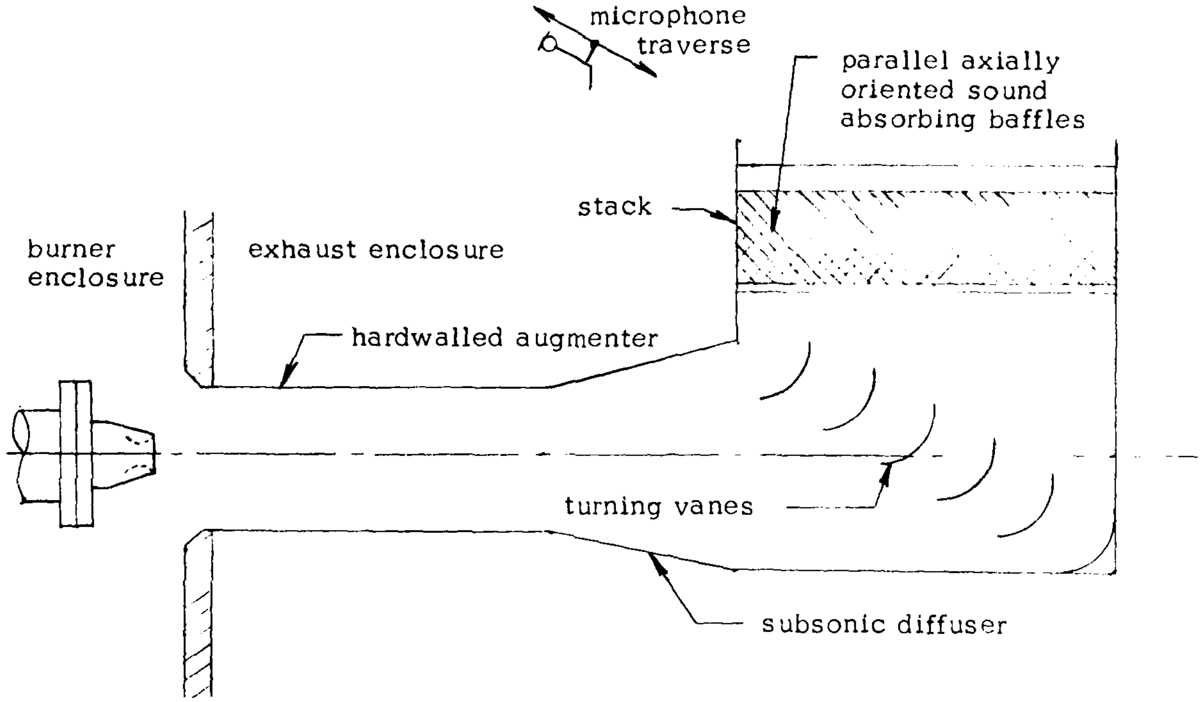

Figure 2.0-6. Experimental Arrangement for the Acoustic Tests on the Stack with Sound Absorbing Baffles

Water manometers, bourdon tube pressure gages, iron-constantan thermocouple and venturi flow meters were used to measure the aerodynamic/thermodynamic information required from the tests (pressure, temperature and flow). The microphone traverse yielded the space-time-average sound pressure generated in the exhaust room by the sound power existing from the augmenter and the stack. A complete summary of the test program, including the test series designation and run numbers which correspond to those on the data sheets provided in the separate Data Appendix is included in Table 2.0-1. For definition of the symbols used in this table and in the rest of the report, see the list of symbols and Figures 3.0-1, 4.2-1, 4.3-1 and 4.4-1.

TABLE 2.0-1. HUSH HOUSE 1/15 SCALE MODEL TEST PROGRAM

Test Series	Type of Test	Nozzle Press. Ratio λ_N	Nozzle Total Temp. T_{T_N} °R	Nozzle Axial Position X_N in.	Nozzle Lateral Position	Nozzle Deflection $\alpha°$	Augm. Inlet Config.	Augm. X-Sect. D_A in.	Augm. Length L_A in.	Acoustic Lining Location	Acoustic Lining Design	Subsonic Diffuser Length L_D in.	Exit Acoustic Treatment	P, T & Flow Run No.	Noise Data Run No. (same as P, T & Flow unless noted)
1	Jet Survey	2	3300											8	
1		3	3300											9	
2		2	2300											6	
2		3	2300											7	
3		2	500											146	1
3	Jet Survey	3	500											4	
4	Aero-Acoustic	2	3300	1/2	Center	0	Conical	12.25	72	None		None	None	45 (2.49)	
4		2	500	1/2		0								44 (3.28)	
4		2	3300	4		0								43 (2.51)	
4		2	500	4		0								41 (3.30)	
4		2	3300	10 1/4		0								48 (2.50)	
4		2	500	10 1/4		0								47 (3.30)	
4		2	3300	18 1/2		0								50 (2.38)	
4		2	500	18 1/2		0								49 (3.15)	
5		3	3300	4		0								60 (2.44)	
5		3	500	4		0						None		59 (3.23)	
6		2	3300	4		0						20		66 (3.65)	
6		2	500	4		0						20		65 (4.33)	
6		2	3300	4		0						40		64 (4.08)	
6		2	500	4		0						40		63 (4.64)	
7		2	3300	4		0						None		58 (2.79)	Lowered $P_{T_{sec}}$ loss
7		2	500	4		0								57 (3.58)	Lowered $P_{T_{sec}}$ loss
7		2	3300	4		0								62 (2.88)	Still lower $P_{T_{sec}}$ loss
7	Aero-Acoustic	2	500	4	Center	0	Conical	12.25	72	None		None	None	61 (3.65)	Still lower $P_{T_{sec}}$ loss

Note: **A star next to the test series designation indicates an extra run.**

The number in parentheses next to each run number is the measured augmentation ratio parameter for that point.

TABLE 2.0-1 (continued)

Test Series	Type of Test	Nozzle Press. Ratio λ_N	Nozzle Total Temp. T_{T_N} °R	Nozzle Axial Position X_N in.	Nozzle Lateral Position	Nozzle Deflection α°	Augm. Inlet Config.	Augm. X-Sect. D_A-in.	Augm. Length L_A-in.	Acoustic Lining Location	Acoustic Lining Design	Subsonic Diffuser Length L_D-in.	Exit Acoustic Treatment	P, T & Flow Run No.	Noise Data Run No. (Same as P, T & Flow unless noted)
8	Aero-Acoustic	2	3300	4	center	0	conical with throttle	12.25	72	None		None	None	52 (2.42)	
8		2	500	4	center	0	conical with throttle		72					51 (3.05)	
9		2	3300	4		0	conical		48					35 (2.33)	
9		2	500	4		0			48			None		34 (2.77)	
9		2	3300	4		0			48			20		71 (3.41)	
9		2	500	4		0			48			20		70 (3.86)	
9		2	3300	4		0			96			None		38 (2.61)	
9		2	500	4		0			96			None		40 (3.30)	
9		2	3300	4		0			96			20		68 (3.67)	
9		2	500	4		0			96			20		67 (4.49)	
9*		2	2300	4		0	conical		96			20		69 (3.97)	
10		2	3300	4		0	round		72			None		54 (2.51)	
10		2	500	4		0	round		72					53 (3.43)	
10		2	3300	4		0	sharp edged		72					56 (2.34)	
10		2	500	4		0	sharp edged	12.25	72					55 (3.02)	
11		2	3300	4		0	conical	8	36					22 (1.34)	
11		2	500	4		0			36			None		21 (1.84)	
11		2	3300	4		0			36			24		33 (2.00)	
11		2	500	4		0			36			24		32 (2.33)	
11		2	3300	4		0			48			None		24 (1.35)	
11		2	500	4		0			48			None		23 (1.97)	
11		2	3300	4		0			48			24		30 (1.84)	
11		2	500	4		0			48			24		29 (2.48)	
11*	Aero-Acoustic	2	2300	4	center	0	conical	8	48	None		24	None	31 (2.14)	

TABLE 2.0-1. (continued)

Test Series	Type of Test	Nozzle Press. Ratio λ_N	Nozzle Total Temp. T_{T_N} °R	Nozzle Axial Position X_N-in.	Nozzle Lateral Position	Nozzle Deflection α°	Augm. Inlet Config.	Augm. X-Sect. D_A-in.	Augm. Length L_A-in.	Acoustic Lining Location	Acoustic Lining Design	Subsonic Diffuser Length L_D-in.	Exit Acoustic Treatment	P,T & Flow Run No.	Noise Data Run No. (same as P,T & Flow unless noted)
11	Aero-Acoustic	2	3300	4	center	0	conical	8	60	None		None	None	26 (1.34)	
11		2	500	4		0			60			None		25 (1.91)	
11		2	3300	4		0			60			24		28 (1.77)	
11		2	500	4		0		8	60			24		27 (2.43)	
12		2	3300	4		0		17.5	72			None		14 (3.32)	
12		2	500	4		0			72					13 (3.52)	
12		2	3300	4		0			96					20 (3.42)	
12		2	500	4		0			96					15 (3.91)	
12		2	3300	4		0			120					19 (3.44)	
12	Aero-Acoustic	2	500	4	center	0		17.5	120	None				17 (4.07)	
13	Aero-Thermal	2	2300	4	b $y_{par}=.45$	$\alpha_s=0$ $\alpha_{v_{eff}}=1.6$		15.5 x 9 obround	72	Full Length	BB&N			75 (2.13)	84 (2.17)
13		2	2300	4	b $y_{par}=.45$	$\alpha_s=1$ $\alpha_{v_{eff}}=1.6$			72					76 (2.17)	87 (2.12)
13		2	2300	4	b $y_{par}=.45$	$\alpha_s=3$ $\alpha_{v_{eff}}=1.6$			72					77 (1.90)	85 (1.96)
14		2	2300	4	a $y_{par}=1.0$	$\alpha_s=0$ $\alpha_{v_{eff}}=1.6$			72					74 (2.57)	83 (2.51)
14		2	2300	4	c $y_{par}=.29$	$\alpha_s=0$ $\alpha_{v_{eff}}=1.6$			72					78 (2.14)	
14		2	2300	4	d $y_{par}=.45$ $z_{par}=.69$	$\alpha_s=0$ $\alpha_{v_{eff}}=1.6$			72					79 (2.19)	
15		2	2300	4	b $y_{par}=.45$	$\alpha_s=0$ $\alpha_{v_{eff}}=3.6$			72					80 (2.24)	81 (2.29)
15		2	2300	4	a $y_{par}=1.0$	$\alpha_s=0$ $\alpha_{v_{eff}}=3.6$			72					82 (2.38)	
16	Aero-Thermal	3	2300	4	b $y_{par}=.45$	$\alpha_s=0$ $\alpha_{v_{eff}}=1.6$	conical	15.5 x 9 obround	72	Full Length	BB&N	None	None	121 (1.96)	[illegible]0 (1.98)

FLUIDYNE ENGINEERING CORPORATION

TABLE 2.0-1. (continued)

Test Series	Type of Test	Nozzle Press. Ratio λ_N	Nozzle Total Temp. T_{T_N} °R	Position Axial Position X_N-in.	Nozzle Lateral Position	Nozzle Deflection α°	Augm. Inlet Config.	Augm. X-Sect. D_A-in.	Augm. Length L_A-in.	Acoustic Lining Location	Acoustic Lining Design	Subsonic Diffuser Length L_D-in.	Exit Acoustic Treatment	P, T & Flow Run No.	Noise Data Run No. (same as P, T & Flow unless noted)
17	Acoustic	2	3300	4	b y_{par}=.45	$\alpha_s = 0$ $\alpha_{v_{eff}} = 2.2$	conical	15.5 x 9 obround	72	Full Length	BB&N	None	None	89 (2.01)	
17		2	500	4		$\alpha_s = 0$ $\alpha_v = 0$			72	Full Length				88 (2.50)	
18*		2	3300	4		$\alpha_s = 0$ $\alpha_{v_{eff}} = 2.2$			60	None			None	125 (2.10)	
18		2	3300	4					72	1 upstrm			45° Ramp	130 (2.00)	
18		2	3300	4					72	2				129 (2.01)	
18		2	3300	4					72	3				127 (2.06)	
18		2	3300	4					72	4				128 (2.02)	
18		2	3300	4					72	5				126 (2.12)	
18		2	3300	4					72	6 dnstrm			45° Ramp	124 (2.13)	
18*		2	3300	4					72	6 dnstrm			None	123 (2.23)	
19		2	3300	4					48	Full Length			45° Ramp	109 (1.92)	108 (1.85)
19		2	3300	4					72					98 (1.90)	97 (1.91)
19		2	3300	4		$\alpha_s = 0$ $\alpha_{v_{eff}} = 2.2$			96					111 (1.90)	
19*		2	500	4		$\alpha_s = 0$ $\alpha_v = 0$			72					110 (2.57)	
20		3	3300	4		$\alpha_s = 0$ $\alpha_{v_{eff}} = 1.1$			72					113 & 120 (1.87)	113 (1.62)
														different $P_{T_{sec}}$	
20		1.2	500	4		$\alpha_s = 0$ $\alpha_{v_{eff}} = 0$			72					101 (2.37)	
21	Acoustic	2	3300	1/2	b y_{par}=.45	$\alpha_s = 0$ $\alpha_{v_{eff}} = 2.2$	conical	15.5 x 9 obround	72	Full Length	BB&N	None	45° Ramp	96 (1.90)	

TABLE 2.0-1. (continued)

Test Series	Type of Test	Nozzle Press. Ratio λ_N	Nozzle Total Temp. T_{T_N} °R	Nozzle Axial Position X_N-in.	Nozzle Lateral Position	Nozzle Deflection α °	Augm. Inlet Config.	Augm. X-sect D_A-in.	Augm. Length L_A-in.	Acoustic Lining Location	Acoustic Lining Design	Subsonic Diffuser Length L_D-in.	Exit Acoustic Treatment	P, T & Flow Run No.	Noise Data Run No. (same as P, T & Flow unless noted)
21	Acoustic	2	3300	10	b y_{par} = .45	α_s = 0 $\alpha_{v_{eff}}$ = 2.2	Conical	15.5 x 9 obround	72	Full length	BB&N	None	45° ramp	95 (1.91)	94 (1.91)
21		2	3300	18		α_s = 0 $\alpha_{v_{eff}}$ = 2.2			72					93 (1.90)	
21*		2	500	18		α_s = 0 $\alpha_{v_{eff}}$ = 0			72					91 (2.47)	92 (2.32)
22		2	2300	4		α_s = 0 $\alpha_{v_{eff}}$ = 1.6			72					100 (2.12)	
22		2	500	4		α_s = 0 $\alpha_{v_{eff}}$ = 0			72					99 (2.35)	
22		3	2300	4		α_s = 0 α_v = .8			72					112 (1.81)	
22		3	500	4		α_s = 0 $\alpha_{v_{eff}}$ = 0	Conical		72					114 (2.12)	
23		2	3300	4		α_s = 0 $\alpha_{v_{eff}}$ = 2.2	conical with throttle		72					102 (1.75)	
23		3	3300	4		α_s = 0 $\alpha_{v_{eff}}$ = 1.0	conical with throttle		72		BB&N			115 (1.53)	
24		2	3300	4		α_s = 0 $\alpha_{v_{eff}}$ = 2.2	conical		72	Full length	Miramar	None	45° ramp	118 (1.91)	
25		2	3300	4		α_s = 0 $\alpha_{v_{eff}}$ = 2.2			48	None		36	stack & baffles	131 & 132 (1.26)(1.49)	133 (1.42)
25		2	2300	4		α_s = 0 $\alpha_{v_{eff}}$ = 1.6			48			36		135 (1.71)	
25	Acoustic	2	500	4	b y_{par} = .45	α_s = 0 α_v = 0	conical		48	None	Miramar	36	stack & baffles	144 & 145 (2.62)(2.62)	134 (2.51)

TABLE 2.0-1. (continued)

Test Series	Type of Test	Nozzle Press. Ratio λ_N	Nozzle Total Temp. T_{T_N} °R	Nozzle Axial Position X_N-in.	Nozzle Lateral Position	Nozzle Deflection α°	Augm. Inlet Config.	Augm. X-Sect. D_A-in.	Augm. Length L_A-in.	Acoustic Lining Location	Acoustic Lining Design	Subsonic Diffuser Length L_D-in.	Exit Acoustic Treatment	P, T & Flow Run No.	Noise Data Run No. (Same as P, T & Flow unless noted)
26	Acoustic	2	3300	4	b y_{par}=.45	α_s=0 $\alpha_{v_{eff}}$=2.2	conical	15.5 x 9 obround	72	Full length	BB&N	None	45° porous ramp	106 (1.96)	105 (1.89)
26		2	2300	4		α_s=0 $\alpha_{v_{eff}}$=1.6			72					104 (2.07)	
26		2	500	4		α_s=0 α_v=0			72		BB&N			103 (2.33)	
26*		2	3300	4		α_s=0 $\alpha_{v_{eff}}$=2.2			72		Miramar		45° porous	119 (1.96)	
26*		2	3300	4		α_s=0 $\alpha_{v_{eff}}$=2.2			72		Hybrid		None	136 (2.11)	
26*		2	500	4		α_s=0 α_v=0			72			None		137 & 141 (2.52) (2.78)	
26*		2	3300	4		α_s=0 $\alpha_{v_{eff}}$=2.2			72			36		139 (2.17)	1/16 mesh 70% open screen at X = 72"
26*		2	500	4		α_s=0 α_v=0			72			36		138 & 140 (2.77)(3.02)	1/16 mesh 70% open screen at X = 72"
26*	Acoustic	2	500	4	b y_{par}=.45	α_s=0 α_v=0	conical	15.5 x 9 obround	72	Full length	Hybrid	36	None	142 (2.78)	1/16 mesh 70% open screen at X = 48"

TOTAL TEST COND.	106
TOTAL TEST POINTS	120

2.0.5 Design-Related Conclusions

Careful study of the aerodynamic/thermodynamic and acoustic test data yielded the following design-related conclusions.

1. By using the aircraft jet exhaust momentum flux directed into an augmenter tube, sufficient secondary air can be pumped to cool the exhaust of an afterburning engine even without a subsonic diffuser on the augmenter exit provided that the augmenter cross-section is adequately large and the flow leaving the augmenter is not restricted.

2. At afterburning jet temperature conditions, the augmenter pumping performance (augmentation ratio) varied little over the range of augmenter length-diameter ratios tested (4 to 8), indicating that the augmenter length can be chosen entirely on the basis of the required noise reduction.

3. The augmenter pumping performance did not vary significantly with jet nozzle pressure ratio, the axial position of the nozzle exit or with augmenter entrance configuration (the 45° conical chamfer type of augmenter inlet used in the Miramar Hush House remains the recommended configuration).

4. At afterburning jet temperatures changing from a hard-walled round augmenter to an absorptive obround augmenter with the same cross-sectional area results in a 10% decrease in pumping.

5. With the obround augmenter, moving the jet nozzle centerline laterally off the augmenter center or deflecting it toward the wall results in decreased pumping and elevated wall temperatures.

6. The addition of a 45° exit ramp (deflector baffle) causes a small reduction in pumping performance.

7. As long as a reasonable distance is maintained between the aircraft exhaust nozzle exit and the augmenter entrance ($X_N/D_{AM} \geq 0.33$), there will be no excess pumpdown of the nozzle base pressure inside the Hush House.

8. The acoustically absorptive augmenter configurations provided greater noise reduction than the one specific vertical stack with parallel baffles configuration investigated.

9. Hush House interior noise levels due to jet exhaust increase significantly if the distance between the jet nozzle exit and augmenter inlet is increased above $X_N/D_{NT} \approx 2.0$, while the exterior exhaust noise levels decrease as this distance increases.

10. Due to the large beneficial flow and temperature gradients which "bend" the rays of sound toward the lined augmenter wall, one can achieve much higher insertion loss then one would predict from simple silencer theory.

11. The exit flow, characterized by its speed and velocity, generates aerodynamic noise (self-noise) which places an upper limit on the actual insertion loss achievable by the exhaust system.

12. The presence of an acoustical lining in the upstream end of the augmenter results in a significant reduction in Hush House interior noise due to jet exhaust.

The primary aim of this report section is to provide information extracted from the model test data in a form which makes it useful for the design of future Hush Houses or makes it possible to predict the performance of an existing Hush House with different aircraft installed. The following parts of this section deal with each aspect of the test results and present graphs which can be used for design. The results are then applied to predict the performance of the NAS Miramar Hush House with the F-14A aircraft. Some simplifications have been made in the form of presentation to reduce the amount of difficult calculation necessary to apply the results.

2.1 Augmenter Pumping Performance

The augmenter pumping performance will be of prime interest in two related areas: predicting maximum augmenter wall temperature with a given combination of aircraft and augmenter cross-section and determining the total Hush House inlet air flow for sizing the air inlet. In Section 7.1, the pumping performance was presented in the form of an augmentation ratio parameter, ARP, (equation 6.2.2)

$$ARP = \frac{\dot{W}_{pumped}}{\dot{W}_N} \times \sqrt{\frac{T_{amb.}}{T_{T_N}} \times \frac{mw_N}{mw_{air}}}$$

$\dot{W}_N$ being the jet nozzle flow rate which corresponds, in full scale, to the aircraft exhaust flow rate, $\dot{W}_{aircraft}$ and T_{T_N} and mw_N being the jet exhaust total temperature and molecular weight. This parameter was chosen because the pressure rise sustainable by an ejector is related to the relative momentum fluxes, $\dot{m}v$, of the driving and secondary flows at the entrance to the mixing section (augmenter). For given expansion ratios, the momentum flux of each flow is proportional to $\dot{w}\,a_o$. Since the speed of sound, a_o, is proportional to $\sqrt{\frac{T_T}{mw}}$, the augmentation ratio parameter is proportional to the ratio of pumped flow momentum flux to jet nozzle flow momentum flux. Calculation of pumped air flow is simple, once this parameter is known for a particular case and we will continue to use it in this section as the basis for predictions. Accordingly, Figures 2.1-1, 2.1-2, 2.1-3, and 2.1-4 have been constructed from the available test data to make possible predictions of pumped air flow and, subsequently, augmenter wall temperature (see Section 2.2).

Figure 2.1-1 presents augmentation ratio parameter versus augmenter cross-sectional area to jet nozzle throat area ratio for a variety of configurations without subsonic diffuser. It is limited to cases where the nozzle is centered in the augmenter and undeflected and where the jet nozzle total temperature and pumped air (ambient) temperature are equal. These curves are based upon data presented in Figures 7.1-1 and 7.1-5. Since the model test data showed no appreciate influence of jet nozzle pressure ratio on augmentation ratio parameter, it can be assumed that these curves are valid for most engines, without regard to nozzle pressure ratio. In Figure 2.1-1, curves are presented for augmenter pressure ratios of both 1.000 and 0.995 (1.000 corresponds to zero Hush House pressure depression, while 0.995 would correspond to roughly 2" H_2O total pressure loss). This figure also shows a small reduction in augmentation ratio parameter due to the addition of the 45° deflector ramp. Such a ramp has been a feature of Hush House designs because it deflects both the flow and the noise upward without unduly penalizing augmenter pumping performance. Any major alterations to this basic configuration would have to be studied carefully to make sure that they didn't increase the augmenter exit backpressure and cause a large reduction in cooling air pumping.

Although Hush House augmenters do not typically require an exit subsonic diffuser for adequate pumping performance, the influence of a subsonic diffuser was obtained from the tests. This is shown in Figure 2.1-2 as the ratio of $ARP_{\text{with diffuser}}/ARP_{\text{w/o diffuser}} = K_{\text{diff}}$. This information would be useful in case a vertical stack with baffles were to be added to an absorptive augmenter to increase noise reduction. Such an addition would tend to increase the augmenter backpressure ($P_{T_{exit}} > P_{amb}$) and reduce pumping. A subsonic

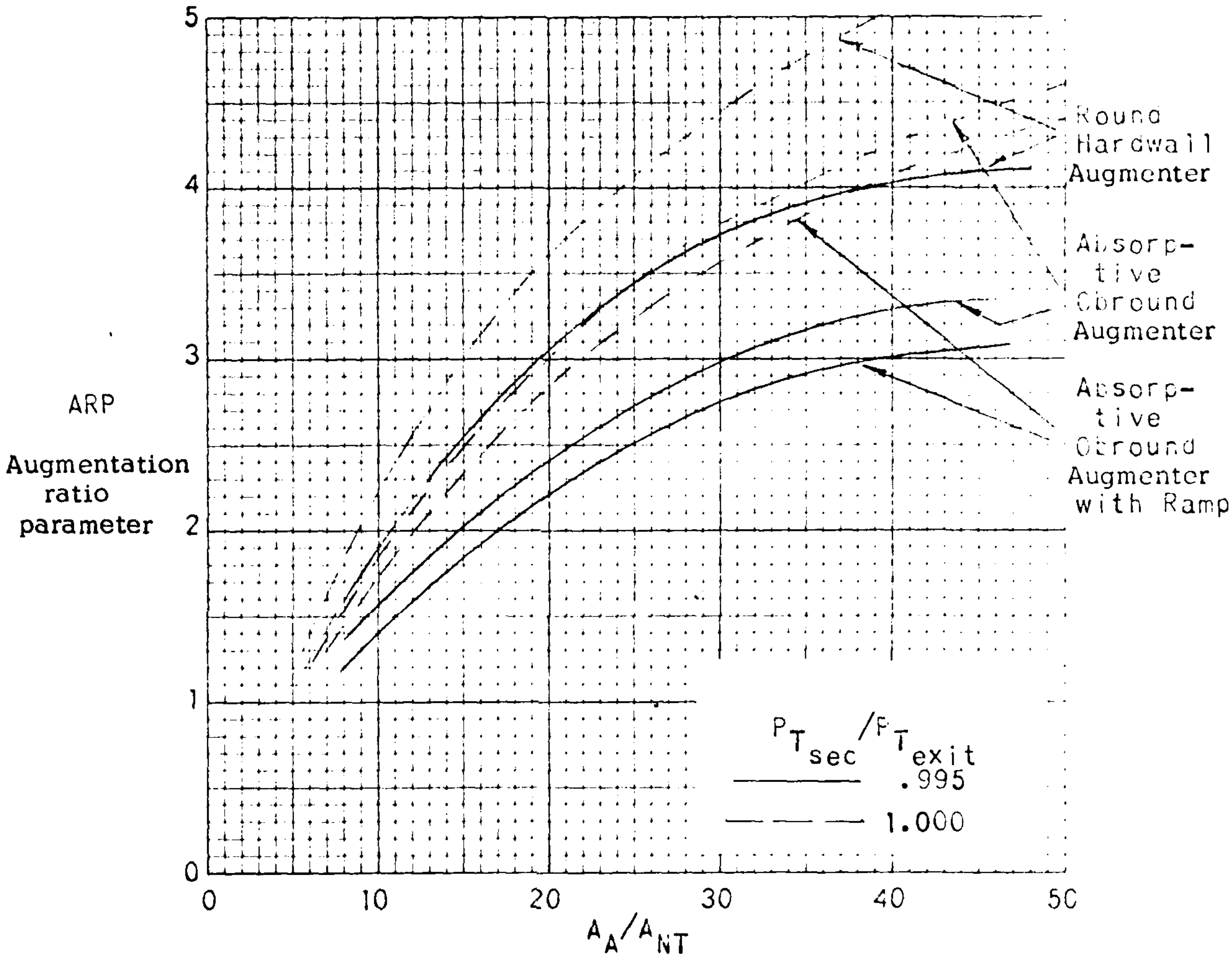

(Augmenter cross-section area/jet nozzle throat area)

$$\text{ARP} = \frac{\dot{W}_{pumped}}{W_N}\sqrt{\frac{T_{amb}}{T_{T_N}} \times \frac{mw_N}{mw_{air}}}$$

FIGURE 2.1-1. AUGMENTER PUMPING PERFORMANCE VERSUS AUGMENTER TO JET NOZZLE THROAT AREA RATIO FOR CASES WITH NO EXIT SUBSONIC DIFFUSER (T_{T_N}/T_{amb} = 1.0, JET CENTERED IN AUGMENTER CROSS SECTION).

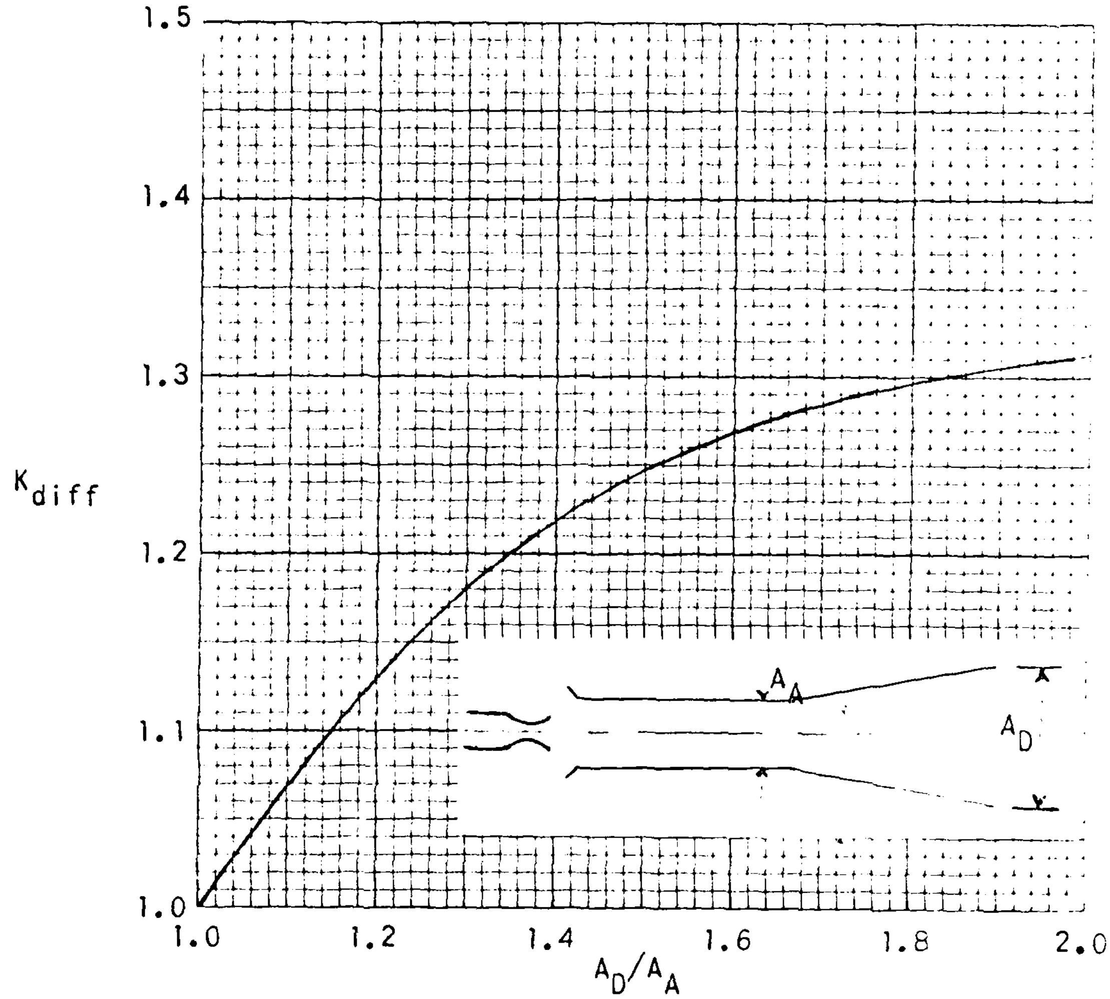

(Subsonic diffuser exit area/augmenter cross-section area)

$$K_{diff} = \frac{ARP_{with\ diffuser}}{ARP_{w/o\ diffuser @ T_{TN}/T_{amb}=1.0}}$$

FIGURE 2.1-2. THE INFLUENCE OF AUGMENTER EXIT SUBSONIC DIFFUSER AREA RATIO ON AUGMENTER PUMPING PERFORMANCE.

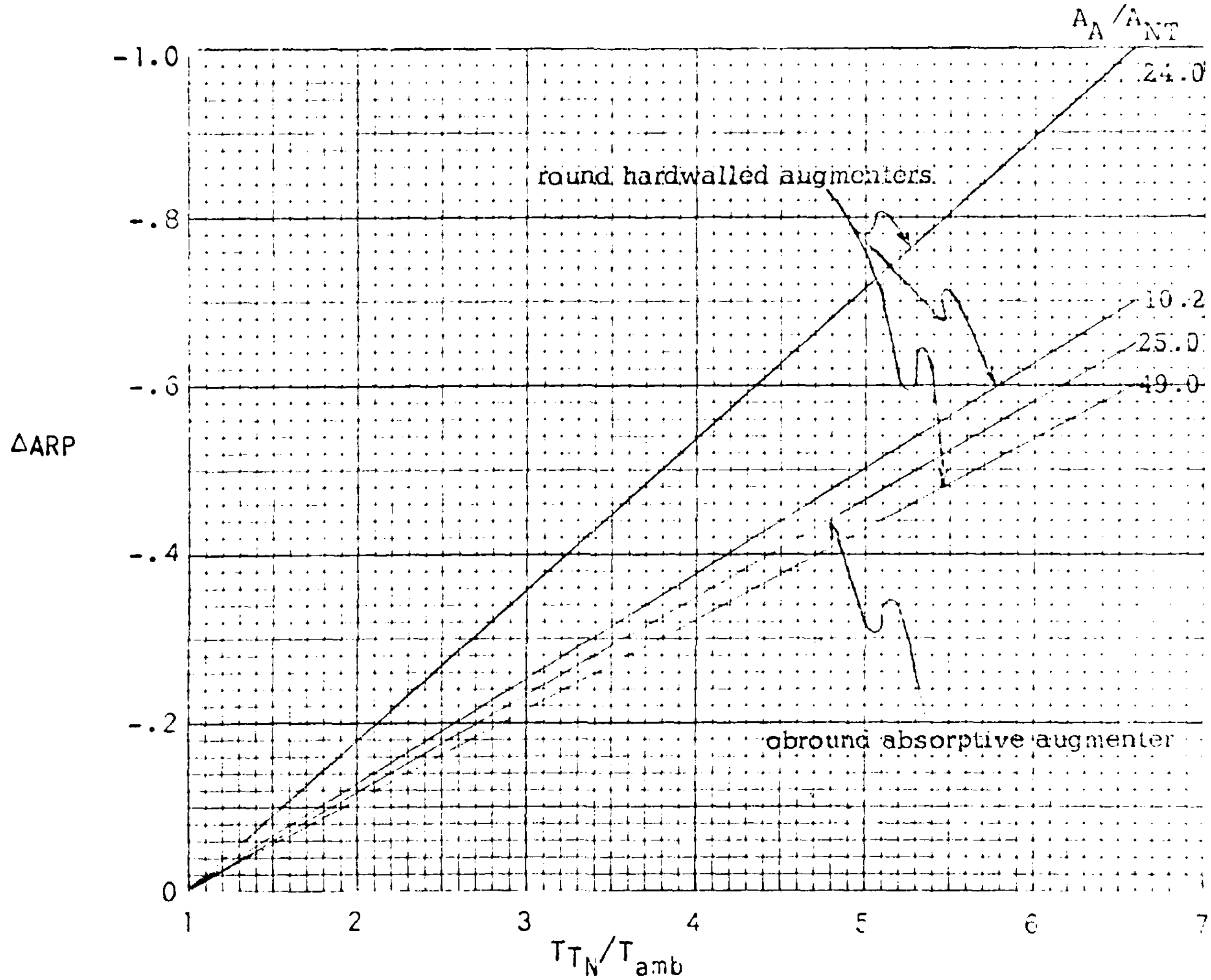

(Jet nozzle total temperature/ambient temperature)

FIGURE 2.1-3. THE INFLUENCE OF JET NOZZLE TO AMBIENT TEMPERATURE RATIO ON AUGMENTER PUMPING PERFORMANCE

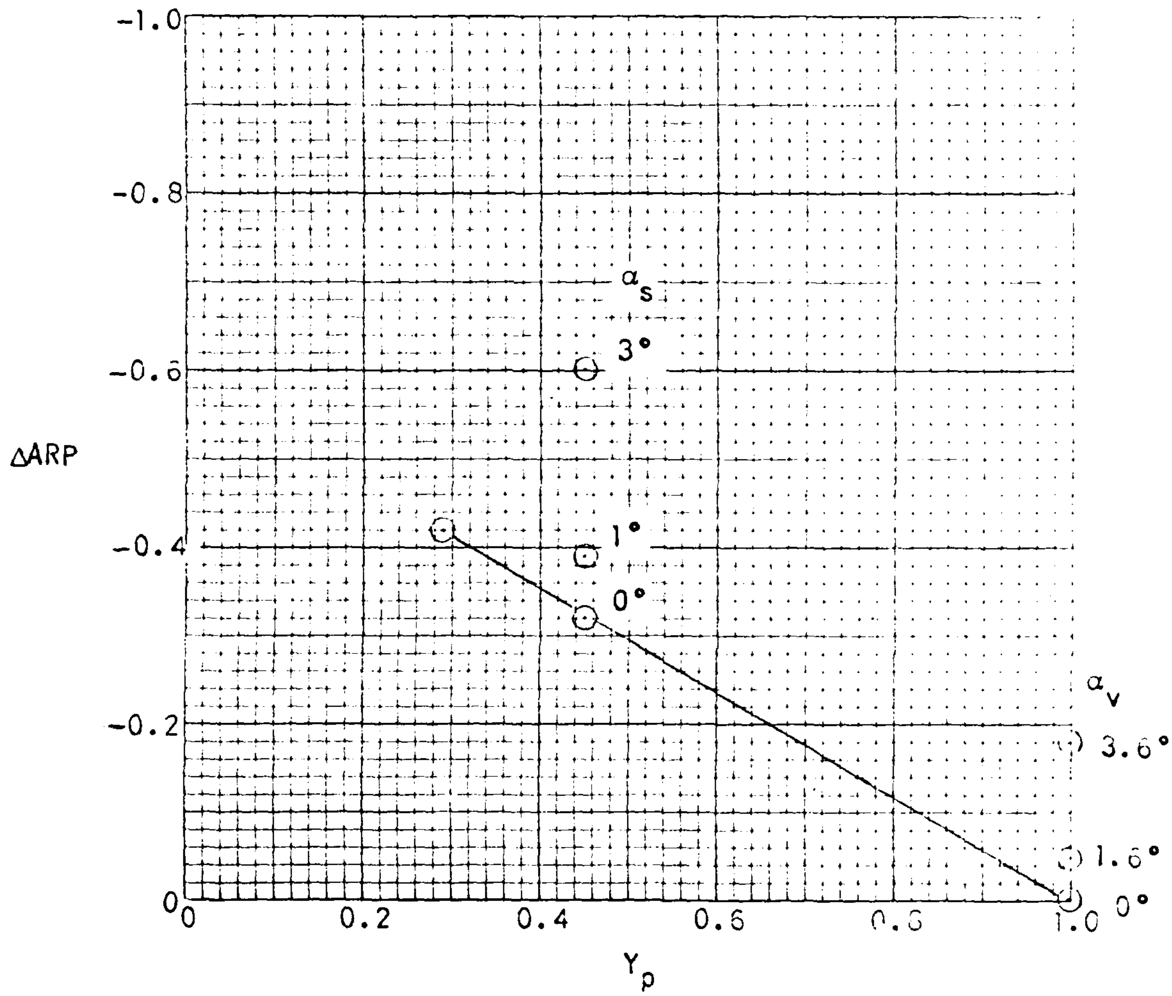

FIGURE 2.1-4. THE INFLUENCE OF JET NOZZLE OFFSET AND DEFLECTION ON AUGMENTER PUMPING PERFORMANCE

diffuser might be required to restore adequate cooling air pumping. To properly estimate the augmentation ratio parameter for a configuration having a diffuser, the correction to Figure 2.1-1 values for the diffuser must be applied before adding the succeeding corrections discussed in the following two paragraphs.

Figure 2.1-3 concerns the same configurations as Figures 2.1-1 and 2.1-2, and provides a correction to the augmentation ratio parameter for jet nozzle total temperature, T_{T_N}, higher than the pumped air temperature, $T_{amb.}$, as it is in every full-scale instance. The model test data run at $T_{T_N}/T_{amb} = 6.6$ correspond almost exactly to an afterburning aircraft run in a Hush House on a 100°F day. Figure 2.1-4 provides an additional correction usable when the jet nozzle is off-center in the augmenter or deflected. It was developed from the model tests run with the obround augmenter. Figure 2.1-3 shows a decrease in augmentation ratio parameter with increasing jet nozzle to ambient temperature ratio. By virtue of the definition of the augmentation ratio parameter, however, the actual augmentation ratio will increase with increasing jet temperature, as illustrated below in Figure 2.1-5 for the case of an obround absorptive augmenter with ramp, $A_A/A_{NT} = 24$, having a centered jet and with $P_{T_{sec}}/P_{T_{exit}} = 0.9975$.

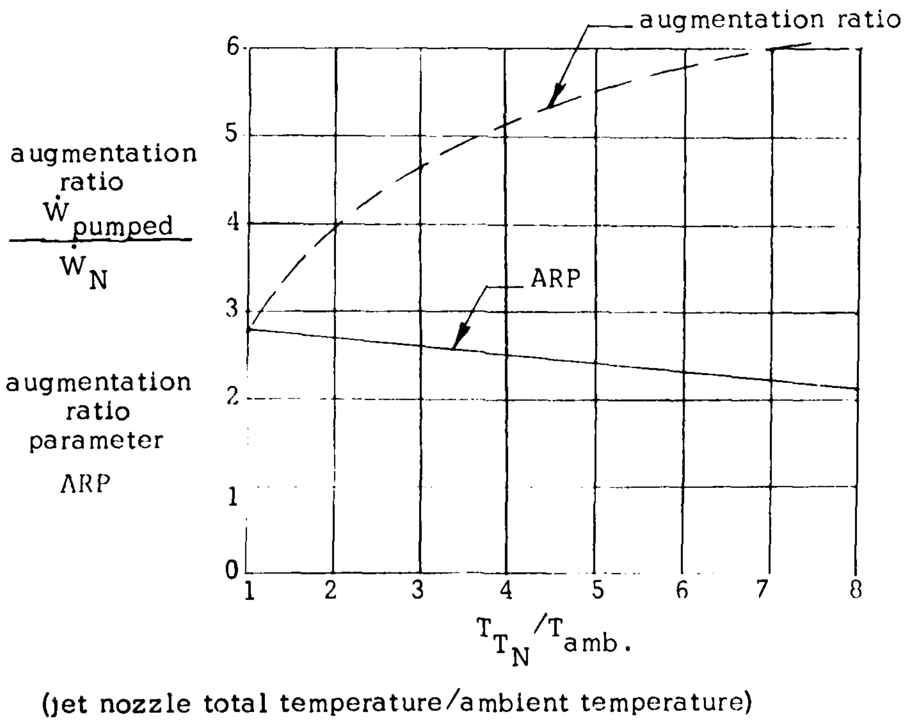

Figure 2.1-5. Augmentation Ratio and Augmentation Ratio Parameter versus Jet Nozzle Stagnation Temperature to Ambient Temperature Ratio

To estimate the augmentation ratio parameter for an arbitrary configuration, the augmentation ratio parameter from Figure 2.1-1 is corrected as follows, using Figures 2.1-2, 2.1-3 and 2.1-4 .

$$ARP = \underset{\text{Fig. 2.1-1}}{ARP} \times \underset{\text{Fig. 2.1-2}}{K_{diff.}} + \underset{\text{Fig. 2.1-3}}{\Delta ARP} + \underset{\text{Fig. 2.1-4}}{\Delta ARP}$$

With the figures provided in this section, along with the inlet total pressure loss versus total Hush House air flow estimated for the NAS Miramar installation, it is possible to estimate the total inlet air flow for the case of the F-14A installed in the NAS Miramar Hush House with one engine in maximum afterburning model (we will assume that the influence of a second idling engine can be neglected). The following engine exhaust characteristics will be assumed for seal level standard conditions.

$\dot{W}_{aircraft} = \dot{W}_N = 250$ pps (aircraft exhaust mass flow rate)

$T_{T_N} = 3700°R$ (exhaust total temperature)

$mw_N = 24$ (exhaust molecular weight)

$A_{NT} = 7.5$ sq. ft. (jet nozzle throat area)

Also, the following information from the full-scale NAS Miramar Hush House design will be extracted and a 100°F day at seal level pressure will be assumed. (Miramar Hush House design estimated total pressure loss through the Hush House air inlet and up to the augmenter entrance is 30% of air flow dynamic pressure through the inlet sounding absorbing baffles where the effective flow area through baffles is assumed to be 285 sq. ft.).

$A_A = 183$ sq. ft. Miramar Hush House augmenter flow area (19' wide x 11' high obround)

$\dot{W}_{inlet}$ pps	$\frac{P_{T_{Hush\ House}}}{P_{amb}}$
2500	.9986
2000	.9984
1500	.9992
1000	.9996

Next, the temperature correction to the engine mass flow rate is made as follows:

$$\dot{W}_{N_{corrected}} = \dot{W}_{N_{std}} \times \sqrt{\frac{T_{amb_{std}}}{T_{amb}}} = 250 \times \sqrt{\frac{520}{560}} = 240 \text{ pps} \quad .$$

From the augmenter and nozzle throat area information, the area ratio, A_A/A_{NT}, is calculated to be 24 and Figure 2.1-1, the augmentation ratio parameter for an obround augmenter having an exit ramp with centered and undeflected engine exhaust can be found for a range of augmenter pressure ratios at $T_{T_N}/T_{amb} = 1.0$.

Figure 2.1-3 can then be used to find a correction to the augmentation parameter of $\Delta ARP = 0.65$ for the jet nozzle to ambient temperature ratio of 6.6. At this point, one further correction, that for jet nozzle (engine exhaust) deflection and offset, must be made to the pumping ratio parameter. For the F-14A, the offset parameter, Y_p, is 0.45 and the deflection α_s equals 1°, giving a correction from Figure 2.1-4 of $\Delta ARP = -0.39$.

$\frac{P_{T_{sec.}}}{P_{amb}} = \frac{P_{T_{sec}}}{P_{T_{exit}}}$	$ARP_{T_{T_N}/T_{amb}} = 1.0$ ctr'd	$ARP_{T_{T_N}/T_{amb}} = 6.6$ ctr'd	ARP_{final} $Y_p = 0.45$ $\alpha_s = 1°$
1.000	3.15	2.50	2.11
.998	2.90	2.25	1.86
.996	2.60	1.95	1.56
.994	2.30	1.65	1.26

With the resulting final ARP value, the pumped air flow rate and total Hush House inlet air flow rate can be calculated for each augmenter pressure ratio case.

$$\dot{W}_{pumped} = \dot{W}_N \times ARP \times \sqrt{\frac{T_{T_N}}{T_{amb}} \times \frac{mw_{amb}}{mw_N}}$$

$$= 240 \times ARP \times \sqrt{\frac{3700 \times 29}{560 \times 24}}$$

$$= 678 \; ARP$$

$$\dot{W}_{inlet} = \dot{W}_{pumped} + \dot{W}_N = 240 + 678 \times ARP$$

$\frac{P_{T_{sec.}}}{P_{T_{exit}}}$	$\dot{W}_{pumped}$ pps	$\dot{W}_{inlet}$ pps
1.000	1451	1692
.998	1273	1513
.996	1058	1298
.994	854	1094

Since the Hush House inlet loss ratio equals the augmenter pressure ratio when $P_{T_{exit}} = P_{amb}$, as in this case, one can plot both the Hush House inlet characteristic and the augmenter pumping performance on the same curve (Figure 2.1-6). The point where the two curves cross will be the operating point for the assumed conditions.

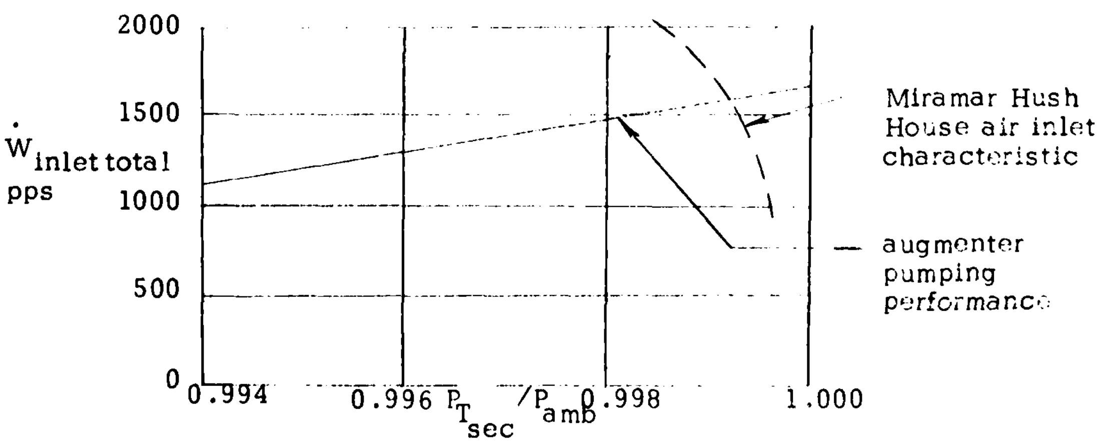

Figure 2.1-6. Total Inlet Flow versus Augmenter Pressure Ratio for the Miramar Hush House

A total inlet air flow of 1580 pps is predicted for the Miramar Hush House under the assumed conditions with an F-14A having one engine operating at maximum afterburning. This corresponds to an augmentation ratio parameter of ARP = 1.97, which is greater than ARP = 1.83 identified in Section 7.1 as being required to limit the mixed exhaust temperature to 800°F.

During the full-scale Miramar Hush House checkout (see Section 8.1), the actual Hush House air mass flow rate was checked against similar predictions of air flow made using the model test data. The predictions fell within 10% of the measured mass flow.

2.2 Maximum Augmenter Wall Temperature

Augmenter wall temperature distributions from the model tests are discussed in Section 7.4 for different jet nozzle offsets and deflections. When the jet is centered in the augmenter and aligned, the high temperature core of the mixing jet is insulated from the augmenter walls by the colder pumped flow. On the other hand, if the jet centerline is moved closer to one wall or is angled toward the wall, there is a tendency for the hot mixing regions to impinge on the augmenter wall. This is illustrated in Figure 2.2-1 below, which shows the relationship between the hot jet centerline temperature and the wall temperature for two nozzle position cases.

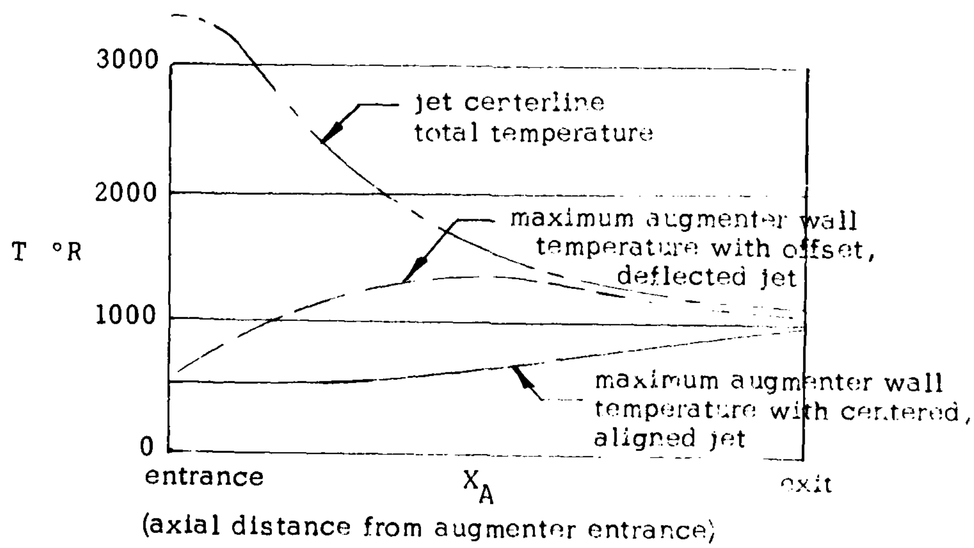

Figure 2.2-1. Relationship between the Jet Temperature and the Augmenter Wall Temperature

Basically, two things determine the maximum wall temperature: (1) the relative amount of ambient air pumped through the augmenter (which determines the mixed average temperature of the jet flow and pumped flow), and (2) the degree of jet exhaust flow impingement on the augmenter wall. Figures 2.2-2, 2.2-3 and 2.2-4 have, therefore, been provided to make possible either the prediction of maximum augmenter wall temperatures for an arbitrary combination of aircraft and augmenter or the design of an augmenter to avoid overheating with a given aircraft. Figure 2.2-2 presents the mixed average temperature parameter as a function of T_{T_N}/T_{amb} and augmentation ratio parameter. Figures 2.2-3 and 2.2-4 give the maximum wall temperature parameter as a function of jet nozzle orientation in relation to the mixed average temperature parameter. To simplify the use of these curves, the mixed temperature and corresponding augmentation ratio parameter are to be determined for the case with the engine exhaust centered in the augmenter and undeflected, giving the resulting form of the presentation

$$\frac{T_{wall\ max_p}}{T_{mix_{p_{\substack{jet\ ctr'd \\ \alpha = 0}}}}}$$

where $T_{wall\ max_p} = \dfrac{T_{wall\ max.} - T_{amb}}{T_{T_N} - T_{amb}}$ (see eqn. 6.4.4 for general definition of temp. param. T_p)

$T_{mix_{p_{\substack{jet\ ctr'd \\ \alpha = 0}}}} = \dfrac{T_{mix} - T_{amb}}{T_{T_N} - T_{amb}}$ (exhaust jet centered and undeflected)

To apply these curves, the applicable curves in Figures 2.1-1, 2.1-2 and 2.1-3 are utilized to get the augmentation ratio parameter for the centered, undeflected exhaust. In design calculations, one will probably assume an augmenter pressure ratio of

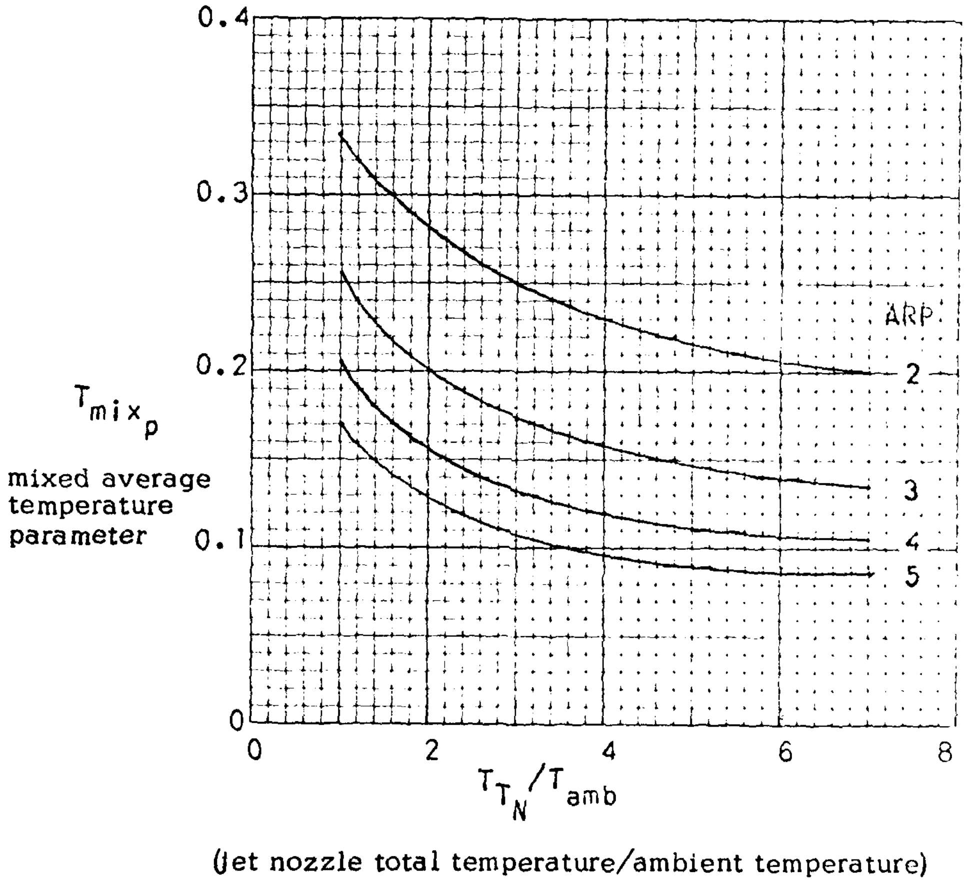

$$T_{mix_p} = \frac{T_{mix} - T_{amb}}{T_{T_N} - T_{amb}}$$

FIGURE 2.2-2. CALCULATED VARIATION OF MIXED AVERAGE TEMPERATURE PARAMETER WITH JET NOZZLE TO AMBIENT TEMPERATURE RATIO AND AUGMENTATION RATIO PARAMETER.

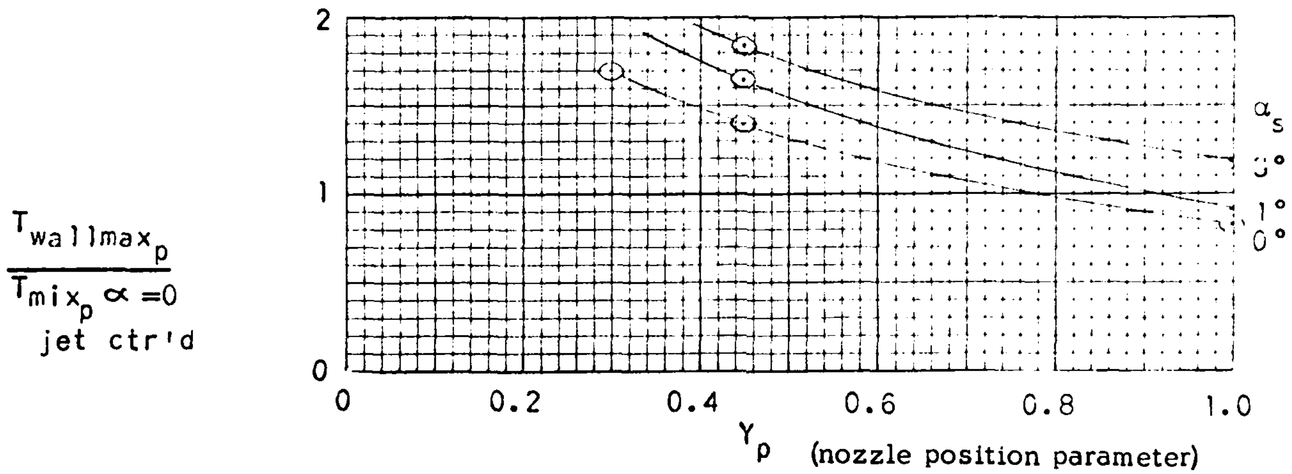

MAXIMUM SIDEWALL TEMPERATURE VARIATION

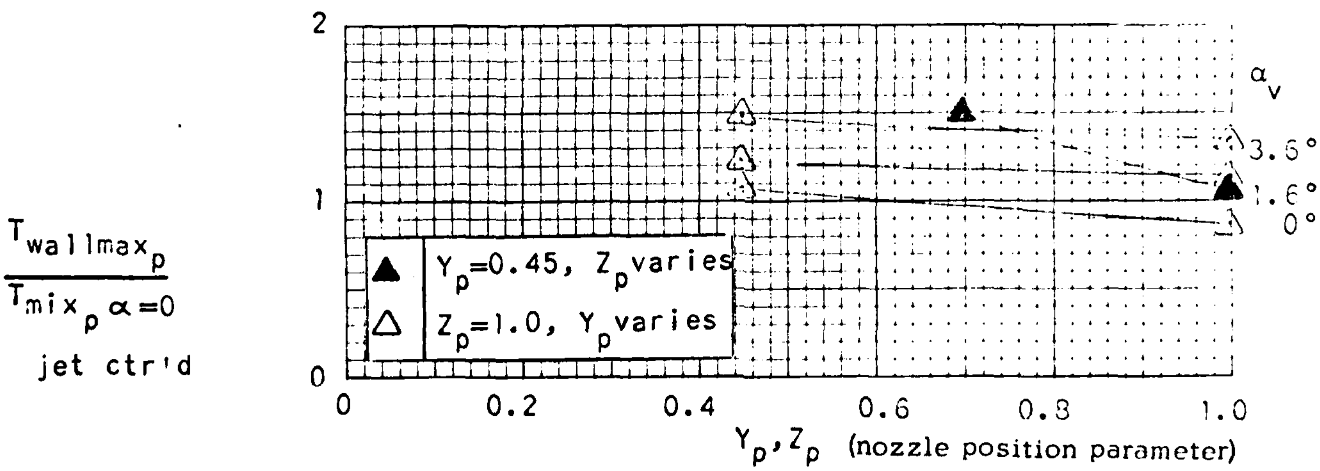

MAXIMUM TOP AND BOTTOM WALL TEMPERATURE VARIATION

Note: Vertical scales defined on Figure 2.2-4

FIGURE 2.2-3. THE VARIATION OF MAXIMUM WALL TEMPERATURE WITH JET NOZZLE LATERAL AND VERTICAL POSITION FOR THE OBROUND AUGMENTER.

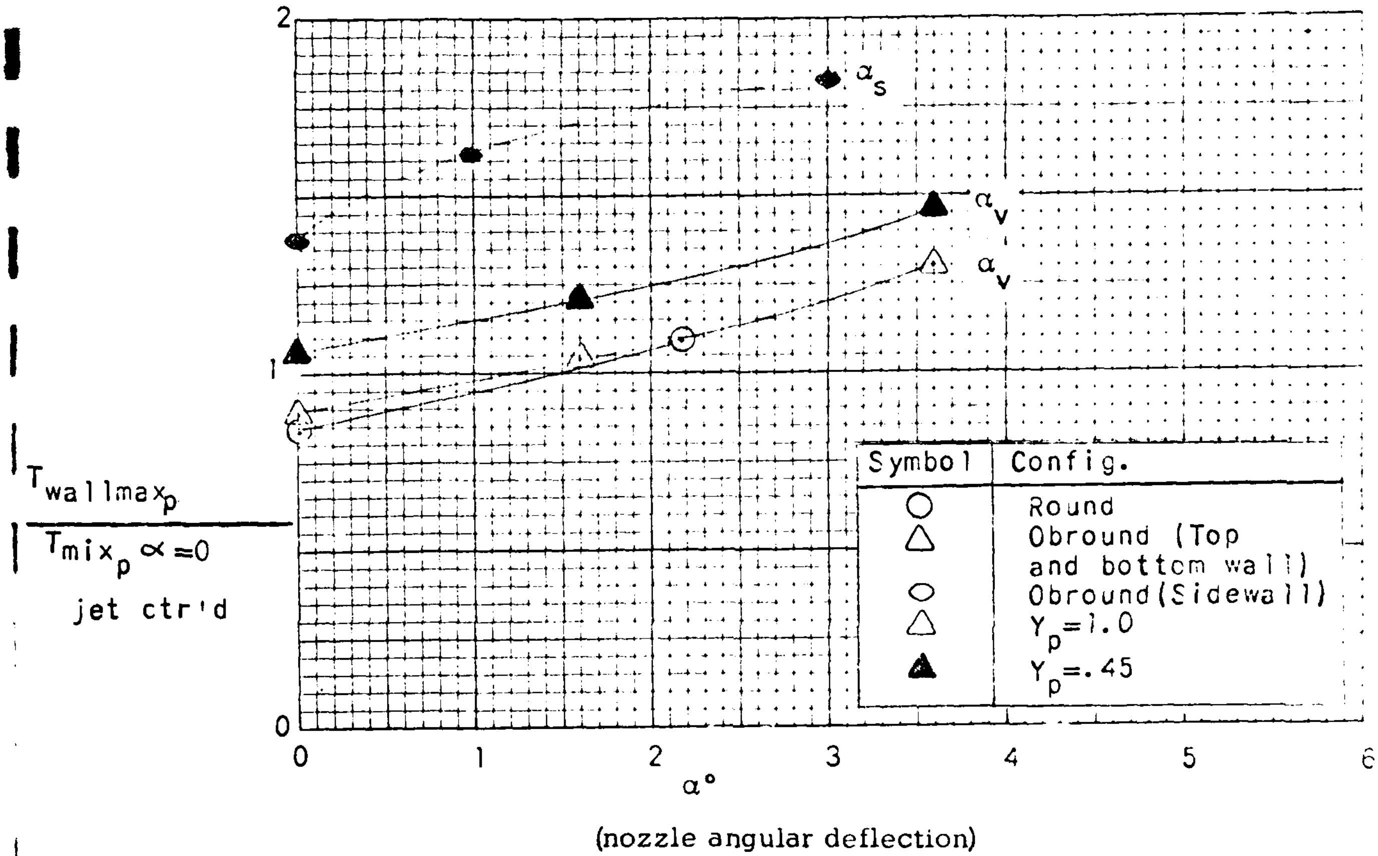

$$\frac{T_{wallmax_p}}{T_{mix_p}\ \alpha=0\ \text{jet ctr'd}} = \frac{\text{maximum wall temperature parameter}}{\text{mixed average temperature parameter for a centered, undeflected jet}}$$

FIGURE 2.2-4. THE VARIATION OF MAXIMUM WALL TEMPERATURE WITH LATERAL AND VERTICAL JET NOZZLE DEFLECTION.

$$\frac{P_{T_{sec.}}}{P_{T_{exit}}} = 0.9975$$

which typically corresponds to a Hush House static pressure depression of 2" H_2O. Next, Figure 2.2-2 is applied to find the mixed temperature parameter, T_{mix_p}. The curves in Figure 2.2-2 were calculated from conservation of energy relationships assuming values of exhaust specific heat which were reasonable at each T_{T_N}/T_{amb} level. Finally, Figures 2.2-3 or 2.2-4 are used to determine the ratio

$$\left.\frac{T_{wall\ max_p}}{T_{mix_p}}\right|_{\substack{jet\ ctr'd \\ \alpha = 0}}$$

from which $T_{wall\ max_p}$ and $T_{wall\ max}$ can be calculated.

These curves will now be applied to the case of the F-14A operating with one engine in maximum afterburning in the NAS Miramar Hush House. From the work done in Section 2.1, it appears that the augmenter pressure ratio will be 0.999. Applying this to Figure 2.1-1 for $A_A/A_{NT} = 24$ with ramp gives

$$ARP_{\substack{ctr'd \\ \alpha=0 \\ T_{T_N}/T_{amb} = 1}} = 2.98$$

which corrects to

$$ARP_{\substack{ctr'd \\ \alpha=0}} = 2.33$$

when $T_{T_N}/T_{amb} = 6.6$ is taken into account. When this is entered in Figure 2.2-2, a mixed temperature parameter for the undeflected, centered jet of $T_{mix_p} = 0.172$ is obtained. Further, using $Y_p = 0.45$ and $\alpha_s = 1°$ describing the configuration with the F-14A, Figure 2.2-3 yields

$$\left. \frac{T_{wall\ max_p}}{T_{mix_p}} \right|_{\substack{jet\ ctr'd \\ \alpha\ =\ 0}} = 1.65$$

This, in turn, provides the final maximum wall temperature parameter, $T_{wall\ max_p} = 1.65 \times 0.172 = 0.284$ and the wall temperature

$$T_{wall\ max_p} = 0.284 = \frac{T_{wall\ max} - 560}{3700 - 560}$$

$$T_{wall\ max} = 1452°R \quad (992°F)$$

The resulting predicted maximum wall temperature of 992°F is much higher than anticipated in the original design. Furthermore, this level was confirmed during the checkout testing on the full-scale Miramar Hush House. This temperature level results from a significant tendency of the offset, deflected jet to impinge on the nearest wall. This can be lowered by design changes which either increase the pumped flow or increase the distance between the engine centerline and the augmenter wall. Increasing the augmenter cross-section will do both of these things. An increase in augmenter width and height of approximately 3 ft. (to 22' x 14') would be needed to lower the maximum wall temperature to 800°F, however, this would reduce the noise reduction effectiveness of a given augmenter length. One might consider the application of air film cooling.

2.3 Data for Acoustical Design

In this section, we present a method for predicting the sound power level (PWL) of exhaust noise (in octave bands) radiated from the augmenter exit of any prospective "Hush House" design. This prediction procedure, which is based on measurements made during scale-model experiments, enables one to estimate

- The octave-band sound power level spectra of jets of various diameters, pressure ratios, and temperatures.
- The differences in radiated sound power level as a function of frequency, among lined augmenter tubes of different lengths, diameters, and lining depths.
- The octave-band sound pressure levels (SPL) of the exhaust noise at various distances from the exit.
- The octave-band sound power levels of interior noise attributable to the exhaust.

The experiments, upon which the prediction method is based, used a BBN-designed scale model of the augmenter lining and oblong cross section. The lining, consisting of a thin porous layer with partitioned airspace behind, was designed to optimize the low-frequency attenuation of the augmenter for the given geometry of the Miramar augmenter. Thus, careful consideration was given to choice of the specific flow resistances of the lining material.

The basic design concept of a lined augmenter to attenuate exhaust noise as depicted in Fig. 2.0-5 is considered to be generally applicable in most situations, where the exhaust noise of the modern-day military jet engines with afterburner must be quieted to meet typical community noise criteria. However, if the noise output or the spectral shape of the engine or the community noise criteria strongly differs from these typical values then a redesign of the liner yielding more effective use of space and materials may be called for.

2.3.1 Prediction of jet sound power level spectra

The PWL spectra of various aircraft are usually available either from the manufacturer or from the environmental noise groups of the aircraft user. If no such data are available, the PWL spectrum of an engine can be estimated using the procedure outlined below. Even when measured full-scale PWL spectra are available, it is recommended that one still use this prediction scheme, compare measured and predicted levels, and, to be conservative, use the higher of these two levels as a design guide.

The octave-band sound power level spectrum of engine exhaust noise is predicted as follows:

1. Calculate from Eq. 2.3.1 the upward shift (PWL_s) of the sound power level spectrum shown in Fig. 2.3.1.

2. Shift the "normalized PWL" curve in Fig. 2.3.1 *vertically* by the dB amount calculated in Step 1.

3. Establish full-scale frequencies by shifting to the right the model-scale frequencies by the factor 0.36 D_N, where D_N is the full-scale nozzle diameter in inches.

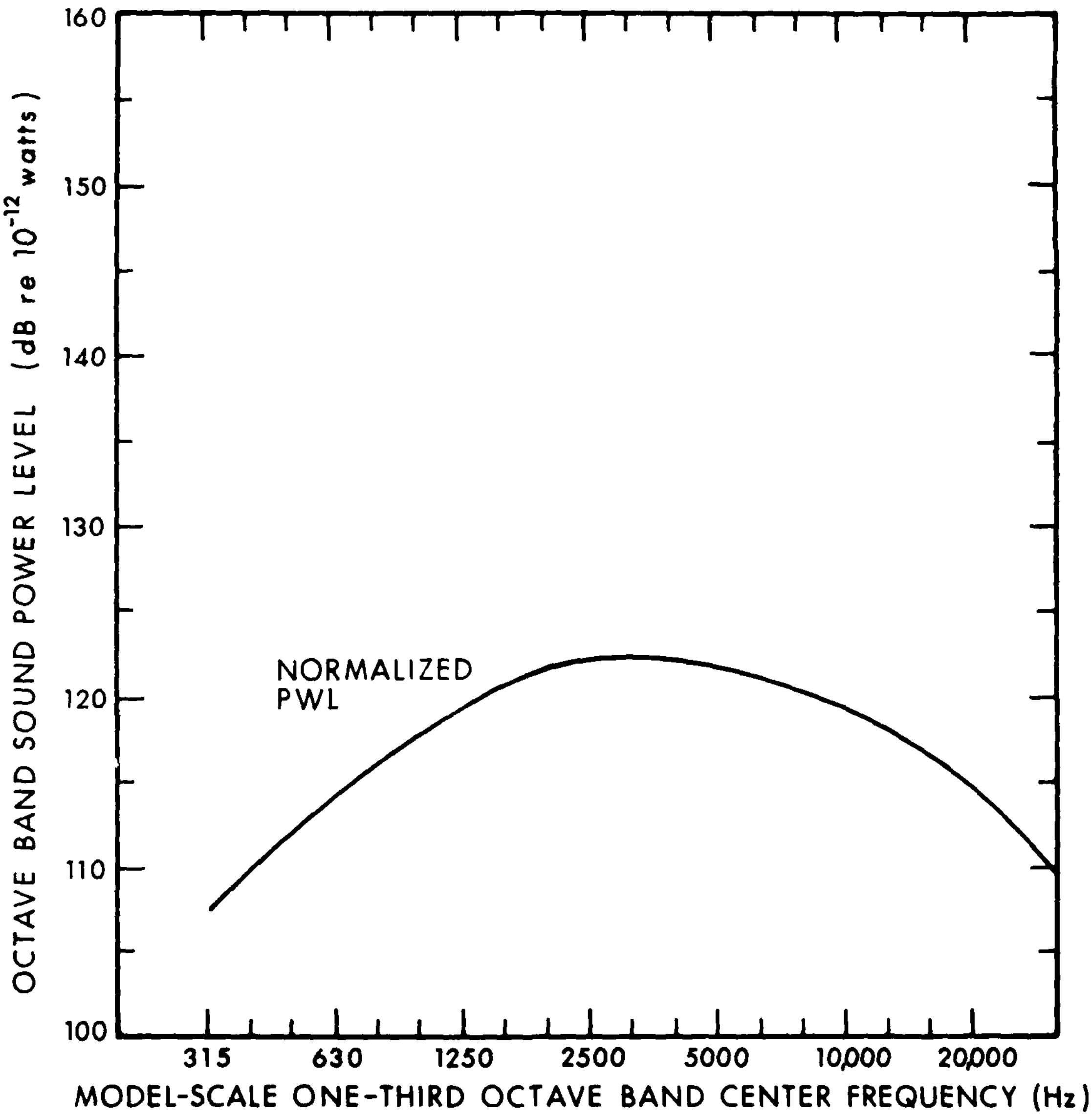

FIG. 2.3.1. NORMALIZED OCTAVE-BAND PWL SPECTRUM TO BE USED WITH EQ. 2.3.1.

$$PWL_S = 20 \log (D_N) + 20 \log (T_{T_N}) + 30 \log (\lambda_N) - 63 \quad , \tag{2.3.1}$$

where T_{T_N} is the jet nozzle total temperature in °Rankin and λ_N is the jet nozzle pressure ratio.

As an example of how to use this procedure, assume a jet characterized by D_N = 41.25 in., T_{T_N} = 3300°R, and λ_N = 2. Equation 2.3.1 yields, for the vertical shift,

$$\begin{aligned} PWL_S &= 20 \log (41.25) + 20 \log (3300) + 30 \log (2) - 63 \\ &= 49 \text{ dB}. \end{aligned}$$

The full-scale frequency scale is obtained by shifting the model-scale frequency scale in Fig. 2.3.1 by the factor 0.36 D_N = 0.36 × 41.25 = 15. Thus, 3000 Hz for the scale model will correspond to 200 Hz for the full-scale jet nozzle.

The prediction procedure, as applied to this example, is illustrated in Fig. 2.3.2, which shows the vertical shift (49 dB) of the normalized PWL curve and the establishment of a full-scale frequency scale (upper abscissa) by shifting the model frequency scale to the right by a factor of 15. The open circles in Fig. 2.3.2 are data points obtained from farfield SPL measurements of an F-14A aircraft operating in its afterburning mode. This spectrum is similar in shape to the predicted one; it is somewhat lower, however, most likely because of a lower jet nozzle total temperature than that used in our prediction.

2.3.2 Augmenter attenuation

Before considering the attenuation characteristics of the lined augmenter, one must first check that the open cross-section is of

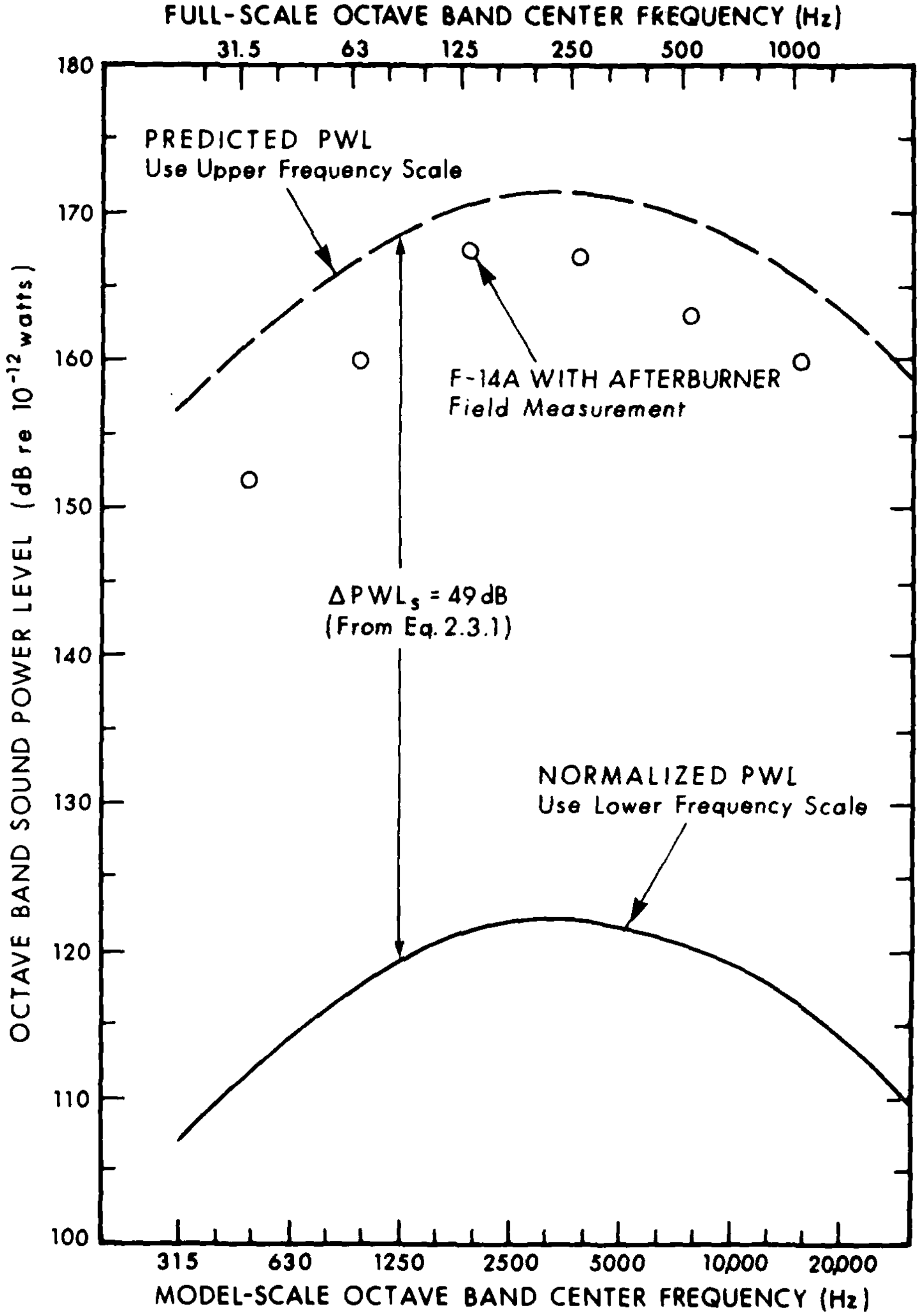

FIG. 2.3.2. PREDICTION OF OCTAVE-BAND PWL SPECTRUM FOR A JET OF D_N = 41 in., T_{T_N} = 3300°R, and λ_N = 3.

sufficient area that the velocity of the exiting flow is minimized to the point where self-noise levels are low enough to meet the noise criteria. We recommend that, until more accurate design information becomes available, the initial cross section be chosen so that the exit velocities listed in Table 2.3.1 are not exceeded. The average exit velocity can be calculated from the total facility mass flow, the mixed average exhaust temperature, and the augmenter cross-sectional area. In listing the maximum velocities, we further assumed that the ratio of maximum to average velocity is 2.4.

TABLE 2.3.1 MAXIMUM PERMISSIBLE EXIT FLOW VELOCITY TO MEET NOISE CRITERIA AT 140 ft FROM THE EXHAUST BOX

Criteria At 140 ft (dBA)	Maximum Permissible Velocity (fps)	
	$V_{mix\ max}$	V_{AV}
75	360	150
80	440	180
85	530	220
90	640	265
95	775	320

The attenuation provided by the augmenter (ΔPWL) depends in a complex manner on a variety of parameters; those considered in this project are discussed in Sec. 7.6.4. Baseline data (ΔPWL_0) are provided in Figs. 2.3.3 and 2.3.4 for a range of pressure ratios (λ_N) and total temperatures (T_{T_N}) covered in the tests. These data were obtained with a single augmenter effective duct diameter of 12.5 in., a duct length of 72 in., a ramp of 45°, and an axial distance (X_N) of 4 in. between the jet nozzle exit and the augmenter entrance. The obround (Miramar) augmenter was used

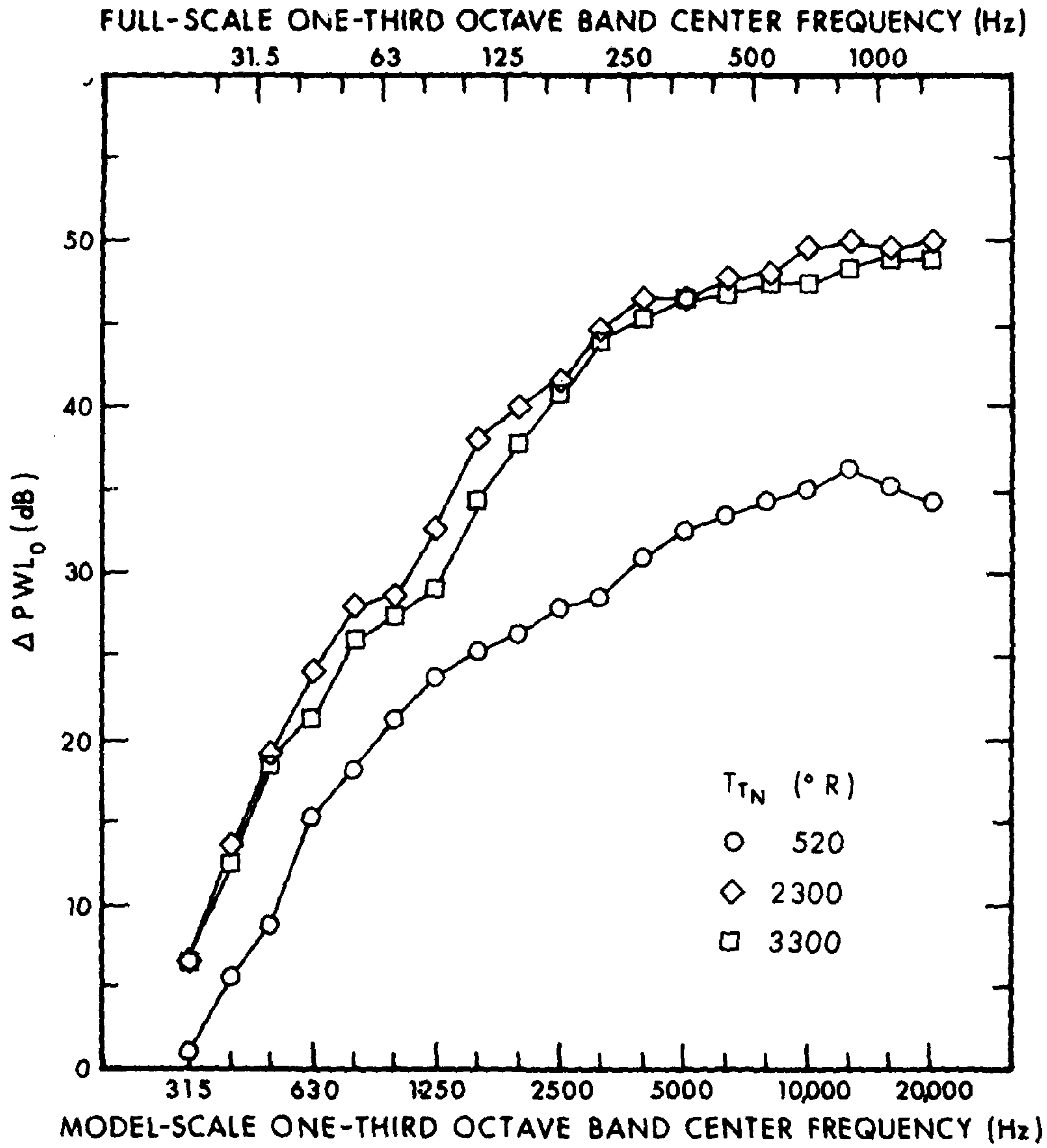

FIG. 2.3.3. ΔPWL FOR 72-in.-LONG BBN AUGMENTER FOR λ_N = 2.

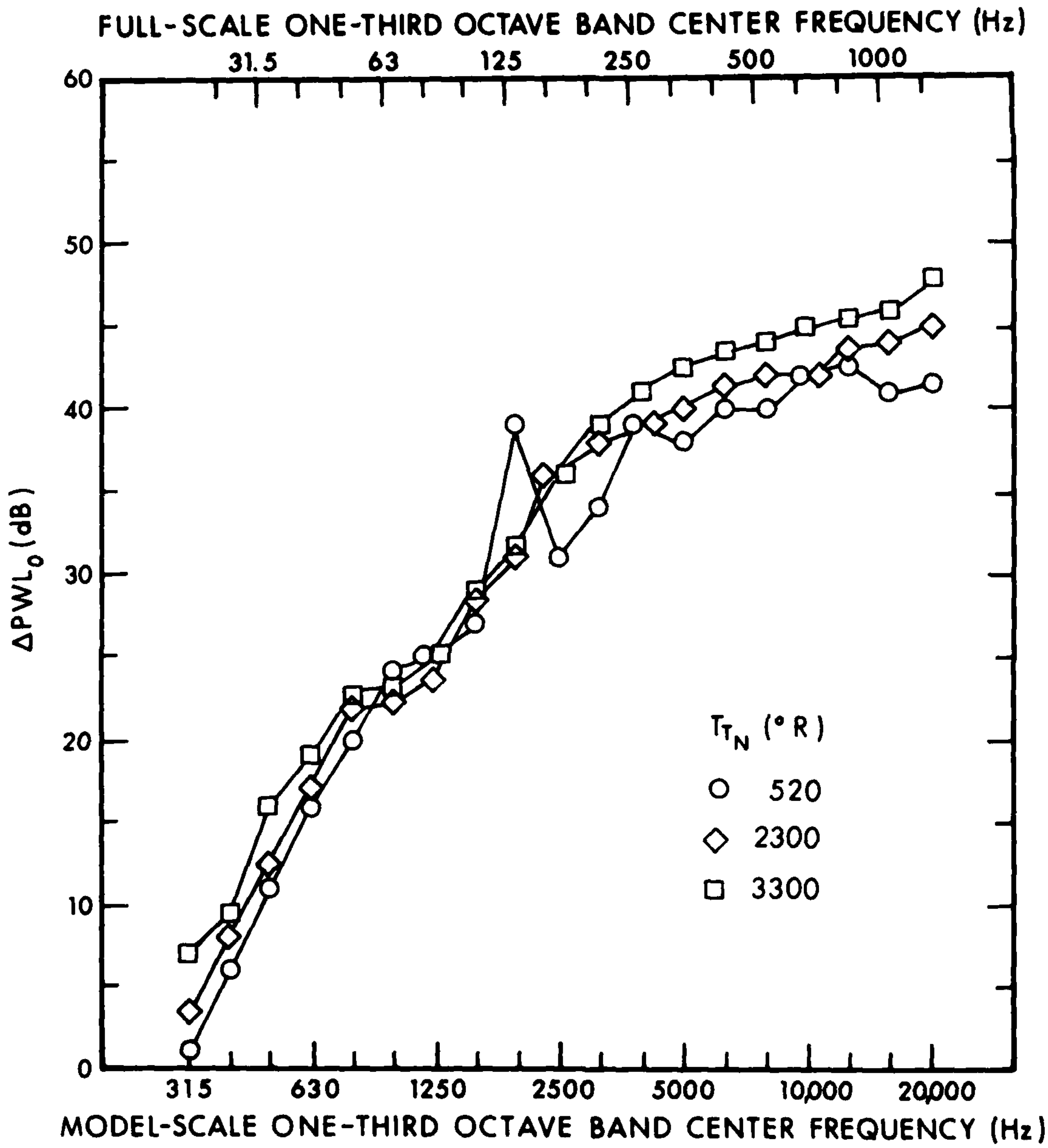

FIG. 2.3.4. ΔPWL_0 FOR 72-in.-LONG BBN AUGMENTER FOR $\lambda_N = 3$.

with the nozzle in the offset F-14 position (Y_p=0.45). To the ΔPWL_0 obtained from Figs. 2.3.3 or 2.3.4, one must add incremental attenuations that account for changes in lined augmenter length (ΔPWL_1), augmenter diameter (ΔPWL_2), axial and radial positions of the engine within the augmenter inlet (ΔPWL_3 and ΔPWL_4), and angular alignment (ΔPWL_5). Methods for estimating these corrections are given below. The final estimate of augmenter attenuation is the sum of the components:

$$\Delta PWL = \Delta PWL_0 + \Delta PWL_1 + \Delta PWL_2 + \Delta PWL_3 + \Delta PWL_4 + \Delta PWL_5 \ . \quad (2.3.2)$$

Augmenter Length

The baseline data (ΔPWL_0) are presented for a model augmenter tube length of 72 in. In Fig. 2.3.5 is shown a correction, ΔPWL_1, to the attenuation provided by the baseline augmenter for dimensionless augmenter lengths of 17.5 and 35.0 – i.e., ratios of augmenter length to nozzle diameter (L_A/D_N). ΔPWL_1 for intermediate lengths can be determined by interpolation.

Augmenter Diameter

All lined augmenter configurations tested had the same cross-sectional dimensions, corresponding in model-scale to the Miramar augmenter. The dimensionless ratio of the equivalent diameter of the augmenter cross section (D_A) and the nozzle diameter (D_N) for all test runs was 4.54. No other augmenter diameters were tested, so the corrections (ΔPWL_2) for augmenter diameter suggested here are based entirely on assumptions guided by theoretical considerations. The analytical models from which they were derived ignored the effects of flow and temperature gradients and so should be used to account only for small variations in the dimensionless effective augmenter length.

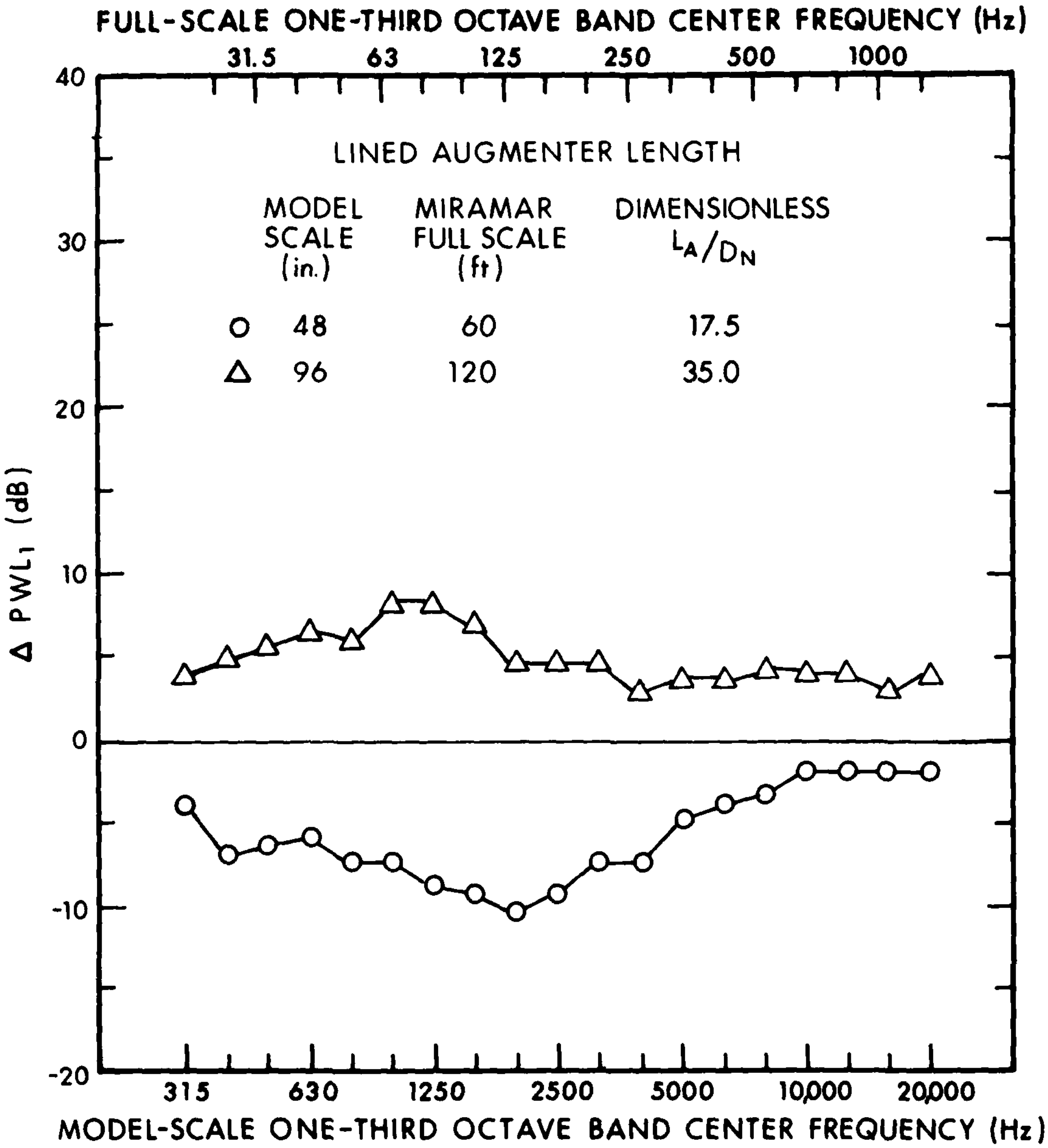

FIG. 2.3.5. CORRECTION TO ΔPWL FOR DIFFERENT AUGMENTER LENGTHS.

At low frequencies, where the wa :length of sound in the augmenter tube is large compared to the tranverse dimensions of the augmenter tube, the correction ΔPWL_2 for a change in the effective diameter of the augmenter is

$$\Delta PWL_2 = \Delta PWL_0 \left(\frac{nD_{AM}}{D_A} - 1 \right) \quad , \tag{2.3.3}$$

where D_{AM} is the effective diameter of the augmenter tube in the model (12 in.) and n is the linear scale factor for the augmenter being designed.

At high frequencies, where the wavelength is smaller than the transverse dimensions of the duct, the correction for the effective diameter of the augmenter tube is

$$\Delta PWL_2 = -10 \log_{10} \left(\frac{D_A}{nD_{AM}} \right) \quad . \tag{2.3.4}$$

A rough estimate of the change in augmenter attenuation with diameter can be synthesized from these two relations by using the first for full-scale frequencies that are less than c/D_A, and the second for full-scale frequencies that are greater than $10c/D_A$. The correction at intermediate frequencies should be faired to provide a smooth progression between these two extreme values.

Nozzle Position

The correction (ΔPWL_3) for three variations in the axial position of the nozzle is presented in Fig. 2.3.6; a correction (ΔPWL_4) for centering the nozzle on the longitudinal axis of the

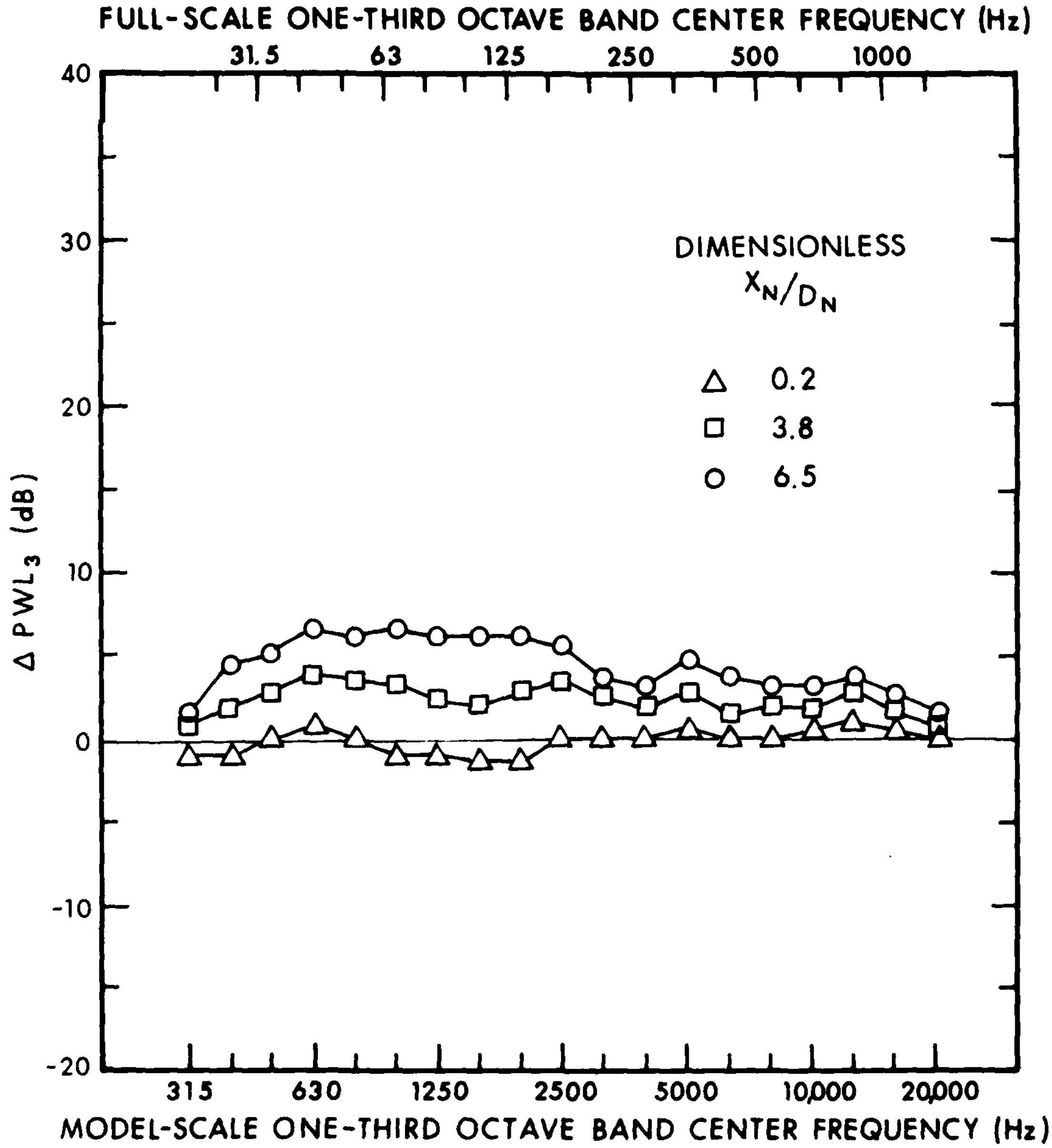

2.3.6. CORRECTION TO ΔPWL FOR DIFFERENT JET NOZZLE AXIAL POSITIONS.

augmenter is provided in Fig. 2.3.7. The corrections for 1° and 3° angular misalignments are given in Table 2.3.2.

TABLE 2.3.2 CORRECTIONS FOR ANGULAR ALIGNMENTS

	Octave-Band Center Frequency (Hz)								
	31	63	125	250	500	1000	2000	4000	8000
ΔPWL_5 for 1°	0	0	0	-1	-2	-2	-2	-2	0
ΔPWL_5 for 3°	0	0	0	-4	-4	-4	-4	-4	0

Choice of Lining

The open cross-sectional area of the augmenter tube must be chosen to satisfy pumping, wall temperature, and self-noise requirements. The capability of the augmenter to attenuate the noise of the engine under test is determined by the type of dissipative lining used and by the length of the lined augmenter. Practically, all linings that provide a high degree of sound absorption in the entire frequency range of interest will yield high sound attenuation. This high absorption coefficient can be achieved either by filling the entire lining depth with a porous sound absorbing material, as illustrated in Fig. 2.0.5, or by concentrating near the augmenter wall a relatively thin layer of porous material backed by an airspace, as shown schematically in the same figure.

The lowest frequency where substantial attenuation is achievable is determined by the total thickness of the lining (including the porous layer and the airspace behind). A reasonable choice is to have the average thickness of the lining correspond to 1/6 wavelength at room temperature for the lowest frequency of interest.

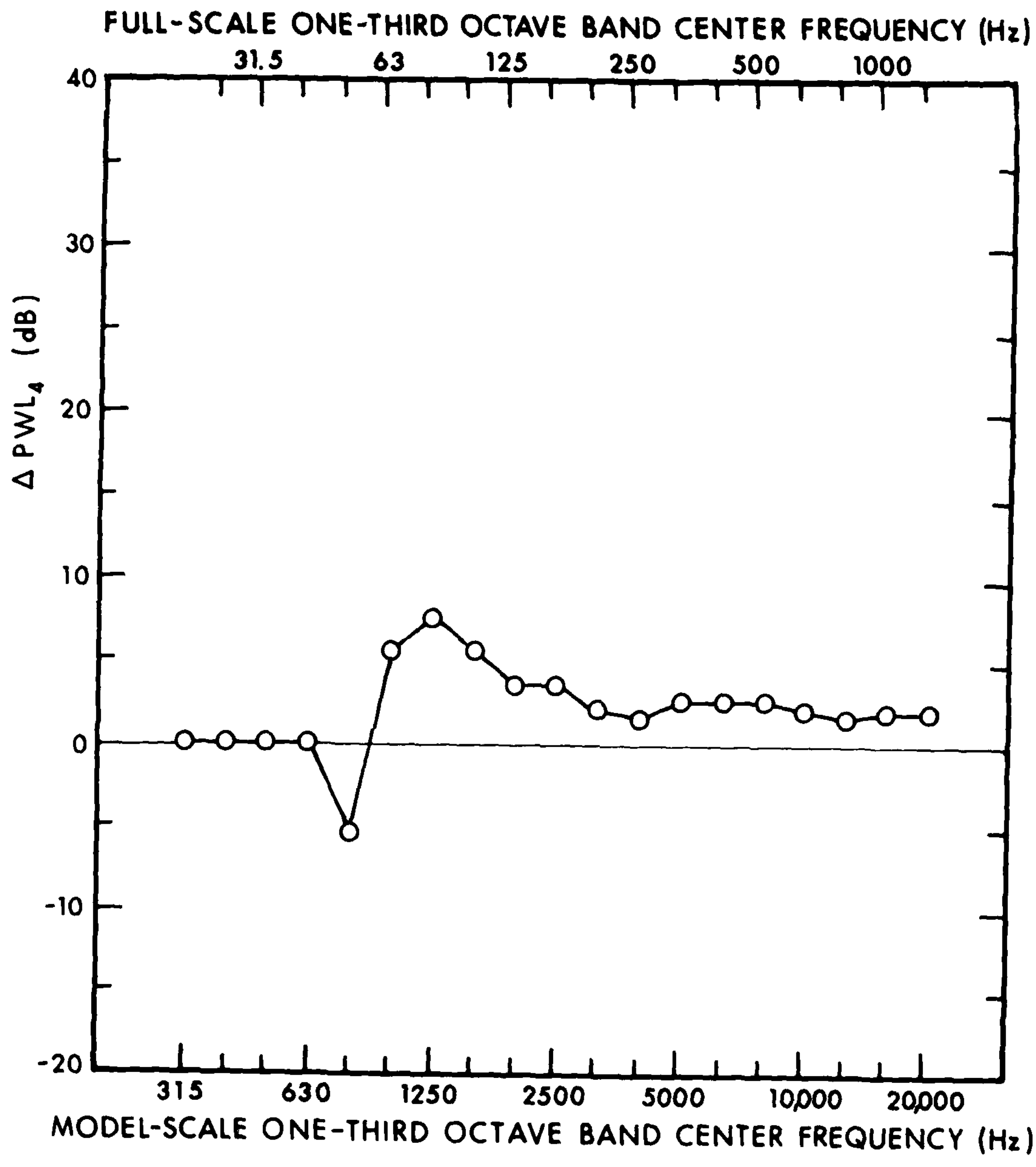

FIG. 2.3.7. CORRECTION TO ΔPWL FOR CENTER POSITION OF JET NOZZLE.

Both the scale-model and the full-scale results indicate that the type of "fully-packed" lining used in the Miramar Hush House can be effective. This full-scale lining consisted of a 6-in.-thick layer of 6 lb/ft^3 density Rockwool with a specific flow resistance of 440 mks rayls/in. (i.e., 1.07 ρc/in.) at room temperature; the remaining airspace was filled with the same material at 3.5 lb/ft^3 density which at room temperature has a specific flow resistance of approximately 200 mks rayls/in. (0.5 ρc/in.).

The thin porous lining backed by an airspace (i.e., the one identified as the BBN lining in the scale-model experiments) may provide better low-frequency attenuation than the "fully packed" lining. As a practical rule, the lining thickness should be between 4 in. and 12 in. and the total flow resistance should be in the range of 1600 to 5000 mks rayls (4 to 12 ρc) at room temperature.

The specific choice of lining materials is dictated by temperature and mechanical stability considerations and by availability. Accordingly, each material which fulfills these requirements and has the above-listed *or up to 50% lower* specific flow resistance can be used.

2.3.3 Estimation of sound pressure level spectra

The exhaust PWL radiated by the augmenter outlet is estimated by subtracting the attenuation (ΔPWL) calculated in accordance with Sec. 2.3.2 from the free-field sound power level of the jet (obtained from experimental data or scaled up from model data by the method of Sec. 2.3.1):

$$PWL_{outlet} = PWL_{free} - \Delta PWL \quad .$$

The octave-band SPL at a distance R from the augmenter outlet is then given by

$$SPL = PWL_{outlet} - 20 \log R + 3 + DI(\phi) \quad , \qquad (2.3.5)$$

where R is the distance (in ft) from the center of the exhaust stack and DI is the directivity correction in (dB) for sound propagation parallel to the ground. The directivity correction as a function of frequency and directivity angle (ϕ) was determined experimentally for the full-scale Miramar exhaust with a 45° exhaust ramp. (See Sec. 8.2.) The angle is defined as being 0° in the downstream direction along the centerline of the exhaust stack, and increasing in the direction of the engine which is running in maximum afterburner. For example, 90° is perpendicular to the augmenter axis and is to the right (looking upstream) if the starboard engine of the F-14A is running and to the left if the port engine is running.

TABLE 2.3.3 DIRECTIVITY OF THE MIRAMAR EXHAUST FOR F-14A WITH ONE ENGINE IN MAXIMUM AFTERBURNER.

Direction	Octave-Band Center Frequency (Hz)									
	31	63	125	250	500	1000	2000	4000	8000	
ϕ = 0°	0	1	2	2	3	2	3	2	3	DI(ϕ), dB
ϕ = 45°	1	1	2	3	4	3	4	3	4	
ϕ = 90°	-1	-1	-1	1	1	1	2	1	1	
ϕ = 270°	-1	-4	-3	-3	-3	-3	-2	-3	-2	
ϕ = 315°	-1	-1	-1	-1	0	-1	-1	-2	-2	

For a practical application of this exhaust noise prediction scheme, the reader is referred to the example calculation carried out in Sec. 2.4.

2.3.4 Prediction of interior noise levels

In addition to the exhaust, other noise sources affect interior noise levels – e.g., engine inlet and casing noise. Thus, we cannot present here a quantitative design of Hush House interior acoustic treatment.

Parameters that affect exhaust SPLs in the interior of a Hush House are

- Jet sound power level
- Jet nozzle position, especially axial distance from the augmenter inlet (Fig. 7.6.14)
- Augmenter lining (Fig. 7.6.15)
- Acoustical absorbing material on walls and ceiling (it is assumed that the floor will be hard)
- Position in the Hush House (i.e., distance and direction from the jet nozzle).

General guidelines for minimizing exhaust noise in the Hush House interior are:

1. Place the jet nozzle as close as possible to the augmenter inlet. (Remember, however, that exterior exhaust noise decreases with increasing X_N.)

2. Treat the bell mouth of the augmenter and the walls around it acoustically to provide sound absorption coefficients very close to unity and mid and high frequencies. (Doing so will provide absorption for the significant acoustic energy radiated by the jet at angles between 20° and 80° forward of the jet axis.)

3. Line the augmenter from the inlet to at least 9 jet diameters downstream of the inlet.

4. Make sure that the lined augmenter has sufficient attenuation that, at all frequencies, the sound returning to the Hush House through reflections from the end of the augmenter tube is low compared to the noise of the free jet propagating forward. (This condition can usually be met if the attenuation of the augmenter tube exceeds 10 dB.)

5. If SPLs in the Hush House must not exceed the levels measured at corresponding locations in free field by more than 2 or 3 dB, line all interior surfaces (except the floor) with sound absorbing material providing, at all frequencies of interest, an absorption coefficient of 98% or better.

2.4 Exhaust Noise Prediction

Using (1) the measured free-field sound power output of the F-14A aircraft operating in its afterburning mode [*A-1*] and (2) the ΔPWL vs frequency curves obtained from our scale-model study and corrected for the 1° angular alignment, we have predicted the octave-band sound pressure level spectra and the A-weighted sound pressure level for various exhaust configurations at the closest point to the augmenter exhaust on the 250-ft radius centered on the aircraft engine exhaust. The calculations are summarized in Tables 2.4.1, 2.4.2, and 2.4.3.. The octave-band exhaust sound pressure levels have been predicted for (1) a full-scale version of the 72-in.-long lined BBN augmenter with a 45° exit ramp, (2) the full-scale Miramar augmenter with a 45° exit ramp, and (3) a full-scale version of the stack-and-baffle configuration using a hard augmenter tube, a subsonic diffuser, and turning vanes.

The predicted levels are plotted in Fig. 2.4.1. This figure also includes, for comparison, a curve of octave-band sound pressure levels, each of which would produce a sound level of 85 dBA. Comparing the octave-band sound pressure levels predicted for the three different exhaust configurations with each other and with the 85-dBA curve, one can conclude that

(1) A full-scale version of the BBN augmenter combined with a 45° exit ramp is expected to meet the 85-dBA criterion at 250 ft for all directions;

(2) The full-scale Miramar Hush House exhaust is expected to meet the 85-dBA criterion at 250 ft for all directions, provided that the attenuated jet noise and not the self-noise controls the exit noise in the 125-Hz and 250-Hz octave bands.

TABLE 2.4.1. CALCULATION OF A-WEIGHTED SOUND LEVEL DUE TO EXHAUST NOISE ON THE 250-FT RADIUS IN THE DOWNSTREAM DIRECTION FOR A FULL-SCALE BBN AUGMENTER.

Description	OCTAVE-BAND CENTER FREQUENCY (Hz)									
	dBA	31.5	63	125	250	500	1000	2000	4000	8000
F-14A PWL*		153	160	168	167	163	160	159	158	157
ΔPWL, BBN Augmenter (scaled from Model Data)		18	27	37	46	47	49	50†	50†	50†
ΔPWL_5		0	0	0	-1	-2	-2	-2	-2	0
Exhaust PWL, Downstream End of Augmenter		135	133	131	112	118	113	111	110	107
Distance Correction = -20 log 140 ft + 3		-40	-40	-40	-40	-40	-40	-40	-40	-40
SPL at 250 ft = PWL -20 log 140 ft + 3		95	93	91	82	78	73	71	70	67
A-Weighting		-40	-26	-16	-9	-3	0	1	1	-1
A-Weighted Octave Band Sound Level at 250 ft		55	67	75	73	75	73	72	71	66
dBA at 250 ft	81‡									

*F-14A sound power level (in dB re 10^{-12} Watt) with starboard engine at 100% rpm, zone 3 afterburner, port engine at idle. Aerospace Medical Research Laboratory Test 73-016-001, Run 03, Wright-Patterson AFB, Ohio.

†Estimated.

‡No adjustment for directivity effects in this calculation.

TABLE 2.4.2. CALCULATION OF A-WEIGHTED SOUND LEVEL DUE TO EXHAUST NOISE ON THE 250-FT RADIUS IN THE DOWNSTREAM DIRECTION FOR THE FULL-SCALE MIRAMAR HUSH HOUSE.

Description	OCTAVE-BAND CENTER FREQUENCY (Hz)									
	dBA	31.5	63	125	250	500	1000	2000	4000	8000
F-14A PWL*		153	160	168	167	163	160	159	158	157
ΔPWL, Miramar Augmenter (scaled from Model Data)		12	26	32	45	49	51	50†	50†	50†
ΔPWL_5		0	0	0	-1	-2	-2	-2	-2	0
Exhaust PWL, Downstream End of Augmenter		141	134	136	123	116	111	111	110	107
Distance Correction = -20 log 140 ft + 3		-40	-40	-40	-40	-40	-40	-40	-40	-40
SPL at 250 ft = PWL -20 log 140 ft + 3		101	94	96	83	76	71	71	70	67
A-Weighting		-40	-26	-16	-9	-3	0	1	1	-1
A-Weighted Octave Band Sound Level at 250 ft		61	68	80	74	73	71	72†	71†	66†
dBA at 250 ft	83‡									

*F-14A sound power level (in dB re 10^{-12} Watt) with starboard engine at 102% rpm, zone 3 afterburner, port engine at idle. Aerospace Medical Research Laboratory Test 73-016-001, Run 03, Wright-Patterson AFB, Ohio.

†Estimated.

‡No credit has been taken for directivity effects in this calculation.

TABLE 2.4.3. CALCULATION OF A-WEIGHTED SOUND LEVEL DUE TO EXHAUST NOISE ON THE 250-FT RADIUS IN THE DOWNSTREAM DIRECTION FOR A FULL-SCALE EXHAUST STACK WITH ACOUSTIC BAFFLES.

Description	OCTAVE-BAND CENTER FREQUENCY (Hz)									
	dBA	31.5	63	125	250	500	1000	2000	4000	8000
F-14A PWL*		153	160	168	167	163	160	159	158	157
ΔPWL, Stack with Baffles (scaled from Model Data)		6	12	17	27	37	48	50[†]	50[†]	50[†]
ΔPWL_5		0	0	0	-1	-2	-2	-2	-2	0
Exhaust PWL from Top of Stack		147	148	151	141	128	114	111	110	107
Distance Correction = -20 log 140 ft + 3		-40	-40	-40	-40	-40	-40	-40	-40	-40
SPL at 250 ft + PWL -20 log 140 ft + 3		107	108	111	101	88	74	71	70	67
Stack Directivity, D.I.		-6	-8	-9	-11	-11	-12	-13	-13	-13
SPL at 250 ft = PWL -20 log 140 ft + 3 + D.I.		101	100	102	90	77	62	58[†]	57[†]	54[†]
A-Weighting		-40	-26	-16	-9	-3	0	1	1	-1
A-Weighted Octave Band Sound Level at 250 ft		61	74	86	81	74	62	59	58	53
dBA at 250 ft	88									

*F-14A sound power level (in dB re 10^{-12} Watt) with starboard engine at 102% rpm, zone 3 afterburner, port engine at idle. Aerospace Medical Research Laboratory Test 73-016-001, Run 03, Wright-Patterson AFB, Ohio.

[†]Estimated.

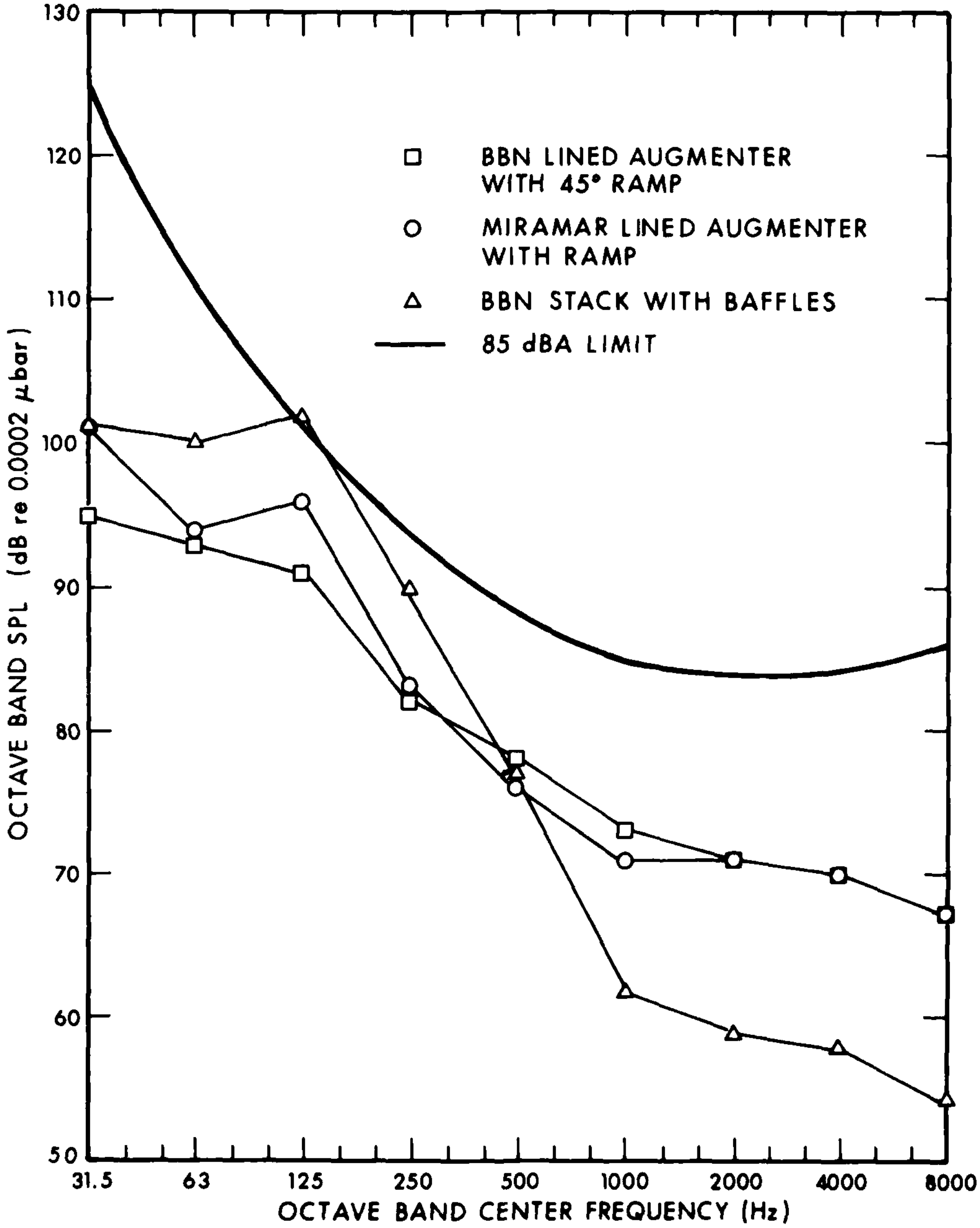

FIG. 2.4.1. PREDICTED SPL AT CLOSEST POINT ON 250-ft RADIUS, F-14A WITH AFTERBURNER COMPARED WITH 85-dBA CURVE.

Should the self-noise control the level in these octave bands, there is the possibility that the 85-dBA level will be exceeded in the downstream direction, because the directivity index of the self-noise in this direction is substantially higher than that of the attenuated jet noise.

As reported in detail in Sec. 8, the acoustical performance of the full-scale Miramar Hush House has been evaluated experimentally by measuring exhaust noise spectra at different distances and at various angles from the exit plane while an F-14A aircraft was operating with one engine in zone 5 afterburner and the other engine was idling. From these data, we have calculated the octave-band sound power level spectrum at 250 ft of exhaust noise emanating from the stack. The spectrum is shown as the solid curve in Fig. 2.4.2; the dotted curve in that figure is the sound power level spectrum predicted (i.e., Line 4 of Table 2.4.2) using the source sound power level spectra of Line 1 in Table 2.4.2 and the augmenter attenuation estimated from our scale-model studies.

Comparison of these two curves shows a satisfactory agreement between the measured and predicted spectra. The largest discrepancy — i.e., the one at 125 Hz — may well be the result of ground reflection effects in the source strength data of Ref. 1. The discrepancy above 2000 Hz is due to our conservative estimation of augmenter attenuation at these high frequencies, which are beyond the upper frequency limit where scale-model data were available. Referring back to Fig. 2.4.1, one can see that these high frequencies do not contribute to the A-weighted exhaust noise.

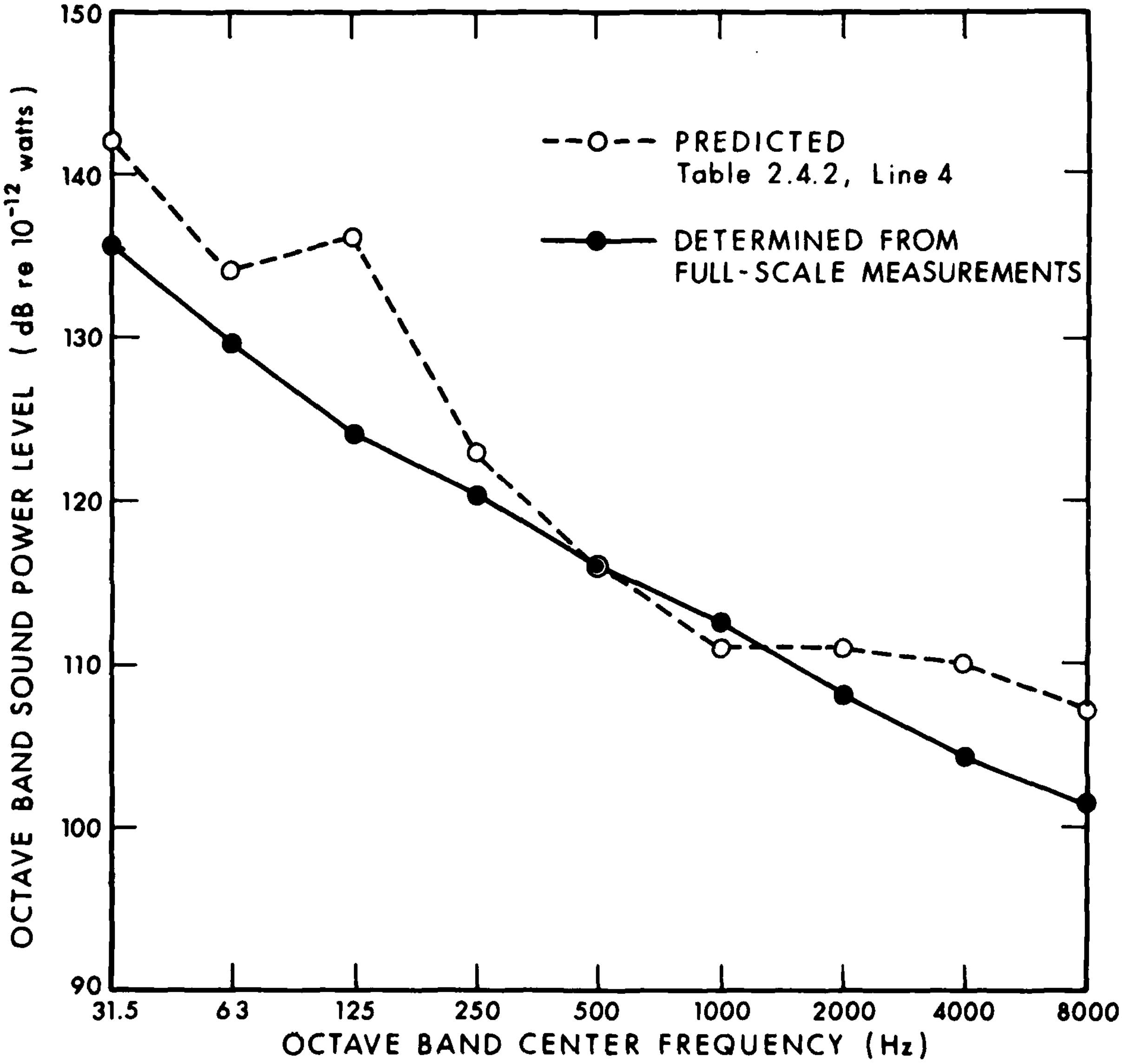

FIG. 2.4.2. PREDICTED AND MEASURED PWL SPECTRA OF THE EXHAUST NOISE FOR THE FULL-SCALE MIRAMAR HUSH HOUSE.

2.5 Augmenter Design Procedure

The application of the data presented in Sections 2.1, 2.2 and 2.3 to the design of a typical sound-absorbing augmenter and Hush House for one or more aircraft and operating situations is a trial-and-error procedure. One must assume augmenter cross-sectional sizes, lengths, etc. and estimate how each assumed design performs in terms of augmenter wall temperature and external noise with one or more aircraft. A block diagram summarizing the augmenter design procedure is presented in Figure 2.5-1.

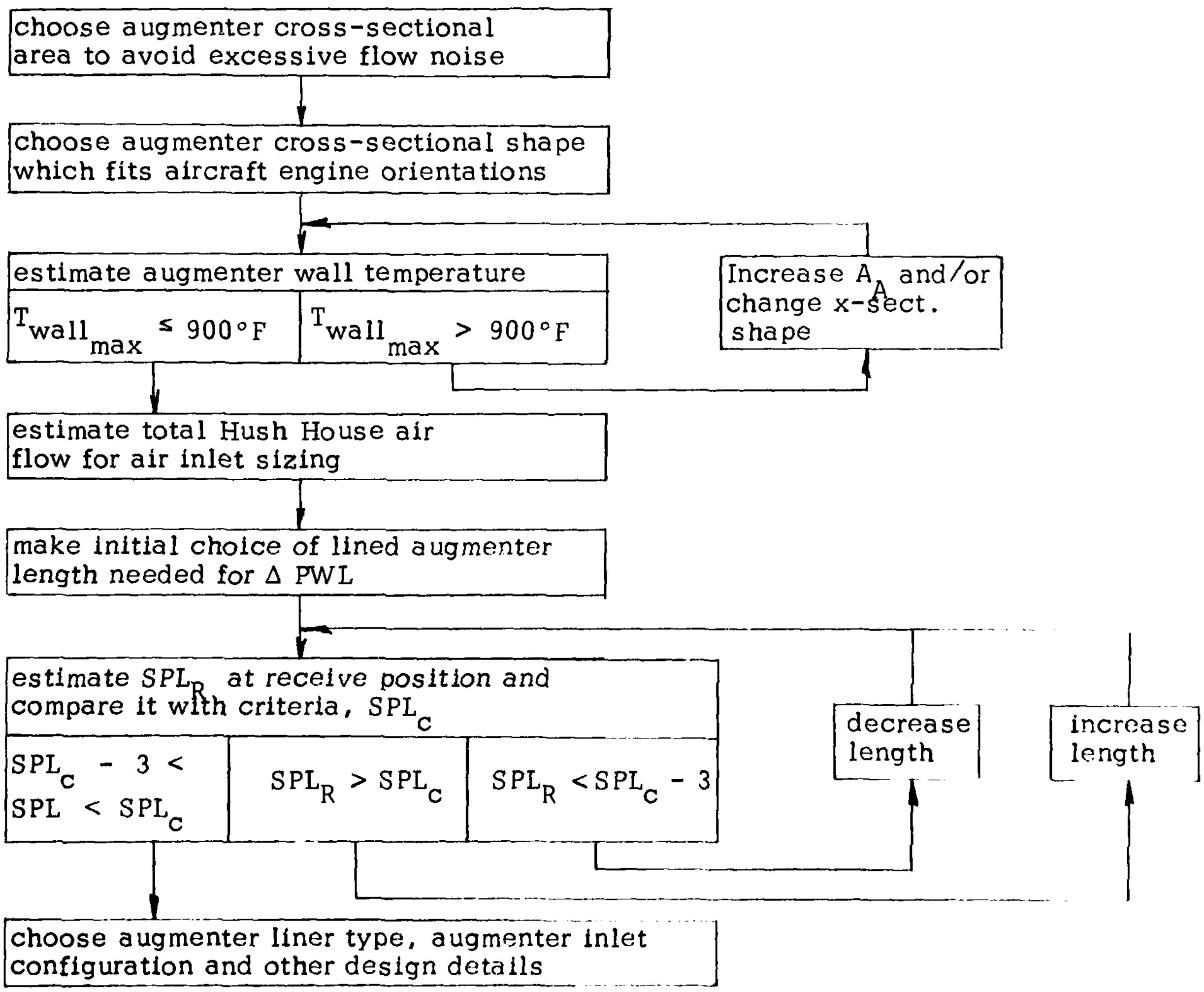

FIGURE 2.5-1. BLOCK DIAGRAM OF AUGMENTER DESIGN PROCEDURE

The first step in the design procedure is to find the augmenter cross-sectional shape of smallest area which will 1) provide a low enough augmenter exit flow velocity so that the noise created by the flow leaving the augmenter is not excessive and 2) avoid excessive wall temperatures ($T_{\text{wall acceptable}} \leq 900°F$).

To keep the noise generated by the augmenter exit flow within acceptable limits in meeting a particular noise requirement, the ratio of augmenter cross-sectional area to maximum jet nozzle throat area must satisfy the criteria listed in Table 2.5-1.

TABLE 2.5-1

Ratio of Augmenter Cross-Sectional Area to Maximum Jet Nozzle Throat Area required to Avoid Excessive Augmenter Exit Flow Noise

Noise Criteria at 250 ft.	One Engine at Max. RPM $A_A/A_{NT} \geq$	Two Engines at Max. RPM $A_A/A_{NT} \geq$
95 dBA	18	16
85 dBA	24	21
75 dBA	30	26

where: A_A is the augmenter cross-sectional area

A_{NT} is the jet nozzle throat area neglecting the throat area of idling engines

After determining the minimum augmenter cross-sectional area which will satisfy the flow noise requirement, an augmenter cross-sectional shape which best suits the various aircraft engine placements should be selected and various cross-sectional sizes having areas equal to or greater than the noise related minimum should be assumed. Figures 2.1-1, 2.1-3, 2.2-2, 2.2-3 and 2.2-4 should then be applied as discussed in Section 2.2 to estimate the maximum augmenter wall temperature for each augmenter cross-section size with the aircraft configuration and engine power setting identified as most critical from an augmenter wall temperature standpoint (if one aircraft type to be accommodated had offset or deflected afterburning engines, such as the F-14, it would be the likely aircraft to assume in calculating the augmenter wall temperature). From the results of these wall temperature calculations, it will be possible to select the augmenter cross-section of smallest area with which both the noise and wall temperature limitation can be met.

After the augmenter cross-section has been sized, Figures 2.1-1, 2.1-3 and 2.1-4 can be applied to determine the maximum air flow rate through the Hush House for air inlet sizing. The critical aircraft and engine operating conditions, with respect to maximum air flow, may be different from that for sizing the augmenter. In the case of a Hush House for the F-14A, one engine operating in maximum afterburning sizes the augmenter cross-section, but two engines operating in maximum non-A/B generate the largest air flow.

The final step in the augmenter design procedure is to determine the absorptive augmenter length required to meet the external noise criteria. This requires the application of known or estimated aircraft noise data, along with the data presented in Section 2.3 and the desired external noise specification. Again, the critical aircraft and/or operating condition from a noise standpoint could conceivably be different from those which sized the augmenter cross-section or gave the maximum Hush House inlet air flow. In determining the augmenter noise reduction required to meet the external noise specification, it is, of course, necessary to remember that the augmenter exit noise is only one noise source; others being noise escaping through the Hush House air inlet and that transmitted through the walls.

Special consideration may have to be given to the sizing of the augmenter entrance or to the incorporation of suitable entrance baffles when designing to accommodate aircraft with unusual jet nozzle orientations. The A-6 is an example of such an aircraft. It has a distance between jet exhaust nozzle centers of 7 ft. and a lateral outward jet deflection of 6°, plus a long-distance between the nozzle exits and the tail. Thus, capture of the exhaust jets is difficult. Since this aircraft has non-afterburning engines, augmenter wall heating is not a problem and the basic augmenter cross-section would not ordinarily be sized for this aircraft if it is only one of a group being adapted.

3.0 FACILITY DESCRIPTION

As mentioned in Section 2.0, the test facility consisted of two reverberant rooms separated by a sound insulating wall through which the augmenter projected in most tests. One of these rooms, referred to as the burner enclosure, corresponded to the Hush House interior; the other, the exhaust enclosure, corresponded to the out-of-doors. Figures 3.0-1 and 3.0-2 are a plan view and elevation view, respectively, showing the relationship between these two rooms. The volume of the burner room was approximately 1630 cu. ft. and that of the exhaust room, 5460 cu. ft.

In order to eliminate significant flanking noise sources, insure good reverberation characteristics at frequencies up to 20,000 Hz and contain all of the significant noise, these rooms had to be properly sized and their walls, including the separating wall, carefully designed and constructed. With jet and meter flow velocity information supplied by FluiDyne, BB&N made estimates of the various primary and secondary source noise levels and specified acceptable wall surface treatment and wall construction and insulation procedures needed to insure that the principal noise being measured was not masked by some flanking noise and could be measured accurately. As a result of their design inputs, the walls were constructed with plywood surfaces and these surfaces, in both the burner enclosure and exhaust enclosure, were painted with a primer and epoxy paint and the joints between sheets of plywood were sealed to avoid leaks which would reduce both the sound transmission loss and the achievable reverberation time. The wall and roof surfaces of both enclosures were supported on 2x6 framing. The burner enclosure had plywood both inside and outside of the framing and a 4" thick insulating fiberglass fill to reduce sound transmission. The exhaust enclosure walls had only the interior plywood surface, while its roof had plywood on both sides for structural purposes. The separating wall, which formed the upstream wall of the exhaust enclosure, was similar to the burner enclosure walls, except where it formed the interface between the burner enclosure and exhaust enclosure. Since this area was critical from a sound transmission standpoint, a third plywood barrier was installed on the burner enclosure side and the 1" space between it and the basic wall was filled with fiberglass. This surface was structurally isolated from the basic wall to minimize noise transmission. In addition, all corners in the burner enclosure were carefully caulked. Acoustically sealed access doors were placed in the burner enclosure and the separating wall. BB&N also considered the reverberation characteristics of the exhaust enclosure in determining an acceptable size for the exhaust ports and vents in the exhaust enclosure.

Figures 3.0-3 and 3.0-4 contain photos showing general views of the burner and exhaust enclosures, as well as photographs of the principal facility instrumentation installed in each. Microphones having a traverse length of 6 ft. were placed in both enclosures. Data from these microphones were recorded simultaneously using a precision multi-track tape recorder. Figure 3.0-3 also contains a view of the secondary (pumped) flow meter. Design of the burner enclosure to be acoustically tight essentially insured air tightness as well. All of the air pumped by the ejector action of the model jet nozzle was metered by this installation. The augmenter total pressure ratio, $P_{T_{sec}}/P_{T_{exit}}$, was varied during the test program by varying the length of subsonic diffuser on the secondary flow meter. Secondary flow meter instrumentation included secondary air meter inlet total pressure, total temperature and throat static pressure. Burner enclosure (Hush House interior) pressure and temperature (ambient temperature) and exhaust enclosure (ambient) pressure and temperature were also recorded. These all appear in Figure 3.0-2.

FLUIDYNE ENGINEERING CORPORATION

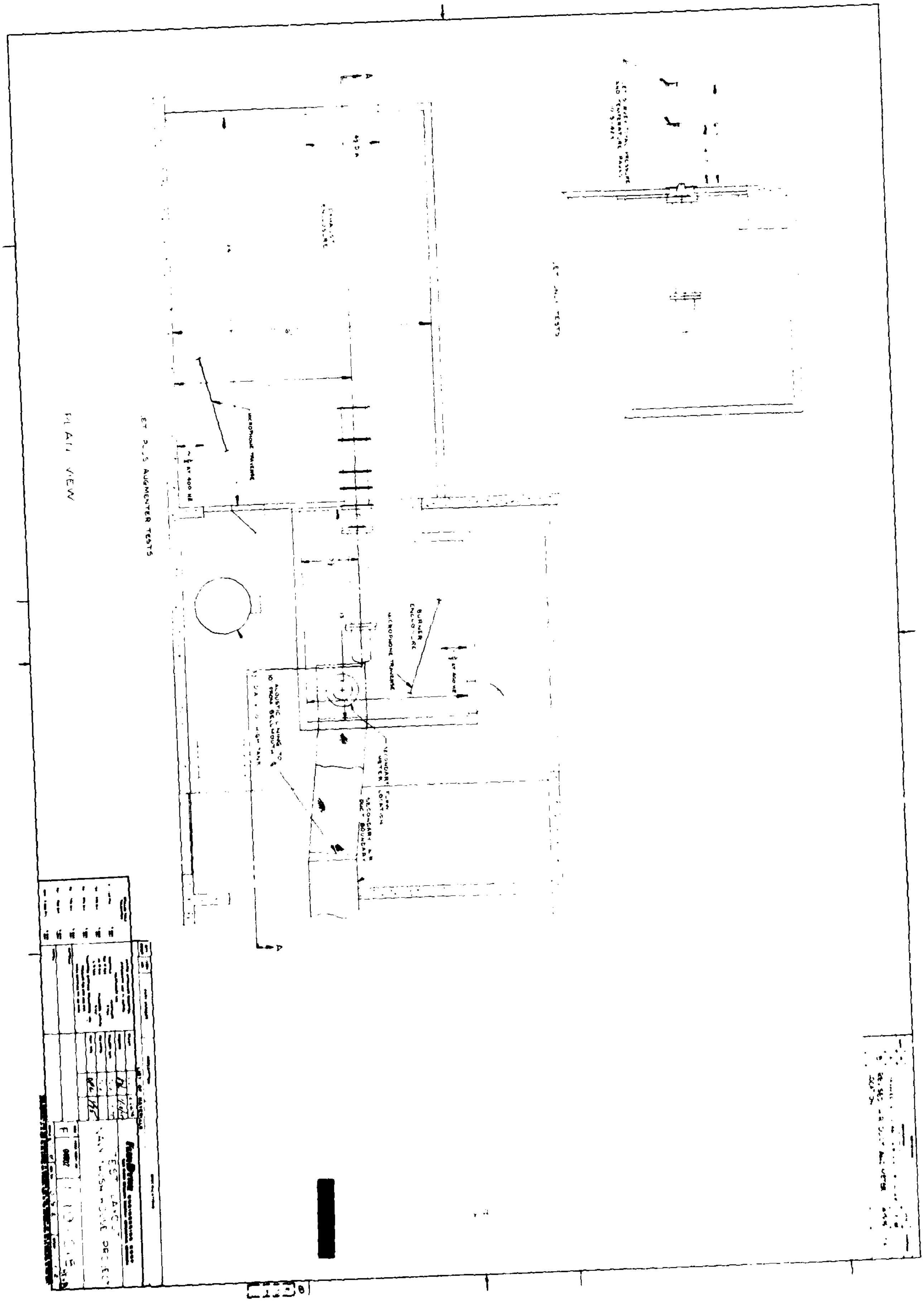

FIGURE 3.0-1 OVERALL TEST LAYOUT - PLAN VIEW

AD-A109 848 FLUIDYNE ENGINEERING CORP MINNEAPOLIS MINN F/G 14/2
AERODYNAMIC AND ACOUSTIC TESTS OF A 1/15 SCALE MODEL DRY COOLED--ETC(U)
OCT 75 J L GRUNNET, I L VER, G GETTER N62467-74-C-0490

UNCLASSIFIED NL

2 OF 4
AD A
109848

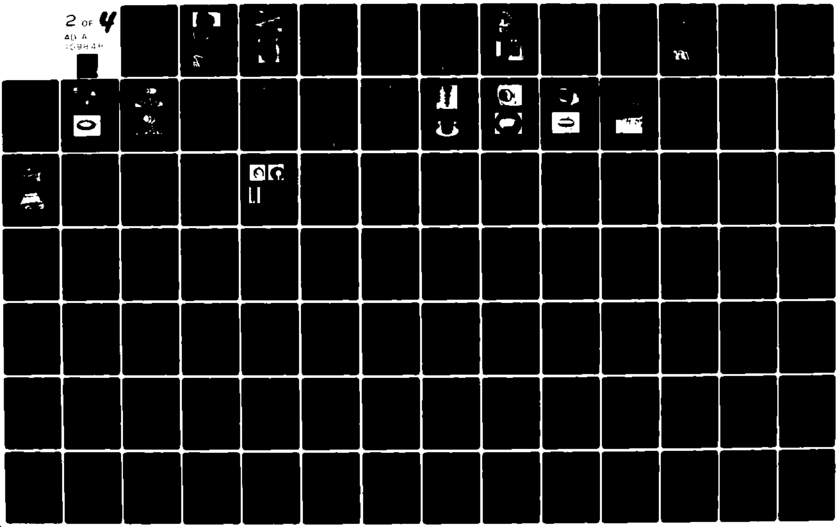

2 OF 4

AD A

09848

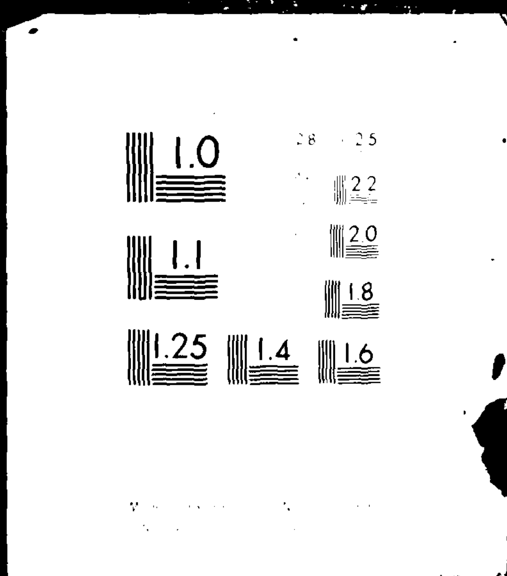

FluiDyne ENGINEERING CORPORATION

FLUIDYNE ENGINEERING CORPORATION

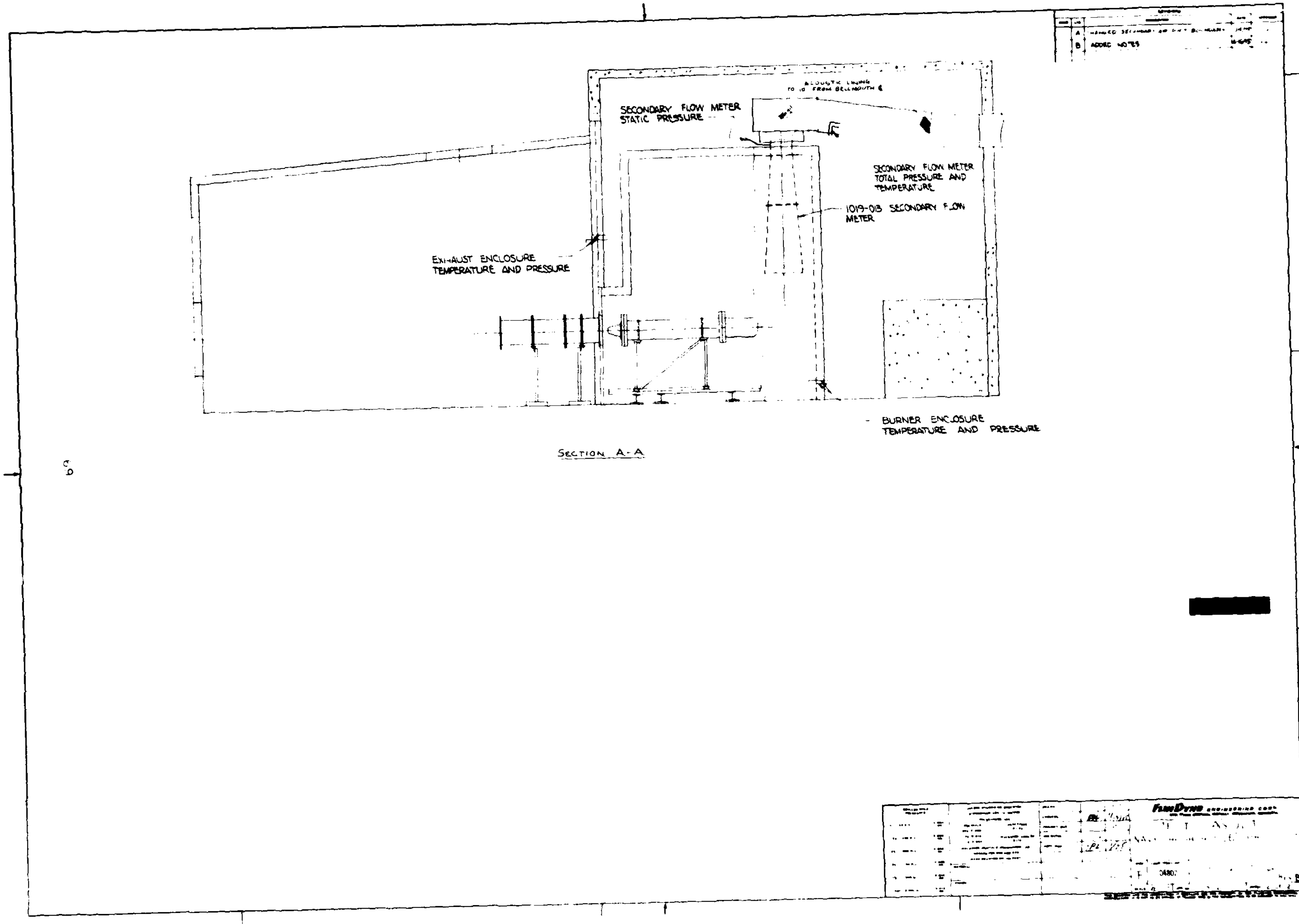

FIGURE 3.0-2 OVERALL TEST LAYOUT - ELEVATION

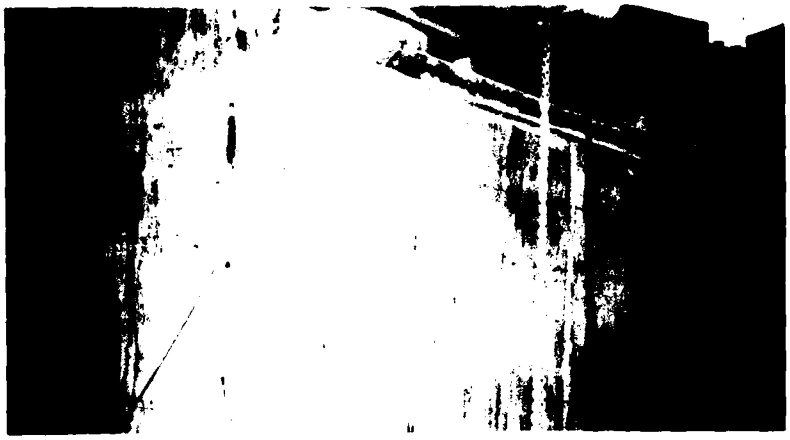

a. External View of Burner Enclosure

b. Burner Enclosure Interior Showing Secondary Flow Meter

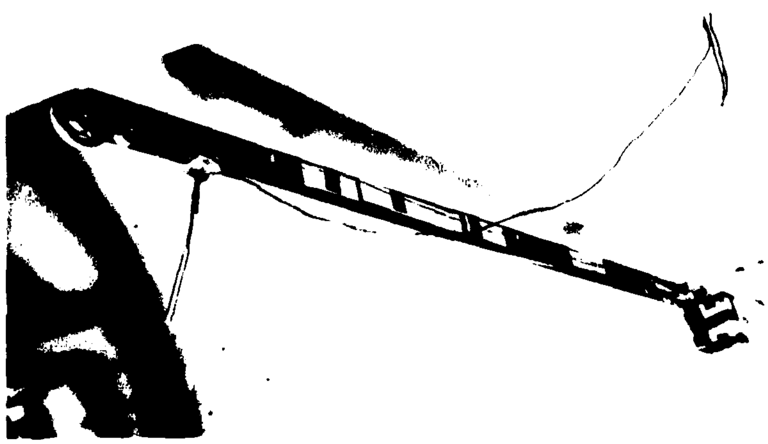

c. Burner Enclosure Interior Showing Microphone Traverse

FIGURE 3.0-3. PHOTOGRAPHS OF BURNER ENCLOSURE

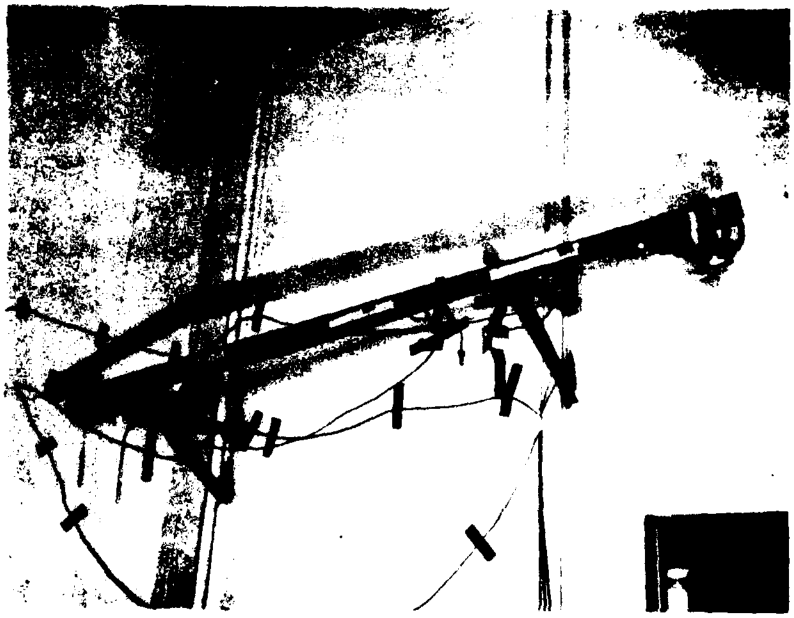

a. Exhaust Enclosure Interior showing Microphone Traverse

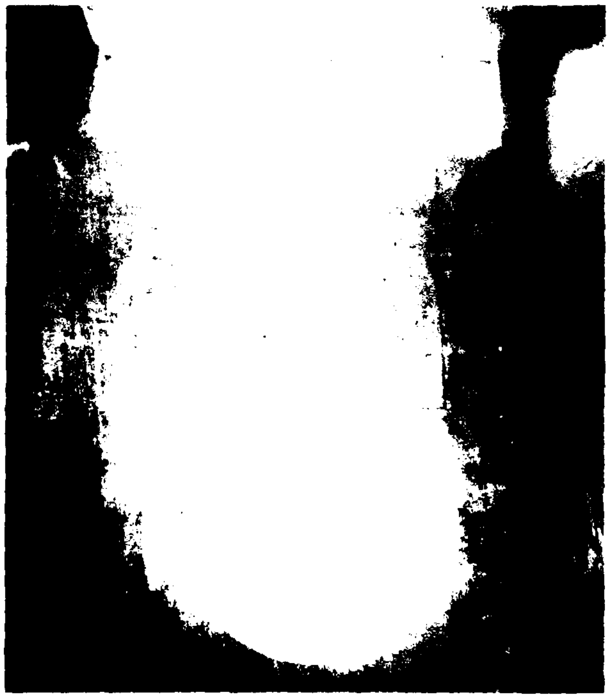

b. Exhaust Enclosure Interior Showing Exhaust and Ventilation Openings

FIGURE 3.0-4. PHOTOGRAPHS OF EXHAUST ENCLOSURE

4.0 MODEL DESCRIPTION

Basically, the model geometry simulated, at 1/15 scale, the F-14A with one P&W TF-30P412 engine operating in maximum afterburning mode installed in the Miramar Hush House with its 90 ft. long obround, acoustically treated, augmenter tube and ramp. For the test program, the jet nozzle was operated over a range of pressure ratios and jet total temperatures, and at different locations and deflections relative to the inlet of the augmenter. Different lengths of acoustically treated augmenters were run, two different acoustic liner designs were tested (including simulation of the full-scale Miramar treatment) and tests were run with and without the augmenter exit ramp. In addition, different lengths and diameters of round, hard-walled augmenters were run with and without subsonic diffusers principally to obtain augmenter pumping data and a hard-walled obround augmenter with exhaust stack and acoustic baffles was tested. The following subsections describe the model hardware which made it possible to economically test with such a wide range of variables.

4.1 Burner, Nozzle and Stand

Figures 4.1-1, 4.1-2 and 4.1-3 contain, respectively, a drawing of the nozzle liner simulating the F-14A engine in maximum afterburning mode, a drawing of the burner, nozzle and stand assembly and photographs of the burner and stand and the burner control panel. The burner itself was designed and built by FluiDyne and operates using propane and air as the combustants. These are metered through choked ASME contoured metering nozzles and injected into the burner at several circumferential locations to enhance mixing. There are two separate combustant supply paths, one to the pilot burner and the other to the main burner. A high intensity spark ignition system is used to ignite the pilot burner. The burner control system utilizes solenoid operated valves in such a way that operation is essentially automatic once pilot and main burner air and propane meter pressures have been preset on the control panel (Figure 4.1-3b) and the safety interlock switch located in the test area has been turned on. Pushing the start button opens the pilot propane valve and

FLUIDYNE ENGINEERING CORPORATION

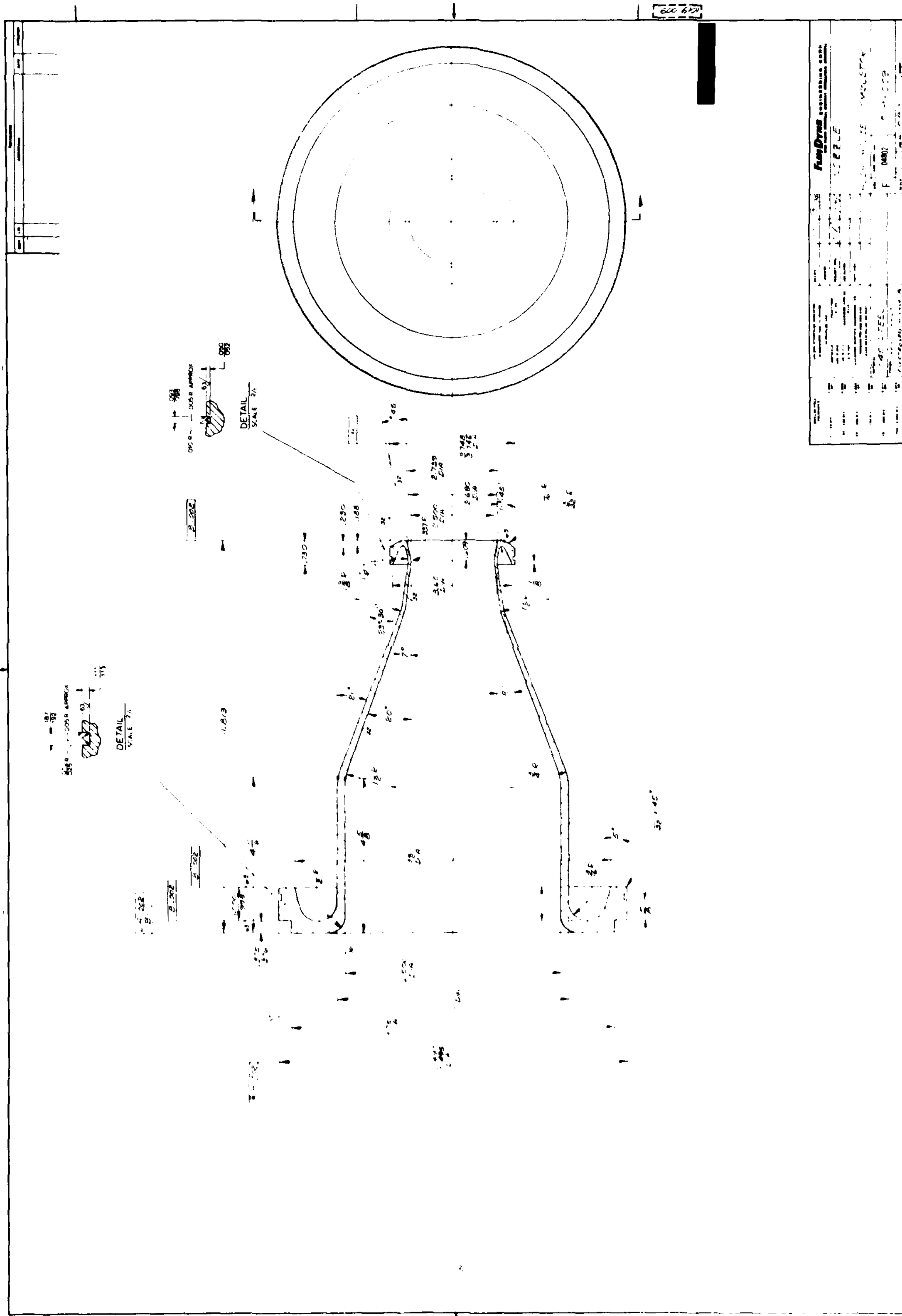

FIGURE 4.1-1 NOZZLE FOR SIMULATING AFTERBURNING F-14A AT 1/15 SCALE

FLUIDYNE ENGINEERING CORPORATION

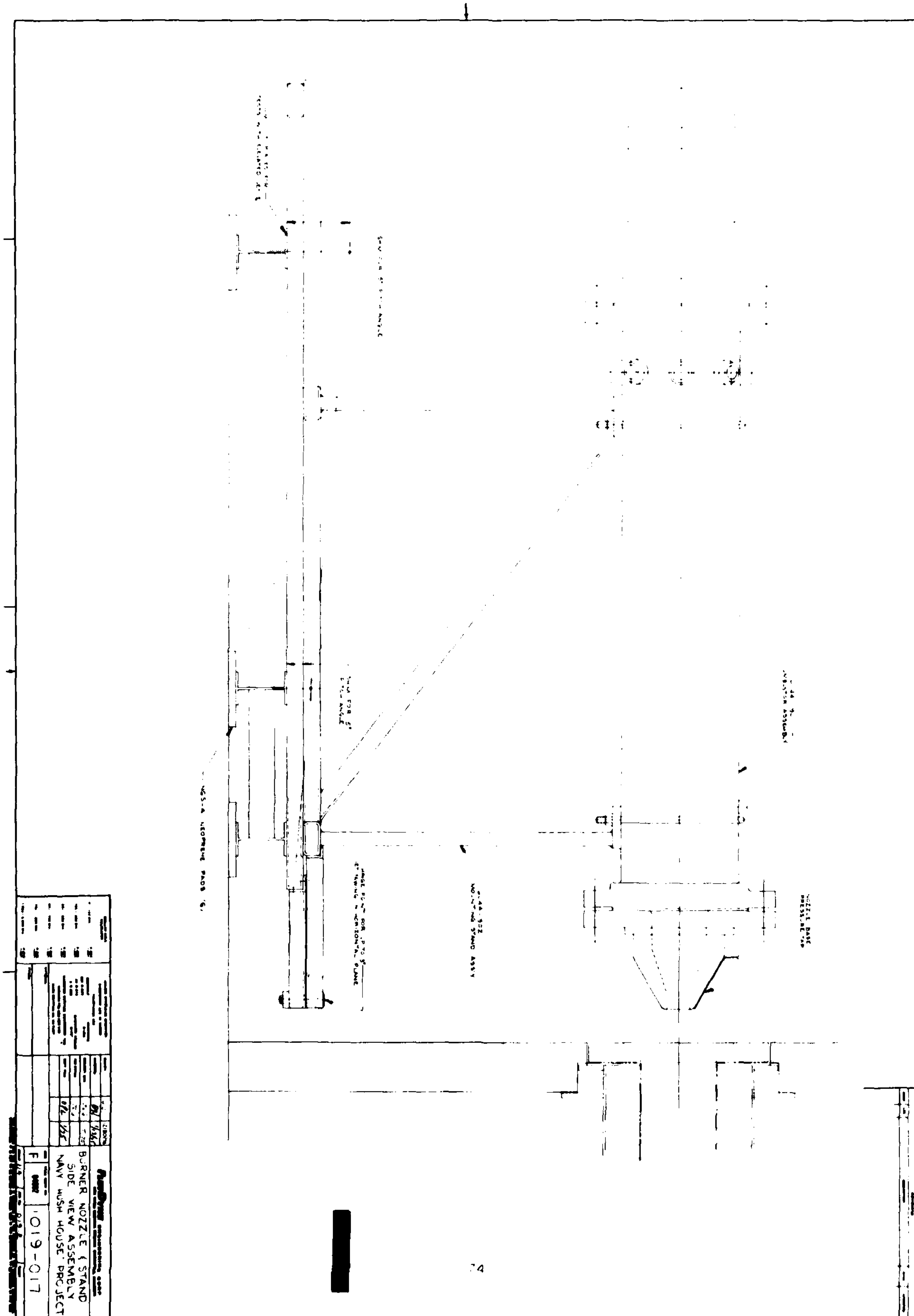

FIGURE 4.1-2 BURNER, NOZZLE AND ADJUSTABLE STAND ASSEMBLY

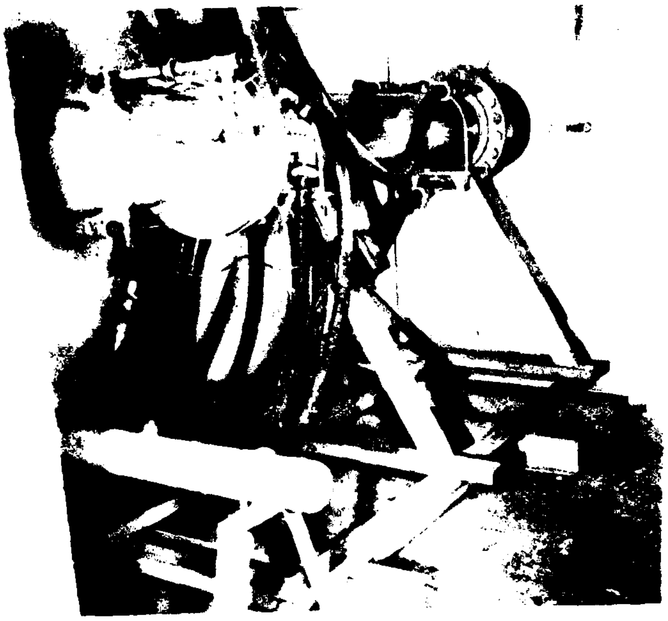

a. Burner, Nozzle and Adjustable Stand Assembly

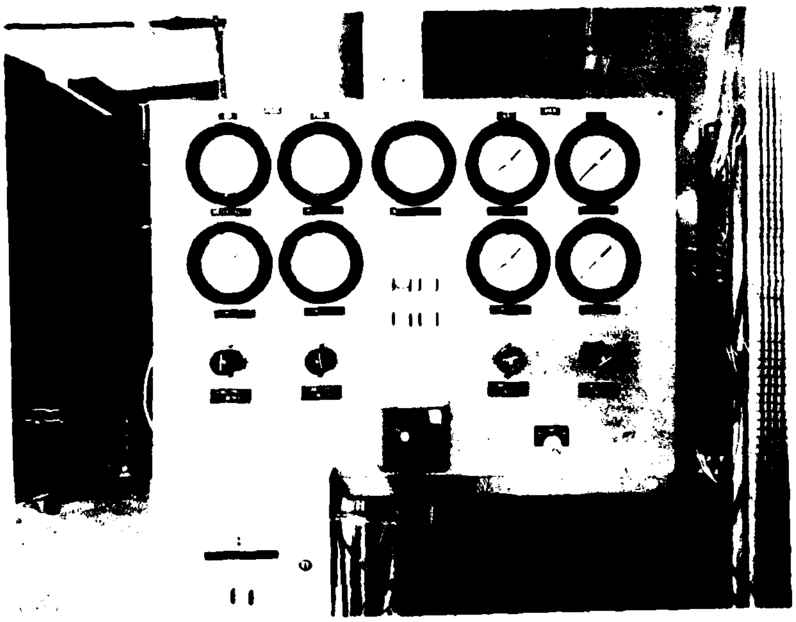

b. Burner Control Panel

FIGURE 4.1-3. PHOTOGRAPHS OF BURNER SYSTEM energizes the ignition. When the pilot burner internal thermocouple senses ignition, the main combustant flows come on and ignite. Usually final, manual adjustment of the controls is used to get the exact jet nozzle pressure ratio condition desired. If, for some reason, the main combustant flow doesn't ignite, a propane "sniffer" in the exhaust enclosure automatically shuts the combustant flow off. The burner proper (Figure 4.1-2) has a 7 in. inside diameter by 6 ft. long, ceramic lined, combustion chamber with an inner steel liner to prevent expulsion of spalled ceramic by the burner. This inner liner is uncooled so it is equipped with a thermocouple and limit switch. If the liner temperature exceeds 900°F, the burner shuts off (at 3000°F, this limits runs to about 30 seconds duration). The burner can be turned off manually by pushing the stop button on the control panel or by pushing the safety interlock switch stop button down in the test area. Pushing either stop button opens the safety interlock switch so that it must be turned on manually in the test area before another run can be made. The burner is capable of running cold (no combustion) and over a range of "hot" temperatures from 1400°R to 3500°R. It is also capable of withstanding internal pressures as high as 300 psia. Burner system instrumentation consists of primary and pilot propane and air meter total pressures and primary air and propane meter total temperatures, as well as a combustion chamber pressure measurement which corresponds to the jet nozzle total pressure P_{T_N}.

The 1/15 scale F-14A model jet nozzle is flanged to the downstream end of the burner combustion chamber and has a 2.50 in. diameter throat and 2.74 in. exit diameter (Figure 4.1-1). Because of the high heat flux at the nozzle throat, the entire nozzle is water-jacketed and a centrifugal water pump recirculates about 80 gpm of cooling water through the water jacket. An external nozzle base surface pressure tap was placed about 1/4" away from the nozzle exit to make possible a determination of the effect of Hush House operation on the aircraft nozzle base pressure.

The adjustable stand shown in Figures 4.1-2 and 4.1-3 made it possible to place the jet nozzle exit in different positions relative to the augmenter entrance. The stand was built with two base frames, resting on lateral I-beams, making possible axial and lateral translation in addition to lateral deflection, using a hinge point which remained at the same axial location as the jet nozzle exit. Marks were scribed on the I-beam cross members for the different lateral positions and other scribe marks made angular settings easily obtainable. Shims were also provided for raising the jet centerline and for vertical plane angular deflection. Adjustments made during the test program included varying the axial position of the nozzle exit from 18" away from the augmenter entrance to a position contiguous with it, moving the nozzle centerline laterally from jet centered-in-augmenter to a 4.6" offset, vertical positions of centered and 1" above center, lateral angular deflections of 0°, 1° and 3° and vertical angular deflections of 0° and 2°. Furthermore, for the jet survey testing (Figure 4.1-4), the hinge which was used for lateral angular adjustment was removed and the entire burner assembly slid downstream so that the jet nozzle projected into the exhaust enclosure. To make such a wide range of adjustments possible, the principal burner supply flows were brought in using rubber hoses. This also provided sound isolation, as did the rubber pads which were placed under the lateral I-beams and supported the entire burner, nozzle and stand assembly.

4.2 Round, Hard-Walled Augmenters with Auxiliary Equipment and Instrumentation

Three different diameters of round, hard-walled augmenter (8", 12.25" and 17.5" inside diameter) were built and used in the aero-acoustic testing to find the influence of augmenter cross-section to jet nozzle throat area ratio, A_A/A_{NT}, on pumping performance and noise generation. These diameters correspond to A_A/A_{NT} values of 10.25, 24.01 and 49.0. The augmenter tubes were built in short flanged sections, making it possible to test each size through a range of length-diameter, L_A/D_A, ratios corresponding to nominally 4, 6 and 8. These length-diameter ratios were chosen because they are representative of current Hush House augmenter design and because they also cover the range from slightly degraded augmenter pumping performance (shorter than optimum L_A/D_A) to more than adequate length for good pumping. Subsonic diffusers were provided for the 8" and 12.25" diameter augmenters. The overall length of the diffuser for the 8" diameter augmenter is 24" which, with a diffuser half-angle of 4°, gives a diffuser area ratio, A_D/A_A, of 2.02. The 12.25" diameter augmenter was provided with two 20 in. lengths of subsonic diffuser so that diffuser area

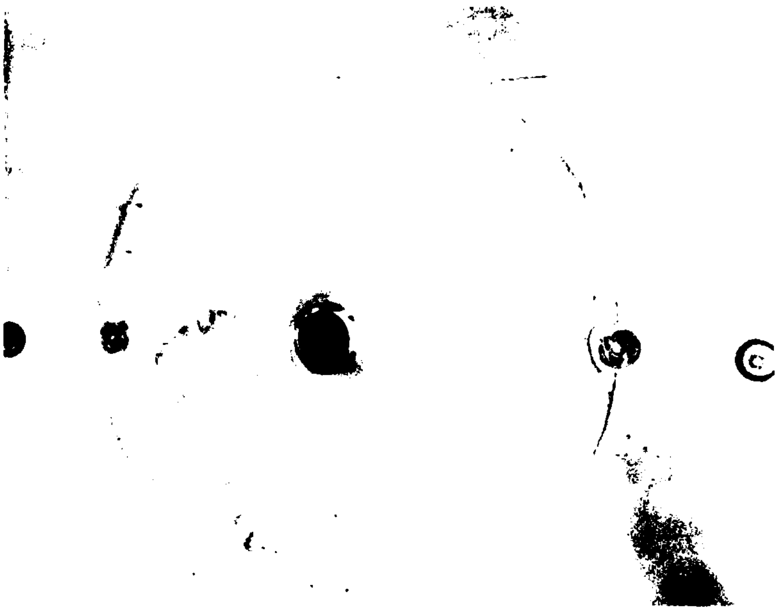

a. Jet Survey Test Setup

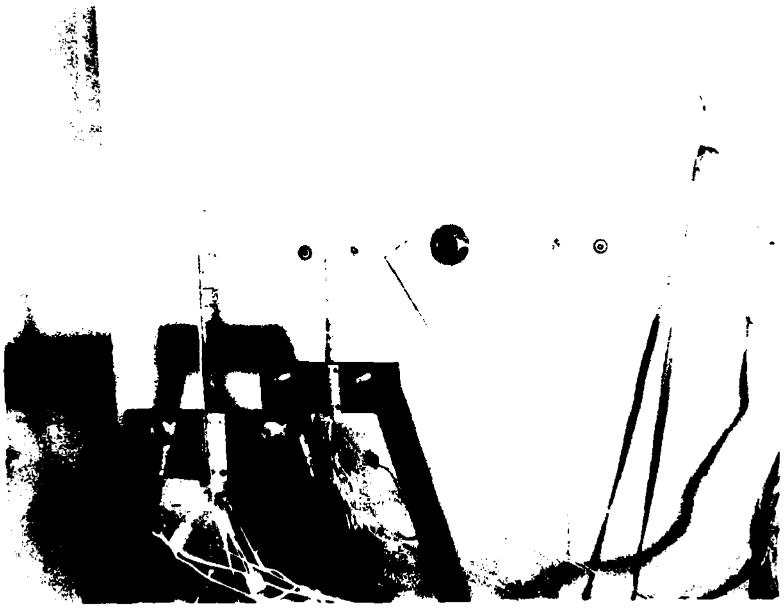

b. Jet Survey Test Setup Showing Rakes

FIGURE 4.1-4. PHOTOGRAPHS OF JET SURVEY SETUP ratios, A_D/A_A, of 1.51 and 2.13 could be tested. Drawings and photos of the three augmenter sizes and the two stands which supported all of the augmenters tested in this program appear in Figures 4.2-1, 4.2-2, 4.2-3 and 4.2-4. As with the burner stand, the augmenter stands rested on resilient rubber pads to prevent noise transmission into the floor. Also, the augmenter entrance was always isolated from the separating wall through which it projected.

In addition to having two subsonic diffuser lengths, the 12.25" diameter augmenter was provided with the conical augmenter entrance typical of all other augmenters plus a round entrance and a sharp-edged entrance for investigation of the influence of the augmenter entrance "bellmouth" geometry on pumping and noise generation. An inlet throttle was also tested. These various inlet configurations are shown in Figure 4.2-1. The 12.25" diameter augmenter was subjected to more tests than the other two because its cross-sectional area corresponds to that of the 1/15 scale model obround augmenter.

All three of the augmenter sizes were provided with wall static pressure taps spaced 1 ft. apart and, those having a subsonic diffuser, had one static pressure tap centered lengthwise in each subsonic diffuser section. Consistent with the more extensive testing on the 12.25" diameter augmenter, it was equipped with two cross-sectional total pressure-total temperature survey rakes making it possible to study jet mixing progress inside of this augmenter. The rakes appear on Figures 4.2-1 and 4.2-3.

4.3 Obround Augmenters with Auxiliary Equipment and Instrumentation

These augmenters, which were used in the aero-thermal and acoustic testing, were all the same cross-section configuration, namely, a 15.5" wide by 9" high, aspect ratio (15.5/9) = 1.72, obround, simulating the NAS Miramar F-14A augmenter at 1/15 scale. In every case, with hard or absorptive wall, the obround liner sections were supported inside the same 17.5" diameter flanged shell sections that formed the 17.5" diameter hard-walled augmenter during the aero-acoustic testing. Hard and absorptive liner sections were interchangeable so that a hard-walled liner section could be substituted for the absorptive wall

FLUIDYNE ENGINEERING CORPORATION

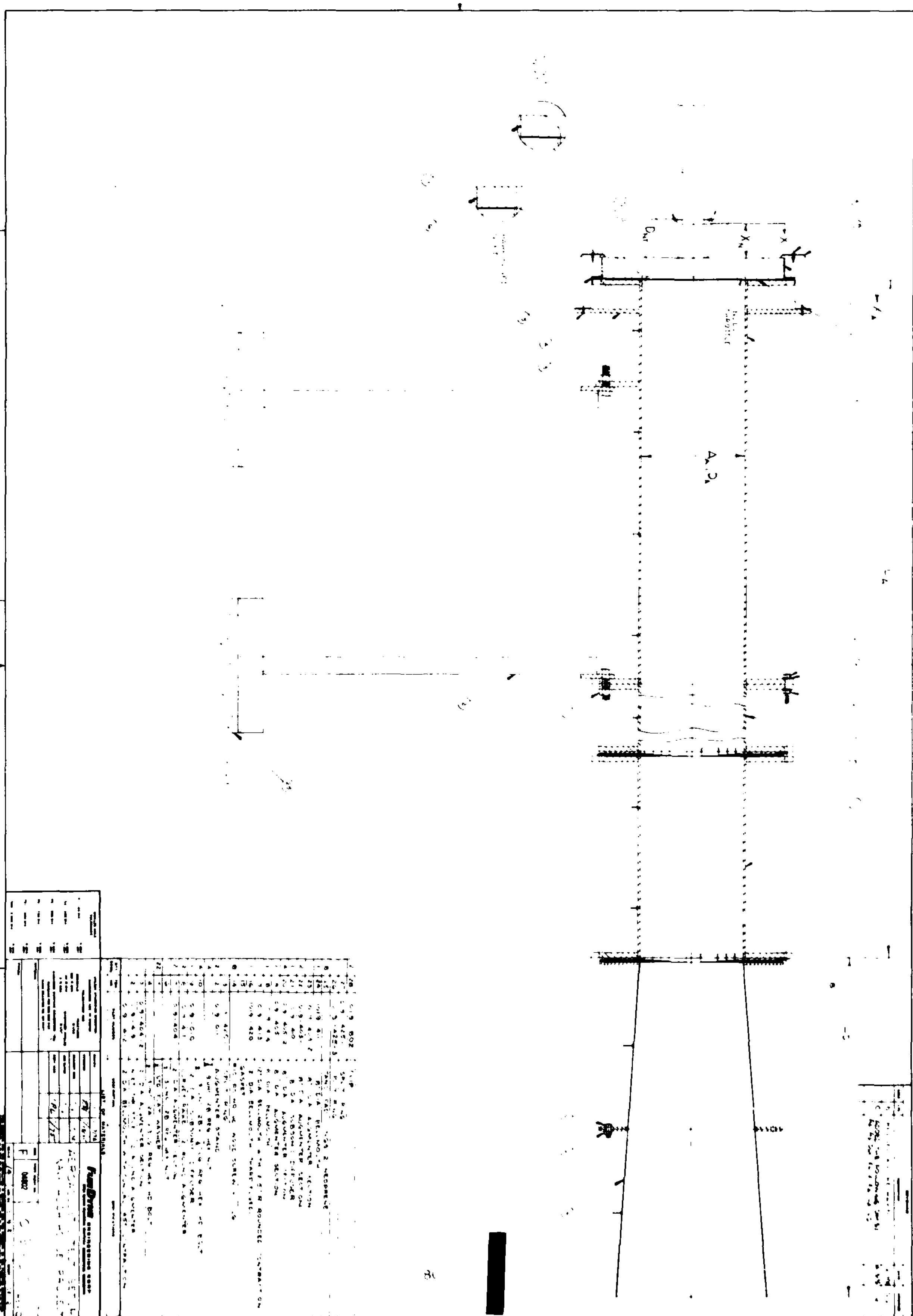

FIGURE 4.2-1 AERO-ACOUSTIC TEST SETUP- 12.25" DIAMETER AUGMENTER

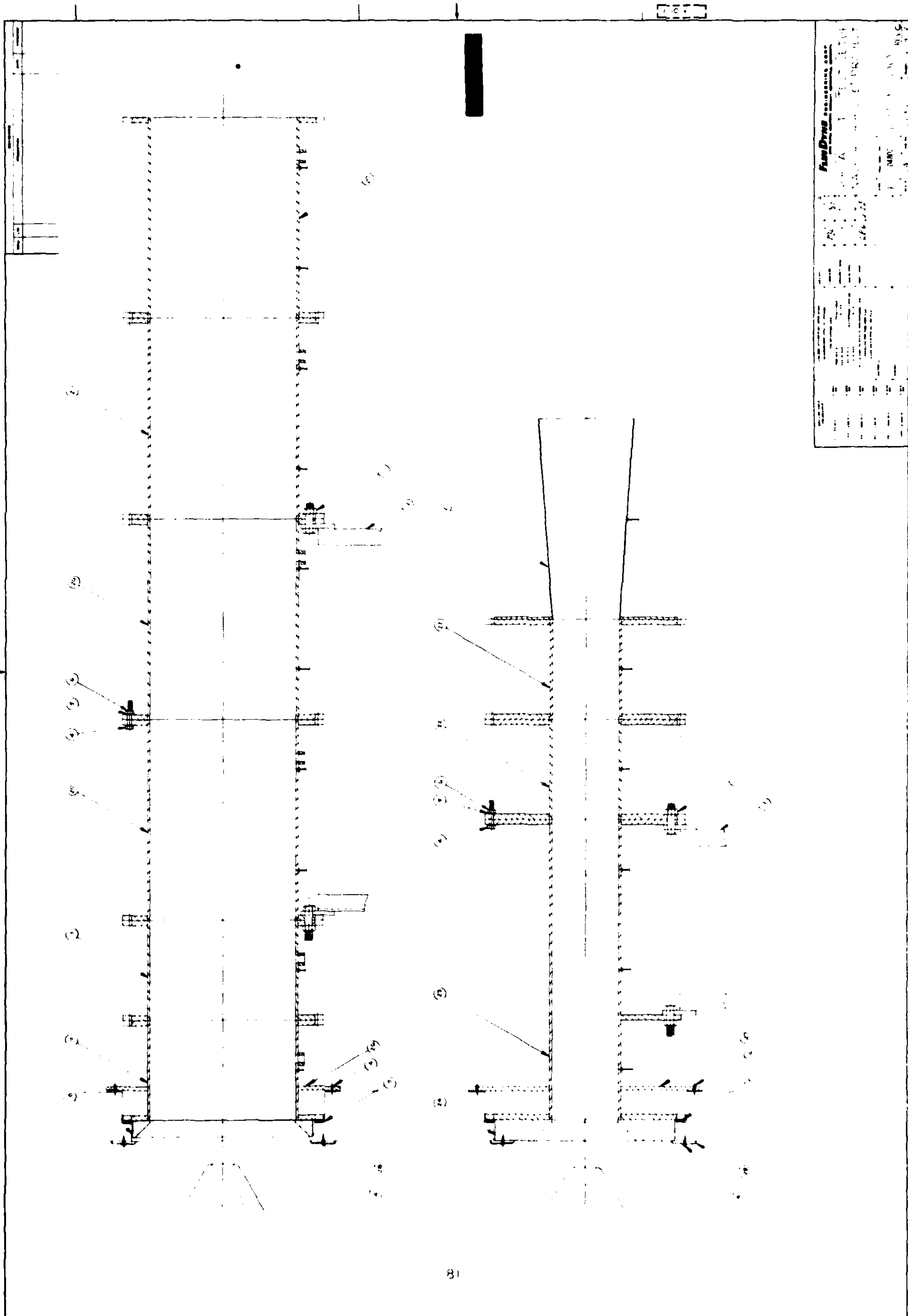

FIGURE 4.2-2 AERO-ACOUSTIC TEST SETUP - 8" and 17.5" DIAMETER AUGMENTERS

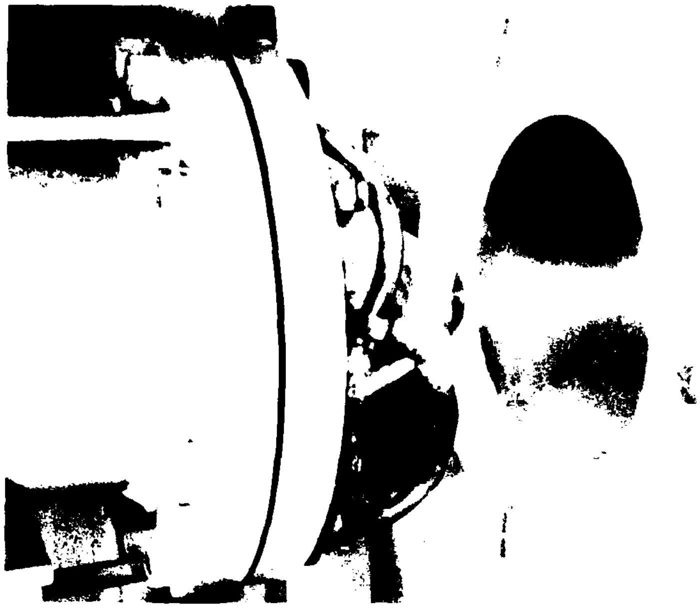

a. Jet Directed into 12.25" Diameter Augmenter

b. Survey Rake for 12.25" Diameter Augmenter

FIGURE 4.2-3. PHOTOGRAPHS RELATED TO AERO ACOUSTIC TEST SETUP

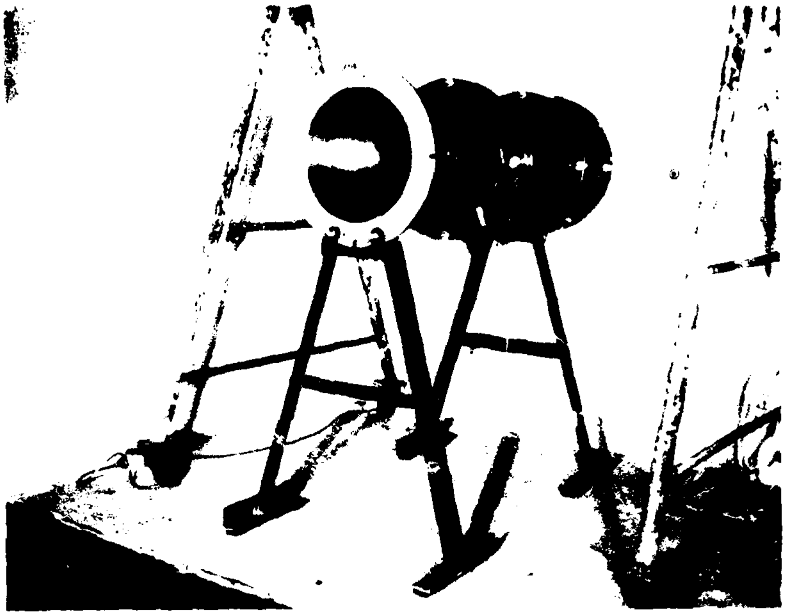

a. 17.5" Diameter Augmenter

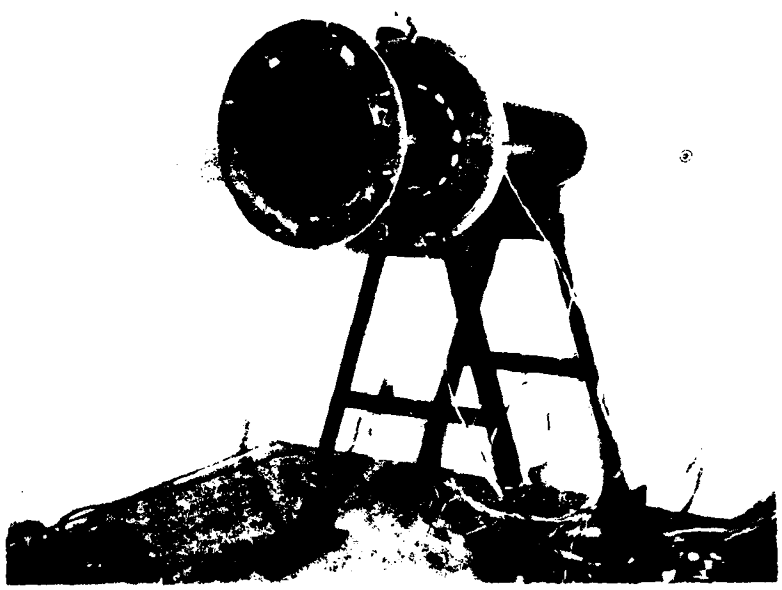

b. 8" Diameter Augmenter with Subsonic Diffuser

FIGURE 4.2-4. PHOTOGRAPHS SHOWING EXHAUST END OF AERO ACOUSTIC TEST SETUP when tests on the latter were complete. By flanging the sections together, a total length of 96 in. of absorptive augmenter corresponding to a full-scale length of 120 ft. could be formed. The augmenter cross-section area to jet nozzle throat area ratio for this configuration is $A_A/A_{NT} = 25$.

For every obround augmenter test, a 45° "conical" augmenter entrance was provided and during the acoustic tests an inlet throttle was also tested (see Figure 4.3-2). During the aero-thermal testing, the augmenter exit flow was not deflected in any way (Figure 4.3-1) whereas the bulk of the acoustic testing was performed with an exit ramp simulating that of the full-scale NAS Miramar Hush House (Figure 4.3-2). For the majority of tests, a full length absorptive liner configuration designed by Bolt, Beranek and Newman was used (Figures 4.3-4b and 4.3-5a). A full length liner configuration simulating the full-scale Miramar Hush House liner was also tested (Figure 4.3-5b). Both of these model scale absorptive liners are also described in Figure 4.3-2. Both utilized an inner, porous mechanical protective liner of Feltmetal (Brunswick Feltmetal 347-10-30-AC3A-A). To accommodate the thermal expansion of the Feltmetal, it was rigidly attached only at the upstream end of each section (Figure 4.3-4a). Feltmetal was also used as the protective surfacing for the ramp and ramp sidewalls. Model scale simulation of the full-scale absorptive liner was achieved by maintaining the same total flow resistance for the thin model liner as the thick full-scale liner has. This required that the model utilize a fiberglass lining (Owens Corning PF-105) having much finer fibers than the full-scale liner, so that the same flow resistance could be obtained with 1/15 of full-scale thickness. Figure 4.3-3 shows a test set-up with 1 ft. of the absorptive liner combined with 5 ft. of hard-walled liner. With the short liner sections, it was possible to test with the 1 ft. absorptive section at any of six axial positions. During all tests with the obround augmenter, the shell was wrapped with fiberglass and this was covered with a lead laminate material (Acousti-jac) to eliminate substantially the transmission through the wall of the augmenter tube.

At the very end of the test program, a configuration consisting of 6 ft. of absorptive augmenter, plus the obround subsonic diffuser from the stack and

FLUIDYNE ENGINEERING CORPORATION

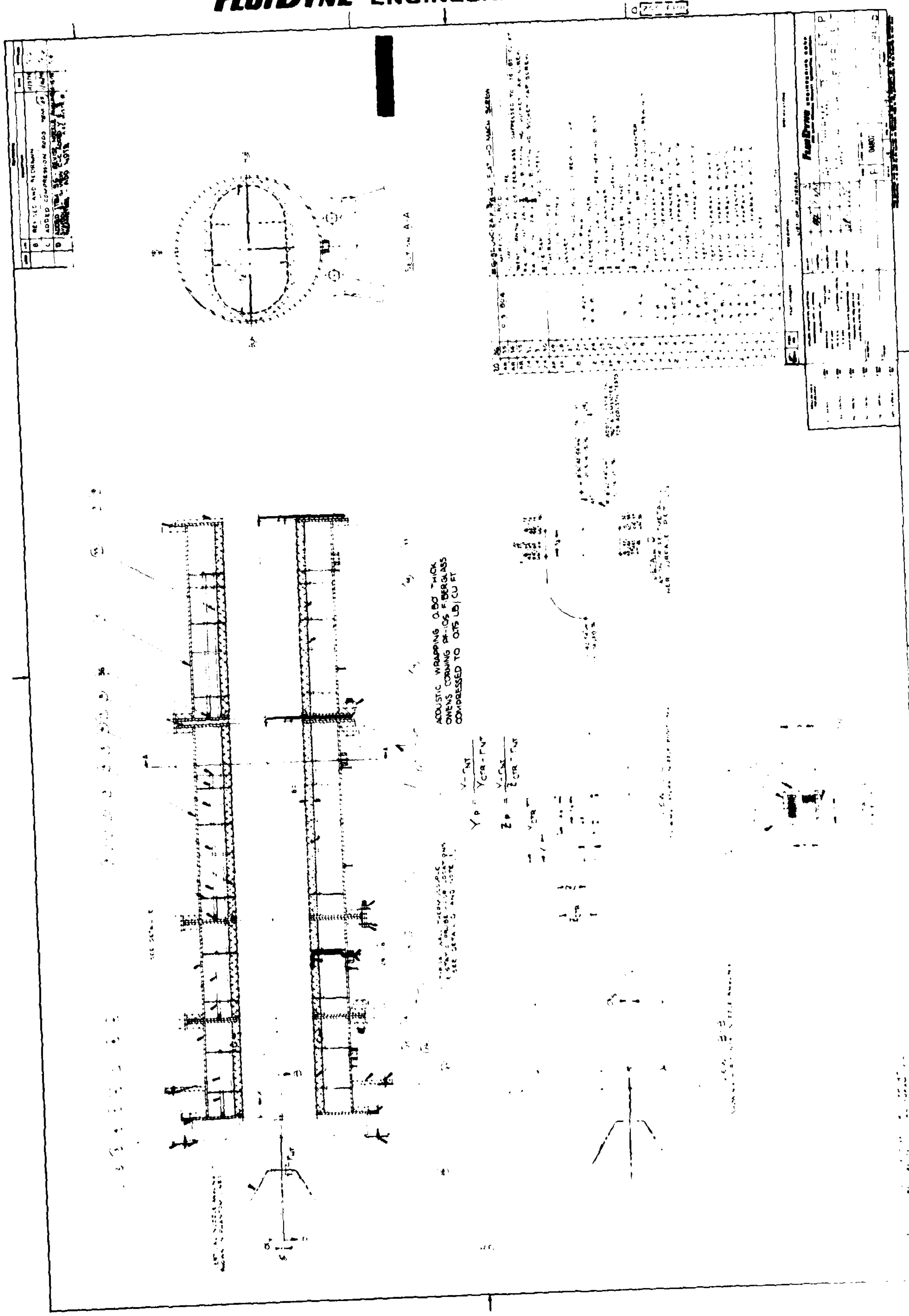

FIGURE 4.3-1 AERO-THERMAL TEST SETUP - 15.5" x 9" OBROUND ABSORPTIVE AUGMENTER

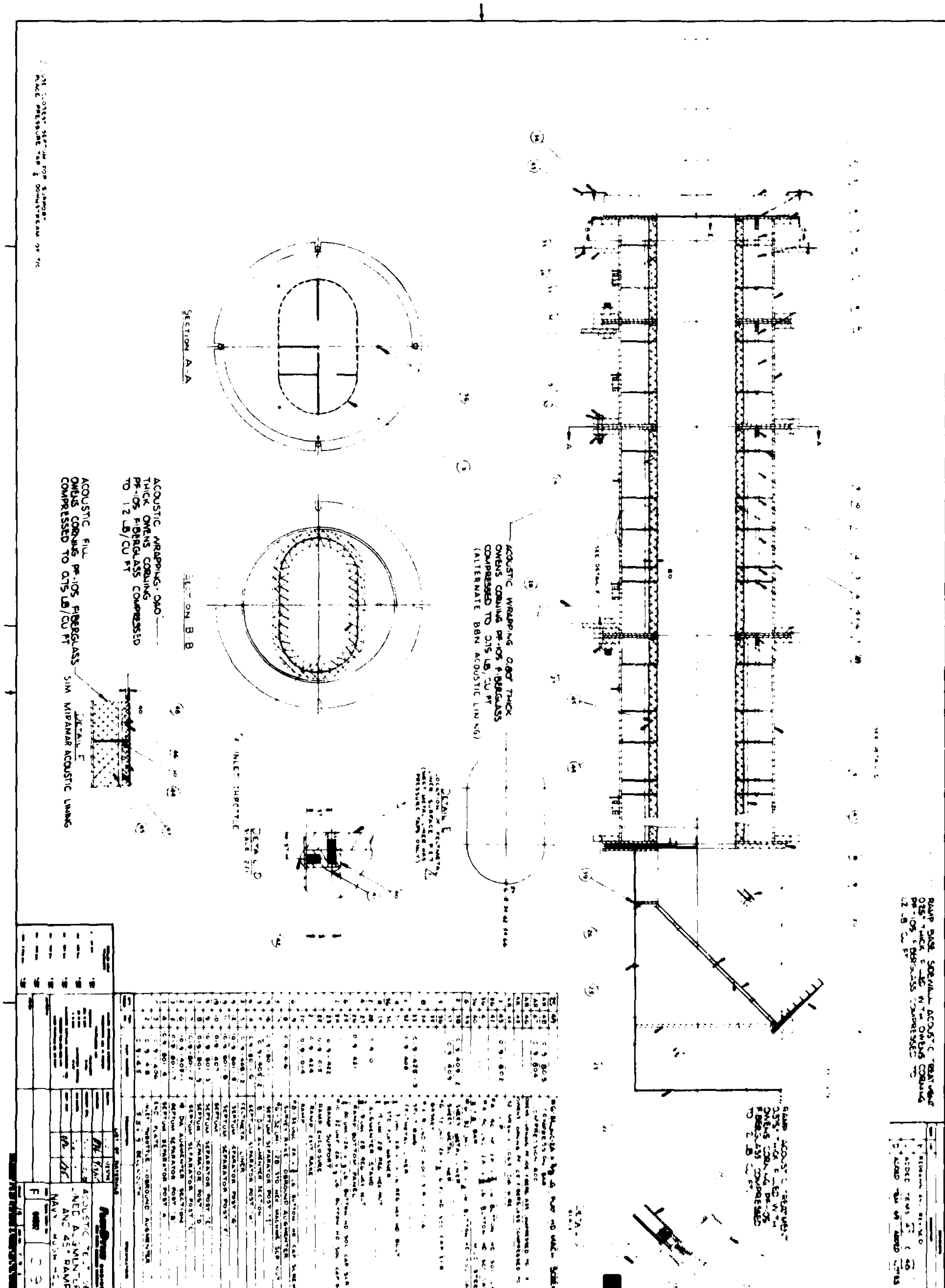

FIGURE 4.3-2 ACOUSTIC TEST SETUP WITH COMPLETE ABSORPTIVE AUGMENTER AND RAMP

FLUIDYNE ENGINEERING CORPORATION

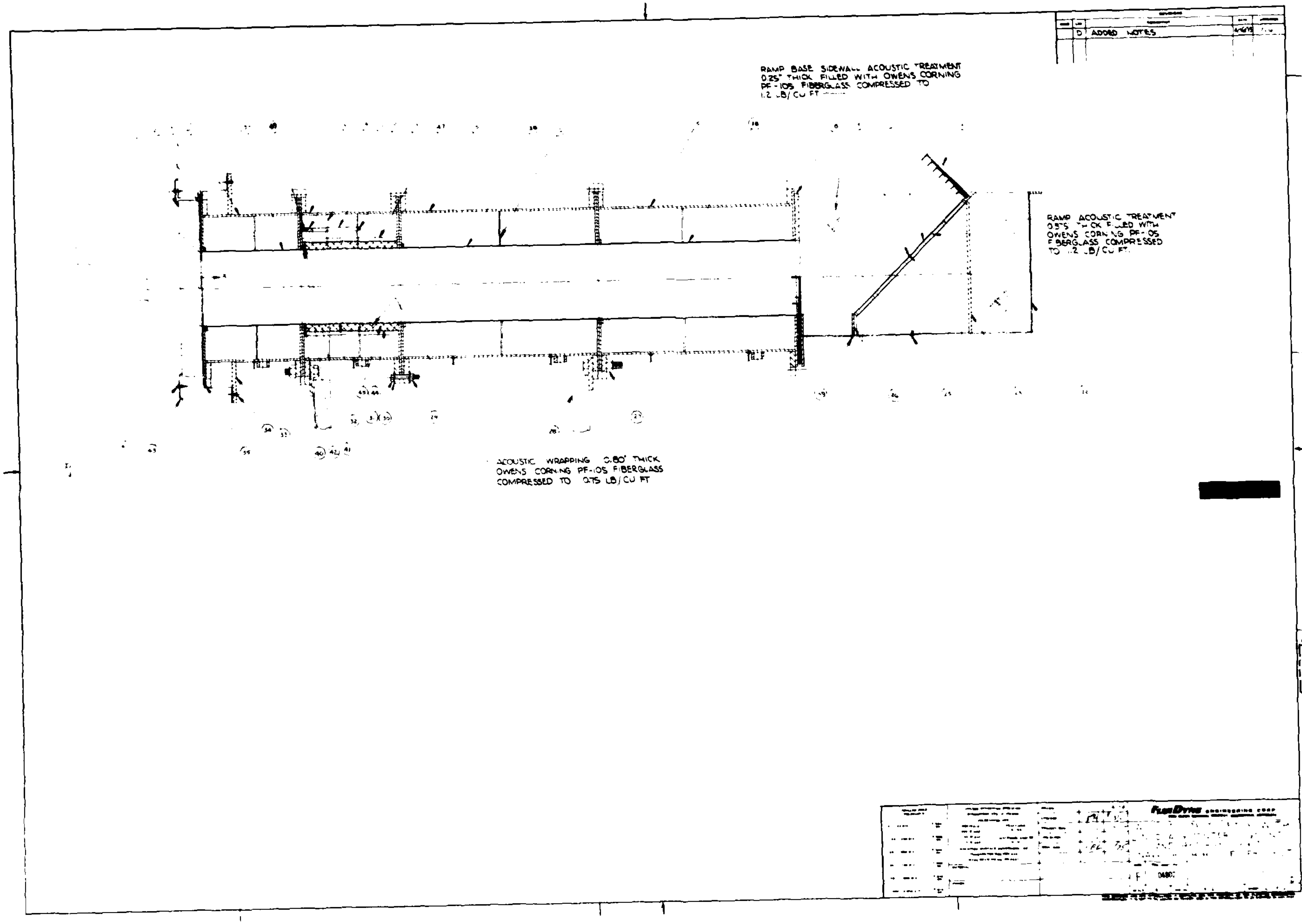

FIGURE 4.3-3 ACOUSTIC TEST SETUP WITH 1' LENGTH OF ABSORPTIVE AUGMENTER

a. Obround Feltmetal Liner and Septums for Sound Absorbing Augmenter Prior to Fiberglass Wrap

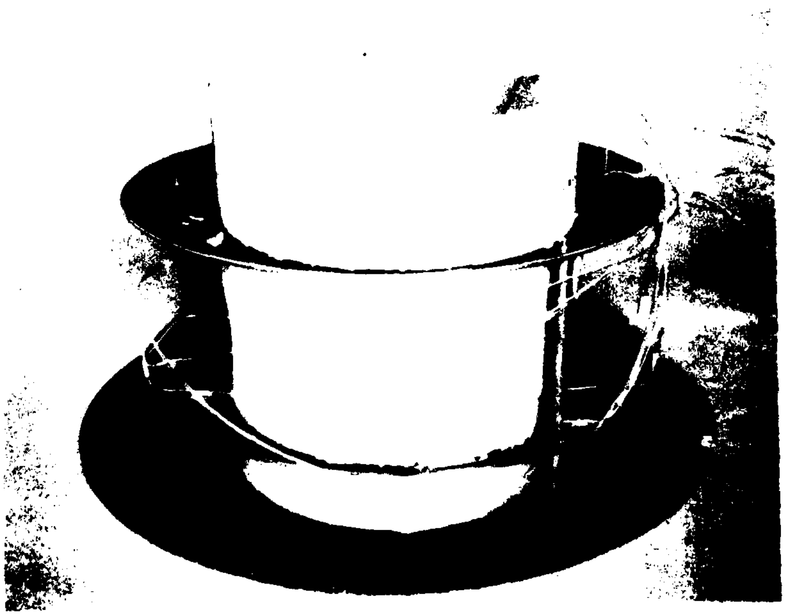

b. Obround Liner and Septums after Fiberglass Wrap (BB&N Design)

FIGURE 4.3-4. PHOTOGRAPHS SHOWING CONSTRUCTION OF SOUND ABSORPTIVE AUGMENTER LINING

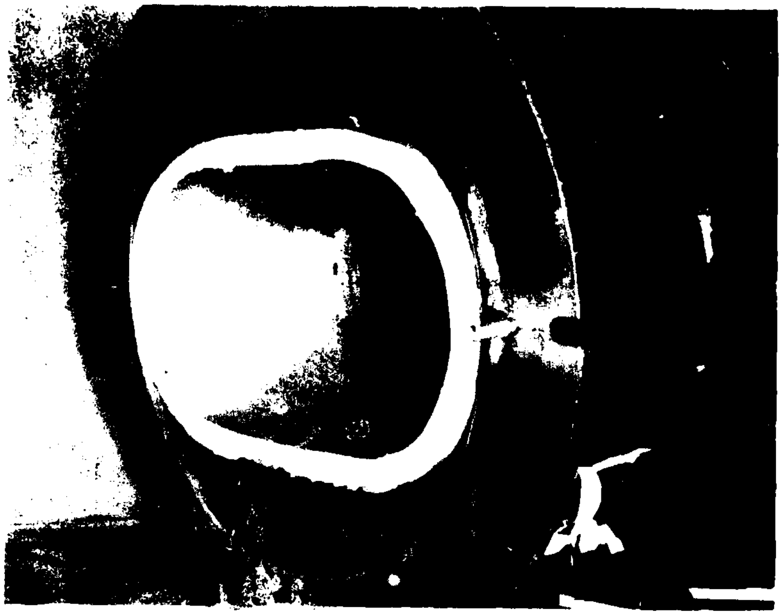

a. BB&N Design Sound Absorbing Liner after Insertion in Shell

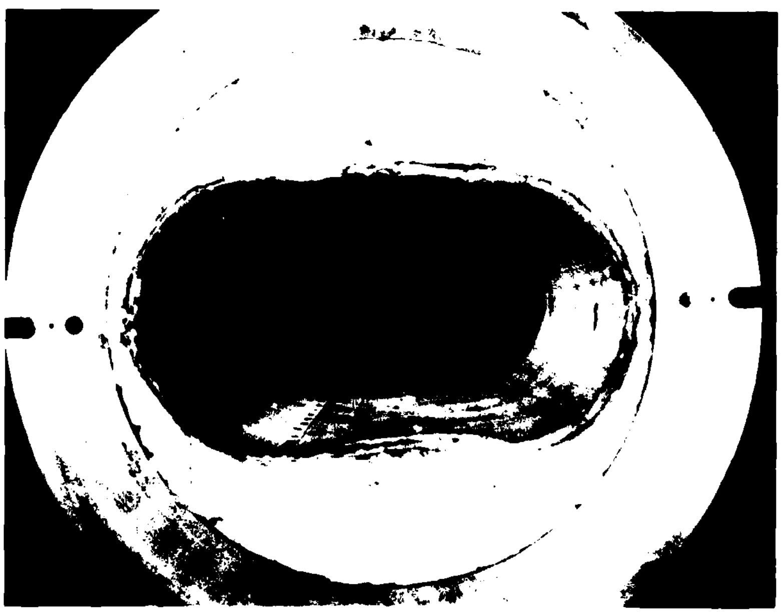

b. Simulated Miramar Sound Absorbing Liner after Insertion in Shell

FIGURE 4.3-5. PHOTOGRAPHS SHOWING THE BB&N AND SIMULATED MIRAMAR SOUND ABSORBING LININGS

a. Finished Section of Sound Absorbing Liner and Shell

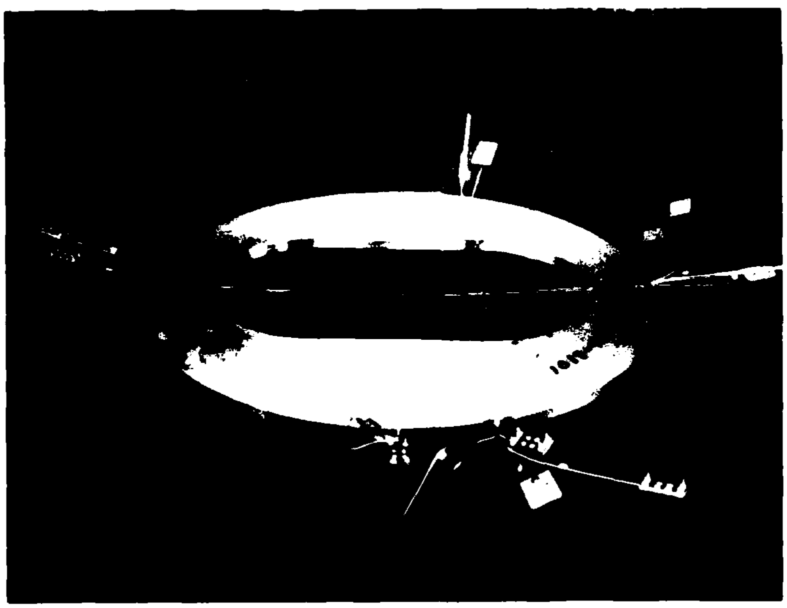

b. Obround Augmentor P_T, T_T Survey Rake

FIGURE 4.3-6. PHOTOGRAPHS RELATED TO THE ACOUSTIC AND AERO THERMAL TEST SETUPS WITH THE SOUND ABSORBING LINER

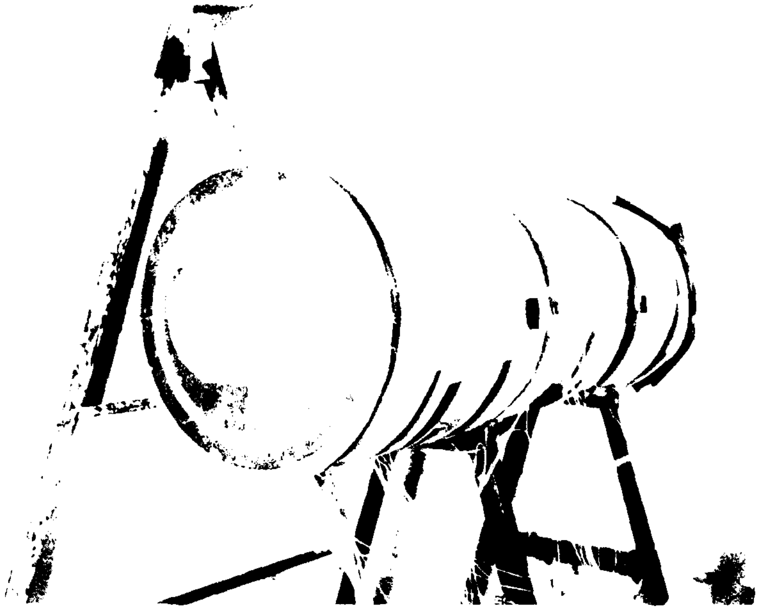

a. Complete Sound Absorbing Augmenter with Lead Exterior Jacket

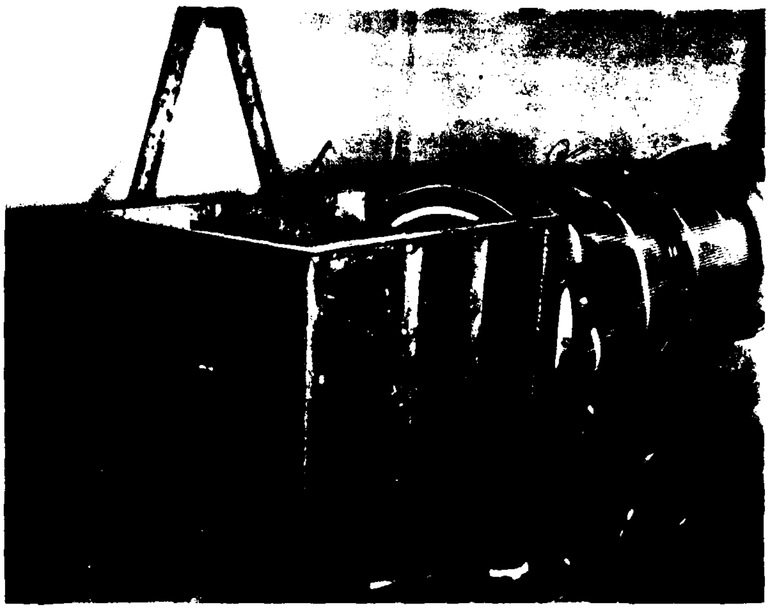

b. Complete Sound Absorbing Augmenter with Ramp and Ramp Exit Rake

FIGURE 4.3-7. PHOTOGRAPHS OF THE COMPLETED SOUND ABSORBING AUGMENTER baffles configuration was tested with a flow distributing screen of 30% solidity placed at the 4 ft. station (Run No. 142). Only limited noise and pumping data were obtained.

The absorptive obround augmenter was extensively instrumented, especially during the aero-thermal testing. The static taps at 1 ft. intervals in the 17.5" diameter shell were utilized and there were static pressure taps and surface thermocouples attached to the inner Feltmetal liner of the augmenter at 1 ft. axial intervals and at various locations on the perimeter for a total of 30 inner liner pressures and 30 thermocouples. These were used to define the jet impingement problem with different jet nozzle orientations relative to the augmenter. The exact arrangement of these surface measurements is shown in Figure 4.3-1. In addition to these surface measurements, the obround augmenter was also equipped with two total pressure-total temperature survey rakes having 12 total pressure probes and 11 total temperature probes each (see Figures 4.3-1 and 4.3-6) and with a ramp exit total pressure survey rake (Figures 4.3-2 and 4.3-7).

4.4 Obround Augmenter Plus Stack and Baffles with Instrumentation

Figures 4.4-1 and 4.4-2 show the final basic configuration which was tested. This consists of a hard-walled obround augmenter of $L_A/D_{AM} = 4.0$, a 36" long hard-walled subsonic diffuser with area ratio, $A_D/A_A = 2.04$, an absorptive wall stack base (which also served as the ramp base in the absorptive obround augmenter tests) containing hard surface turning vanes and an absorptive wall stack containing 21 longitudinally oriented sound absorptive baffles. The absorptive surface of each baffle is protected with a thin Feltmetal of low flow resistance. The stack cross-sectional area was sized to limit the velocity through the baffles to 180 ft./sec., assuming that the baffles occupied one-half of the area. During the initial tests with this configuration, the baffle surface temperature got hot enough to buckle the Feltmetal protective surface, thus reducing the effective flow area through the baffles (see Figure 4.4-1 for gap during test). All exterior surfaces were covered with fiberglass and Acousti-jac lead laminate material to reduce noise transmission so that during the model study, the exhaust noise would consist only of what passed through the baffles or was generated by the stack exit flow.

Instrumentation for the stack and baffles configuration consisted of one augmenter liner wall static pressure tap each foot of length, two axially spaced subsonic diffuser wall static pressure taps, various stack base static pressure taps and between-the-baffles stack pressure taps, as well as two stack exit total temperature probes.

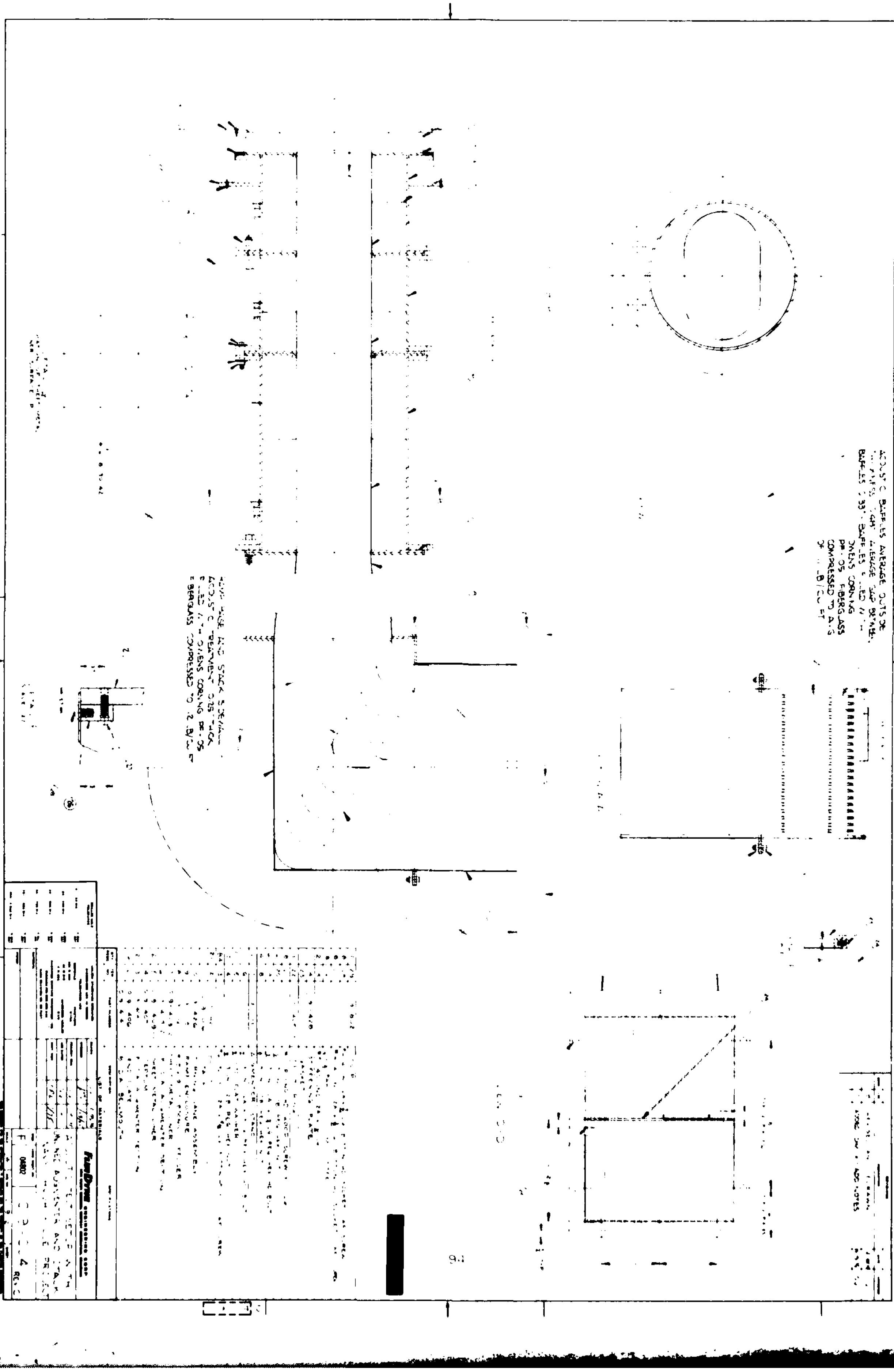

FIGURE 4.4-1 ACOUSTIC TEST SETUP OF HARD-WALLED AUGMENTER WITH ABSORPTIVE (K AND BAFFLES

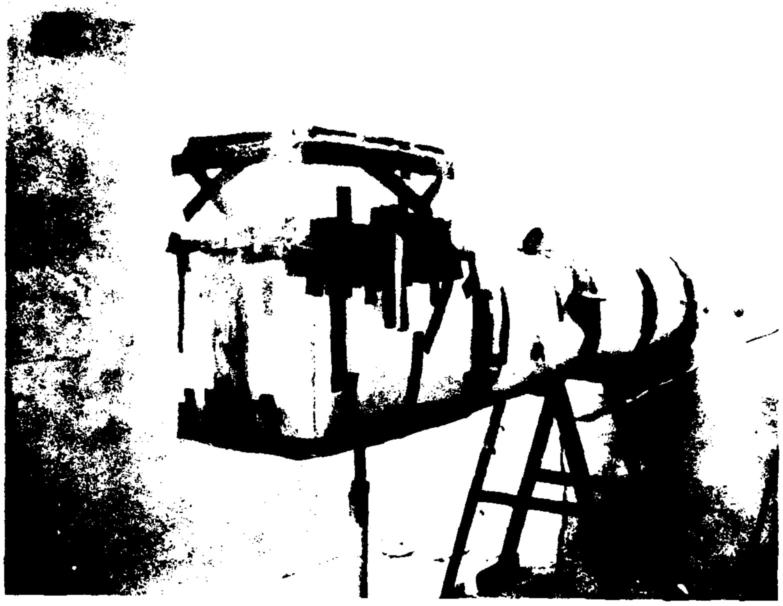

a. Complete Hard-Walled Augmenter with Sound Absorbing Stack and Baffles

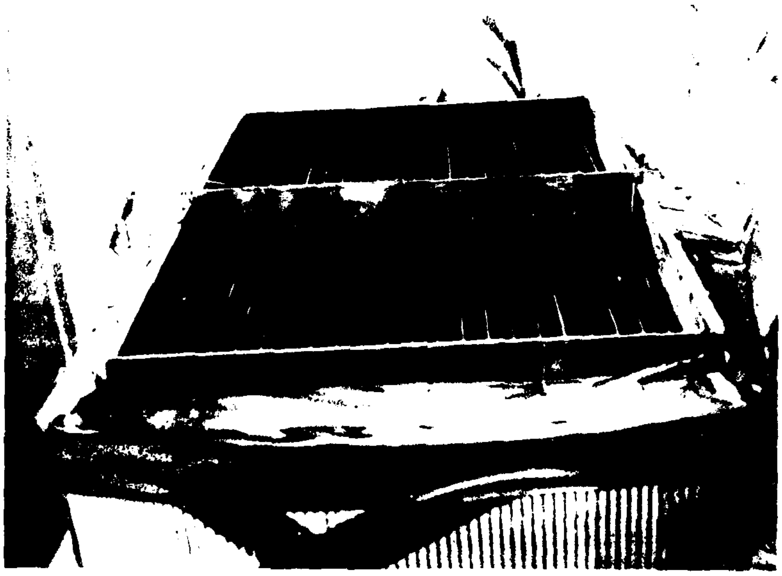

b. Close-Up of Stack and Baffles Exit Showing Exit Temperature Probes

FIGURE 4.4-2. PHOTOGRAPHS OF THE STACK AND BAFFLES ACOUSTIC TEST SETUP

5.0 MEASURING EQUIPMENT

This section is devoted to a description of the pressure, temperature and noise measuring equipment used during the Hush House model tests. Measurement errors associated with the instrumentation are presented and the resulting probable error in some of the calculated quantities is discussed.

5.1 Measuring Equipment used for Aerodynamic/Thermodynamic Data

Aerodynamic/Thermodynamic measurements consisted primarily of pressures and temperatures. These measurements were then used to calculate mass flows, augmentation ratio parameter, pressure ratios and temperature parameters. The equipment used for each measurement and the probable error associated with its use is listed below.

Pressure Measurement

atmospheric pressure, P_{bar}

Taylor aneroid barometer
$\pm$ 0.005 psi probable error

jet nozzle total pressure, P_{T_N}

Heise bourdon tube gauge 0-50 psi range
$\pm$ 0.015 psia probable error with barometer accuracy included

primary air meter total pressure, $P_{T_{am}}$

Seeger bourdon tube gauge 0-200 psig range
$\pm$ 0.062 psia probable error with barometer accuracy included

pilot air meter total pressure, $P_{T_{pm}}$

Ashcroft dura-gauge 0-60 psig range
$\pm$ 0.30 psia probable error

secondary air meter total pressure, $P_{T_{sm}}$,

secondary air meter static pressure, $P_{S_{sm}}$,

and all model pressures

multi-tube water manometers 100 inch range
$\pm$ 0.0064 psia probable error with barometer accuracy included.

The Heise and Seeger gauges are dead-weight calibrated at regular intervals to maintain their accuracy in use.

Temperature Measurement

All temperatures, except outside air temperature were measured with iron-constantan thermocouples using special grade wire. These were recorded either with a Bristol recorder or using reference junctions and a VIDAR digital data acquisition system. In both cases, the accuracy of the thermocouple wire governs the probable error as follows:

up to 530°F the probable error is $\pm$ 2.1°F
above 530°F the probable error is $\pm$ 3/8% of $T_{°F}$
($\pm$ 4°F at T = 1,050°F)

Relative Humidity Measurement

Outdoor relative humidity measurements were taken at regular intervals during each day of testing to aid in the interpretation of the acoustic test data. Since ILG calibrations of the reverberant rooms were taken with each test run, this information is merely supplementary rather than essential. A Lambrecht hygrometer was used for the relative humidity measurement. Its expected accuracy is $\pm$ 2% in relative humidity.

Figure 5.1-1 is a composite showing the test data recorded for a particular run. A manometer board photo, gauge photos and the digital printout of thermocouple data are included.

At this point, it is of interest to consider how the probable errors in the various measurements influenced the accuracy of various calculated quantities. The jet nozzle mass flow, $\dot{W}_N$, retains a probable error of only about $\pm$ 0.25% because the metering nozzles are choked and the principal measurement accuracies are good. The secondary mass flow and augmentation ratio parameter, ARP, on the other hand, may have probable errors as high as $\pm$ 4% at low ARP values of about 2.0 because the secondary venturi flow meter is unchoked and the meter throat Mach number and corresponding isentropic area ratio are very sensitive to inaccuracies in the secondary meter total and static pressure measurements.

Jet Nozzle Total Pressure

Primary Air Meter Total Pressure

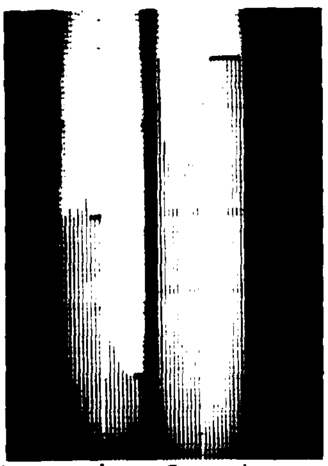

Manometer Board

004511042560
004820391350
004710886460
004610829160
004511465160
004410640360
004310761360
004210653460

Thermocouple Readings

Run No. 43

Barometer Reading =28.775 in. hg.

Outside Air Temperature = 34°F

Pilot Air Meter Pressure= 27 PSIG

Outside Relative Humidity= 71%

FIGURE 5.1-1. DATA TAKEN DURING A TYPICAL TEST

5.2 Acoustical Measurement Equipment

Measurements of sound pressure level were made simultaneously in the two reverberation rooms (burner room and exhaust room) during each jet run. Figure 5.2.1 is a block diagram of the instrumentation used to record and analyze the acoustic signals. In each room, a 1/2-in. Bruel & Kjaer (B&K) Type 4134 microphone was traversed over a 6-ft path during the jet run, after the jet temperature and flow rates had stabilized. The microphone polarization voltage was provided by a General Radio (GR) Type P-42 preamplifier. Signals from the microphone-preamplifier sets were amplified by Ithaco Model 453 amplifiers and recorded on the two "data" channels of a Kudelski Nagra IV-SJ tape recorder. The "cue" channel of the Nagra IV-SJ was used for announcements of run number, gain settings of the Ithaco amplifiers, and attenuator settings of the tape recorder. The identical instrumentation and process was used to record sound pressure levels in each reverberation chamber when a calibrated reference sound source (an "ILG" fan manufactured by ILG Industries, Inc.) was operated in one of the rooms.

During recording, the signal recorded on each data channel was monitored on both the recorder VU meters and on a dual-trace Tektronix Model 531 oscilloscope. This monitoring assured that the recordings were made with the maximum possible signal-to-noise ratio without overloading the input amplifiers. In addition, two system calibration signals were recorded at intervals to assure that the response of the record-playback system remained constant with time:

1. a B&K Type 4220 pistonphone placed over the microphone in each room, and

2. pink noise at the input to the Ithaco amplifier.

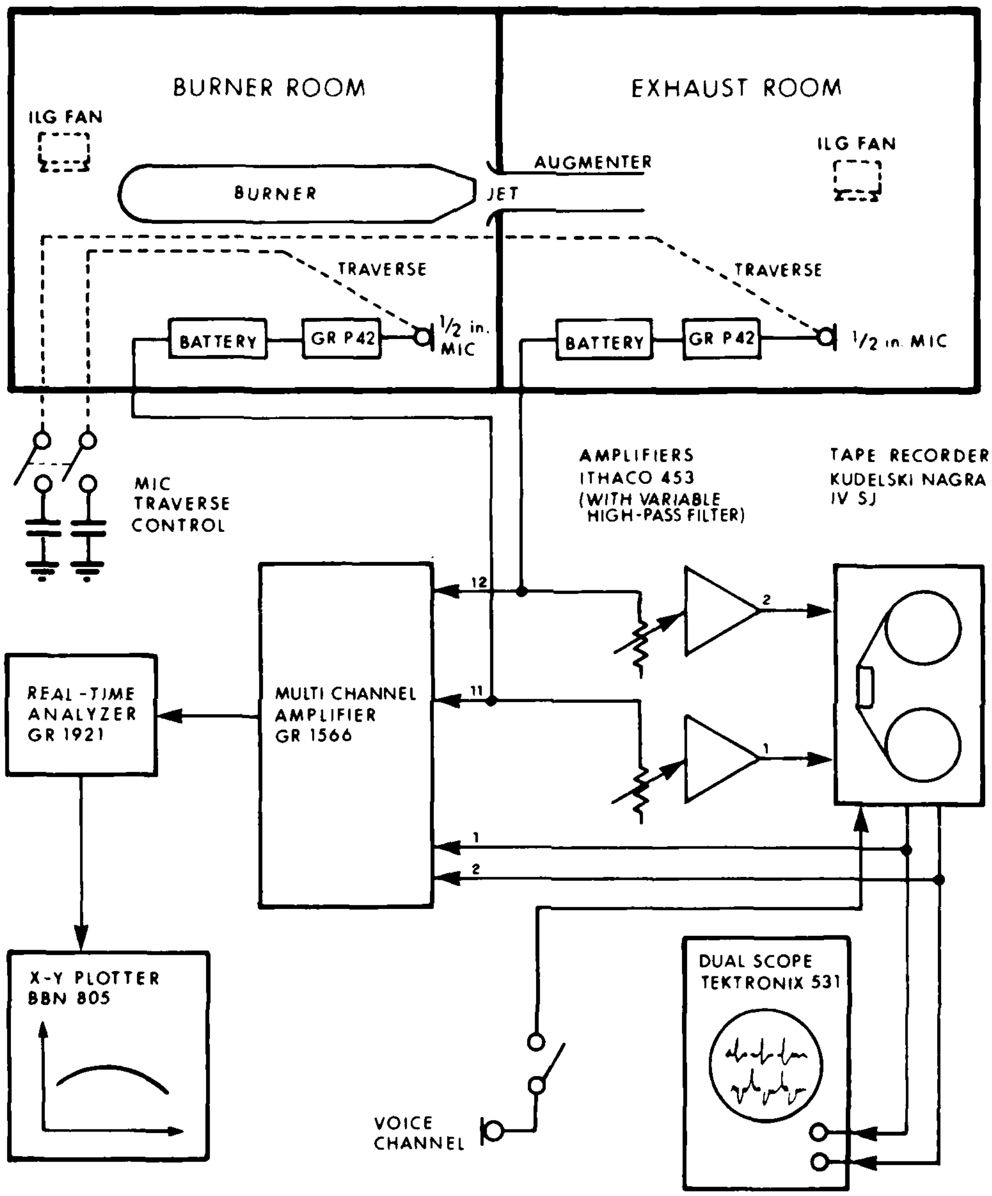

FIG. 5.2.1. BLOCK DIAGRAM OF ACOUSTICAL INSTRUMENTATION.

The B&K pistonphone, which is calibrated to produce a sound pressure level of 124 dB re 0.0002 μbar, also provided the absolute calibration necessary to convert the microphone signal from voltage level to sound pressure level.

When time permitted during the test schedule, the tape-recorded signals were played back through the GR Model 1921 1/3-octave band real-time analyzer. After accounting for both record and playback amplifier gain settings, the output of the GR 1921 was an X-Y plot of 1/3-octave band sound pressure level (in dB re 0.0002 μbar) vs 1/3-octave band center frequency. Figure 5.2.2 is an example of a typical data output, showing data measured in the exhaust room for jet run number 86. Ambient levels (i.e., background noise levels with jet not running) recorded after run 86 are also shown in Fig. 5.2.2. Similar data were plotted for the ILG run. The ILG was run immediately after the jet was shut down in the exhaust room for nearly all runs and somewhat later in the burner room for approximately every second run. For all playback analysis, the signal integration time of the GR 1921 was selected to be 8 sec to correspond to the approximately 9-sec traverse time of the microphones. The 8-sec signal integration occurred continuously as the microphone traversed; thus, the GR 1921 output was a true space-time average of the sound pressure levels along the 6-ft path.

The microphone signals could also be analyzed directly, in "real time", using the GR 1921. This mode was used to check microphone calibration (but not record-playback system calibration) using the B&K pistonphone. This mode of measurement was also used for several analyses for which tape-recording was unnecessary; these included:

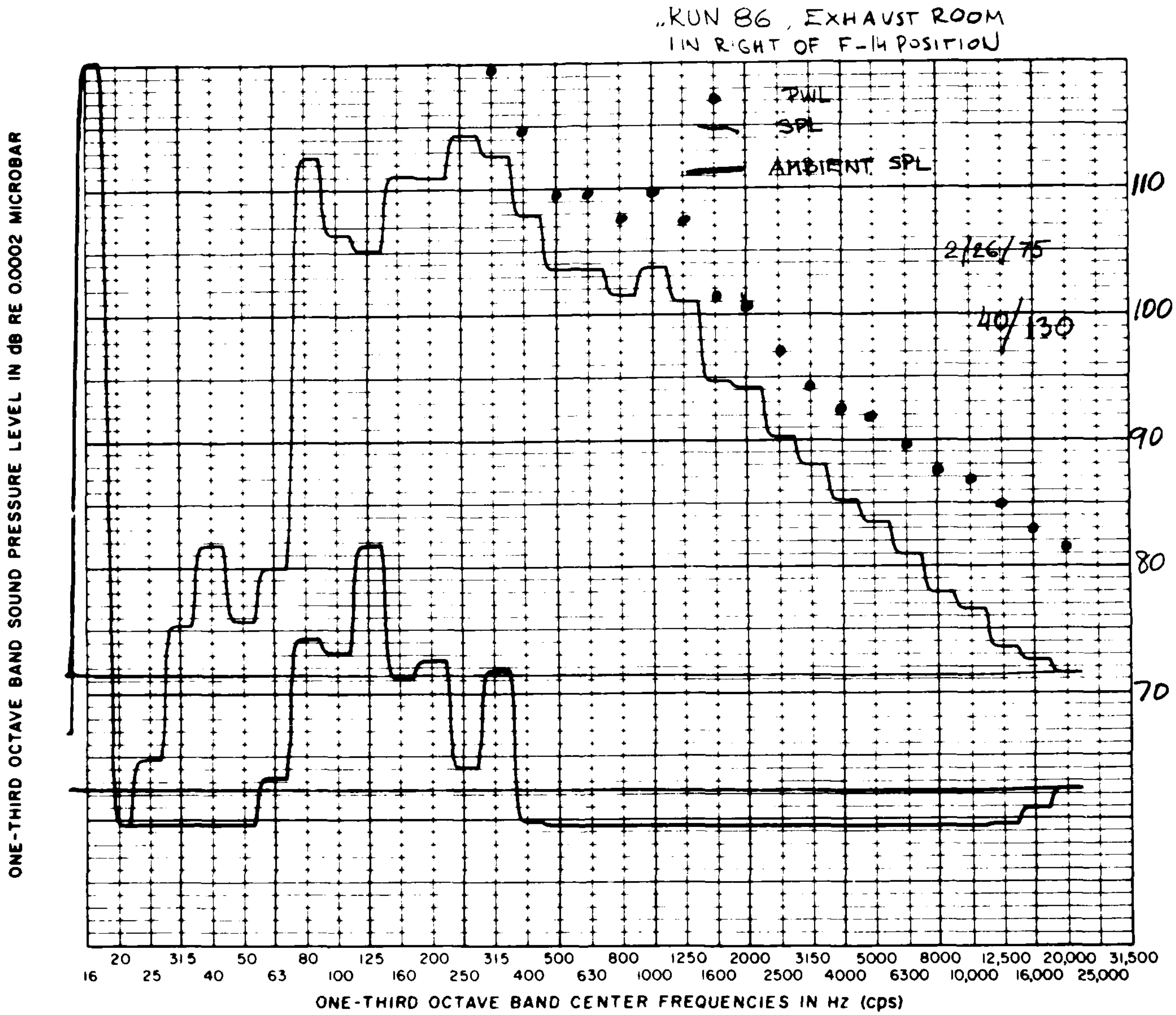

FIG. 5.2.2. EXAMPLE FOR THE RAW DATA PLOTTED PROVIDED BY THE REAL-TIME ANALYZER AND X-Y PLOTTER.

- Initial reverberation room checkout
- Measurement of noise reduction of the dividing wall between rooms
- Measurement of no-flow attenuation of the lined [illegible] using loudspeaker excitation.

The microphone traverses were controlled at a panel located next to the tape recorder. The panel had switches to start, stop, and reverse the microphones as well as lights that indicated the position of each microphone. This set-up allowed announcement of microphone start and stop times on the cue channel of the tape recorder, thus enabling GR 1921 signal integration to begin at the proper time during playback.

The uncertainty of any single measurement of room-average sound pressure level is estimated to have a standard deviation of 1.5 dB at 500 Hz and below, 0.5 dB between 630 and 10,000 Hz, and 1 dB at 12,500 Hz and above.

6.0 DATA ANALYSIS PROCEDURES

The methods used in analyzing the test data are discussed in this section and the data reduction equations listed.

6.1 Jet Nozzle Pressure Ratio, Total Temperature, and Mass Flow Rate

These three quantities, the jet nozzle pressure ratio, λ_N, jet nozzle inlet total temperature, T_{T_N}, and jet nozzle mass flow rate, W_N, are derived from the following five measurements:

Jet nozzle inlet total pressure, P_{T_N}.

Primary air meter inlet total pressure, $P_{T_{AM}}$.

Pilot air meter inlet total pressure, $P_{T_{PM}}$.

Ambient pressure, P_{amb}.

Primary air meter inlet total temperature, $T_{T_{AM}}$.

Jet nozzle pressure ratio is simply the ratio of jet nozzle inlet total pressure to ambient pressure

$$\lambda_N = \frac{P_{T_N}}{P_{amb}} . \qquad \text{(eqn. 6.1.1)}$$

Jet total temperature requires a more complicated relationship. If one neglects the fuel flow (which is relatively small compared to the air flow), assumes that the resulting air flow acts as a perfect gas and assumes continuity between the air meters and jet nozzle throat one develops the following relationship between pressures and temperatures

$$\underset{\text{jet nozzle}}{\frac{P_{T_N} \times A_{NT}}{\sqrt{T_{T_N}}}} = \underset{\text{primary air meter}}{\frac{P_{T_{AM}} \times A_{AM}}{\sqrt{T_{T_{AM}}}}} + \underset{\text{pilot air meter}}{\frac{P_{T_{PM}} \times A_{PM}}{\sqrt{T_{T_{PM}}}}}$$

then assuming that the primary and pilot air meter total temperatures are equal ($T_{T_{PM}} = T_{T_{AM}}$) and introducing the fact that the pilot meter throat area is 6.9% of the primary air meter throat area one derives the following equation which is correct for non-combustion flow conditions.

$$\frac{T_{T_N}}{T_{T_{AM}}} = \left[\frac{A_{NT}}{A_{AM}} \times \frac{P_{T_N}}{\left(P_{T_{AM}} + 0.069\ P_{T_{PM}}\right)} \right]^2$$

For our data reduction process, the presence of the fuel flow at each temperature and the affect of combustion on the nozzle exhaust gas properties were taken into account and the curve shown in Figure 6.1-1 developed. This curve was programmed into our time-sharing computer for data reduction purposes, giving

$$T_{T_N} = T_{T_{AM}} \times \left| \frac{T_{T_N}}{T_{AM}} \right| \doteqdot T_{T_{AM}} \times f \left(\frac{P_{T_N}}{P_{T_{AM}} + 0.069\ P_{T_{AM}}} \right) \quad \text{Fig. 6.1-1}$$

(eqn 6.1.2)

For calculating the total jet nozzle mass flow rate, W_N, the mass flow of the choked primary plus pilot air meters was corrected for the theoretical fuel flow required to give the ratio of T_{T_N}/T_{AM} calculated above (Figure 6.1-2). Again, it was assumed that $T_{T_{PM}} = T_{T_{AM}}$ and that the discharge coefficients of the primary and pilot meters are equal.

$$W_N = \left(0.532 \times \frac{C_{D_{AM}} \times P_{T_{AM}} \times A_{AM}}{\sqrt{T_{T_{AM}}}} + 0.532 \times \frac{C_{D_{PM}} \times P_{T_{PM}} \times A_{PM}}{\sqrt{T_{T_{AM}}}} \right) \left(1 + \frac{\dot{W}_{fuel}}{W_{air\ meters}}\right)$$

$$= \frac{0.532 \cdot C_{D_{AM}} \times A_{AM}}{\sqrt{T_{T_M}}} \left(P_{T_{AM}} + 0.69\ P_{T_{PM}} \right)\ f \left(\frac{T_{T_N}}{T_{T_{AM}}} \right) \quad \text{Fig. 6.1-2}$$

(eqn 6.1.3)

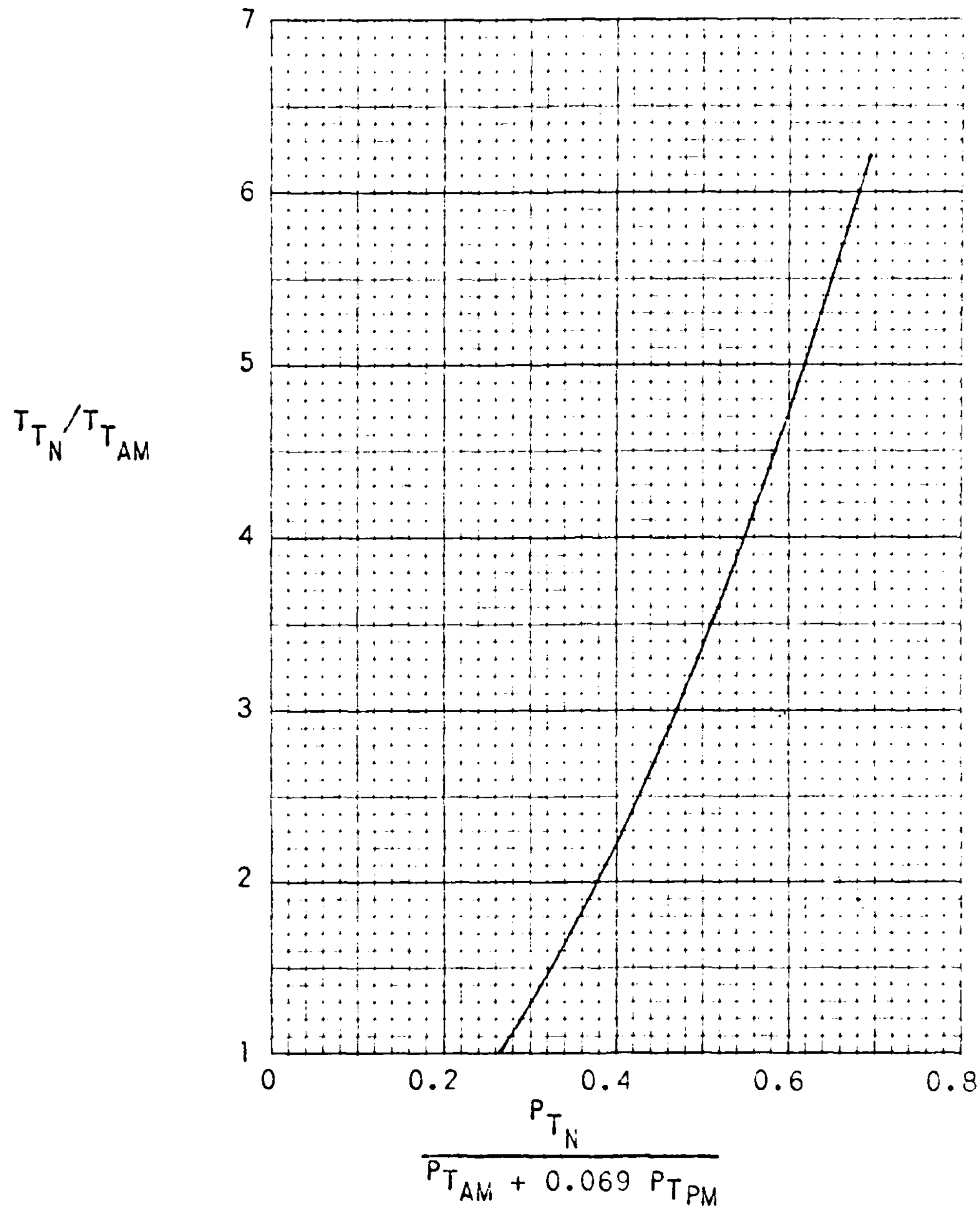

FIGURE 6.1-1. CALCULATED RELATIONSHIP BETWEEN BURNER COMBUSTION TEMPERATURE TO PRIMARY AIR METER TOTAL TEMPERATURE RATIO AND MEASURED JET NOZZLE AND METER TOTAL PRESSURES.

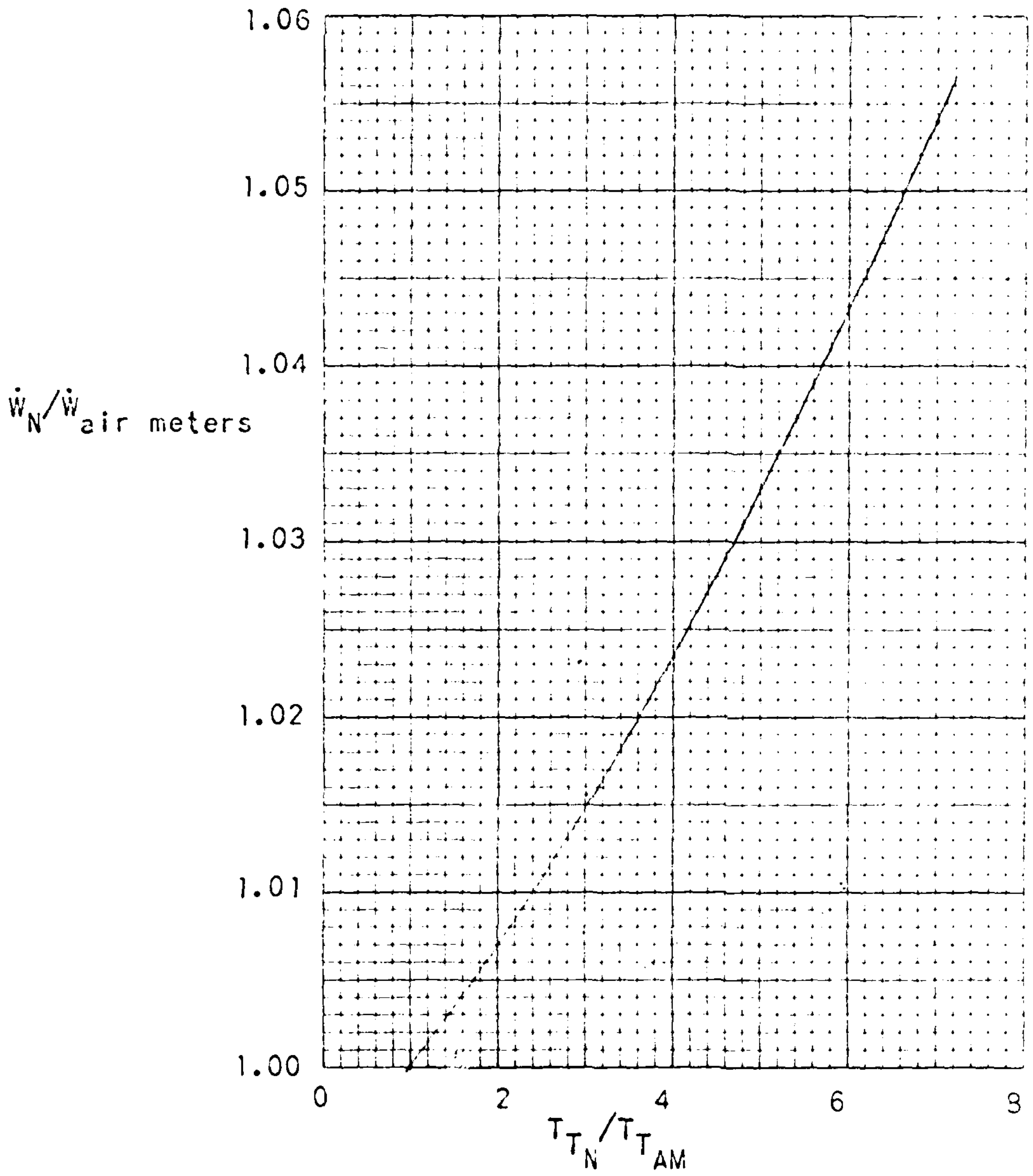

FIGURE 6.1-2. CALCULATED CORRECTION TO THE JET NOZZLE MASS FLOW FOR FUEL FLOW.

The computer program used in calculating jet nozzle pressure ratio, λ_N, jet nozzle total temperature, T_{T_N}, jet nozzle mass flow rate, $\dot{W}_N$, and the following quantities of secondary air flow rate and augmentation ratio parameter are included in the separate Data Appendix under the program title "Mass Flow Data - Project 1019," along with the computer printouts of the calculated results.

6.2 Pumped Air Flow Rate and Augmentation Ratio Parameter

Measurement of augmenter pumping performance was a prime objective of this test program. To accomplish this, a venturi meter with a contoured approach was installed in the ceiling of the burner enclosure and instrumented as follows:

Secondary air meter inlet total pressure, $P_{T_{SM}}$.

Secondary air meter throat static pressure, P_{SM}.

Secondary air meter total temperature, $T_{T_{SM}}$.

The secondary, or pumped, air flow rate, $\dot{W}_{pumped}$, was calculated directly from these measurements

$$\dot{W}_{pumped}\ (WS) = \frac{0.532 \times C_{D_{SM}} \times P_{T_{SM}} \times A_{SM}}{\sqrt{T_{T_{SM}}} \times \left(\frac{A}{A^*}\right)_{M_{sec,\ meter}}} \qquad \text{(eqn 6.2.1)}$$

where: $$\left(\frac{A}{A^*}\right)_{M_{sec.\ meter}} = f\left(\frac{P_{SM}}{P_{T_{SM}}}\right)$$

and can be explicitly defined using compressible flow relationships.

An augmentation ratio parameter, ARP, has been defined as follows:

$$ARP = \frac{\dot{W}_{pumped}}{\dot{W}_N} \times \sqrt{\frac{T_{T_{amb}}}{T_{T_N}} \times \frac{mw_N}{mw_{air}}} \qquad \text{(eqn 6.2.2)}$$

where: $\dfrac{\dot{W}_{pumped}}{\dot{W}_N}$ = augmentation ratio .

The augmentation ratio parameter is formed from the augmentation ratio by multiplying each flow rate by its corresponding $\sqrt{T_T/mw}$. For a given geometry, etc., the augmentation ratio parameter is, therefore, proportional to the ratio of pumped flow momentum flux to primary (nozzle) flow momentum flux.

In this relationship, the pumped flow corresponds to outside, ambient temperature air which passes through the Hush House. If the above expression for $\dot{W}_{pumped}$ is put in a slightly approximate but more basic form

$$\dot{W}_{pumped} = \frac{K \times \sqrt{mw_{air}} \times C_{D_{SM}} \times P_{T_{SM}} \times A_{SM}}{\sqrt{T_{T_{SM}}} \times \left(\frac{A}{A*}\right)_{M_{sec.\ meter}}}$$

and a similar approximate equation for the jet nozzle mass flow is introduced

$$\dot{W}_N = \frac{K \times \sqrt{mw_N} \times C_{D_N} \times P_{T_N} \times A_{NT}}{\sqrt{T_{T_N}}}$$

and, in addition, it is assumed that the burner enclosure temperature which corresponds to T_{amb} is equal to the secondary air meter total temperature, $T_{T_{SM}}$, and the throat discharge coefficients of the meter and nozzle are equal, the following simple equation develops for deriving ARP from the test data:

$$ARP = \frac{P_{T_{SM}} \times A_{SM}}{P_{T_N} \times A_{NT} \times \left(\frac{A}{A*}\right)_{M_{sec.\ meter}}} = \frac{41}{(A/A*)_{M_{sec.\ meter}}} \times \left(\frac{P_{T_{SM}}}{P_{T_N}}\right) \quad \text{(eqn 6.2.3)}$$

During the testing, the difference between secondary meter total temperature and burner enclosure temperature $(T_{amb.})$ was typically 10°F which would introduce an error of only 1% in ARP.

6.3 Pressure Data Reduction

After conversion from gauge or manometer readings to absolute pressures, the model pressure data were reduced in two different ways: 1) to the ratio of measured pressure to reference ambient pressure, and 2) to a pressure parameter. The ratio is formed as follows:

$$\frac{P}{P_{amb.}} = \frac{P}{P_{EE\ (exhaust\ enclosure)}} \quad . \qquad \text{(eqn 6.3.1)}$$

This form was used throughout the data presentation. The following pressure parameter has some value in the presentation of jet mixing data (where $P = P_{T_{rake}}$) and it appears on the computer printouts in the Data Appendix, but it was not used in the data presentation of this report.

$$P_P = \frac{P - P_{amb.}}{P_{T_N} - P_{amb.}} = \frac{P - P_{EE}}{P_{T_N} - P_{EE}} \quad . \qquad \text{(eqn 6.3.2)}$$

The computer program used to calculate these quantities from the raw test data are included in the separate Data Appendix under the title, "Pressure Data Program - Project 1019."

A special parameter was defined for the jet nozzle base pressure to show how the base pressure would be influenced by Hush House operation.

$$P_{NB_p} = \frac{(P_{NB} - P_{interior})_{\underline{hush\ house}} - (P_{NB} - P_{amb})_{\underline{free\ field}}}{P_{amb}} \qquad \text{(full scale)}$$

(eqn 6.3.3)

$$= \frac{(P_{NB} - P_{BE})_{\underline{with\ augmenter}} - (P_{NB} - P_{EE})_{\underline{jet\ survey}}}{P_{EE}} \qquad \text{(model)}$$

(eqn 6.3.4)

6.4 Temperature Data Reduction

All model temperatures were reduced to the following temperature parameter:

$$T_p = \frac{T - T_{amb}}{T_{T_N} - T_{amb}} = \frac{T - T_{BE} \text{ (burner enclosure)}}{T_{T_N} - T_{BE}} \qquad \text{(eqn 6.4.4)}$$

This parameter is useful because, for jet mixing cases, the value of this parameter at a particular location does not change much with T_{T_N}, which gives results expressed in this form a degree of applicability not characteristic of simple temperature ratios such as T/T_{amb}.

The computer program used to calculate this temperature parameter is included in the separate Data Appendix under the title, "Temperature Data - Project 1019," along with the calculated results printout.

6.5 Analysis of Acoustic Data

The objective of the acoustical measurements was to obtain sound power level spectra for a scale model that could be used to predict the jet exhaust noise in the interior and exterior of the full-scale Hush House. Two reverberation rooms were designed for this purpose — one for the burner and one for the exhaust. (See Sec. 3.) Sound power levels measured in the burner room corresponded to the full-scale sound power levels that would be emitted by the engine exhaust into the Hush House interior, and sound power levels measured in the exhaust room corresponded to full-scale jet exhaust sound power that would radiate from the downstream end of the full-scale augmenter. Sound power levels were measured in the 400 Hz to 16 kHz 1/3-octave bands, which correspond approximately to full-scale 1/3-octave bands from 31.5 to 1000 Hz. Sound power levels estimated for the 1/3-octave bands adjacent to the upper and lower ends of the spectrum (20,000 and 315 Hz, respectively) were also analyzed for comparison.

6.5.1 Measurement of sound power level

The sound power radiated by a source may be measured in a reverberation chamber in two ways: (1) by the absolute method and (2) by the comparison method. Both methods require measuring the room-average sound pressure level ($\overline{SPL}$) in the reverberation room with the noise source operating. The methods differ, however, in the conversion of $\overline{SPL}$ to sound power level (PWL).

In the absolute method, the absorption coefficient is measured (indirectly by measuring room reverberation time) and the PWL is calculated using the following equation:

$$PWL = \overline{SPL} + 10 \log \frac{Vol}{T_{60}} - 13.5 \text{ dB re } 10^{-12} \text{ Watt} \quad , \qquad (5.5.1)$$

where

PWL = sound power level in dB re 10^{-12} Watt

Vol = room volume in m^3

T_{60} = time in sec for SPL in a room to decay 60 dB

$\overline{SPL}$ = room-average sound pressure level in dB re 0.0002 μbar measured in identical room conditions as for the T_{60} measurement.

In the comparison method, the room-average SPL, measured with the unknown source operating, is compared with the room-average SPL measured when a reference sound source of known sound power output is operating. Then,

$$PWL = PWL' + (\overline{SPL} - \overline{SPL}') \text{ dB re } 10^{-12} \text{ Watt} \quad , \qquad (6.5.2)$$

where

PWL' = sound power level of the reference source,

$\overline{SPL}'$ = room-average sound pressure level produced by the reference source, and

$\overline{SPL}$ = room-average sound pressure level produced by the unknown source.

For our measurements in the reverberation rooms of the model Hush House project, we used the absolute method to measure the PWL' of an ILG fan and then measured the sound power of the jet by the comparison method, with the ILG source as the *reference*. Table 6.5.1 gives reverberation times, T_{60}, measured during calibration of the ILG, and the calculations of PWL for each 1/3-octave band for each of the reverberation rooms.

TABLE 6.5.1. CALIBRATION OF THE REFERENCE SOURCE (ILG FAN)

1/3-Octave Band Center Frequency, Hz	BURNER ROOM		EXHAUST ROOM	
	Reverberation Time T_{60}, sec	ILG PWL', dB re 10^{-12} Watt	Reverberation Time T_{60}, sec	ILG PWL', dB re 10^{-12} Watt
400	1.6	76	2.0	77
500	1.6	76	2.1	77
630	1.6	75	2.1	77
800	1.8	75	2.1	77
1000	1.8	75	2.0	77
1250	1.8	76	1.9	78
1600	1.6	76	1.7	77
2000	1.4	76	1.6	77
2500	1.2	75	1.5	76
3150	1.1	75	1.5	75
4000	1.0	74	1.4	75
5000	.9	74	1.3	75
6300	.8	73	1.2	75
8000	.7	73	1.1	74
10000	.6	69	1.1	69
12500	.6	65	1.0	66
16000	.5	62	1.0	63

We chose the comparison method because, once the reference source was calibrated, PWL calculations could be made significantly faster. In addition, determining the $\overline{SPL}'$ of the reference source immediately after the jet was shut down enabled us to account automatically for effects of the changed temperature in the exhaust room on the $\overline{SPL}$ measured during the jet runs.

For each of the 139 jet runs in the test program, jet sound power level was calculated by the following process:

1. Signals from microphones in each room were tape-recorded first with the jet running and then with the ILG running.

2. The tape-recorded signals were played back and analyzed to find jet $\overline{SPL}$ and $\overline{SPL}'$ in each room.

3. $\overline{SPL}'$ was subtracted from ILG PWL' yielding a difference (ΔdB) for each 1/3-octave band from 315 to 20,000 Hz for each room.

4. ΔdB was added to jet $\overline{SPL}$, yielding jet PWL in each 1/3-octave band in each room.

The ILG was not operated in the burner room after each run; when it was not, $\overline{SPL}'$ in the burner room was used from another run with similar temperature and humidity.

6.5.2 Reverberation room checkout

A second reason for measuring reverberation times in the two rooms was to ensure that they actually were reverberation chambers – i.e., that the reverberation times were sufficiently long. The data in Table 6.5.1 show that reverberation times in both rooms were adequate and indicate that the sound fields were sufficiently reverberant to allow accurate calculation of sound power level.

An estimate of the accuracy of measurement of the room-average sound pressure level was obtained using the same microphone traverse and electronic instrumentation as was used during the jet runs (excluding the tape recorder). This procedure is outlined in Ref. A-2, which specifies procedures for "qualifying" a reverberation room for the measurement of broadband sound. (A jet exhaust generates broadband sound.) Room-average SPL was measured using the traversing microphone, with the ILG source placed at eight different locations, resulting in eight values of $\overline{SPL}$ in each 1/3-octave band. The standard deviation of the eight values of SPL (Table 6.5.2) gives an indication of the accuracy of a single measurement of $\overline{SPL}$ of a distributed broadband sound source.

6.5.3 Assessment of flanking noise sources

In addition to the noise sources we wanted to measure in each room, there were several potential contaminating sources *from which* unwanted noise could have entered each room by flanking paths and could have contributed to the total sound power measured. Precautions were taken to assure that noise from these flanking sources did not interfere with our measurements. Figure 6.5.1 shows schematically the flanking noise sources and paths in each room. Ws in this figure indicate acoustic power emitted by noise sources, and $\overline{SPL}_1$ and $\overline{SPL}_2$ represent the room-average sound pressure levels in the two rooms.

Sources and flanking paths in the *former room* in Fig. 6.5.1 are:

1. W_1 is the power from the source we desire to measure – i.e., the power radiated from the jet near the nozzle plus the power radiated from the upstream end of the augmenter. Thus, it would be desirable that only W_1 contribute to $\overline{SPL}_1$.

TABLE 6.5.2. ACCURACY OF MEASUREMENT OF BROADBAND SOUND

1/3-Octave Band Center Frequency, Hz	Standard Deviation of 8 Values of $\overline{SPL}$ Using ILG Source, dB	
	Burner Room	Exhaust Room
400	1.03	1.23
500	1.53	.91
630	.55	.45
800	.44	.29
1000	.31	.44
1250	.25	.48
1600	.40	.35
2000	.39	.35
2500	.42	.30
3150	.31	.33
4000	.47	.29
5000	.45	.30
6300	.59	.23
8000	.42	.46
10000	.55	.32
12500	.72	.30
16000	.67	.35

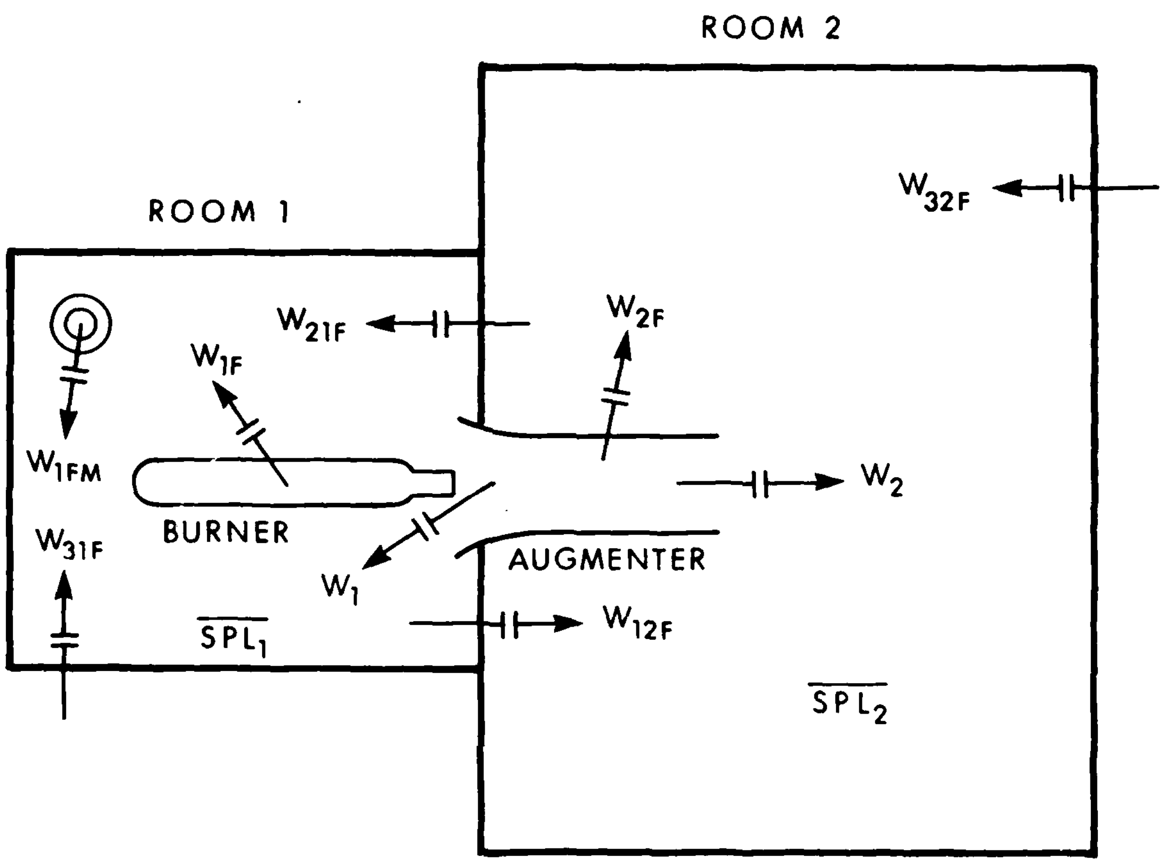

FIG. 6.5.1. FLANKING NOISE SOURCES AND FLANKING PATHS.

2. W_{1F} represents the acoustic power generated by the burner fuel and air supply hoses and manifolds. W_{1F} was measured during the jet survey series when the jet nozzle was completely in the exhaust room. W_{1F} was compared with the measured power in the burner room during later series of runs and was never found to affect burner-room noise levels.

3. W_{1FM} is the power generated by flow through the secondary-air flow meter. This was not measured, but calculations of noise generated by the flow of air through the meter, the speed of which was accurately measured, showed that this source generated noise levels very much lower than the levels measured in the burner room.

4. W_{21F}, the acoustic power propagating through the dividing wall from the exhaust room into the burner room, was calculated by subtraction of a correction, NR_{21} in dB, from the measured noise level in the exhaust room. NR_{21} was measured, in each 1/3-octave band, by placing a high-power loudspeaker in the exhaust room and measuring $\overline{SPL}_2$ in the exhaust room and $\overline{SPL}_1$ in the burner room (using the same microphone traverse as for the jet runs); then $NR_{21} = \overline{SPL}_2 - \overline{SPL}_1$ in each band. W_{21F} was never found to affect W_1.

5. W_{31F}, the power generated by external noise sources, is the cause of "background" noise in the *burner room*. Background noise in the burner room was measured at frequent intervals (after approximately every fourth jet run and after approximately every second ILG run). Neither jet noise nor ILG noise was affected by W_{31F}.

Sources and flanking paths in the *exhaust room* in Fig. 6.5.1 are:

1. W_2, the acoustic power emitted from the downstream end of the augmenter, is the sum of the jet sound power which has been attenuated by aeroacoustic effects and by the augmenter lining. It was necessary to verify that only W_2 contributed to the measured $\overline{SPL}_2$ in the exhaust room.

2. W_{2F} is the acoustic power transmitted through the walls of the augmenter. While W_{2F} will be a real source in a full-scale Hush House, no attempt was made to scale model the augmenter tube wall structure acoustically, and since the goal was to measure only W_2, it was desired to suppress W_{2F}. Calculations were made which showed that W_{2F} would be a possible contaminant only during jet runs in which acoustic absorbing material was placed near the downstream end of the augmenter – for example, during the tests of the stack with baffles and with the 12-in. lined augmenter section at the downstream end of the augmenter. For these tests, the exterior of the augmenter shell was wrapped with acoustical insulation consisting of approximately 3-in.-thick glass fiber material covered with lead-aluminum sheet weighing approximately 1 lb/ft^2. As a precaution, this same wrapping was applied to the outside shell of the augmenter for all tests of the lined obround augmenter.

3. W_{12F} is the acoustic power transmitted through the wall dividing the burner room and the exhaust room. This source was a potential problem during runs with a fully lined obround augmenter, when W_2 was significantly less than W_1. W_{12F} was calculated by subtracting a correction, NR'_{12} from the measured $\overline{SPL}_1$. $NR'_{12} = NR_{12} + \Delta NR$, where NR_{12} was measured by placing a loudspeaker in the burner room and ΔNR is an estimate correction term, for high frequencies, which accounted for the fact that noise reduction between the two rooms was greater with

flow (i.e., with the jet running) than without flow because of the refraction of sound rays into the acoustic lining of the augmenter. (Of course, NR was measured with the jet off.) Thus, the W_{12F} caused an $\overline{SPL}_{12F}$ in the exhaust room given by

$$\overline{SPL}_{12F} = \overline{SPL}_1 - NR'_{12} \quad .$$

In all cases, $\overline{SPL}_{12F}$ was sufficiently less than $\overline{SPL}_2$. Accordingly, it was verified that W_{12F} did not contribute to $\overline{SPL}_2$.

4. W_{32F} is the acoustic power generated in the exhaust room by external noise sources. As was the case in the burner room, background noise levels were frequently measured. A form of W_{32F}, electrical noise in the tape record-playback system, was the only background noise found to be a problem. This noise was encountered only during jet runs with a fully lined augmenter and was caused by the fact that the dynamic range of the acoustic spectrum in the exhaust room exceeded the available dynamic range of the tape record-playback system. The reason for the large dynamic range of the noise in the exhaust room was that the attenuation of the lined augmenter was significantly higher at high that at low frequencies; thus, the jet noise in the exhaust room had much higher SPLs at low frequencies that at high frequencies. The problem was solved by artificially reducing the dynamic range of the electrical signal into the tape recorder to an amount that the record-playback system could tolerate without adding noise of its own. This was accomplished by passing the input signal to the recorder through a high-pass electrical filter (i.e., attenuating the low frequencies while leaving the high frequencies unaffected). During playback and analysis,

this attenuation was added back in, using the individually variable gains on the 1/3-octave filters in the GR Model 1925 Filter Set (a component of the GR 1921 Real-Time Analyzer) to achieve an overall flat frequency response in the record-playback-analysis system. In this way, electrical noise was decreased, and no background noise affected $\overline{SPL}_2$.

7.0 PRESENTATION OF RESULTS

Reduced test data from the model test program are presented and discussed in this section of the report. To facilitate an orderly, digestible presentation, not all of the test data are presented here. For a complete tabulation of all test data, refer to the Data Appendix.

7.1 Augmenter Pumping Performance

Accurate measurement of augmenter pumping performance was one of the principal goals of this test program. Adequate augmenter pumping is essential in a full scale, dry cooled installation to lower the exhaust temperature and, thereby, protect the exhaust acoustic treatment. To maintain a mixed exhaust temperature of 800°F (1260°R) while running with an afterburning engine on a 100°F (560°R) day requires that the jet exhaust pump a cooling air flow rate equal to 5.30 times the jet exhaust flow rate. A number of references contain ejector pumping information which might be used to predict pumping performance for a dry cooled augmenter. References A/T-4, 5 and 6 contain pumping information covering a variety of configurations and test conditions. They have the disadvantage of being limited to fairly high augmenter pressure rise, relatively low pumping ratio and low augmenter cross-section to nozzle throat area ratio cases. Reference A/T-7 contains data relating directly to the case of interest, but the jet nozzle total temperature equals ambient temperature for all of the tests and very little information relating pumping performance to augmenter pressure rise is present. Nevertheless, the data in these references indicates that mass flow ratios of six or over are feasible for a properly sized augmenter.

To facilitate correlation of augmenter pumping data, the test data from this program have been reduced to an augmentation ratio parameter, ARP, defined as follows:

$$ARP = \frac{\dot{W}_{pumped}}{\dot{W}_N} \times \sqrt{\frac{T_{amb}}{T_{T_N}} \times \frac{mw_N}{mw_{air}}} \quad .$$

This definition ratios the equivalent pumped and primary flow momentum fluxes. It has the advantage of being primarily configuration oriented, having only a weak sensitivity to the temperature ratio, $^{T}T_N/T_{amb}$. The augmentation ratio parameter corresponding to the mass flow ratio of 5.30, mentioned above as necessary to give $T_{mix} = 800°F$ on a 100°F day with afterburning, would be ARP ~ 1.83.

Figure 7.1-1 contains a summary of augmenter pumping performance wherein the augmentation ratio parameter, ARP, is plotted versus jet nozzle to ambient temperature ratio, $^{T}T_N/T_{amb}$, for a number of selected test configurations at an augmenter length diameter ratio of nominally 6.0. Pumping performance for each test configuration is included in the test program summary, Table 2.0-1. Considering the afterburning case on a 100°F day ($^{T}T_N/T_{amb} = 6.6$) one observes in Figure 7.1-1 that an ARP of 1.83 is obtainable, even without a subsonic diffuser, if the augmenter cross-section to jet nozzle throat area ratio, A_A/A_{NT}, is made large enough . It is also apparent that a subsonic diffuser on the downstream end of the augmenter increases pumping, whereas changing from a round to an AR = 1.7 obround cross-section reduces pumping. Pumping performance does not appear to be sensitive to jet nozzle pressure ratio, λ_N.

The consistent drop in augmentation ratio parameter with increasing jet nozzle to ambient temperature ratio, $^{T}T_N/T_{amb}$ shown in Figure 7.1-1, is of particular interest. While it is a secondary effect, it is nevertheless, larger than might have been expected on the basis of typical ejector performance data and is probably related to the low loss, high augmentation ratio situation which is characteristic of dry cooled augmenter installations. At high jet nozzle to ambient temperature ratios, there is a significant exchange of heat from the jet flow to the pumped flow in the mixing region. This increases the volume flow of the pumped flow and requires that it accelerate, producing an additional pressure drop, which must be overcome by the jet momentum, and a resulting drop in pumping performance. When the ejector situation corresponds to a lower augmentation ratio and a higher pumped flow pressure rise (higher loss), this additional pressure drop due to heat exchange is smaller relative to the

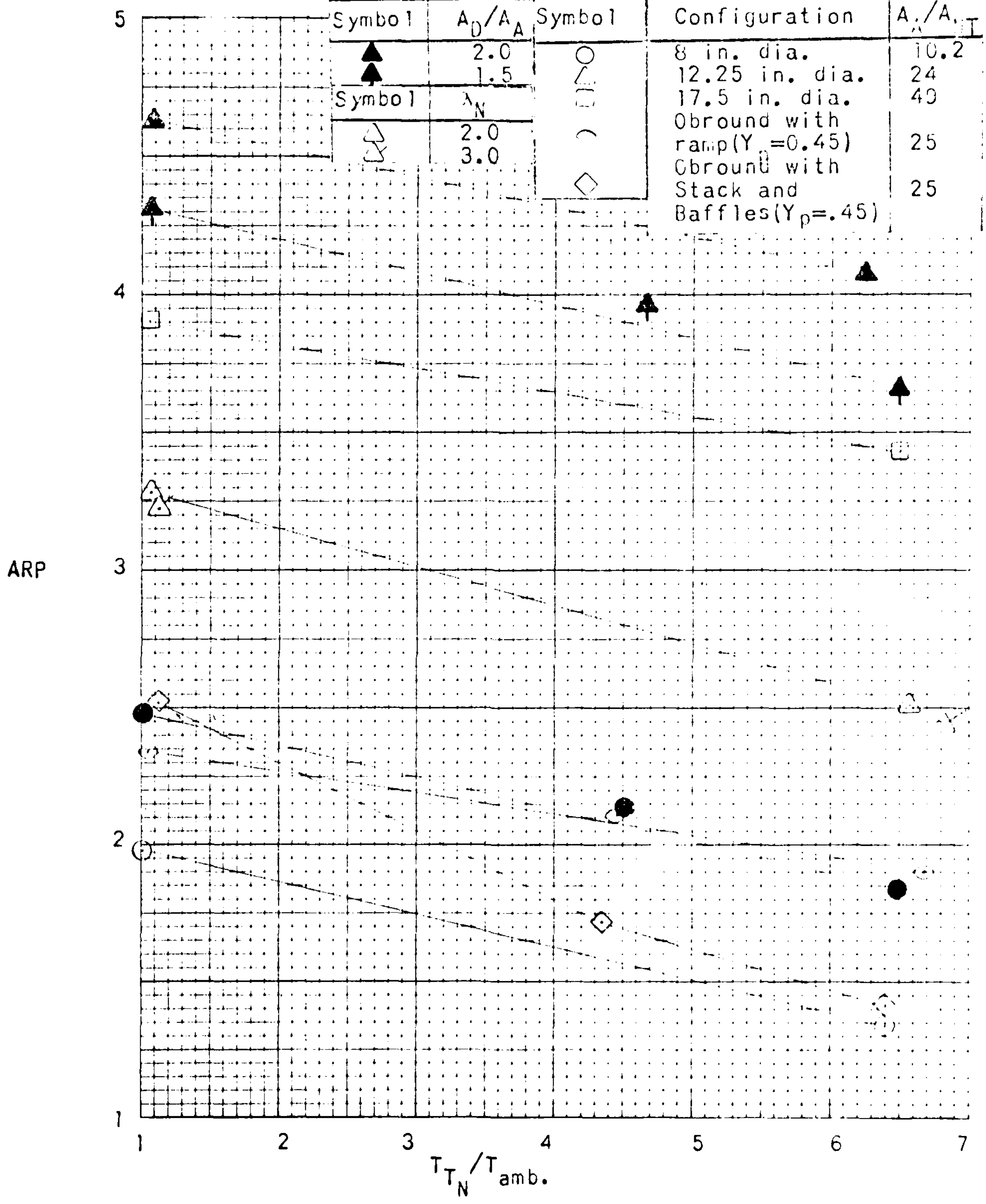

FIGURE 7.1-1. SUMMARY OF AUGMENTER PUMPING PERFORMANCE (AUGMENTATION RATIO PARAMETER, ARP, vs. T_{T_N}/T_{amb})(X_N/D_{NT}=1.6,L_A/D_{AM}=6)

overall pressure rise required and the drop in pumping performance is correspondingly less. Note that, although the augmentation ratio parameter decreases with increasing jet temperature to pumped flow temperature ratio, the augmentation ratio actually increases.

Augmenter length - diameter ratio is one of the geometric variables influencing pumping performance. Figures 7.1-2 (for cases without subsonic diffuser) and 7.1-3 (for cases with subsonic diffuser) present the pumping performance as a function of augmenter length-diameter ratio, L_A/D_A, over the range tested. Both figures show little change in pumping performance above $L_A/D_A = 6$, but some decrease in performance as L_A/D_A is reduced below 6. Although the ${}^{T}T_N/T_{amb} = 1.0$ (${}^{T}T_N = 500°R$) test results show better pumping performance than at higher ${}^{T}T_N$, they also exhibit a greater decrease in pumping as augmenter length-diameter ratio is reduced This probably arises because mixing progresses more rapidly with the higher gas viscosity associated with high jet temperature and so is closer to completion at any given distance from the nozzle exit. At ${}^{T}T_N/T_{amb} = 6.6$, the variation in pumping performance is no greater than 10% over the range of L_A/D_A values tested.

A comparison of the data in Figure 7.1-3 for an augmenter having an exit subsonic diffuser with the data taken without diffuser (Figure 7.1-2) shows an increase of roughly 50% in ARP due to the diffuser at ${}^{T}T_N/T_{amb} = 6.6$. A subsonic diffuser area ratio of 2.0 gave about 7% better pumping performance than one with $A_D/A_A = 1.5$.

During the tests with both the 12.25" round and the 15.5" x 9" obround augmenters, the jet nozzle exit was moved axially relative to the augmenter entrance from a point contiguous with the augmenter entrance to a point 18" (7.2 nozzle diameters) upstream of the entrance (Figure 7.1-4). No appreciable variation in pumping performance was experienced because the augmenter entrance area is 24 times larger than the jet nozzle throat area and jet capture is no problem within the X_N/D_{NT} range tested. The bulk of the test program was run with $X_N/D_{NT} = 1.6$. Moving the nozzle away from the augmenter entrance did have an appreciable influence on burner enclosure (Hush House interior) noise as is reported in Section 7.6.

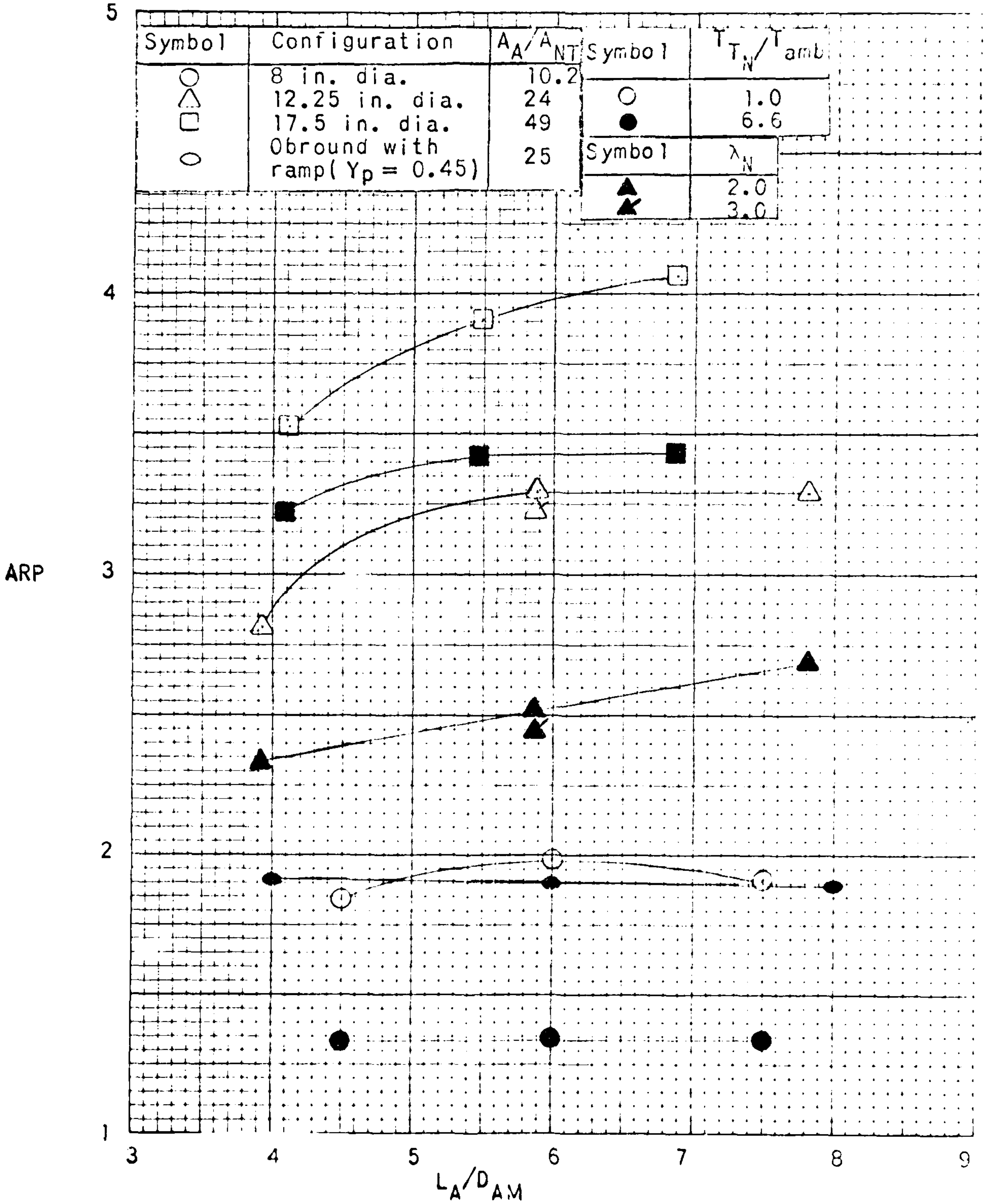

FIGURE 7.1-2. AUGMENTER PUMPING PERFORMANCE VS. AUGMENTER LENGTH-DIAMETER RATIO FOR CASES WITH NO EXIT SUBSONIC DIFFUSER.

(X_N/D_{NT} = 1.6)

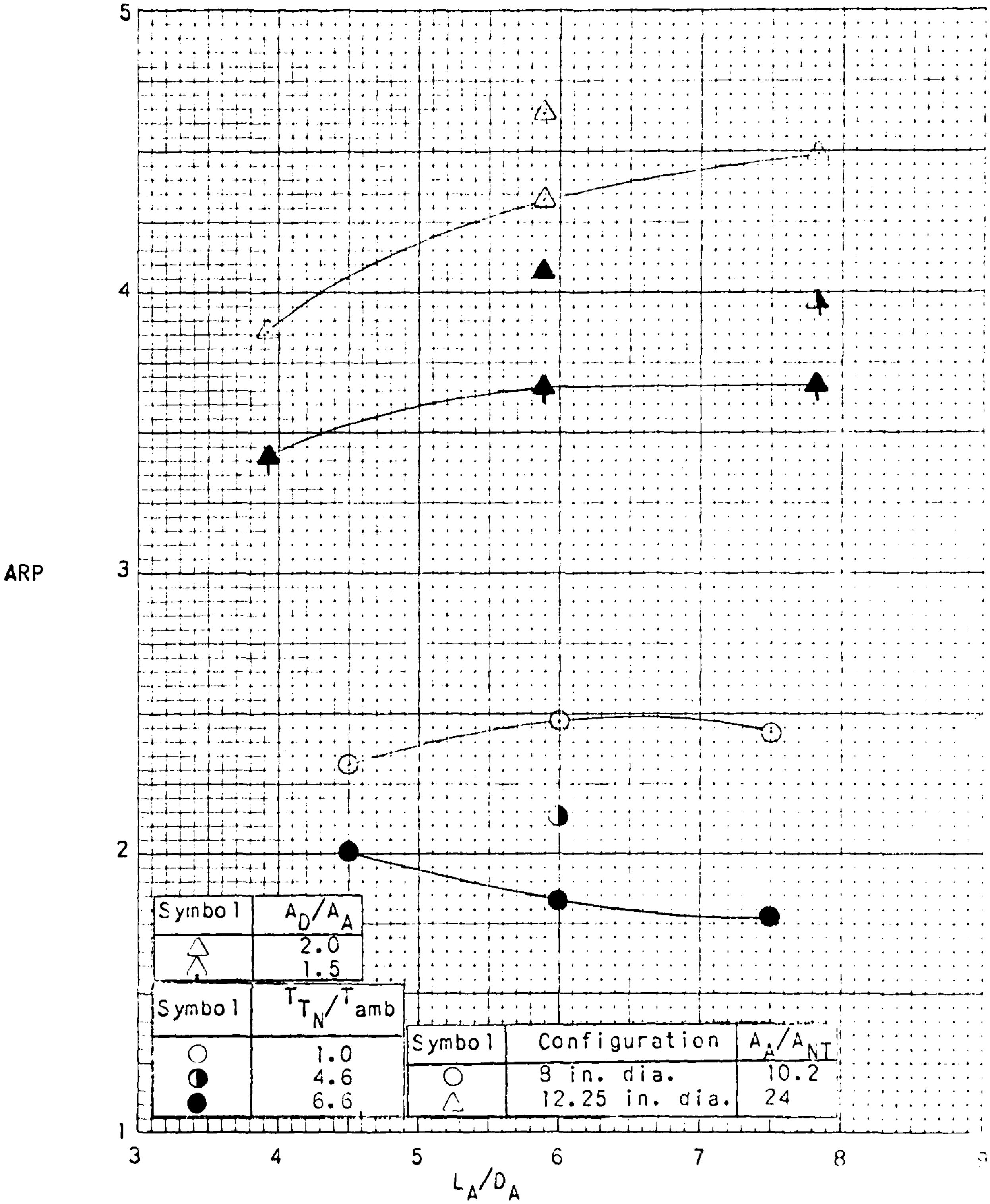

FIGURE 7.1-3. AUGMENTER PUMPING PERFORMANCE VS. AUGMENTER LENGTH-DIAMETER RATIO FOR CASES WITH EXIT SUBSONIC DIFFUSER

$(X_N/D_{NT} = 1.6)$

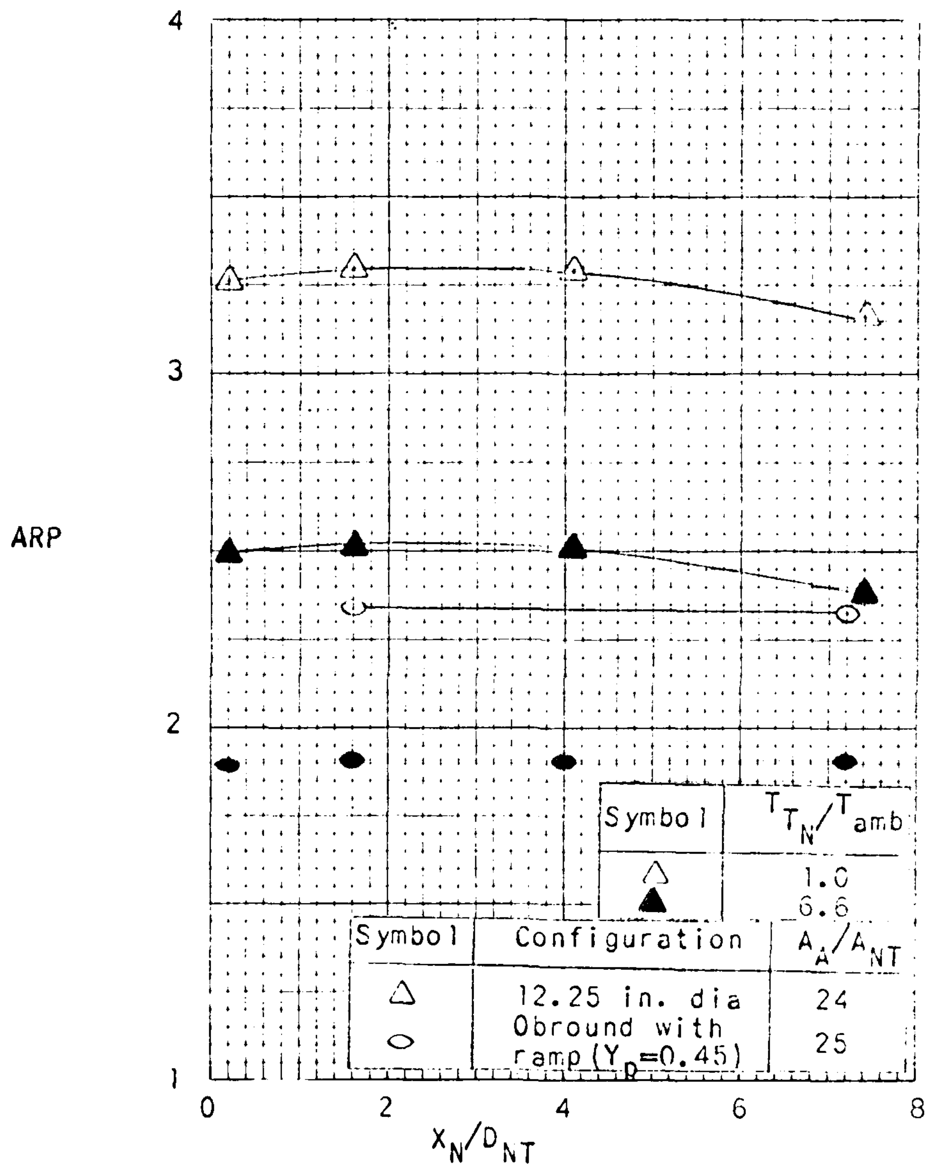

FIGURE 7.1-4. AUGMENTER PUMPING PERFORMANCE VS. JET NOZZLE EXIT TO AUGMENTER ENTRANCE SPACING PARAMETER.
$(A_A/A_{NT_{nom}}=25, L_A/D_{A\bar{M}}=6, \lambda_N=2)$

The augmenter entrance geometry was also varied with the 12.25" diameter round augmenter. Most runs were made with the standard, conical, augmenter entrance configuration, but runs were also made with a rounded entrance, a sharp edged entrance and with the conical entrance plus an inlet throttle (see Figure 4.2-1). These changes had relatively small influence on pumping performance, as shown by the tabulation below:

Inlet Configuration	ARP @ ${}^{T}T_N/T_{amb} = 1$	ARP @ ${}^{T}T_N/T_{amb} = 6.6$
conical	3.30	2.51
rounded	3.43	2.50
sharp-edged	3.02	2.34
conical plus throttle	3.05	2.41

The inlet throttle was also applied to the obround augmenter and at ${}^{T}T_N/T_{amb} = 6.6$ resulted in a drop in pumping performance of ARP = -0.15. The inlet throttle was tested because it was felt that, for many full-scale designs, an augmenter properly sized from jet impingement and noise standpoints might pump more than the required amount of cooling air unless throttled.

During the aero-thermal testing with the 15.5" x 9" obround augmenter, the jet centerline was moved laterally and vertically and also deflected relative to the augmenter centerline. The jet nozzle orientations and the obround cross-section both had a significant effect on pumping performance, as is shown in Figure 7.1-5. Changing from a round to an aspect ratio 1.7 obround cross-section resulted in a 10% decrease in pumping ratio parameter at ${}^{T}T_N/T_{amb} = 4.6$, $A_A/A_{NT} = 25$. Perhaps as much as half of this decrease is due to the porous, sound-absorbing liner which limits the rate of pressure rise. As the jet centerline was moved off the centerline of the augmenter or deflected a reduction in pumping performance occurred. The data point at $Y_P = 0.45$ and $\alpha_S = 1°$ corresponds to the F-14A configuration. Most of the data shown in Figure 7.1-5 were run with no augmenter exit ramp. One point from the acoustic testing is included to show the influence of the ramp on pumping performance.

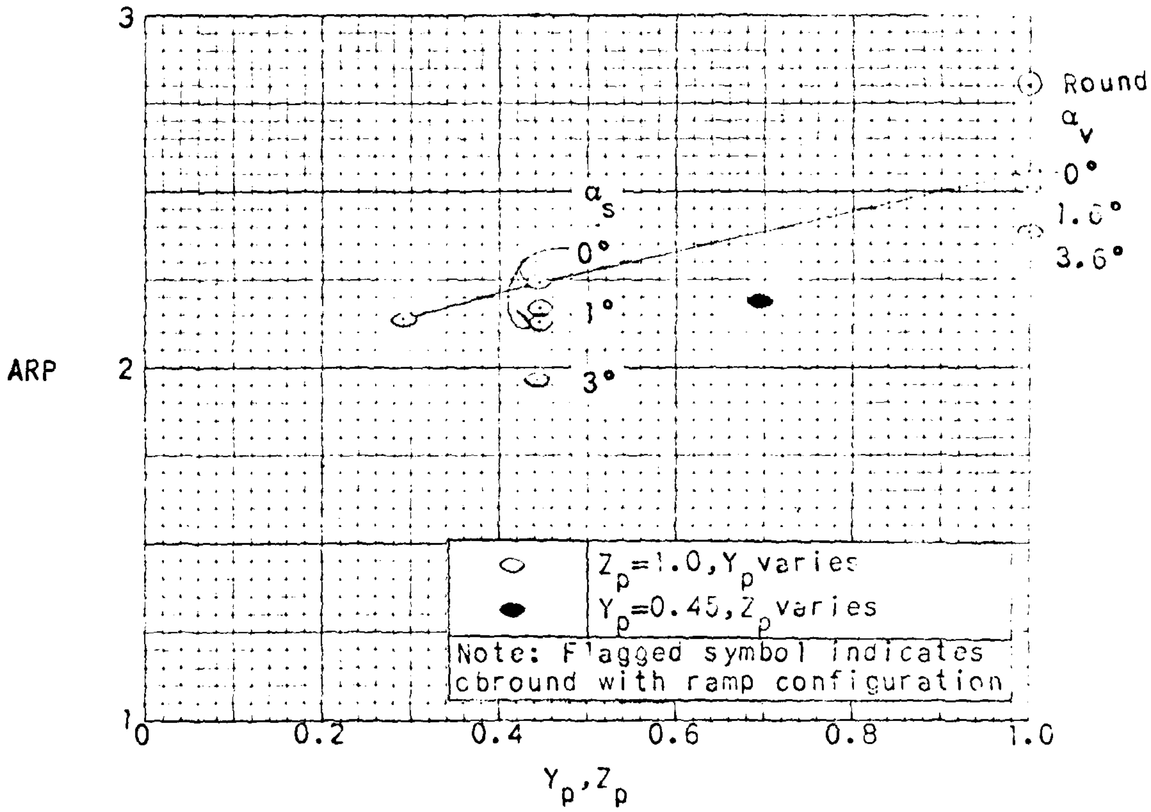

FIGURE 7.1-5. OBROUND AUGMENTER PUMPING PERFORMANCE WITH DIFFERENT NOZZLE POSITIONS AND INCLINATIONS (A_A/A_{NT}=25, X_N/D_{NT}=1.6, $L_A/D_{A\overline{M}}$=6, T_{T_N}/T_{amb}=4.6, λ_N=2.0)

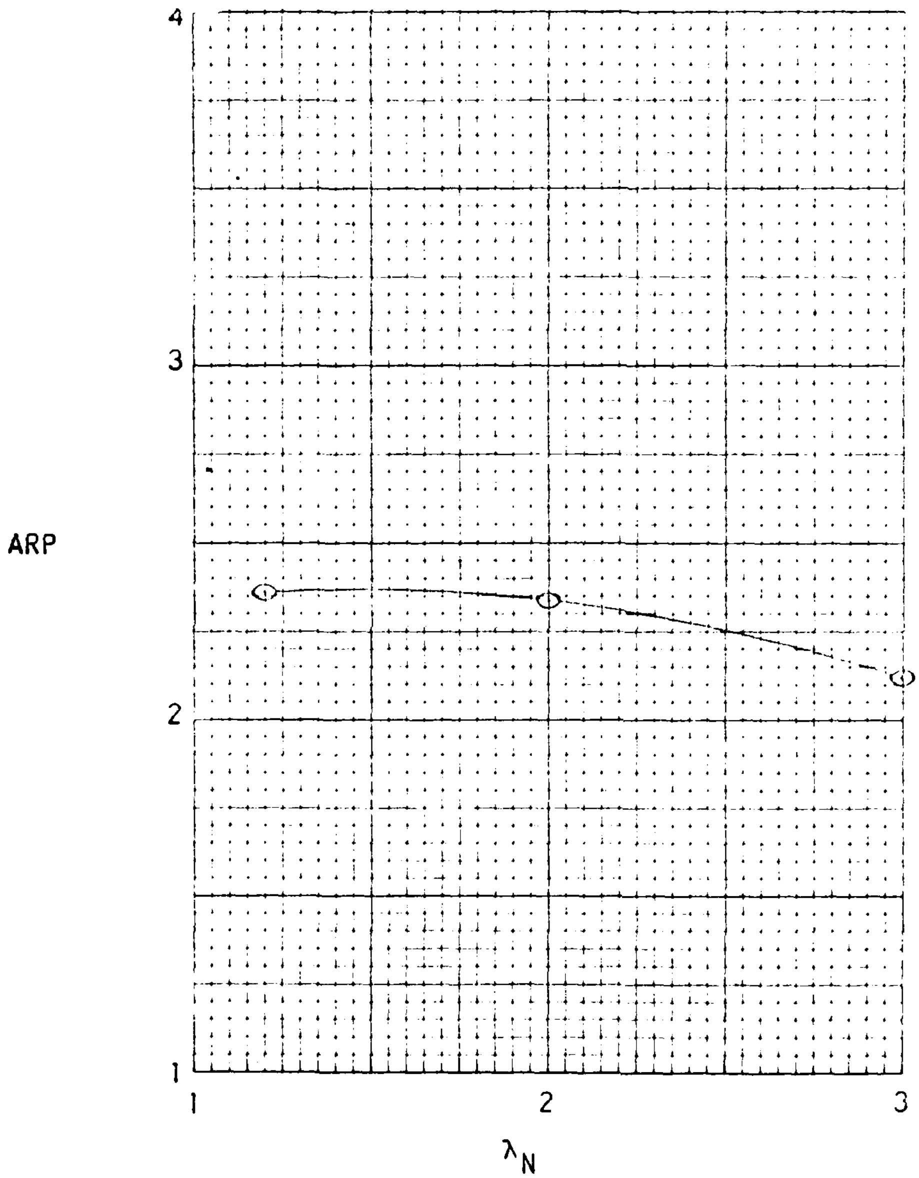

FIGURE 7.1-6. AUGMENTER PUMPING PERFORMANCE VS. JET NOZZLE PRESSURE RATIO FOR OBROUND AUGMENTER WITH RAMP AT $T_{T_N}/T_{amb} = 1.0$.

$(A_A/A_{NT}=25, L_A/D_{AM}=6, Y_p = 0.45)$

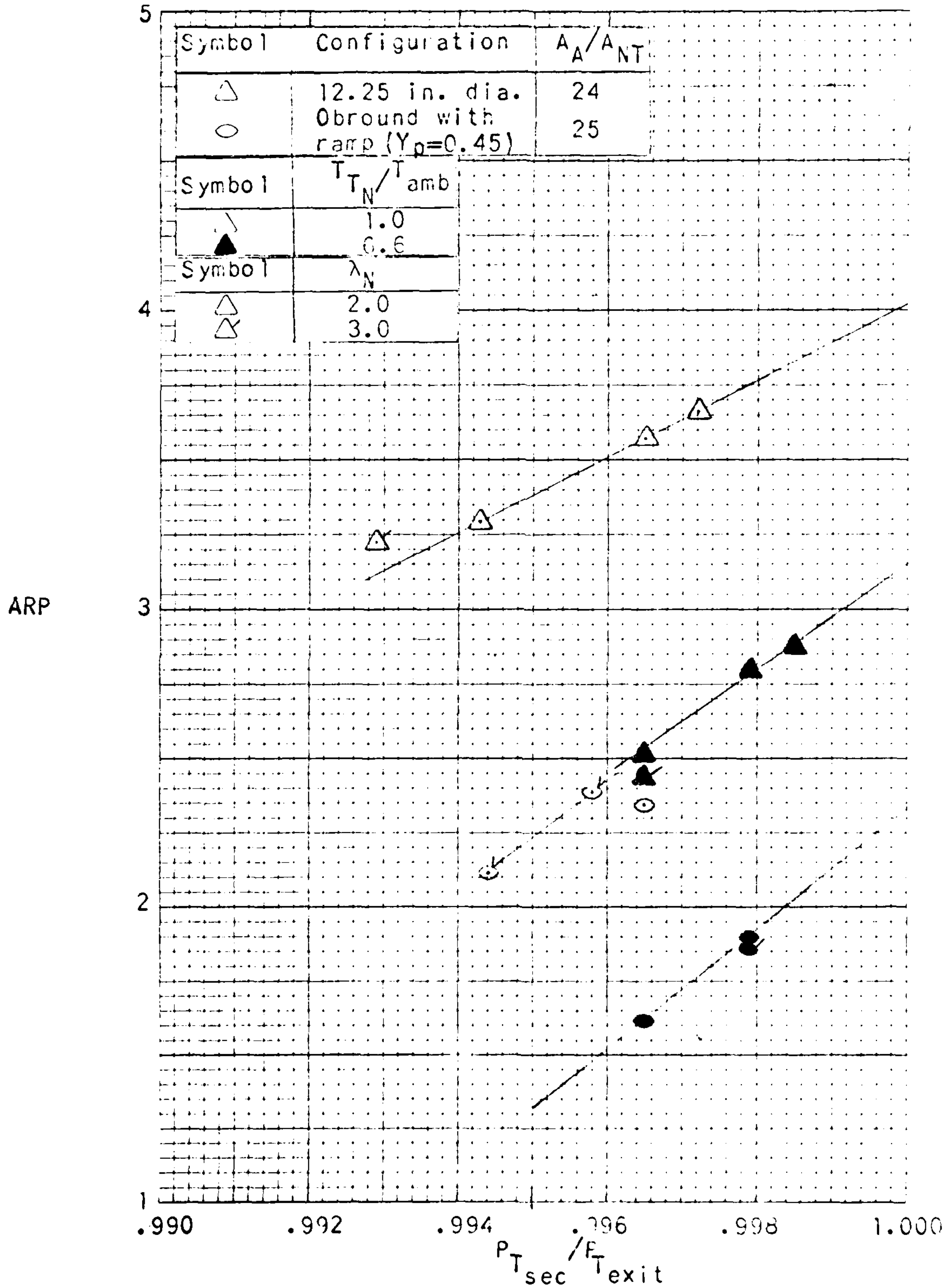

FIGURE 7.1-7. AUGMENTER PUMPING PERFORMANCE VS. AUGMENTER PRESSURE RATIO.
$(A_A/A_{NT_{nom}}=25, X_N/D_{NT}=1.6, L_A/D_A=6)$

Figure 7.1-6 shows the variation in pumping performance with jet nozzle pressure ratio, λ_N . The apparent drop in performance with λ_N occurs because no attempt was made to keep the inlet loss constant for this series of runs and, as a result, the inlet loss and corresponding augmenter pressure rise is higher at $\lambda_N = 3$ than at 2 or 1.2. The low pressure ratio, $\lambda_N = 1.2$, point was run specifically to make sure adequate pumping occurred at low jet nozzle pressure ratios so as to prevent recirculation of exhaust gases within the Hush House. The data point does indicate adequate pumping for this near-idling condition.

Up to this point, augmenter pressure rise or pressure ratio has not been presented as a variable influencing pumping performance. The bulk of the test points presented in Figures 7.1-1 through 7.1-6 correspond to a nominal augmenter pressure ratio, ${}^{P}T_{sec}/{}^{P}T_{exit}$ of 0.995 (2" H_2O loss in total pressure through the Hush House inlet). Specific tests were run to define the influence of augmenter pressure ratios on pumping performance. These runs were accomplished by adding subsonic diffuser lengths onto the secondary air metering nozzle, thereby reducing the loss between outside barometric pressure and the burner enclosure (Hush House) interior. The results of these tests are presented in Figure 7.1-7. These data show an essentially linear variation in augmentation ratio parameter with ${}^{P}T_{sec}/{}^{P}T_{exit}$, a slope which is not a strong function of configuration or ${}^{T}T_N/T_{amb}$ and no significant effect of jet nozzle pressure ratio, λ_N .

7.2 Augmenter Longitudinal Pressure Distribution

Augmenter longitudinal wall pressure data are of diagnostic value in understanding the mixing progress in the augmenter, as well as the influence of loss elements placed in the flow path. Selected examples of these data are presented in this subsection.

Figure 7.2-1 contains longitudinal pressure distributions taken during the aero-acoustic testing for the three different round augmenter sizes at two different jet nozzle total temperatures without subsonic diffuser. A comparison between the data for the different augmenter sizes indicates a lower entrance pressure or, i.e., a higher augmenter entrance velocity (higher specific flow in pps per square foot) for the smaller diameter augmenter especially at the low jet nozzle temperature. The data for the two jet nozzle temperatures or temperature ratios demonstrates the influence of heat exchange between a hot jet flow and a cold pumped flow wherein the pressure drop associated with heat exchange and acceleration of the secondary flow reduces the overall pressure rise experienced with a given jet momentum.

Figure 7.2-2 also contains data for the three sizes of round augmenters, this time for different augmenters length-diameter ratios, L_A/D_A. The data show that the pressure rise along the augmenter is somewhat reduced for the shorter overall length diameter ratios. This corresponds to a lack of adequate mixing between the jet flow and pumped flow and a reduced pumping performance.

Longitudinal augmenter wall pressures from the 12.25" diameter round augmenter tests with different nozzle exit to augmenter entrance spacings are presented in Figure 7.2-3. These data suggest that the completeness of mixing in the augmenter is a function of the distance between this jet nozzle exit and the augmenter exit, rather than just the augmenter length-diameter ratio.

The influence of augmenter entrance geometry on augmenter pressure distribution is shown in Figure 7.2-4. There is little difference between the distributions for the conical and rounded entrances, but the sharp-edged and throttled entrances both show increased local velocities (lower wall pressures) associated with the local flow restriction at the entrance (which reduced the pumping performance).

Pressure distributions for the 12.25" diameter round augmenter with and without a subsonic diffuser are shown in Figure 7.2-5. Here, lower static pressures appear with the higher flow ratio (higher entrance Mach numbers) associated with application of the subsonic diffuser. The static pressure rise in the two subsonic diffuser lengths are also shown. The static pressure drop associated with the exchange of heat between the jet flow and secondary flow is especially well illustrated by the two cases with subsonic diffusers.

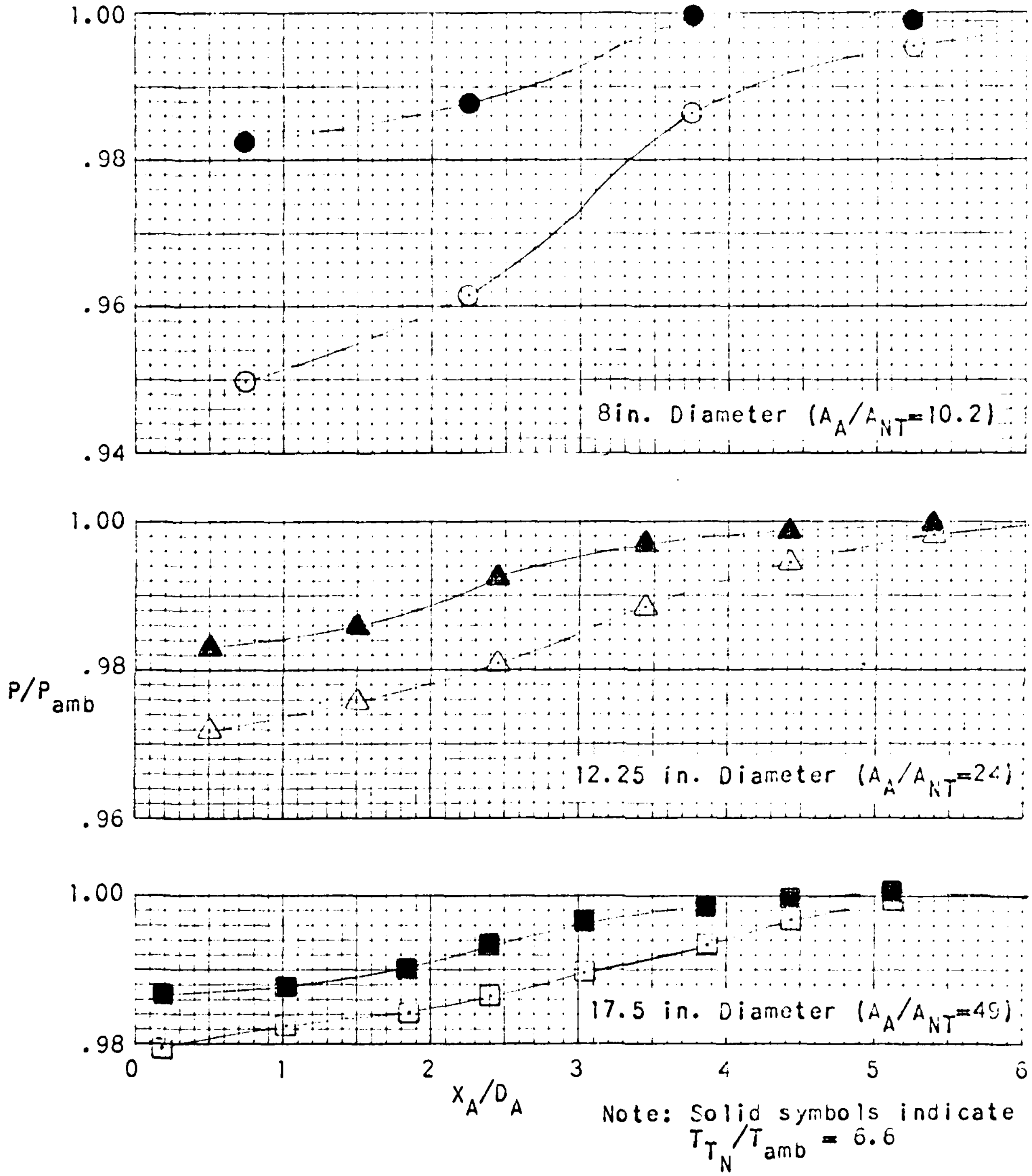

FIGURE 7.2-1. LONGITUDINAL PRESSURE DISTRIBUTION FOR THREE SIZES OF ROUND AUGMENTER HAVING NO SUBSONIC DIFFUSER AT JET NOZZLE TO AMBIENT TEMPERATURE RATIOS OF 1.0 AND 6.6.
$(X_N/D_{NT}=1.6, L_A/D_A=6, \lambda_N=2.0)$

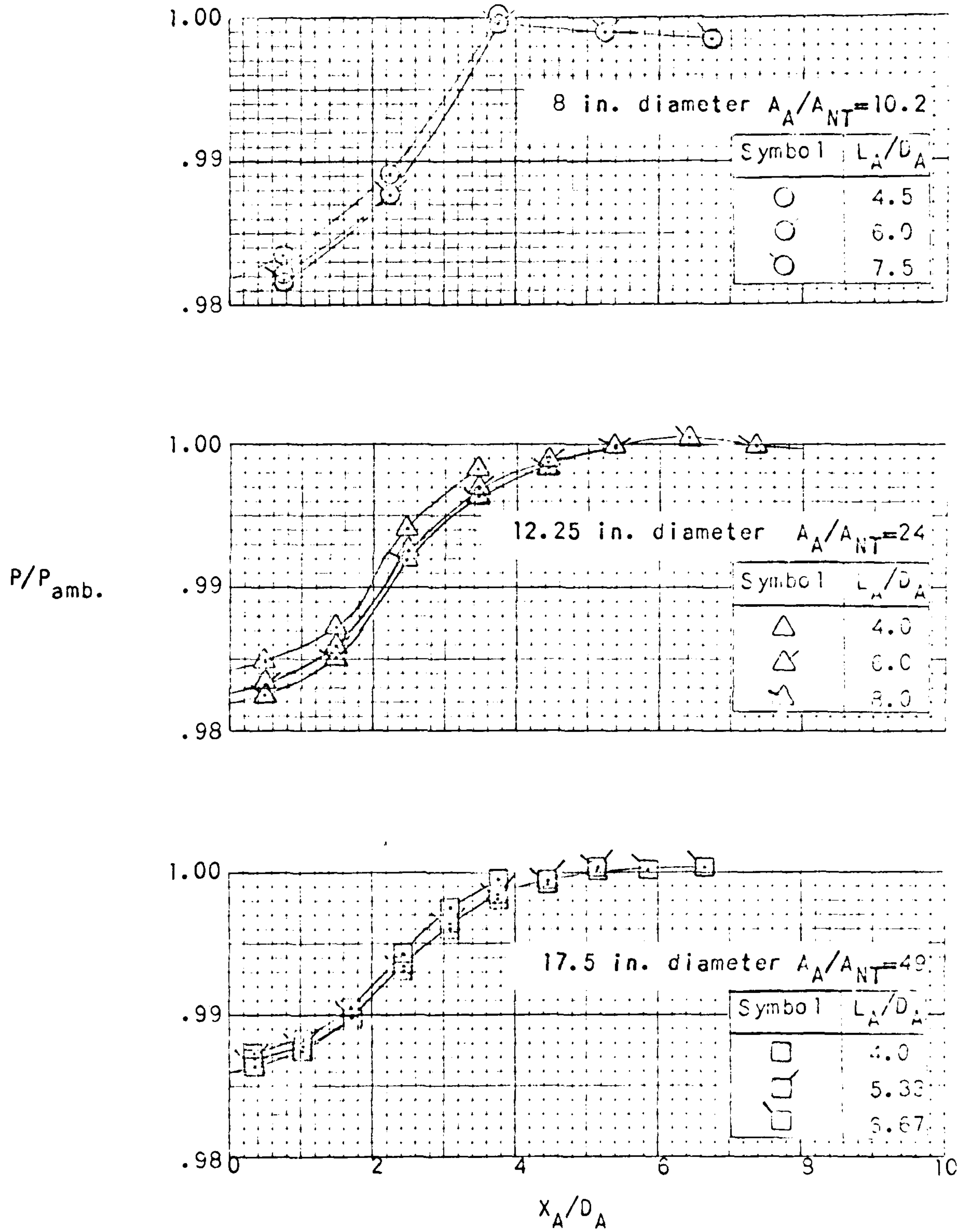

FIGURE 7.2-2. LONGITUDINAL PRESSURE DISTRIBUTION FOR THREE SIZES OF ROUND AUGMENTER HAVING NO SUBSONIC DIFFUSER WITH VARYING AUGMENTER LENGTH-DIAMETER RATIO. $(X_N/D_{NT}=1.6, T_{T_N}/T_{amb}=6.6, \lambda_N=2.0)$

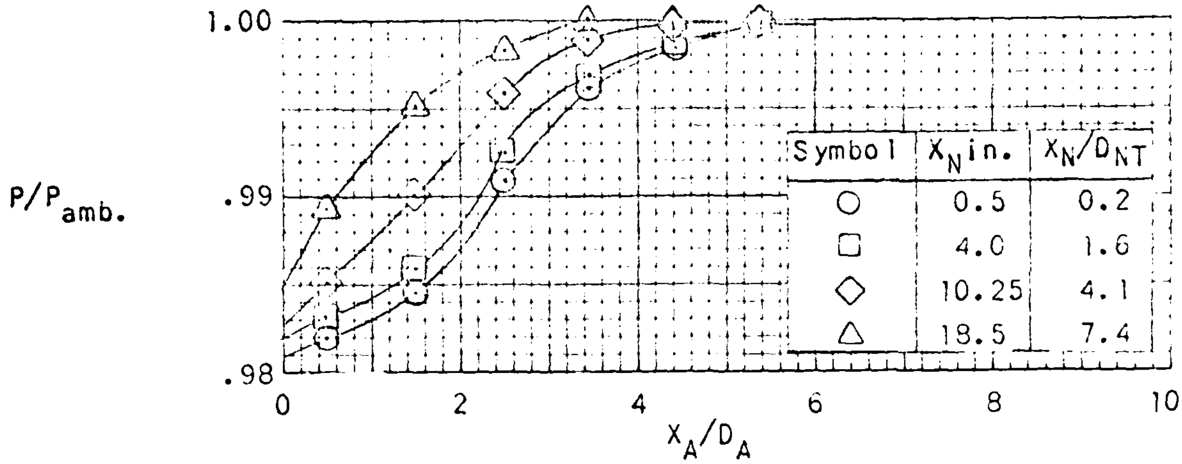

FIGURE 7.2-3. LONGITUDINAL PRESSURE DISTRIBUTION FOR 12.25 IN. DIAMETER AUGMENTER HAVING NO SUBSONIC DIFFUSER AT VARIOUS JET NOZZLE TO AUGMENTER ENTRANCE SPACINGS.
$(A_A/A_{NT}=24, L_A/D_A=6, T_{T_N}/T_{amb}=6.6, \lambda_N=2.0)$

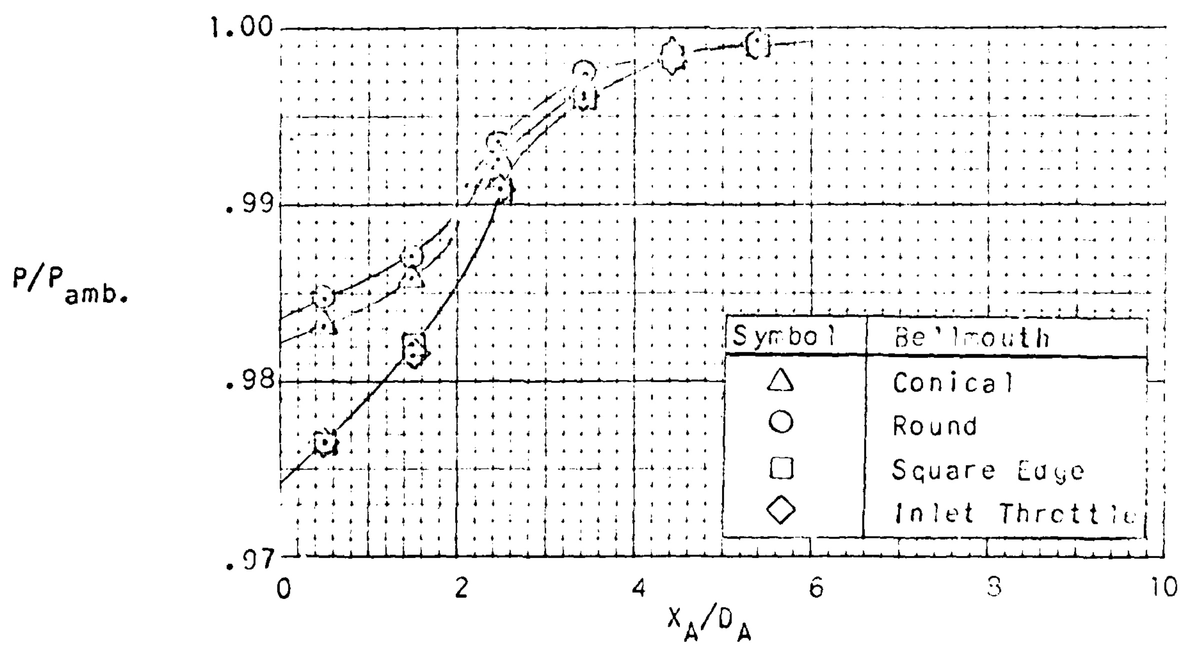

FIGURE 7.2-4. LONGITUDINAL PRESSURE DISTRIBUTION FOR THE 12.25 IN. DIAMETER AUGMENTER HAVING NO SUBSONIC DIFFUSER WITH VARIOUS AUGMENTER ENTRANCE CONFIGURATIONS.
$(A_A/A_{NT}=24, X_N/D_{NT}=1.6, L_A/D_A=6, T_{T_N}/T_{amb}=6.6, \lambda_N=2.0)$

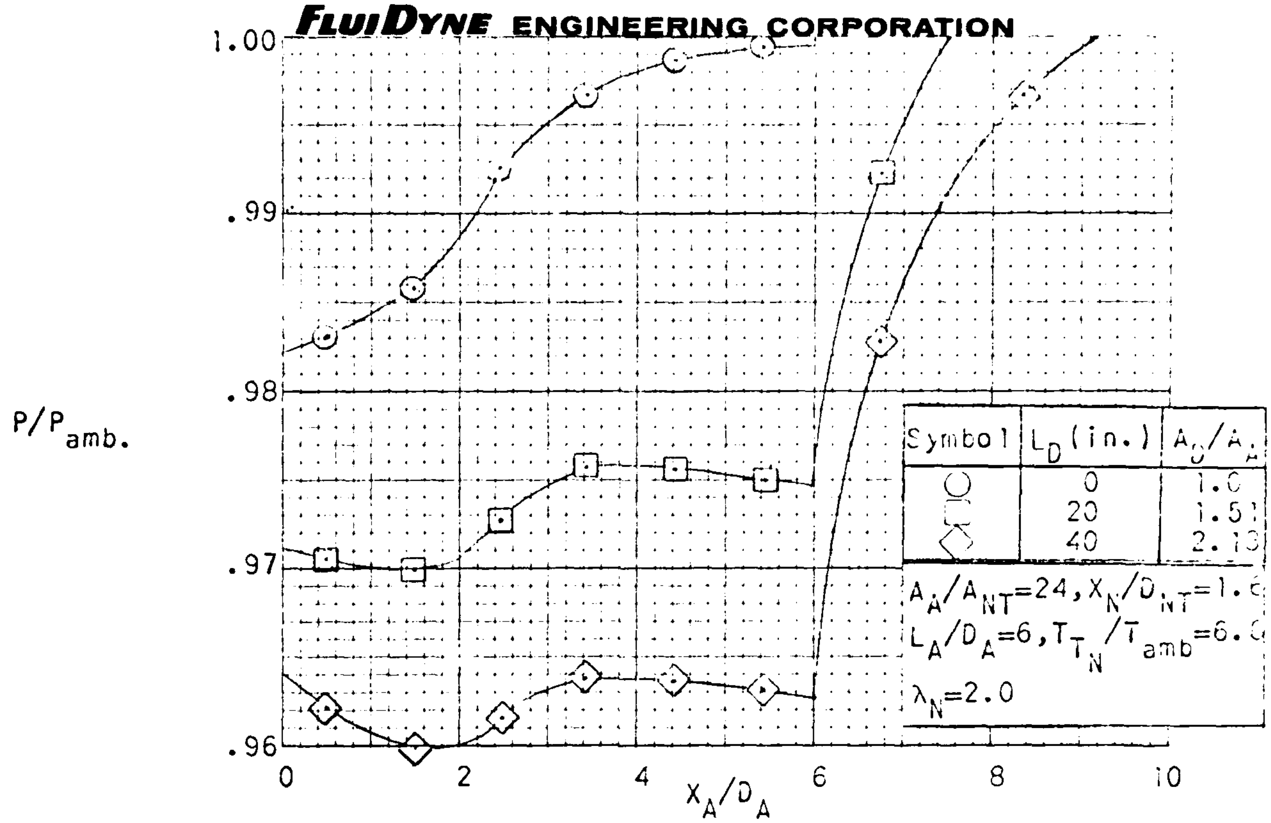

FIGURE 7.2-5. LONGITUDINAL PRESSURE DISTRIBUTION FOR THE 12.25 IN. DIAMETER AUGMENTER FOR VARIOUS EXIT SUBSONIC DIFFUSER LENGTHS

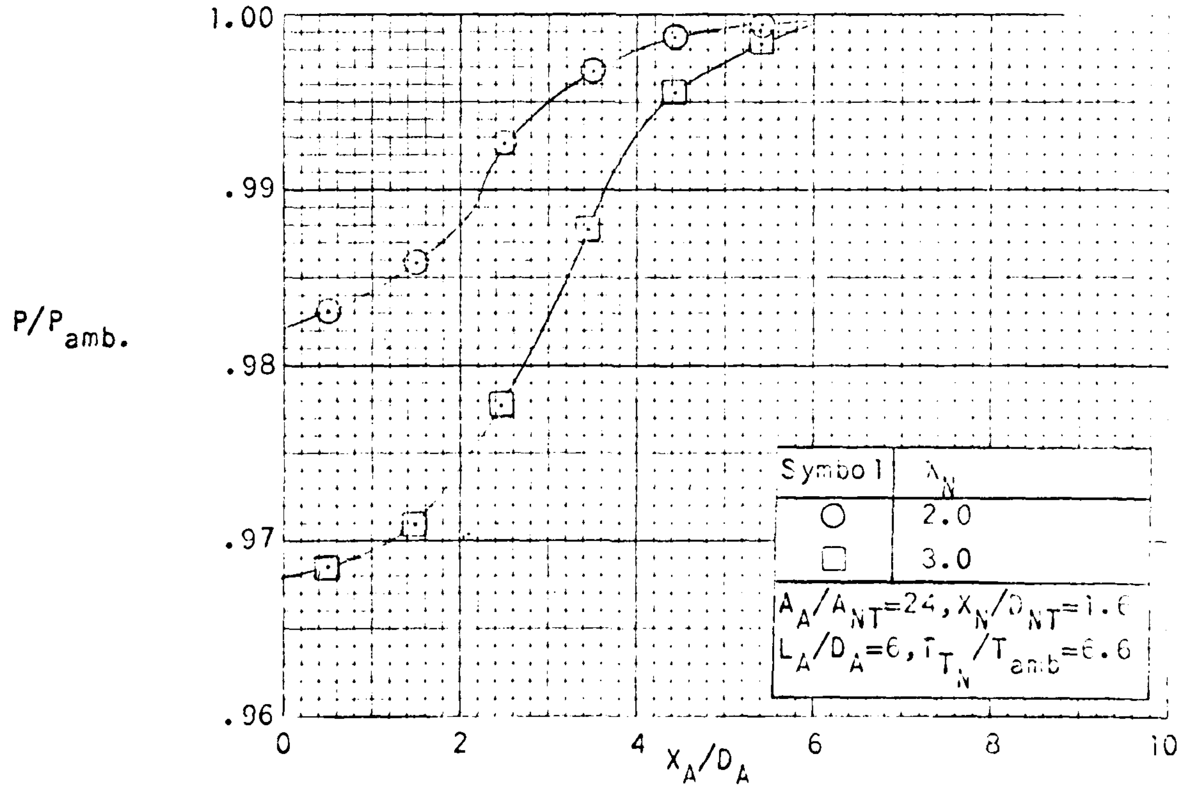

FIGURE 7.2-6. LONGITUDINAL PRESSURE DISTRIBUTION FOR THE 12.25 IN. DIAMETER AUGMENTER HAVING NO EXIT SUBSONIC DIFFUSER AT JET NOZZLE PRESSURE RATIOS OF 2.0 AND 3.0.

Since pumping performance expressed as ARP doesn't vary with jet nozzle pressure ratio, the secondary mass flow will vary in proportion to primary mass flow or, i.e., with jet nozzle total pressure to ambient pressure ratio, other things remaining constant. One would, consequently, expect a higher inlet Mach number and the lower augmenter wall pressures shown in Figure 7.2-6 for the $\lambda_N = 3.0$ case.

The 12.25" diameter round augmenter and the 15.5" x 9" obround augmenter have the same cross-sectional area. Consequently, their longitudinal pressure distributions are compared in Figure 7.2-7 at different jet nozzle total temperatures. The data illustrate the lower inlet Mach number which corresponds to the lower pumping performance with the obround augmenter.

Figure 7.2-8 shows the effects of nozzle offset and deflection during the aero-thermal tests on longitudinal pressure distribution. Here, reduced pumpingperformance reveals itself in a lower inlet Mach number (higher entrance pressure) and reduced augmenter pressure rise, with the centered, undeflected jet position providing maximum performance and the offset jet with 3° lateral deflection providing the lowest performance.

Adding the exit ramp to the obround augmenter for the acoustic tests back-pressured the augmenter slightly, as shown in Figure 7.2-9. This resulted in a small decrease in a pumping performance illustrated in Figure 7.1-5.

Figure 7.2-10 shows the influence of jet nozzle exit to augmenter entrance spacing on the obround augmenter pressure distribution just as Figure 7.2-3 showed the effect with the 12.25" diameter round augmenter. Again, it appears that the completeness of mixing at the augmenter exit is largely a function of the distance between the nozzle exit and augmenter exit expressed in nozzle throat diameters, i.e., as X/D_{NT}.

The effects of jet nozzle pressure ratio, λ_N, on augmenter longitudinal pressure distribution appear in Figure 7.2-11 for the obround augmenter. Data for the 12.25" diameter round augmenter were presented in Figure 7.2-6. Both figures show the lower augmenter entrance pressures and higher pressure rises corresponding to increased pumped flow at higher pressure ratios.

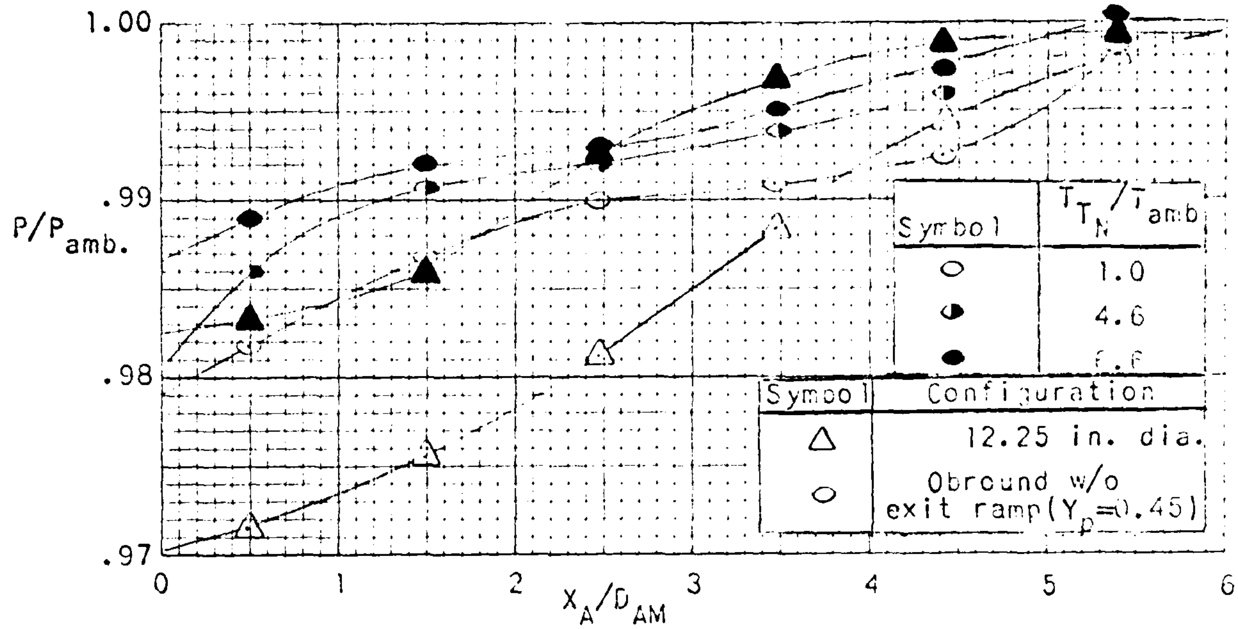

FIGURE 7.2-7. LONGITUDINAL PRESSURE DISTRIBUTION FOR BOTH THE 12.25 IN. DIAMETER AND THE OBROUND AUGMENTER AT VARIOUS JET NOZZLE TO AMBIENT TEMPERATURE RATIOS. $(A_A/A_{NT}=25, X_N/D_{NT}=1.6, L_A/D_{AM}=6, \lambda_N=2.0)$

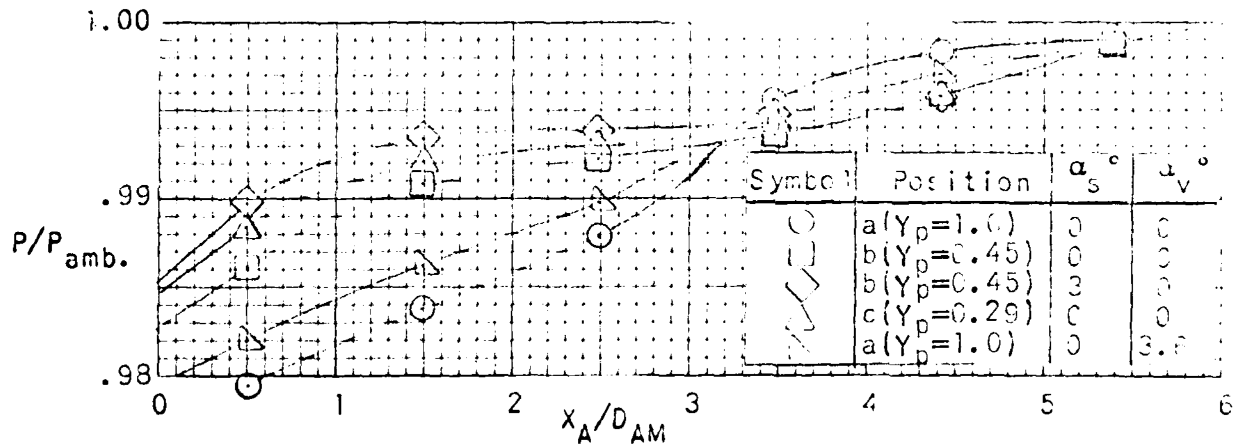

FIGURE 7.2-8. LONGITUDINAL SHELL PRESSURE DISTRIBUTION FOR THE OBROUND AUGMENTER WITHOUT RAMP WITH VARIOUS NOZZLE POSITIONS AND INCLINATIONS. $(A_A/A_{NT}=25, X_N/D_{NT}=1.6, L_A/D_{AM}=6.0, T_{T_N}/T_{amb}=4.6, \lambda_N=2.0)$

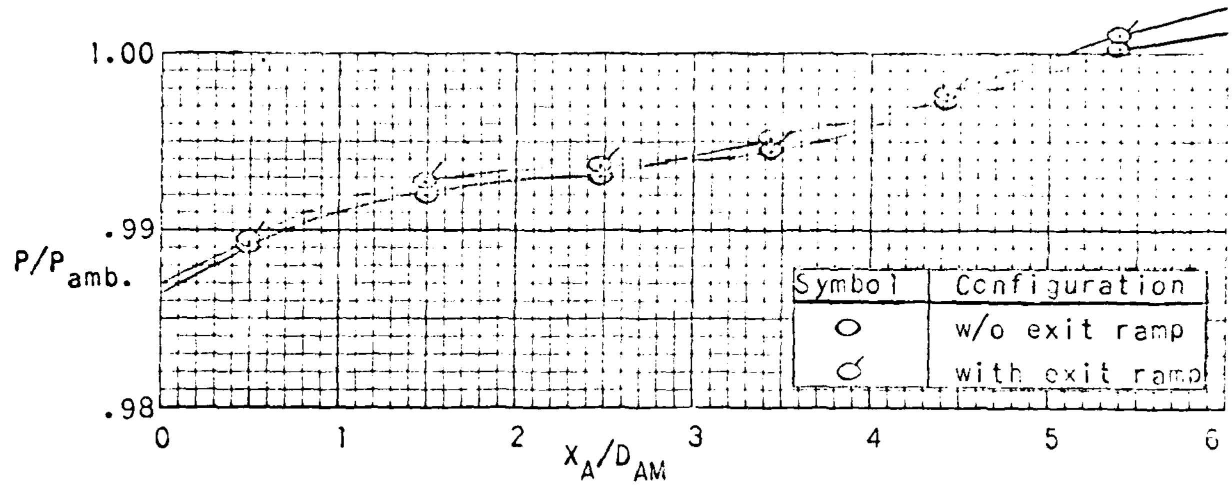

FIGURE 7.2-9. LONGITUDINAL SHELL PRESSURE DISTRIBUTION FOR THE OBROUND AUGMENTER WITH AND WITHOUT EXIT RAMP. (A_A/A_{NT}=25, X_N/D_{NT}=1.6, L_A/D_{AM}=6, T_{T_N}/T_{amb}=6.6, λ_N=2.0, Y_p= 0.45)

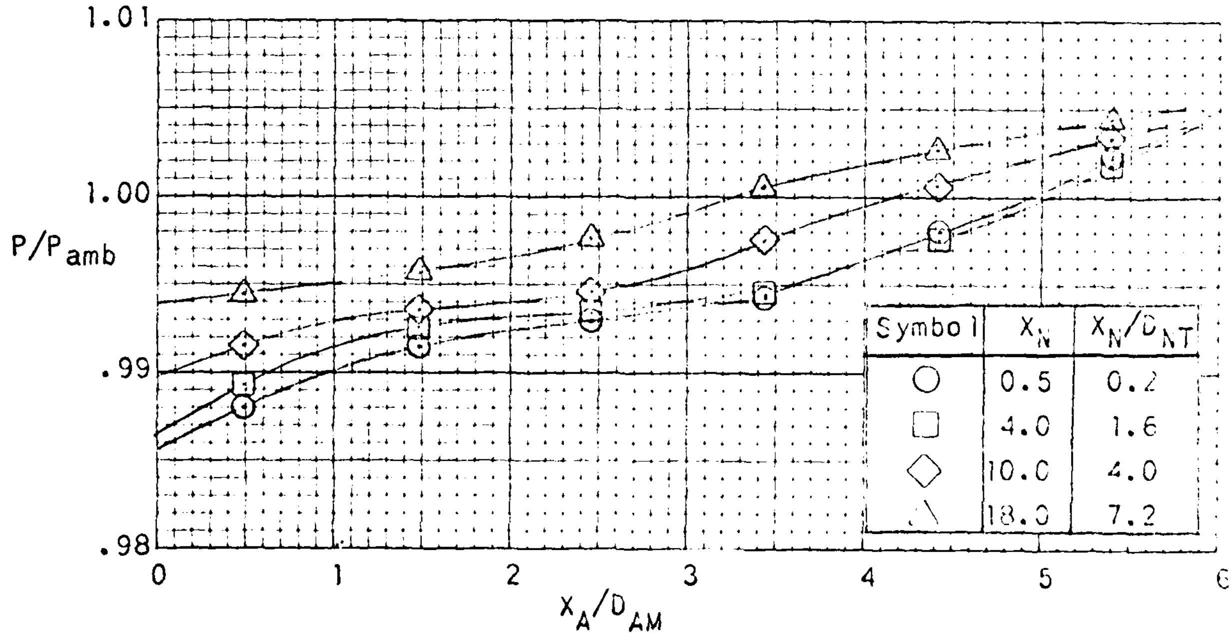

Symbol	X_N	X_N/D_{NT}
○	0.5	0.2
□	4.0	1.6
◇	10.0	4.0
△	18.0	7.2

FIGURE 7.2-10. LONGITUDINAL SHELL PRESSURE DISTRIBUTION FOR THE OBROUND AUGMENTER WITH EXIT RAMP AT VARIOUS JET NOZZLE EXIT TO AUGMENTER ENTRANCE SPACINGS. (A_A/A_{NT}=25, L_A/D_{AM}=6, T_{T_N}/T_{amb}=6.6, λ_N=2.0, Y_p=0.45)

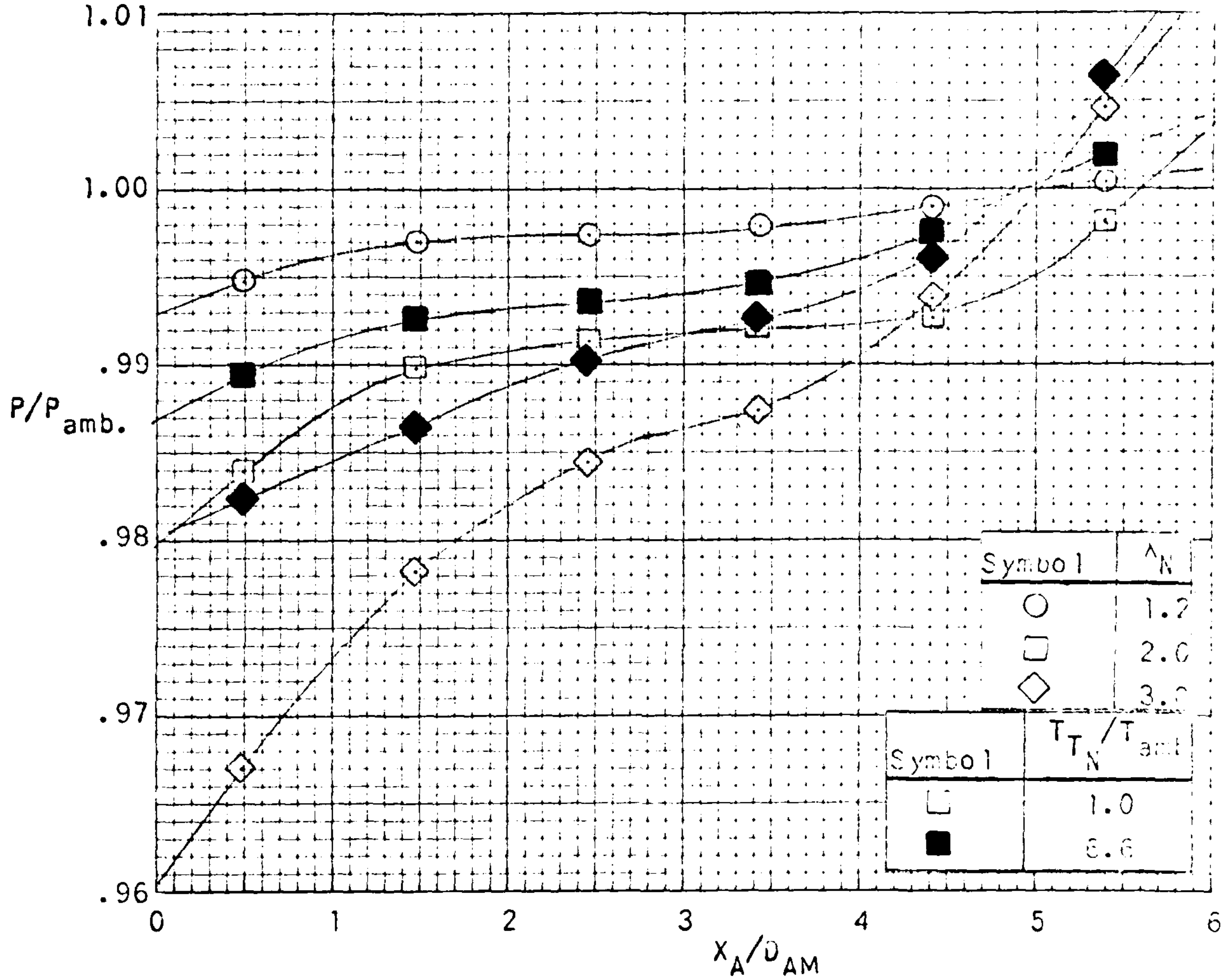

FIGURE 7.2-11. LONGITUDINAL SHELL PRESSURE DISTRIBUTION FOR THE OBROUND AUGMENTER WITH EXIT RAMP AT T_{T_N}/T_{amb} = 1.0 AND 6.6 FOR VARIOUS JET NOZZLE PRESSURE RATIOS. (A_A/A_{NT}=25, X_N/D_{NT}=1.6, $L_A/D_{A\bar{M}}$=6, Y_ρ=0.45)

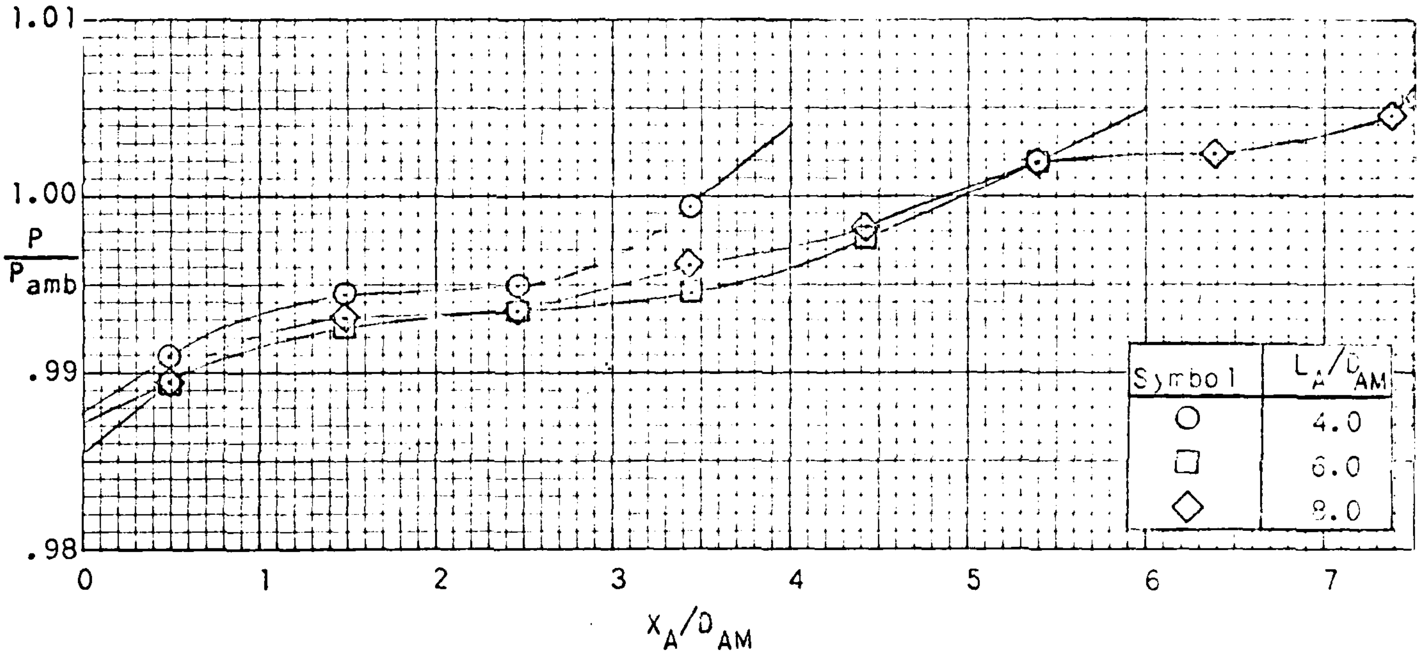

FIGURE 7.2-12. LONGITUDINAL SHELL PRESSURE DISTRIBUTION FOR THE OBROUND AUGMENTER WITH EXIT RAMP FOR THREE AUGMENTER LENGTH-DIAMETER RATIOS. (A_A/A_{NT}=25, X_N/D_{NT}=1.6, T_{T_N}/T_{amb}=6.6, λ_N=2.0, Y_p=0.45)

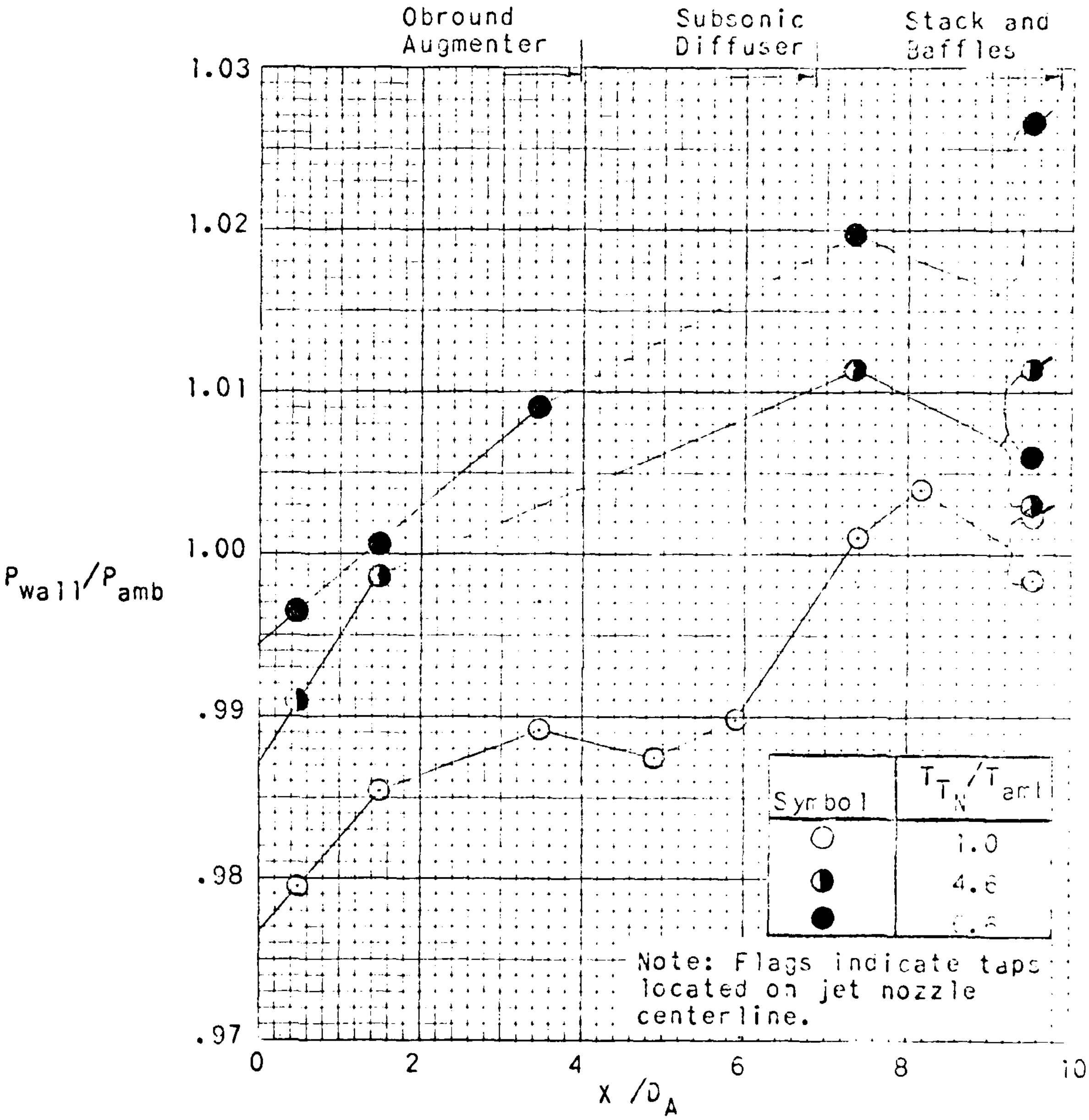

FIGURE 7.2-13. STREAMWISE PRESSURE DISTRIBUTION FOR THE STACK AND BAFFLES CONFIGURATION AT T_{T_N}/T_{amb} = 1.0, 4.6, AND 6.6.
(A_A/A_{NT}=25, X_N/D_{NT}=1.6, $L_A/D_{A\overline{M}}$=4, λ_N=2.0, Y_p=0.45)

Augmenter longitudinal pressure distribution for different obround augmenter length-diameter ratios are presented in Figure 7.2-12 (see Figure 7.2-2 for corresponding round augmenter data). Both figures indicate that the lower pumping performance with a shorter than optimum augmenter length reveals itself in a lower augmenter pressure rise between inlet and exit.

The final longitudinal pressure distribution plot presents data from the tests with the stack and baffles configuration (Figure 7.2-13). The principal feature of this plot is the increase in augmenter back-pressure with jet nozzle total temperature. The higher exhaust volume flow associated with the higher jet temperature results in greatly increased pressure drop through the baffles. This, in turn, resulted in a significant drop in pumping performance with jet nozzle to ambient temperature ratio, ${}^{T}T_N/T_{amb}$, as shown in Figure 7.1-1. The effect was aggravated by wrinkling of the feltmetal baffle skin from high jet temperature operation. Another phenomenon which shows up in the Figure 7.2-13 is the difference in the between-the-baffles pressure from one side of the stack to the other. This occurred because of the persistence of the exhaust jet which still hadn't mixed completely at the stack entrance. Here, again, high jet temperature and a persistent hot core increased this effect.

7.3 Total Pressure and Total Temperature Surveys

Total pressure and total temperature surveys were made during the jet survey to study the jet mixing progress of the free jet and also inside of the 12.25" diameter round and the 15.5" x 9" obround augmenters to study jet mixing progress inside of an augmenter. In addition, a total pressure survey rake was installed on the augmenter exit ramp for some tests to study the mixing progress in the flow leaving the ramp and lateral total temperature distribution information was obtained at the exit of the stack in the stack-and-baffles configuration. During tests with the sound absorbing augmenter liner, it was necessary to test a configuration with the rakes to get the survey data and then test without the rakes to obtain noise data which was free of rake noise. These total pressure and total temperature surveys provide a wealth of data which has been valuable in interpreting both the wall heating effects and the noise data.

7.3.1 Jet Survey

The jet survey was run with the jet nozzle exit located in the exhaust enclosure and with no jet confinement (free jet). Two identical total pressure-total temperature rakes were set up on the jet axis; one 4 ft. 7 in. from the jet nozzle exit (upstream), the other 6 ft. 7 in. from the nozzle exit (downstream). These distances were chosen because they correspond almost exactly to the distance between the jet nozzle exit and the augmenter cross-section rakes during tests with both the 12.25" diameter round augmenter and the obround augmenter. The jet survey data were taken at jet nozzle pressure ratios of $\lambda_N = 2.0$ and 3.0, and at nominal jet nozzle total temperatures of 500°R (ambient), 2300°R and 3300°R, which correspond to ${}^{T}T_N/T_{amb} = 1.0$, 4.6 and 6.6. Figure 7.3-1 contains all of the rake data taken at a pressure ratio of 2.0, while the nozzle pressure ratio 3.0 data appear in Figure 7.3-2. In each case, there was an almost exact correllation between the pressure and temperature parameters.

Considering the pressure ratio 2.0 data in Figure 7.3-1 first, one observes the reduction in peak total temperature and pressure between the upstream and downstream rakes for each temperature condition corresponding to more complete mixing and lower core velocity at the downstream location. Also, one will note that the higher the relative jet nozzle temperature, the more complete the mixing at each station implying that mixing progresses faster with higher jet temperature. The pressure ratio 3.0 data in Figure 7.3-2 show some of these same trends with one notable difference: namely, that the data for ${}^{T}T_N/T_{amb} = 1.0$ display a lower, total pressure than where the jet is hot, reversing the trend measured at $\lambda_N = 2.0$. This appeared to be related to the formation of normal shock waves in the jet near the nozzle exit and was accompanied by the generation of discrete frequency noise. These shocks and the discrete frequency noise were not present at the higher jet nozzle total temperatures. Otherwise, the pressure ratio 3.0 data exhibit higher core pressures than at pressure ratio 2.0 both because of the higher nozzle total pressure and because of the tendency of the potential flow jet core to persist longer when it is supersonically expanded.

One feature of both the pressure ratio 2.0 and 3.0 data is the apparent depression of the core center below the geometric jet centerline with hot flow. A close examination of Figures 7.3-1 and 2 reveals a greater depression at $T_{T_N}/T_{amb} = 6.6$ (3300°R) than at 4.6 (2300°R), a greater depression at $\lambda_N = 2.0$ than at 3.0 and a greater depression at the downstream rake location, indicating that the phenomenon must be an effective downward deflection of the jet at high jet nozzle total temperatures. What is apparently happening is that, within the burner mixing section, convection occurs at high jet nozzle total temperatures which results in a hot, high total pressure core running along the top of the burner mixing section, while the colder, low total pressure gas near the walls drifts to the bottom of the mixing section. When this flow exits through the jet nozzle, it effectively deflects the jet centerline downward. This angular deflection, $\alpha_{v_{eff}}$ is presently in Figure 7.3-3 as calculated from the rake data for each of the pressure ratio, temperature ratio cases. This is not expected to be a feature of actual engine and afterburner operation.

The jet survey rake data were also reduced to give maximum mixed core velocity and these values ratioed to the ideal expanded jet velocity giving $\frac{V_{mix\ max}}{V_{jet}}$ for comparison with similar results from the augmenter cross-section rake data. The ideal jet velocity values used in the ratio are as follows:

T_{T_N} °R	V_{jet} fps, $\lambda_N = 2.0$	V_{jet} fps, $\lambda_N = 3.0$
500	1056	1302
2300	2221	2737
3300	2660	3278

The resulting velocity ratios are plotted in Figure 7.3-16 versus dimensionless distance from the nozzle exit X/D_{NT}.

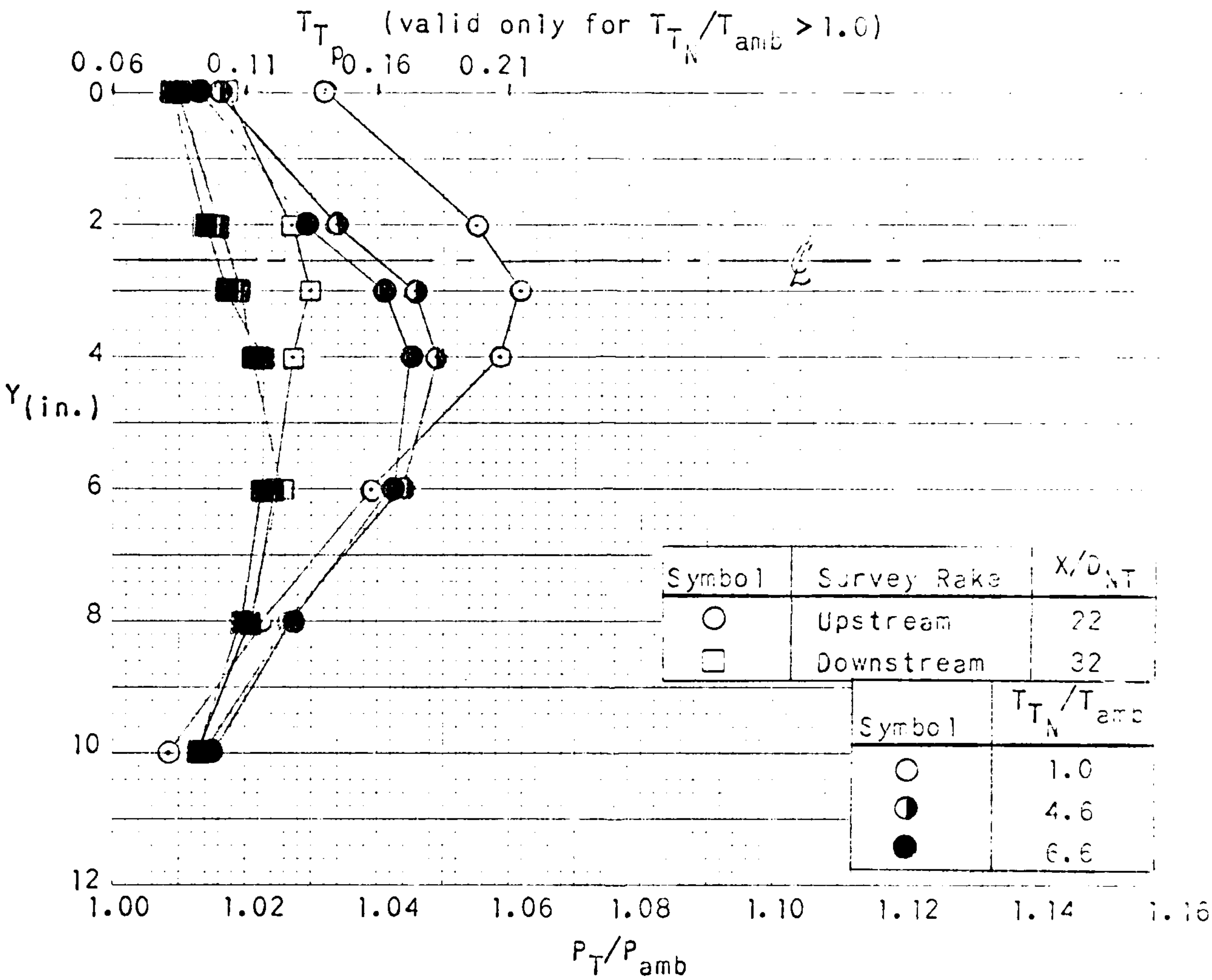

FIGURE 7.3-1. JET SURVEY RAKE TOTAL PRESSURE AND TOTAL TEMPERATURE DISTRIBUTIONS ($\lambda_N = 2.0$).

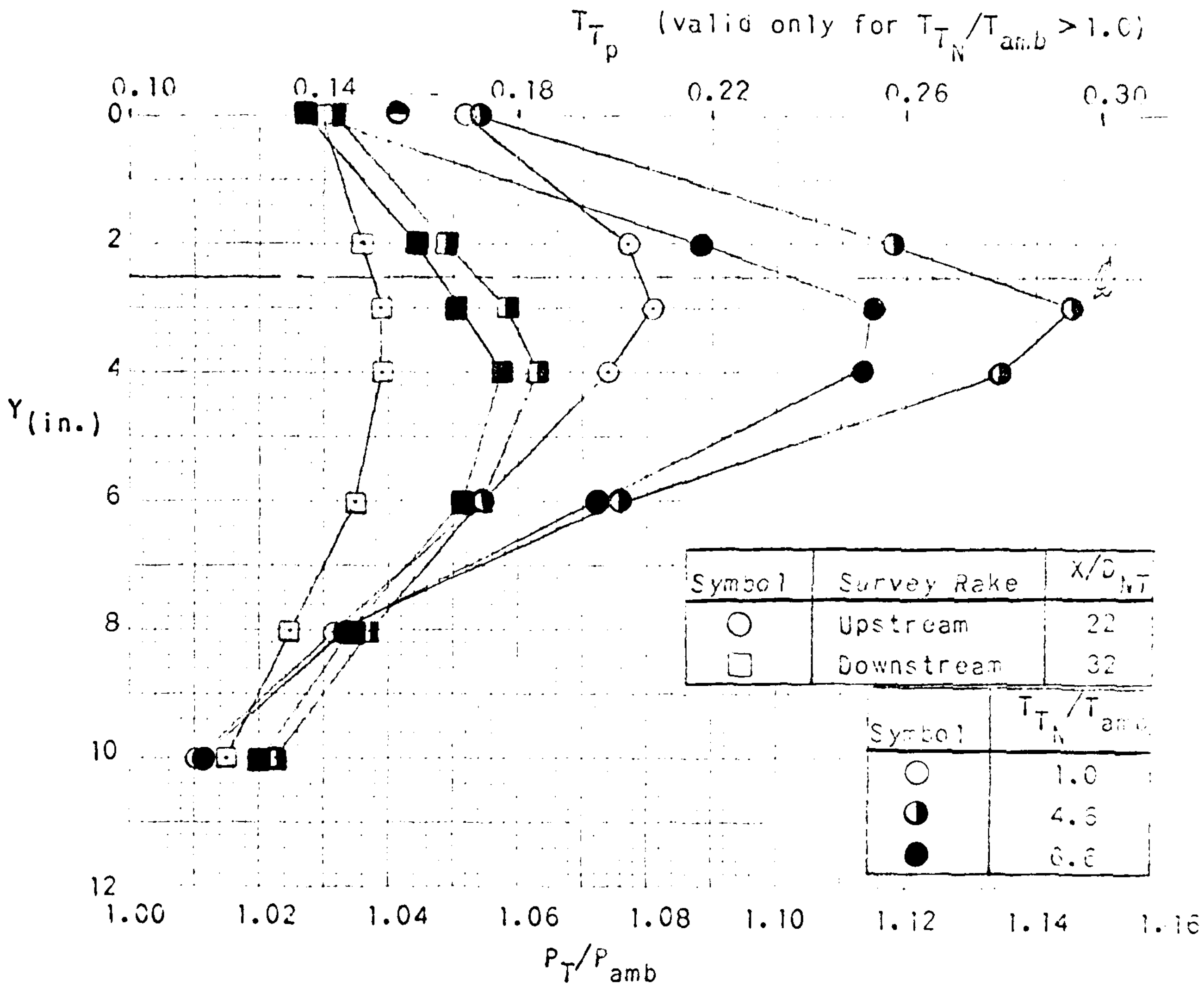

FIGURE 7.3-2. JET SURVEY RAKE TOTAL PRESSURE AND TOTAL TEMPERATURE DISTRIBUTIONS (λ_N = 3.0).

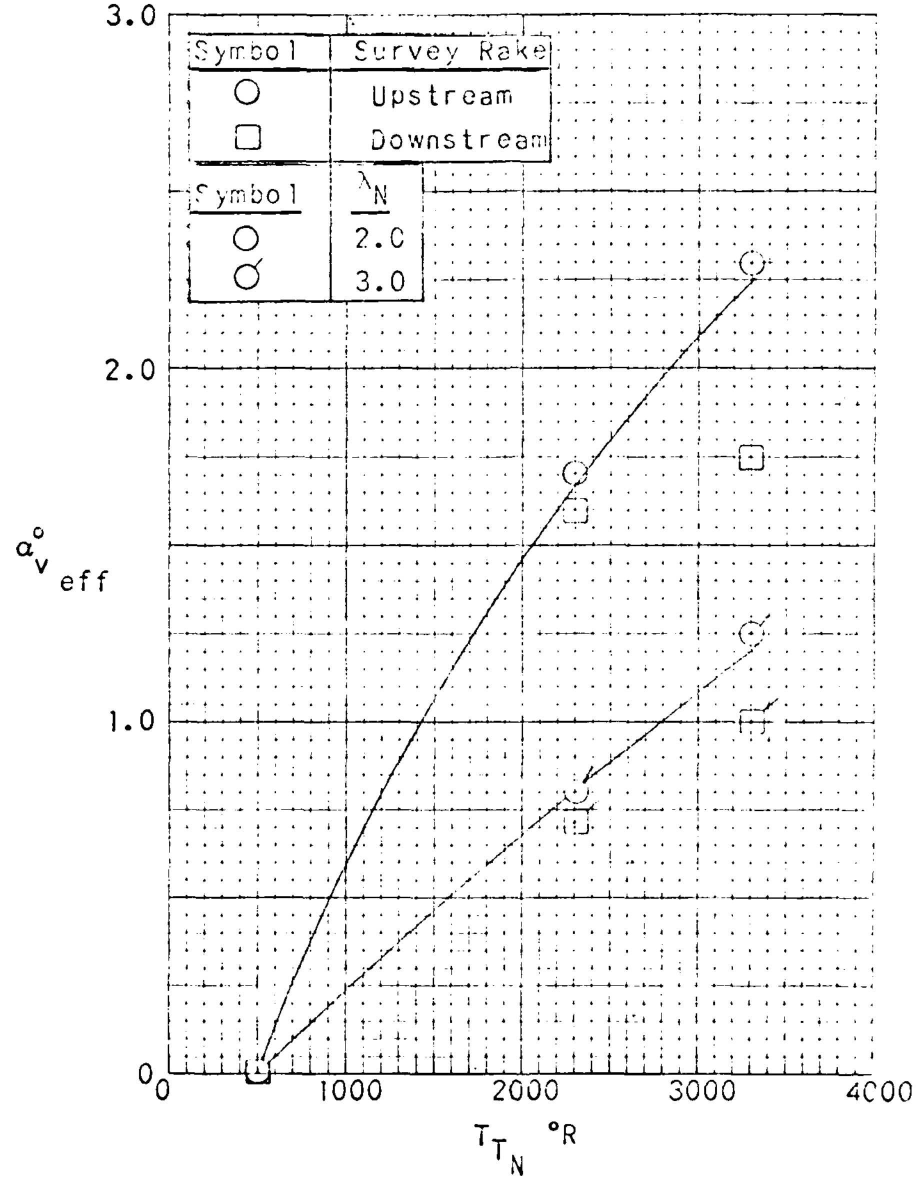

FIGURE 7.3-3. APPARENT JET ANGULAR DEFLECTION AT ELEVATED JET TEMPERATURE DUE TO BURNER INTERNAL CONVECTION

7.3.2 Augmenter Cross-Section Surveys

Augmenter cross-section total pressure-total temperature surveys were taken with both the 12.25" diameter round and the 15.5" x 9" obround augmenters. At elevated jet temperatures, these data were influenced by the convection induced downward jet deflection described in the preceding subsection and presented in Figure 7.3-3. For the graphical presentation herein, the augmenter cross-section survey data have been corrected to remove the effects of this deflection, except where it is of interest to show the influence of vertical jet deflection, α_v .

Figures 7.3-4, -5, -6, -7 and -8 contain the survey results from the aero-acoustic tests with the 12.25" diameter round augmenter. Typically, the survey rakes were placed at the augmenter exit and at the station two feet upstream of the exit. Figure 7.3-4 shows the survey results for three augmenter length-diameter ratios at two jet nozzle total temperatures. As with the jet survey, there was a direct correlation between total temperature parameters and total pressure parameter, thus enabling both temperature and pressure data to be represented by the same curve using different scales for temperature and pressure. It is apparent from Figure 7.3-4, that mixing inside of the augmenter progresses more rapidly at elevated jet temperature just as in the free jet case. One can also observe how mixing progresses as one gets farther away from the jet nozzle exit. Figure 7.3-5 presents a comparison of data taken at two different axial stations with different overall augmenter length-diameter ratios. These curves show that the extent of mixing is primarily a function of distance from the jet nozzle exit expressed in nozzle throat diameters and is not much affected by overall length-diameter ratio, L_A/D_A.

The effects of jet nozzle pressure ratio are illustrated in Figure 7.3-6 for the $^{T}T_N/T_{amb} = 6.6$ case. The jet survey results are generally confirmed again, wherein the higher jet nozzle pressure ratio results in increased core total pressure.

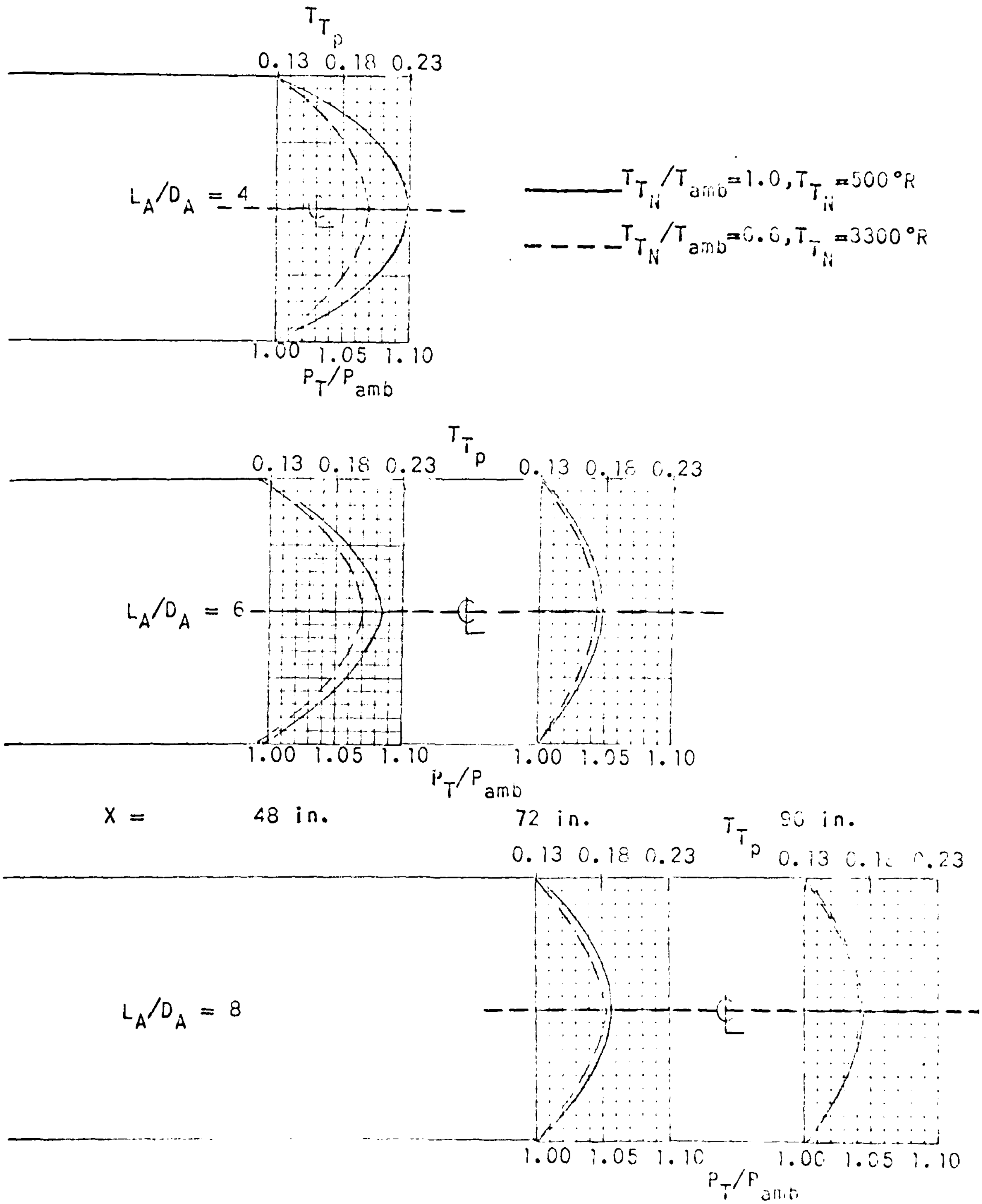

FIGURE 7.3-4. CROSS-SECTION TOTAL PRESSURE AND TEMPERATURE DISTRIBUTIONS WITH THE 12.25 IN. AUGMENTER HAVING NO SUBSONIC DIFFUSER FOR VARIOUS AUGMENTER LENGTH-DIAMETER RATIOS.
$(A_A/A_{NT}=24, X_N/D_{NT}=1.6, \lambda_N=2.0)$

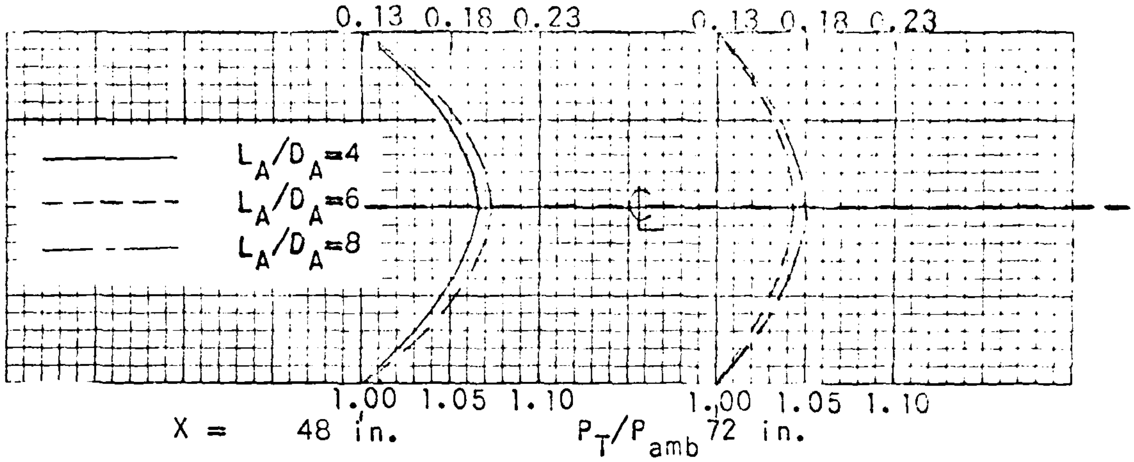

FIGURE 7.3-5. CROSS-SECTION TOTAL PRESSURE AND TEMPERATURE DISTRIBUTIONS FOR THE 12.25 IN. DIAMETER AUGMENTER HAVING NO EXIT SUBSONIC DIFFUSER SHOWING THE INFLUENCE OF AUGMENTER LENGTH-DIAMETER RATIO ON THE DISTRIBUTION AT A PARTICULAR STATION. $(A_A/A_{NT}=24, X_N/D_{NT}=1.6, T_{T_N}/T_{amb}=6.6, \lambda_N=2.0)$

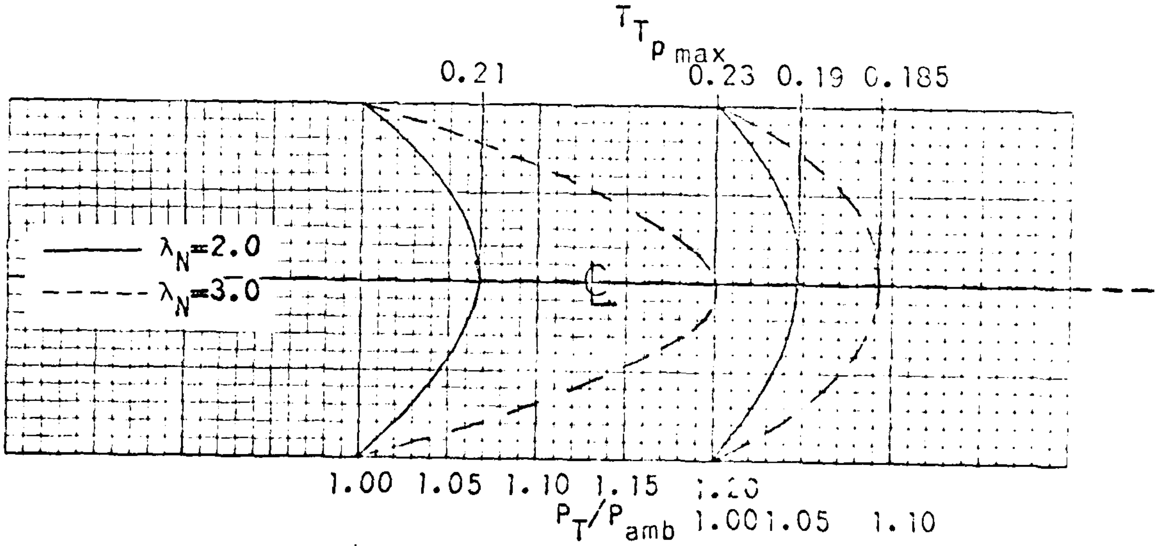

FIGURE 7.3-6. CROSS-SECTION TOTAL PRESSURE AND TEMPERATURE DISTRIBUTIONS FOR THE 12.25 IN. DIAMETER AUGMENTER HAVING NO EXIT SUBSONIC DIFFUSER FOR JET NOZZLE PRESSURE RATIOS OF 2.0 AND 3.0. $(A_A/A_{NT}=24, X_N/D_{NT}=1.6, L_A/D_A=6, T_{T_N}/T_{amb}=6.6)$

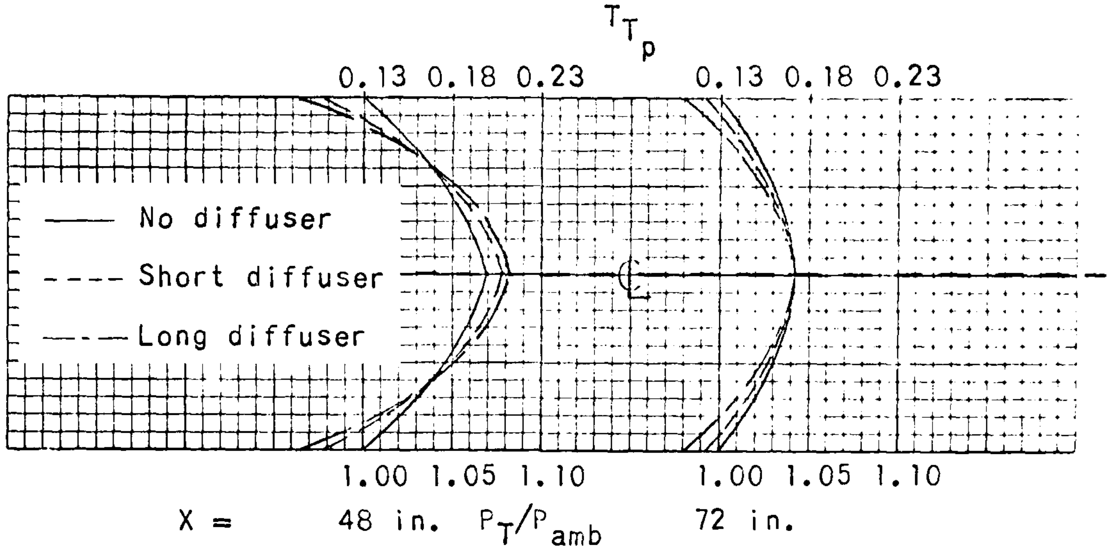

FIGURE 7.3-7. CROSS-SECTION TOTAL PRESSURE AND TEMPERATURE DISTRIBUTIONS FOR THE 12.25 IN. DIAMETER AUGMENTER WITH AND WITHOUT EXIT SUBSONIC DIFFUSER.
$(A_A/A_{NT}=24, X_N/D_{NT}=1.6, L_A/D_A=6, T_{T_N}/T_{amb}=6.6, \lambda_N=2)$

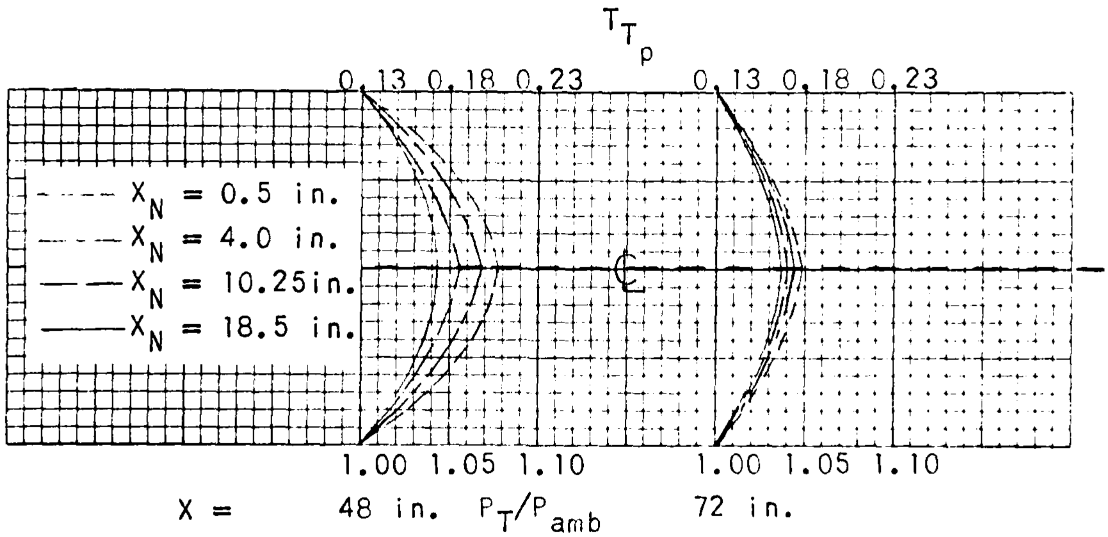

FIGURE 7.3-8. CROSS-SECTION TOTAL PRESSURE AND TEMPERATURE DISTRIBUTIONS FOR THE 12.25 IN. DIAMETER AUGMENTER HAVING NO EXIT SUBSONIC DIFFUSER FOR VARIOUS JET NOZZLE EXIT TO AUGMENTER ENTRANCE SPACINGS.
$(A_A/A_{NT}=24, L_A/D_A=6, T_{T_N}/T_{amb}=6.6, \lambda_N=2)$

Figures 7.3-7 and 7.3-8 demonstrate again that the principal parameter influencing the degree of mixing completion is the dimensionless distance from the jet nozzle exit to the survey station. Figure 7.3-7 presents the survey results taken with and without a subsonic diffuser on the augmenter exit. Addition of a diffuser resulted in a significant increase in pumped flow and yet one observes only a small increase in mixed core total pressure. The influence of increased pumped flow appears mainly in reduced total pressure near the augmenter wall. Figure 7.3-8 shows the influence of moving the jet nozzle exit axially with respect to the augmenter entrance. Again, if one were to plot mixed core total pressure ratio, P_T/P_{amb}, versus dimensionless axial distance between nozzle exit and rake, X/D_{NT}, this dimensionless distance would appear as the prime correlating variable.

These augmenter survey data have been reduced to give the maximum mixed core velocity and the ratio $\frac{V_{mix\ max}}{V_{jet}}$ with an augmenter in the same way as the jet survey data were reduced. The results have been plotted in Figures 7.3-17 and 18 versus dimensionless distance from the jet nozzle exit, X/D_{NT}, along with selected points from the jet survey results for comparison. Such data would be useful in correlating augmenter self-noise, that is, the noise produced by the flow leaving the augmenter and such a correlation is discussed in Section 7.6.4.

Total pressure-total temperature rake survey data from the aero-thermal tests with the obround augmenter could not be presented in the same manner as those data from the round augmenter because the jet centerline orientation was purposely changed relative to the augmenter centerline to define wall heating, pumping and noise effects. Consequently, the presentation form used in Figures 7.3-9, -10, -11, -12, -13, -14 and -15 was used to depict the influence of jet nozzle centerline orientation on the survey results, as well as the effect of mixing. In this presentation, the data are presented as a series of isolines in the augmenter cross-section for both rake stations. Each isoline corresponds to a particular total pressure to ambient pressure ratio and temperature parameter. This presentation makes it easy to see how the test variables influence the location of the maximum velocity core and the extent of mixing. The location of the jet nozzle center is shown in each case. To add universality to the data, lateral and vertical nozzle position parameters were defined as illustrated in Figure 4.3-1. $Y_p = 1.0$ and $Z_p = 1.0$ correspond to a jet centered in the augmenter, while $Y_p = 0$ or $Z_p = 0$ would correspond to the jet grazing the augmenter wall.

The influence of lateral jet nozzle centerline translation at $\lambda_N = 2.0$ is found by comparing Figures 7.3-9 for the centered jet with Figure 7.3-10 for a 3.6" lateral jet centerline offset $(Y_p = 0.45)$. Two things are of particular interest: 1) the lateral offset jet is somehow carried over to the near sidewall so that the mixed core location is closer to the wall than the jet nozzle centerline and 2) the maximum core total pressure and velocity at either survey station are higher with the offset jet (i.e., mixing is not as complete). These effects are increased when the jet is moved still closer to the sidewall (Figure 7.3-13) or deflected toward the sidewall (Figure 7.3-12).

A comparison of Figure 7.3-10 for $\lambda_N = 2.0$ with Figure 7.3-11 for $\lambda_N = 3.0$ shows a decreased tendency of the jet flow to be carried to the sidewall at higher jet nozzle pressure ratio. Figures 7.3-14 and 7.3-15 showing the effects of vertically deflecting the jet nozzle centerline indicate that vertical deflection does not result in as severe a tendency of the jet to be carried to the near wall, as does lateral translation and deflection. The maximum core total pressures are not increased as much either.

The tendency of the laterally translated or deflected jet to be carried to the sidewall is felt in two other areas; maximum wall temperature, discussed in subsection 7.4 and in the generation of augmenter exit self-noise discussed in Section 7.6. The rake survey results have here, again, been reduced to $\frac{V_{mix\ max}}{V_{jet}}$. These results, for the obround augmenter, are presented in Figure 7.3-19 showing the effects of jet centerline lateral translation and deflection. Data from the jet survey and round augmenter survey are included for comparison. In addition to Figure 7.3-19, Figure

Isoline	P_T/P_{amb}	T_{T_P}
1	1.02	.16
2	1.04	.18
3	1.06	.20
4	1.08	.215

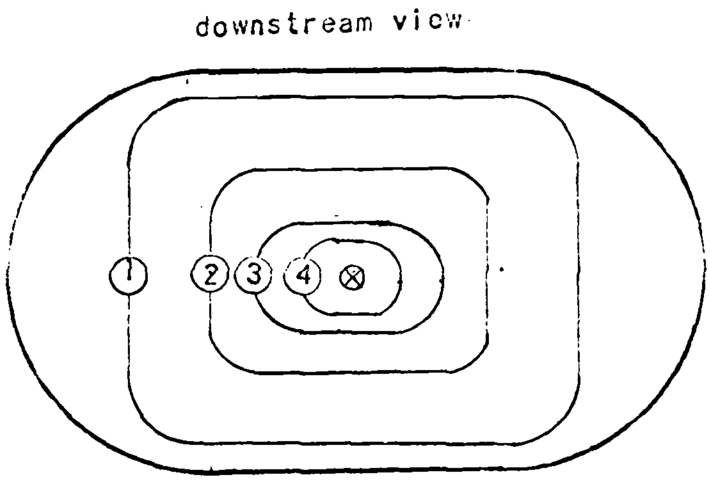

a. 48 in. Station

Isoline	P_T/P_{amb}	T_{T_P}
1	1.02	.16
2	1.03	.17
3	1.04	.18

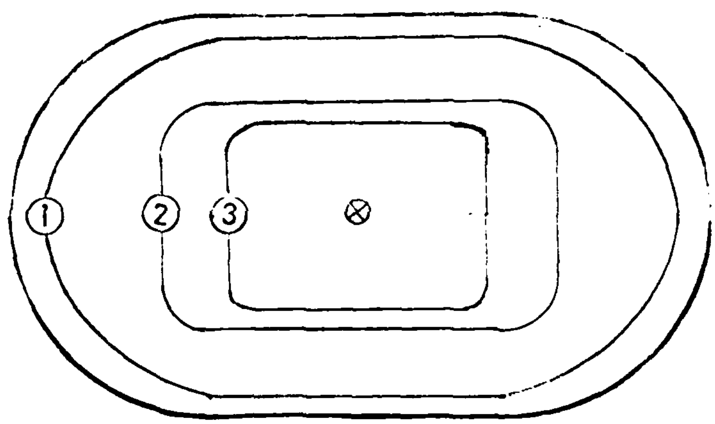

b. 72 in. (Exit) Station

FIGURE 7.3-9. CROSS-SECTION TOTAL PRESSURE AND TEMPERATURE CONTOURS FOR THE OBROUND AUGMENTER WITH THE JET CENTERED (POSITION a, Y_P = 1.0). (A_A/A_{NT}=25, X_N/D_{NT}=1.6, L_A/D_{AM}=6, T_{T_N}/T_{amb}=4.6, λ_N=2.0)

Isoline	P_T/P_{amb}	T_{T_P}
1	1.02	.16
2	1.04	.20
3	1.06	.23
4	1.08	.25

downstream view

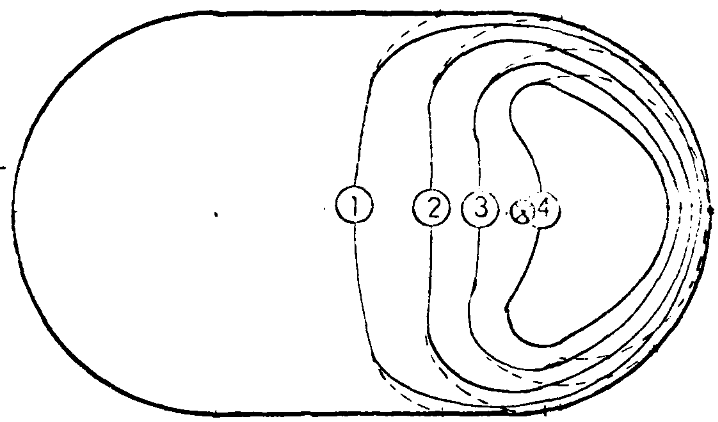

a. 48 in. Station

Isoline	P_T/P_{amb}	T_{T_P}
1	1.02	.16
2	1.03	.18
3	1.04	.20
4	1.06	.23

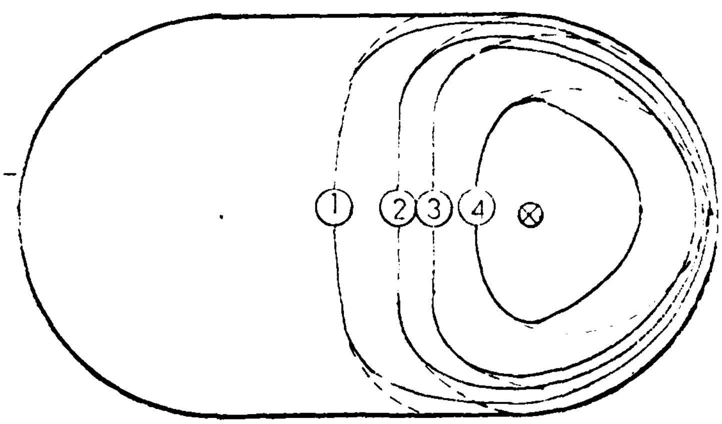

b. 72 in.(Exit) Station

FIGURE 7.3-10. CROSS-SECTION TOTAL PRESSURE AND TEMPERATURE CONTOURS FOR THE OBROUND AUGMENTER WITH THE JET IN THE F-14A LOCATION (POSITION b, $Y_P = .45$) AND UNDEFLECTED.

($A_A/A_{NT}=25, X_N/D_{NT}=1.6, L_A/D_{AM}=6, T_{T_N}/T_{amb}=4.6, \lambda_N=2.0$)

Isoline	P_T/P_{amb}	T_{T_P}
1	1.04	.16
2	1.08	.20
3	1.12	.23
4	1.16	.25
5	1.20	.26

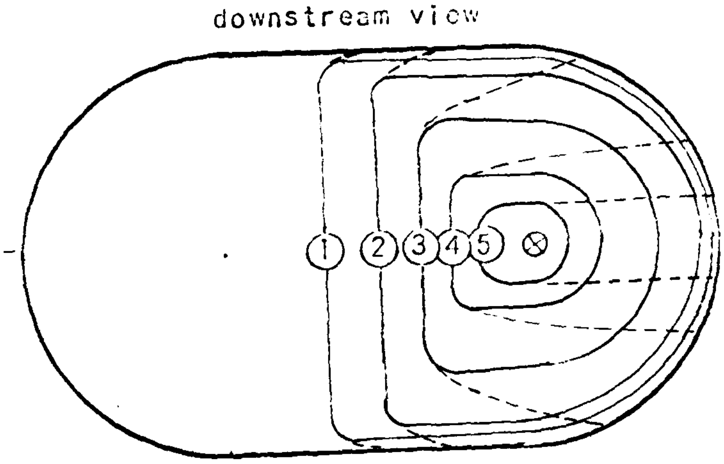

a. 48 in. Station

Isoline	P_T/P_{amb}	T_{T_P}
1	1.04	.16
2	1.08	.20
3	1.10	.215
4	1.12	.23

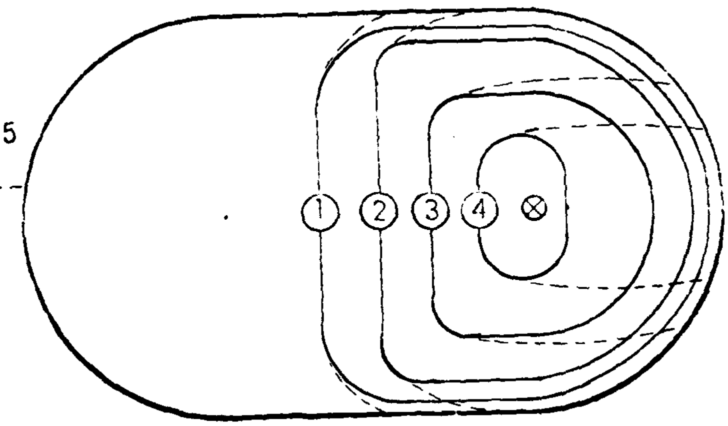

b. 72 in. (Exit) Station

FIGURE 7.3-11. CROSS-SECTION TOTAL PRESSURE AND TEMPERATURE CONTOURS FOR THE OBROUND AUGMENTER WITH THE JET IN THE F-14A LOCATION (POSITION b, Y_P = .45) AND UNDEFLECTED AT A JET NOZZLE PRESSURE RATIO OF 3.0.
(A_A/A_{NT}=25, X_N/D_{NT}=1.6, L_A/D_{AM}=6, T_{T_N}/T_{amb}=[illegible].6, λ_N=3.0)

Isoline	P_T/P_{amb}	T_{T_P}
1	1.02	.16
2	1.04	.20
3	1.06	.23
4	1.08	.25
5	1.10	.26

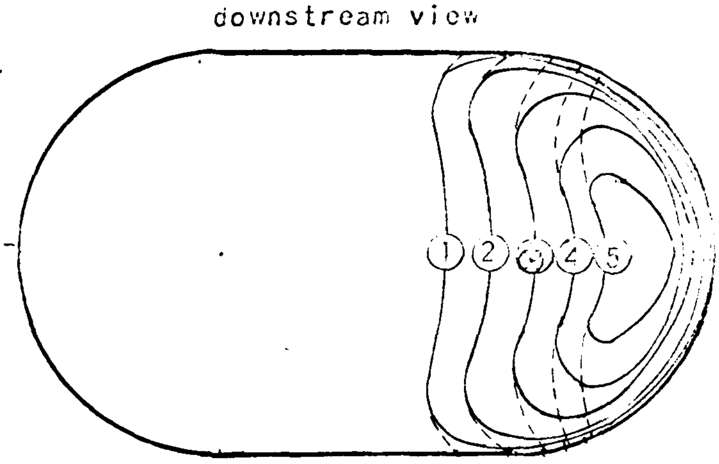

a. 48 in. Station

Isoline	P_T/P_{amb}	T_{T_P}
1	1.02	.16
2	1.03	.18
3	1.04	.20
4	1.06	.23

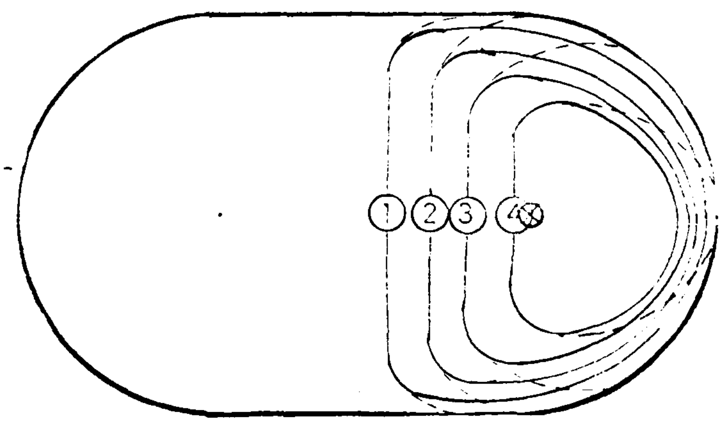

b. 72 in. (Exit) Station

FIGURE 7.3-12. CROSS-SECTION TOTAL PRESSURE AND TEMPERATURE CONTOURS FOR THE OBROUND AUGMENTER WITH THE JET IN THE F-14A LOCATION (POSITION b, Yp = .45) AND DEFLECTED 3° LATERALLY TOWARD THE NEAR WALL OF THE AUGMENTER.

$(A_A/A_{NT}=25, X_N/D_{NT}=1.6, L_A/D_{AM}=6, T_{T_N}/T_{amb}=4.6, \lambda_N=2.0)$

Isoline	P_T/P_{amb}	T_{T_P}
1	1.02	.16
2	1.04	.20
3	1.06	.23
4	1.08	.25
5	1.10	.26

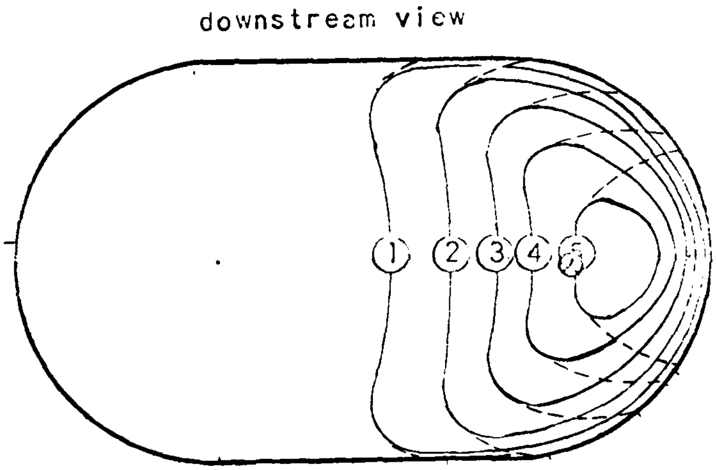

a. 48 in. Station

Isoline	P_T/P_{amb}	T_{T_P}
1	1.02	.16
2	1.03	.18
3	1.04	.20
4	1.06	.23

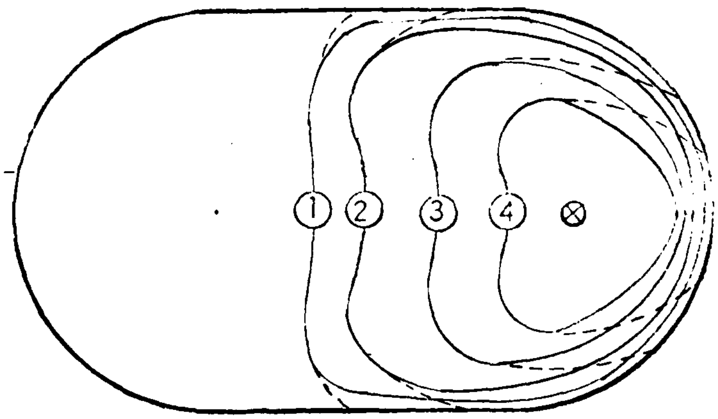

b. 72 in.(Exit) Station

FIGURE 7.3-13. CROSS-SECTION TOTAL PRESSURE AND TEMPERATURE CONTOURS FOR THE OBROUND AUGMENTER WITH THE JET IN POSITION c (Y_P = .29) AND UNDEFLECTED.
(A_A/A_{NT}=25, X_N/D_{NT}=1.6, L_A/D_{AN}=6, T_{T_N}/T_{amb}=4.3, λ_N=2.0)

Isoline	P_T/P_{amb}	T_{T_P}
1	1.02	.16
2	1.04	.18
3	1.06	.20
4	1.08	.215

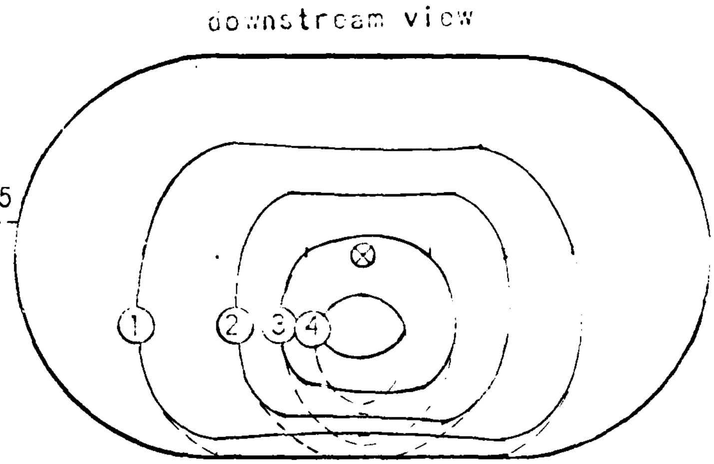

a. 48 in. Station

Isoline	P_T/P_{amb}	T_{T_P}
1	1.02	.16
2	1.03	.17
3	1.04	.18
4	1.06	.20

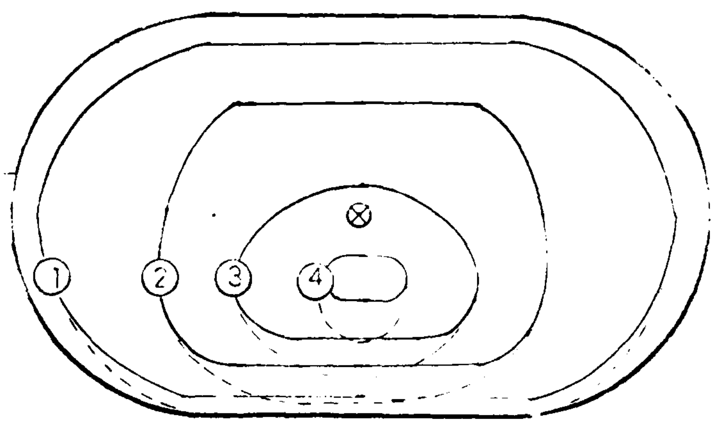

b. 72 in. (Exit) Station

FIGURE 7.3-14. CROSS-SECTION TOTAL PRESSURE AND TEMPERATURE CONTOURS FOR THE OBROUND AUGMENTER WITH THE JET CENTERED (POSITION a, Yp = 1.0) AND DEFLECTED DOWNWARD 1.6°.

$(A_A/A_{NT}=25, X_N/D_{NT}=1.6, L_A/D_{AM}=6, T_{T_N}/T_{amb}=4.8, \lambda_N=2.0)$

AD-A109 848 FLUIDYNE ENGINEERING CORP MINNEAPOLIS MINN F/G 14/2
AERODYNAMIC AND ACOUSTIC TESTS OF A 1/15 SCALE MODEL DRY COOLED--ETC(U)
OCT 75 J L GRUNNET, I L VER, G GETTER N62467-74-C-0490

UNCLASSIFIED NL

3 OF 4

AD A 109848

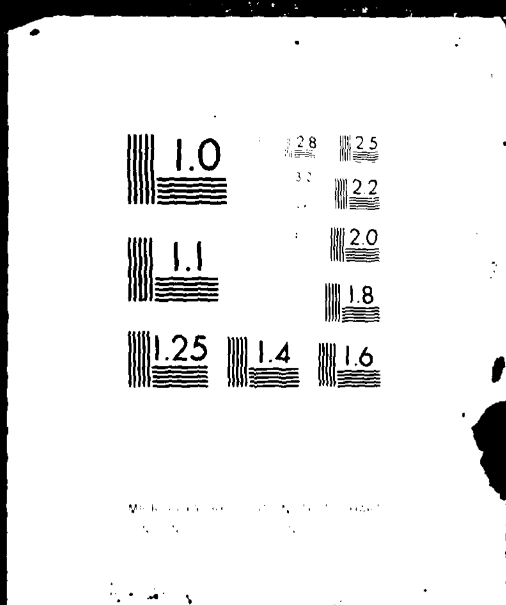

FLUIDYNE ENGINEERING CORPORATION

Isoline	P_T/P_{amb}	T_{T_P}
1	1.02	.16
2	1.04	.18
3	1.06	.20
4	1.08	.215

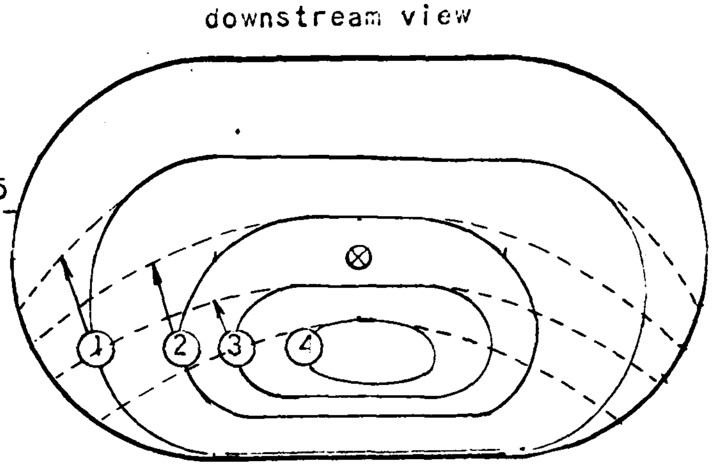

a. 48 in. Station

Isoline	P_T/P_{amb}	T_{T_P}
1	1.02	.16
2	1.03	.17
3	1.04	.18
4	1.06	.20

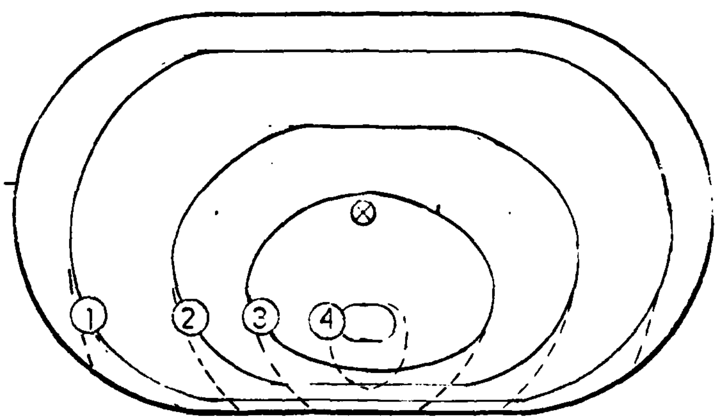

b. 72 in.(Exit) Station

FIGURE 7.3-15. CROSS-SECTION TOTAL PRESSURE AND TEMPERATURE CONTOURS FOR THE OBROUND AUGMENTER WITH THE JET CENTERED (POSITION a, Yp = 1.0) AND DEFLECTED DOWNWARD 3.6°.

$(A_A/A_{NT}=25, X_N/D_{NT}=1.6, L_A/D_{AM}=6, T_{T_N}/T_{amb}=4.6, \lambda_N=2.0)$

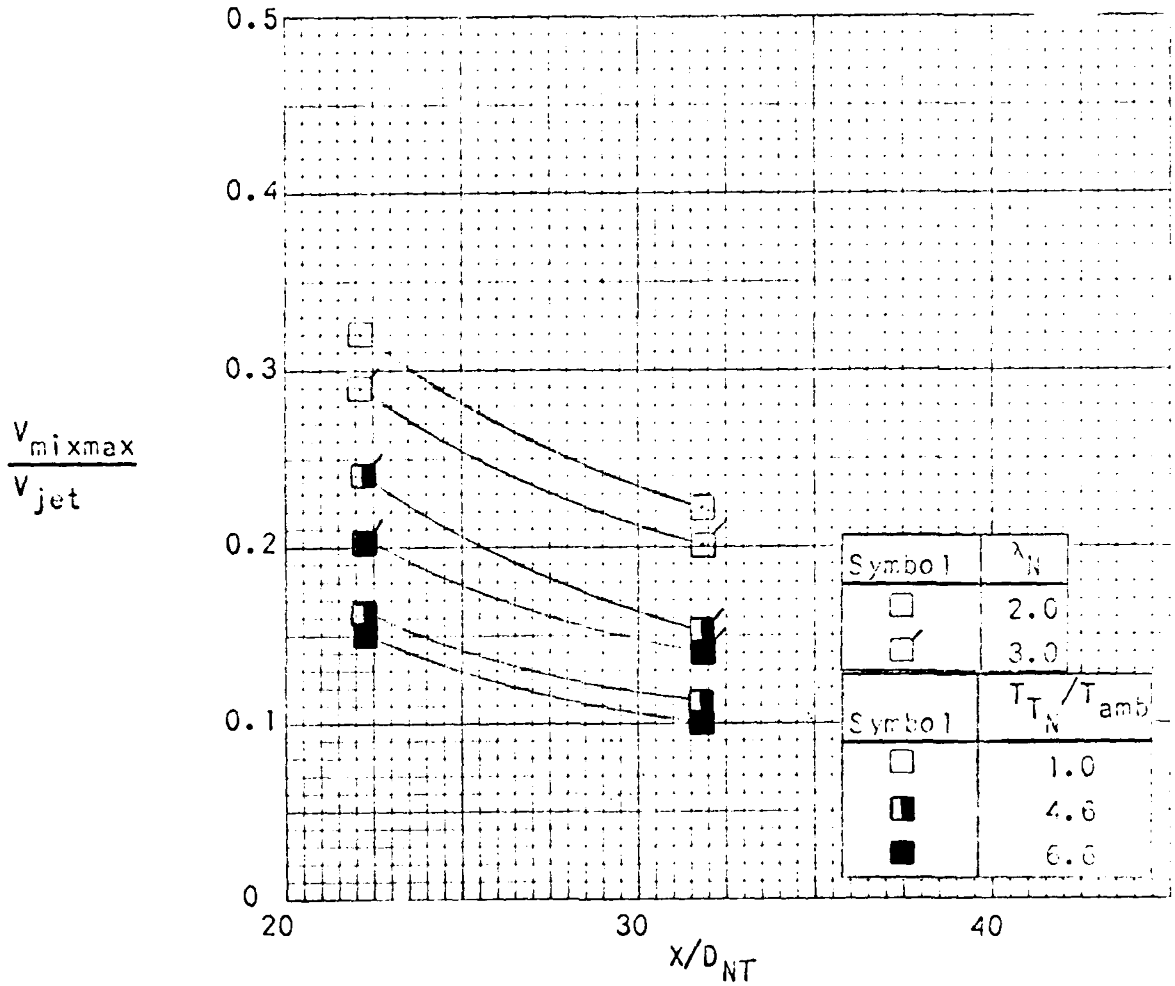

FIGURE 7.3-16. MAXIMUM MIXED VELOCITY TO JET VELOCITY RATIO VERSUS AXIAL LOCATION FROM THE JET SURVEY RESULTS.

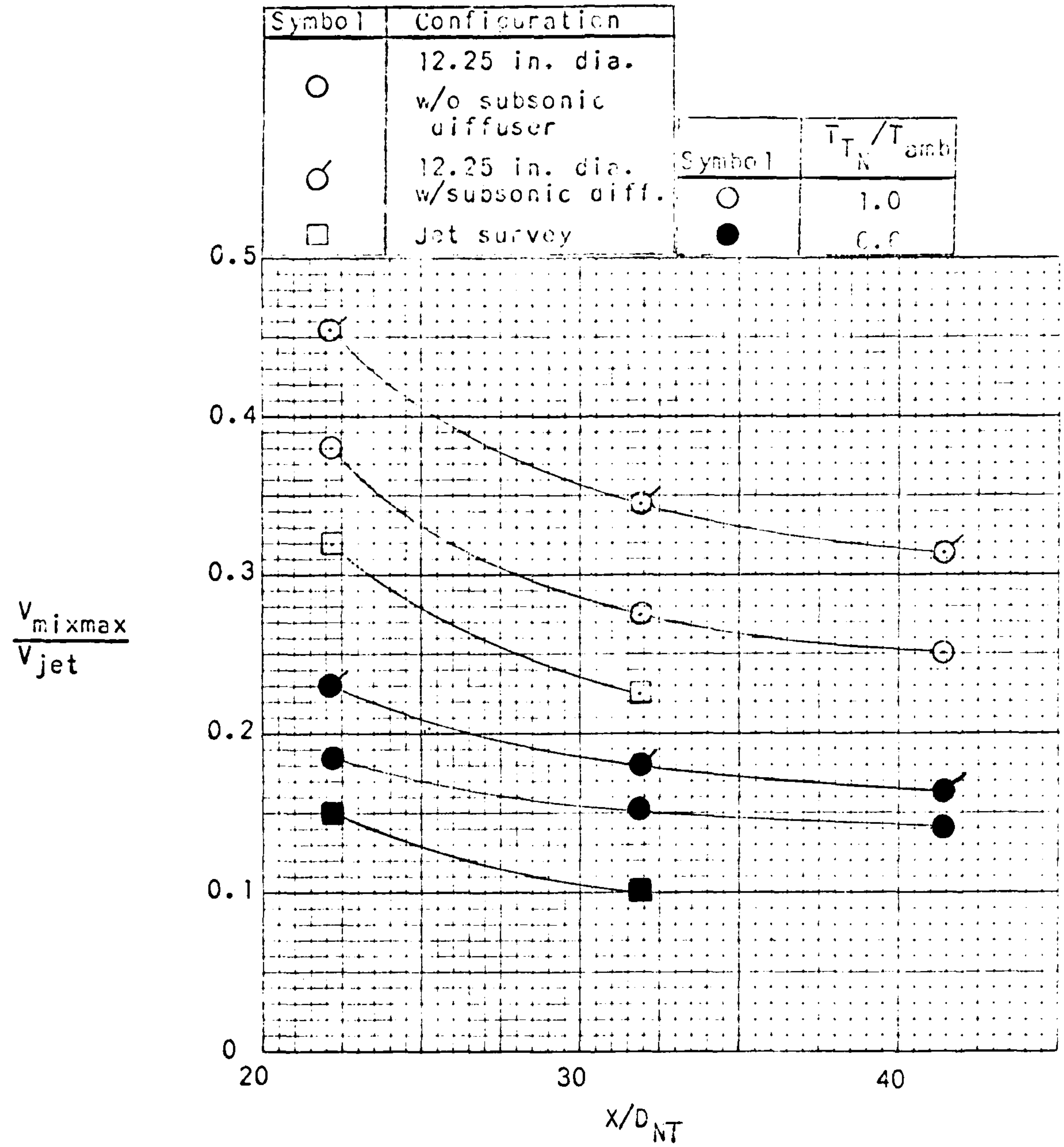

FIGURE 7.3-17. MAXIMUM MIXED VELOCITY TO JET VELOCITY RATIO VERSUS AXIAL LOCATION FOR THE 12.25 IN. DIAMETER AUGMENTER WITH AND WITHOUT EXIT SUBSONIC DIFFUSER (JET SURVEY RESULTS SHOWN FOR COMPARISON) (λ_N=2.0)

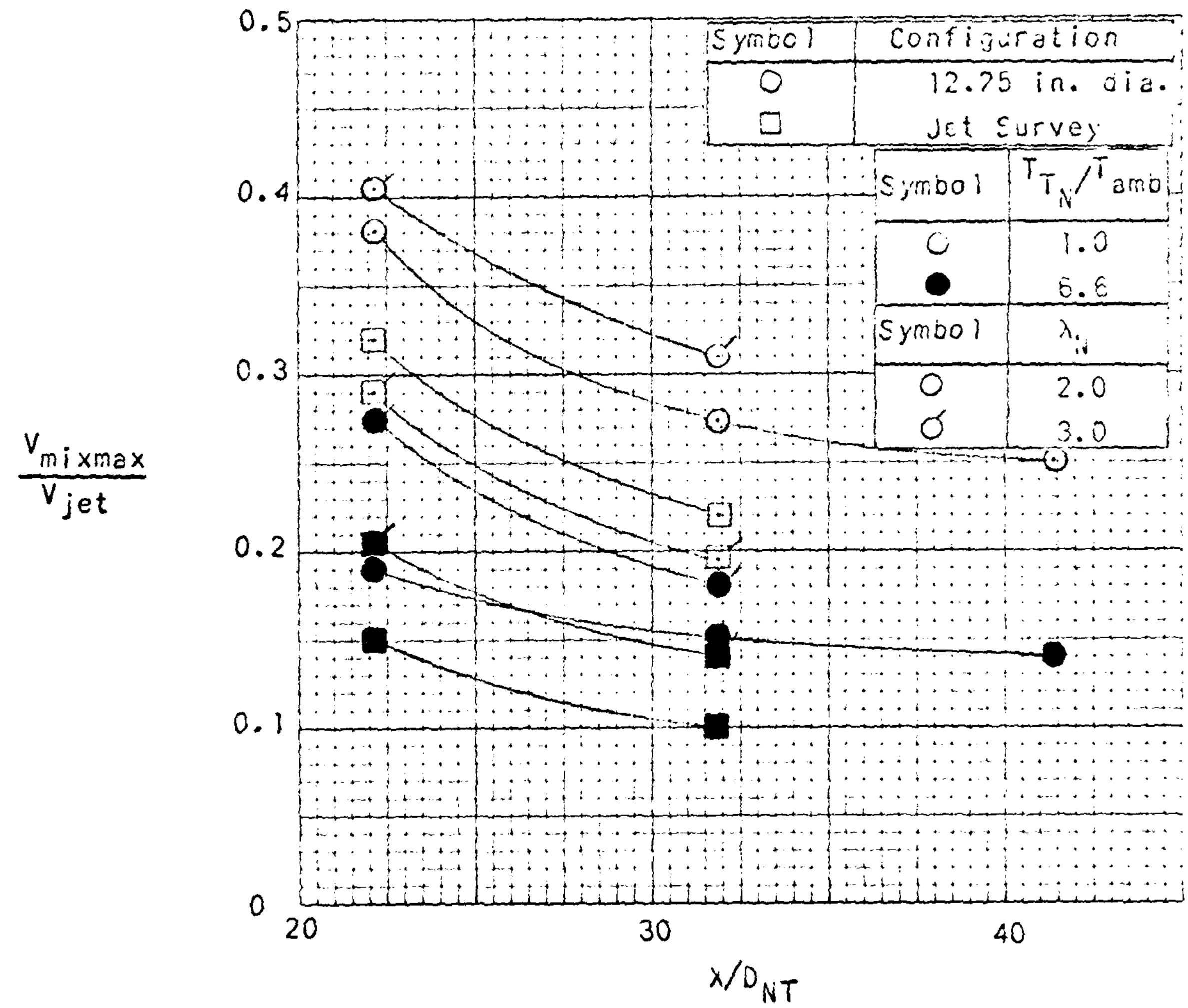

FIGURE 7.3-18. MAXIMUM MIXED VELOCITY TO JET VELOCITY RATIO VERSUS AXIAL LOCATION FOR THE 12.25 IN. DIAMETER AUGMENTER HAVING NO EXIT SUBSONIC DIFFUSER FOR JET NOZZLE PRESSURE RATIOS OF 2.0 AND 3.0 (JET SURVEY RESULTS SHOWN FOR COMPARISON).

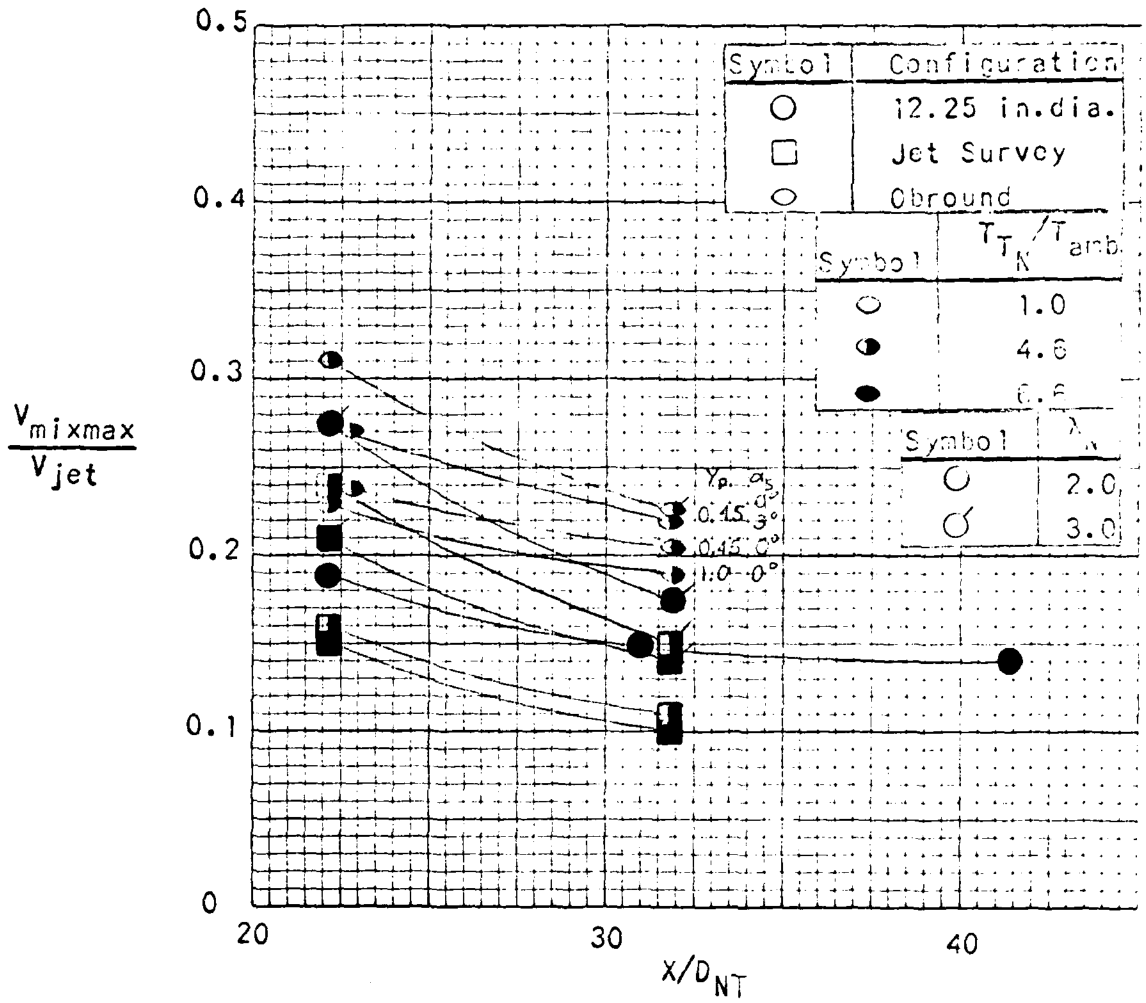

FIGURE 7.3-19. MAXIMUM MIXED VELOCITY TO JET VELOCITY RATIO VERSUS AXIAL LOCATION FOR THE OBROUND AUGMENTER (JET SURVEY RESULTS AND 12.25 IN. DIAMETER AUGMENTER RESULTS SHOWN FOR COMPARISON).

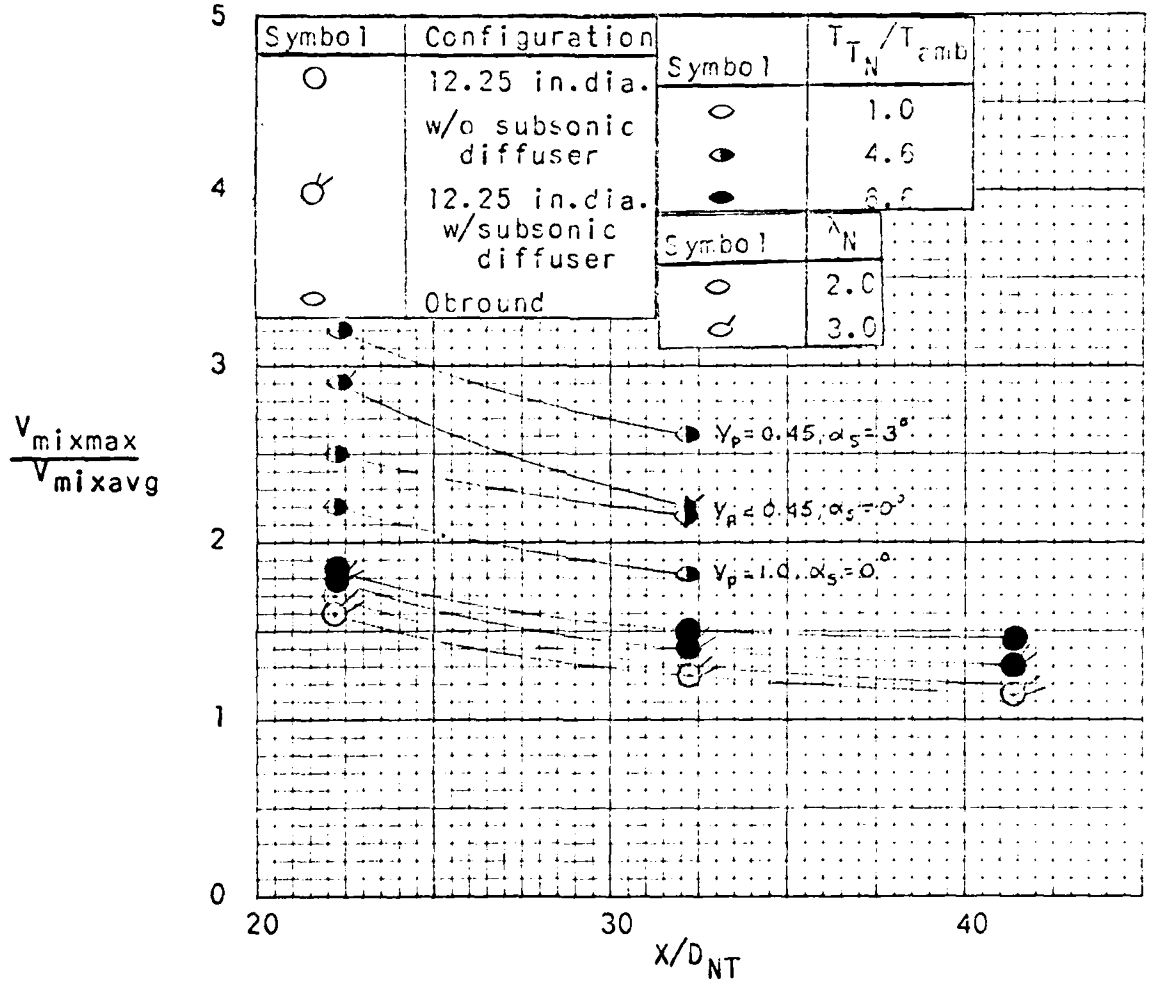

FIGURE 7.3-20. MAXIMUM MIXED VELOCITY TO AVERAGE MIXED FLOW VELOCITY RATIO VERSUS AXIAL LOCATION FOR SELECTED AUGMENTER CONFIGURATIONS.

7.3-20 has been prepared to show the ratio $\frac{V_{mix\ max}}{V_{mix\ avg.}}$, thus giving some idea of how the various parameters influence the mixed velocity distribution. When $\frac{V_{mix\ max}}{V_{mix\ avg.}}$ is equal to 1.0, the velocity profile would be flat. The results have a bearing on the interpretation of the self-noise data. They indicate, for example, that with an obround augmenter having a laterally offset jet centerline, the velocity profile is far from flat

$$\left(\frac{V_{mix\ max}}{V_{mix\ avg.}} > 2 \quad \text{at } X/D_{NT} = 32 \right)$$

so that the principal resulting self-noise would be generated by a small, persistent, high velocity core of flow, rather than by a uniform, distributed mass flow leaving the augmenter.

7.3.3 Augmenter Exit Ramp Surveys

Figure 7.3-21, -22 and -23 present total pressure rake data taken during the acoustic tests at the point where the mixed flow leaves the obround augmenter exit ramp. In every case, the flow appears to have distributed itself into a fairly thin sheet. Each of the three figures shows the influence of a particular variable. In Figure 7.3-21, the rake total pressure distribution is plotted for two jet nozzle exit to augmenter entrance spacings. Since the larger X_N spacing results in a longer flow path between the nozzle exit and the rake, mixing has progressed farther and the maximum total pressure is lower. Similarly, the data in Figure 7.3-22 shows the ramp rake total pressure distribution for two different augmenter lengths. Here again, the longer flow path represented by the longer augmenter results in a lower peak total pressure. Figure 7.3-23 presents the rake data taken at three different jet nozzle pressure ratios and shows the influence of increased jet total pressure on the maximum rake total pressure.

It is of special interest to compare the maximum exit ramp rake total pressure for a particular configuration with the maximum augmenter exit

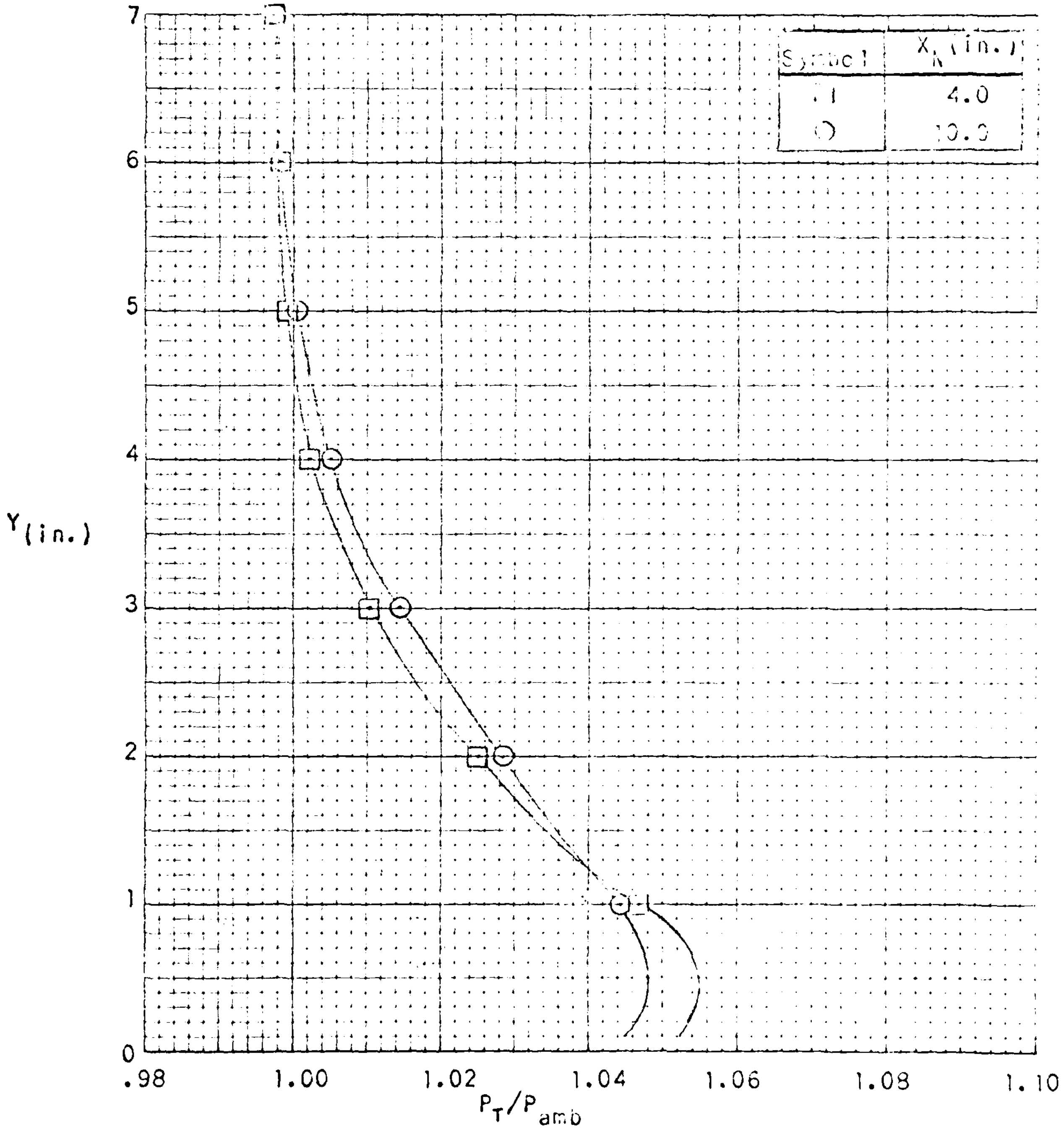

FIGURE 7.3-21. TOTAL PRESSURE DISTRIBUTION AT THE TOP OF THE OGROUND AUGMENTER EXIT RAMP FOR TWO JET NOZZLE TO AUGMENTER ENTRANCE SPACINGS.
(A_A/A_{NT}=25, L_A/D_{AM}=6, T_{TN}/T_{amb}=6.6, λ_N=2.0, Y_p=0.45)

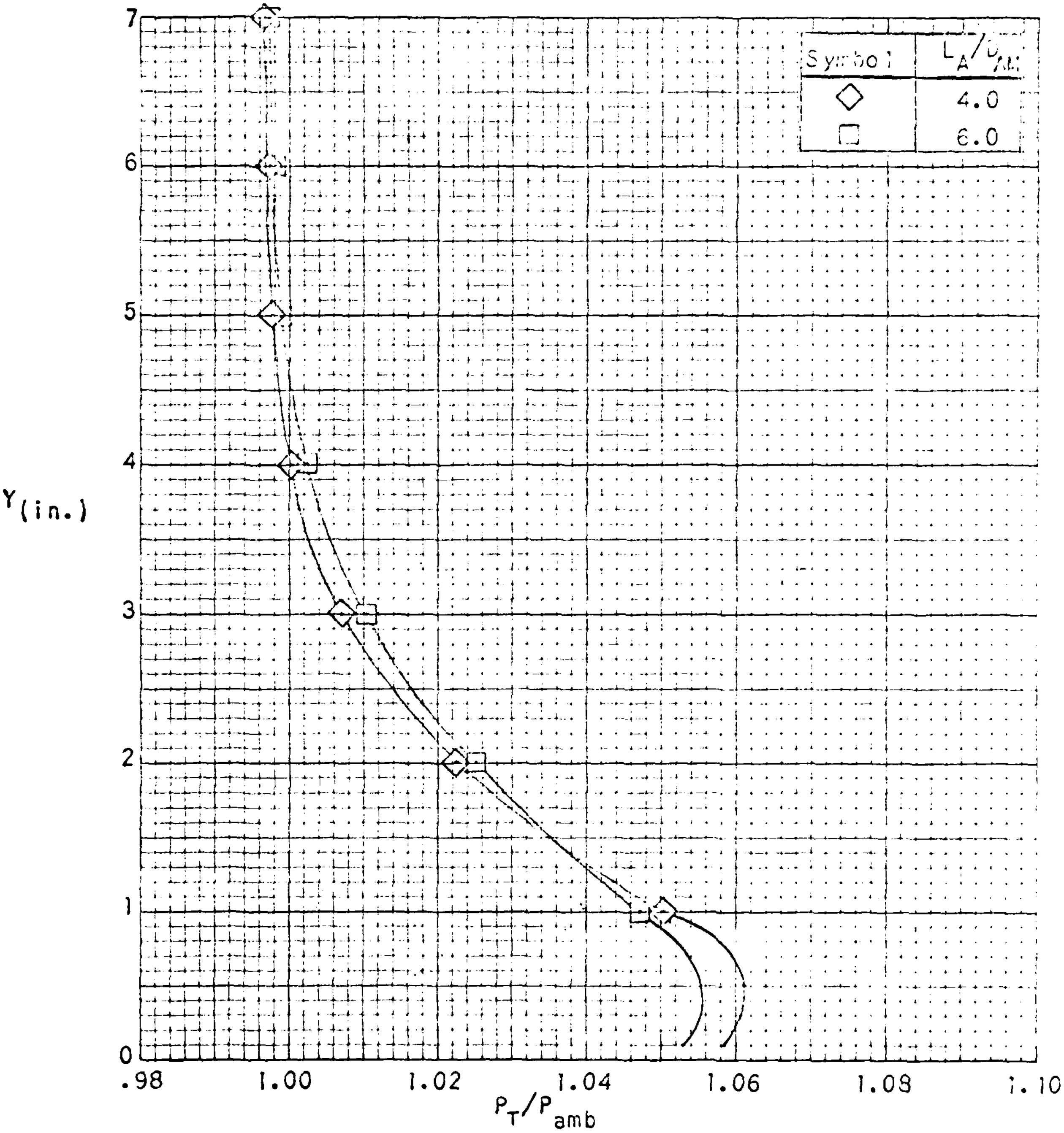

FIGURE 7.3-22. TOTAL PRESSURE DISTRIBUTION AT THE TOP OF THE OBROUND AUGMENTER EXIT RAMP FOR TWO AUGMENTER LENGTH-DIAMETER RATIOS.

(A_A/A_{NT}=25, X_N/D_{NT}=1.6, T_{TN}/T_{amb}=6.6, λ_N=2.0, Y_p=0.45)

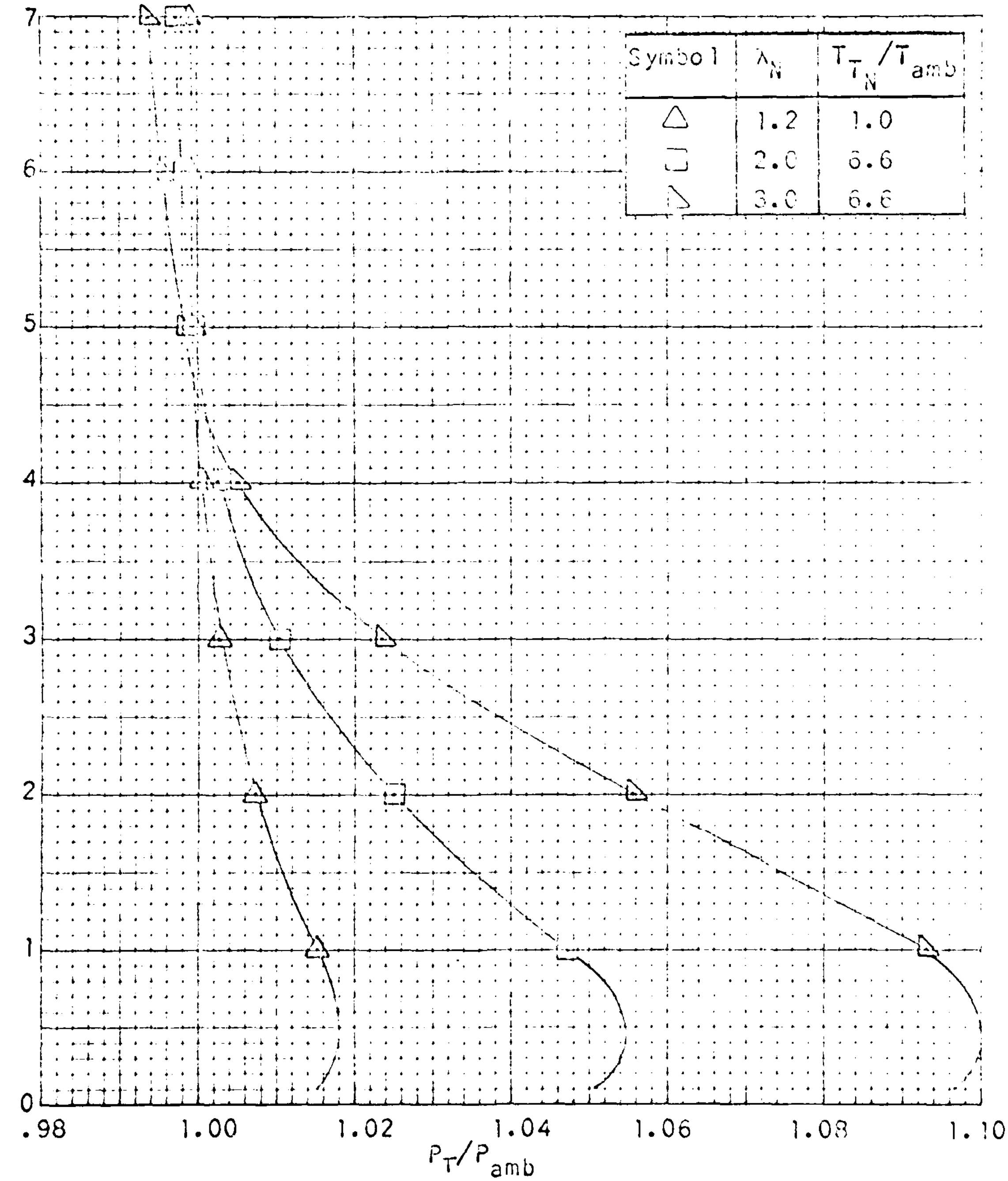

FIGURE 7.3-23. TOTAL PRESSURE DISTRIBUTION AT THE TOP OF THE OBROUND AUGMENTER EXIT RAMP FOR THREE JET NOZZLE PRESSURE RATIOS. (A_A/A_{NT}=25, X_N/D_{NT}=1.6, L_A/D_{AM}=6, Y_p=0.45)

total pressure. This can be done by comparing the maximum exit ramp total pressure from Figure 7.3-22 for the 72" augmenter length with the maximum augmenter exit total pressure from Figure 7.3-10. At the augmenter exit, a maximum total pressure to ambient pressure ratio of about 1.065 is found, while the maximum exit ramp rake total pressure to ambient pressure ratio is found to be 1.052. Considering the geometry (the ramp rake isn't lined up with the jet centerline), one would conclude that the maximum velocity in the flow leaving the ramp is only slightly lower than the maximum velocity leaving the augmenter duct.

7.3.4 Stack Exit Total Temperatures

Two total temperature probes were placed in the stack exit with the stack and baffles configuration. One probe was on the stack centerline, the other was displaced laterally one-half the distance to the stack sidewall. These probes were mounted on a lateral plate which could be reversed end for end. As a result, data was obtained both with the offset probe behind the jet nozzle position and on the opposite side of the stack from the jet nozzle centerline. The data from these probes is presented in Figure 7.3-24 in the form of a temperature parameter where

$$T_{exit_p} = \frac{T_{exit} - T_{amb}}{T_{T_N} - T_{amb}} = \frac{T_{exit} - T_{BE}}{T_{T_N} - T_{BE}} .$$

The results show that the probe behind the jet nozzle experiences much higher total temperatures. The indicated exit temperature parameter of 0.275 corresponds to a temperature of 950°F for an afterburning engine on a 100°F day.

7.4 Augmenter Longitudinal and Perimetral Wall Temperature Distributions

Among the major goals of this test program was the gathering of test data relating to jet impingement on the augmenter wall and resultant augmenter wall heating. To accomplish this, the aero-thermal test program was run with the absorptive obround augmenter having 30 longitudinally and perimetrally distributed

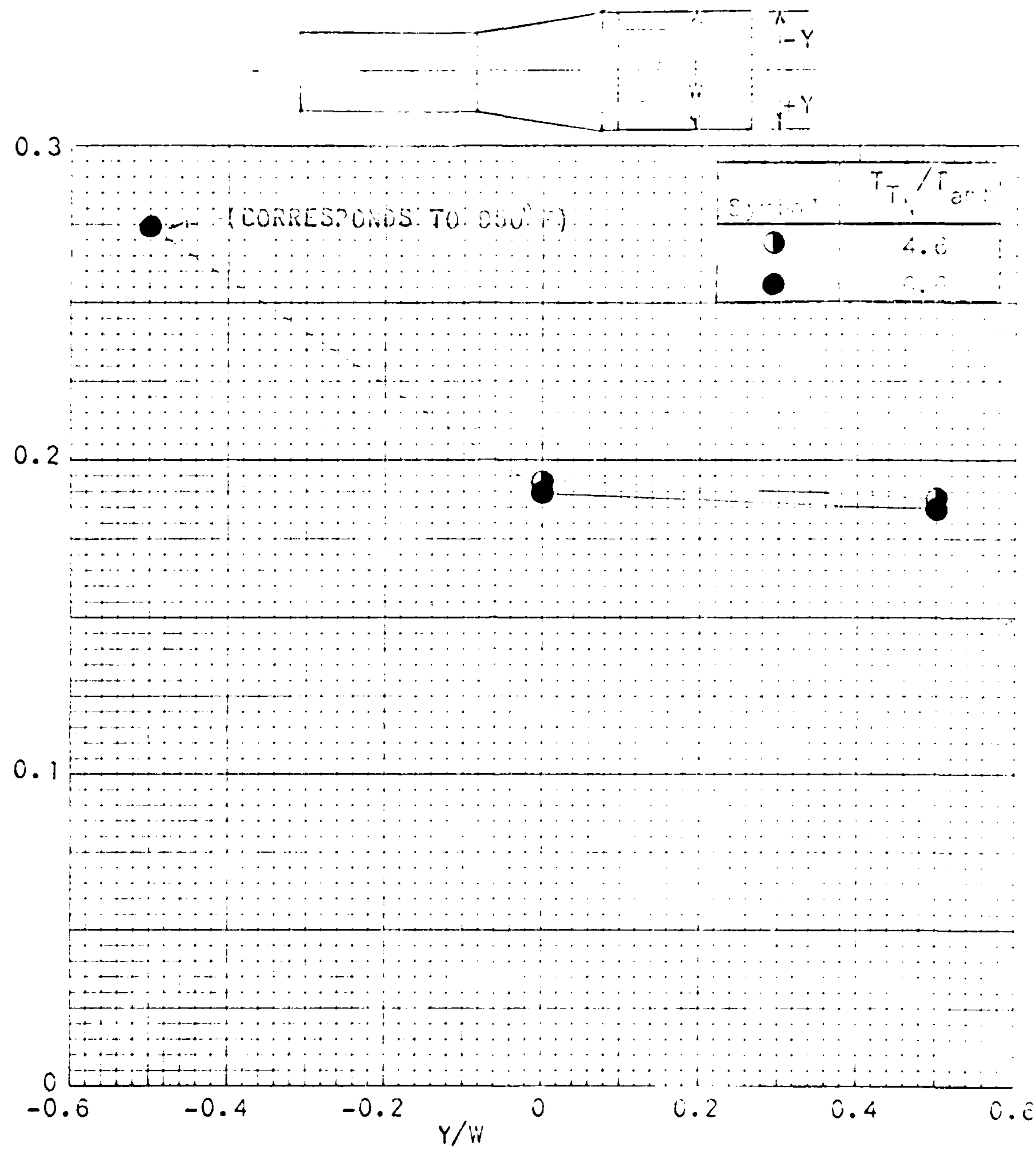

FIGURE 7.3-24. LATERAL TOTAL TEMPERATURE VARIATION AT THE EXIT OF THE STACK AND BAFFLES.
(A_A/A_{NT}=25, X_N/D_{NT}=1.6, L_A/D_{AM}=4, A_D/A_A=2, λ_N=2.0, Y_p=0.45)

wall thermocouples, as well as wall static pressure taps. Tests were run with the jet nozzle centerline oriented in various ways relative to the augmenter centerline to define the influence of aircraft configuration and orientation on the wall heating phenomenon. Here, as with the preceding survey results, corrections have been made to account for the effective jet deflection at elevated temperature, except where it is desired to show the influence of vertical jet nozzle centerline deflection.

The augmenter cross-section survey results for $\lambda_N = 2.0$, discussed in Section 7.3.2, indicated that, with lateral translation or deflection of the jet nozzle centerline relative to the obround augmenter centerline, the jet tended to be carried to the augmenter sidewall. The results of this tendency are graphically illustrated in Figure 7.4-1 which shows the longitudinal distribution of augmenter wall temperature parameter, ${}^{T}wall_p$, for a number of different lateral nozzle centerline locations and deflections. The data in the figure indicate unexpectedly high augmenter sidewall temperatures for a lateral offset and deflection representative of the F-14A aircraft configuration ($Y_p = 0.45$, $\alpha_s = 1°$). Similar top and bottom wall data show appreciable jet impingement effects when the jet is deflected vertically (Figure 7.4-2). Figure 7.4-1 shows, for example, that the orientation corresponding to the F-14A ($Y_p = 0.45$, $\alpha_s = 1°$) results in over 100% greater maximum wall temperature parameter than for the centered, undeflected jet.

Additional obround augmenter sidewall temperature data were obtained during the acoustic testing to find the influences of the augmenter exit ramp and the influence of jet nozzle total temperature and pressure ratio on wall temperature. Figure 7.4-3 shows the distribution of sidewall temperature parameter at $\lambda_N = 2.0$ with and without ramp for nozzle total temperatures of 2300°R and 3300°R (${}^{T}T_N/T_{amb} = 4.6$ & 6.6). The data show a slightly lower maximum wall temperature parameter at ${}^{T}T_N = 3300°R$ than at 2300°R (which is due to a slightly lower mixed temperature parameter; see Section 2.2) and a slight increase in maximum wall temperature parameter when the ramp is added because of the reduction in pumped air.

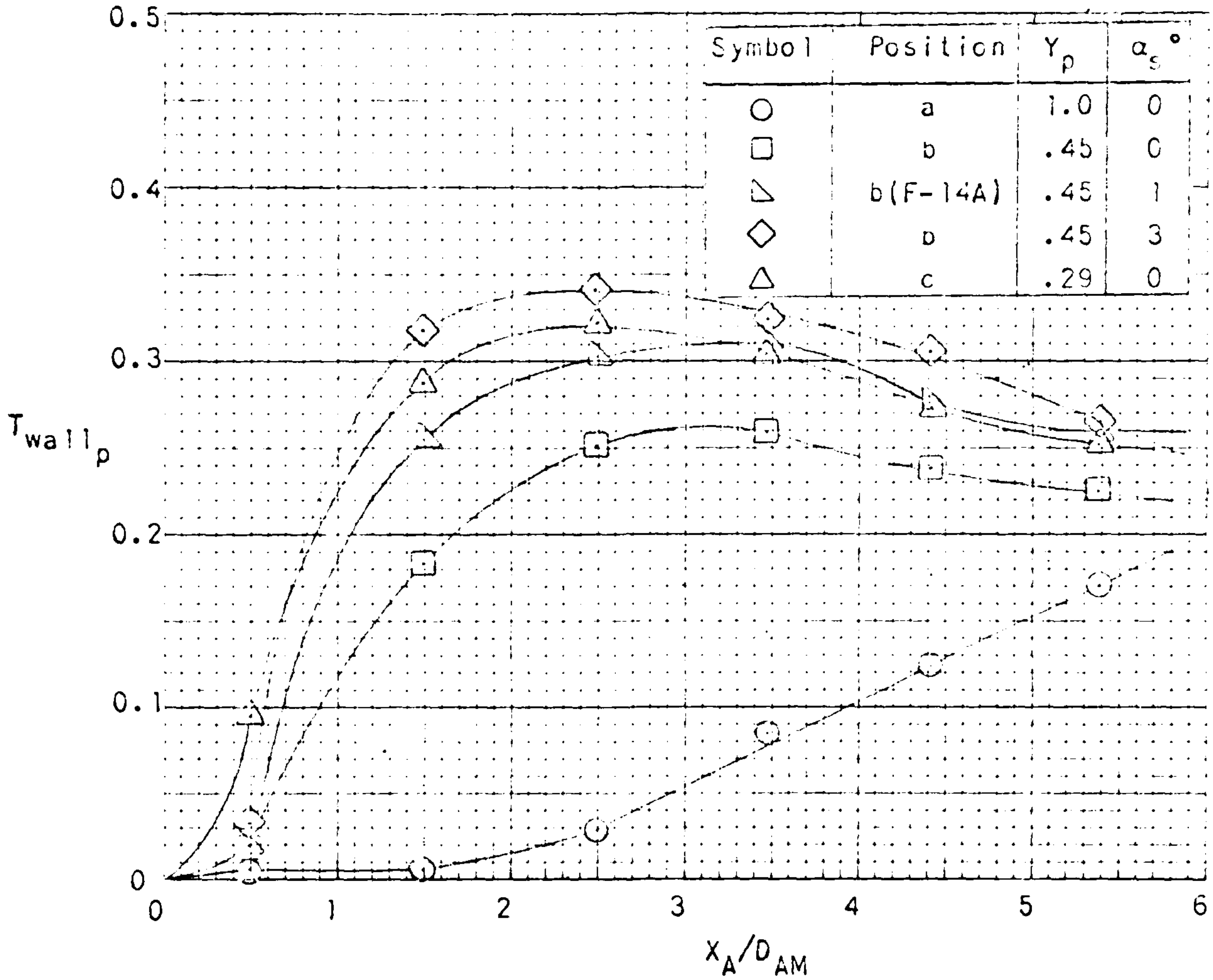

FIGURE 7.4-1. LONGITUDINAL SIDEWALL TEMPERATURE DISTRIBUTION VERSUS JET NOZZLE LATERAL POSITION AND DEFLECTION FOR THE OBROUND AUGMENTER.
(A_A/A_{NT}=25, X_N/D_{NT}=1.6, L_A/D_{AM}=6, T_{T_N}/T_{amb}=4.6, λ_N=2.0)

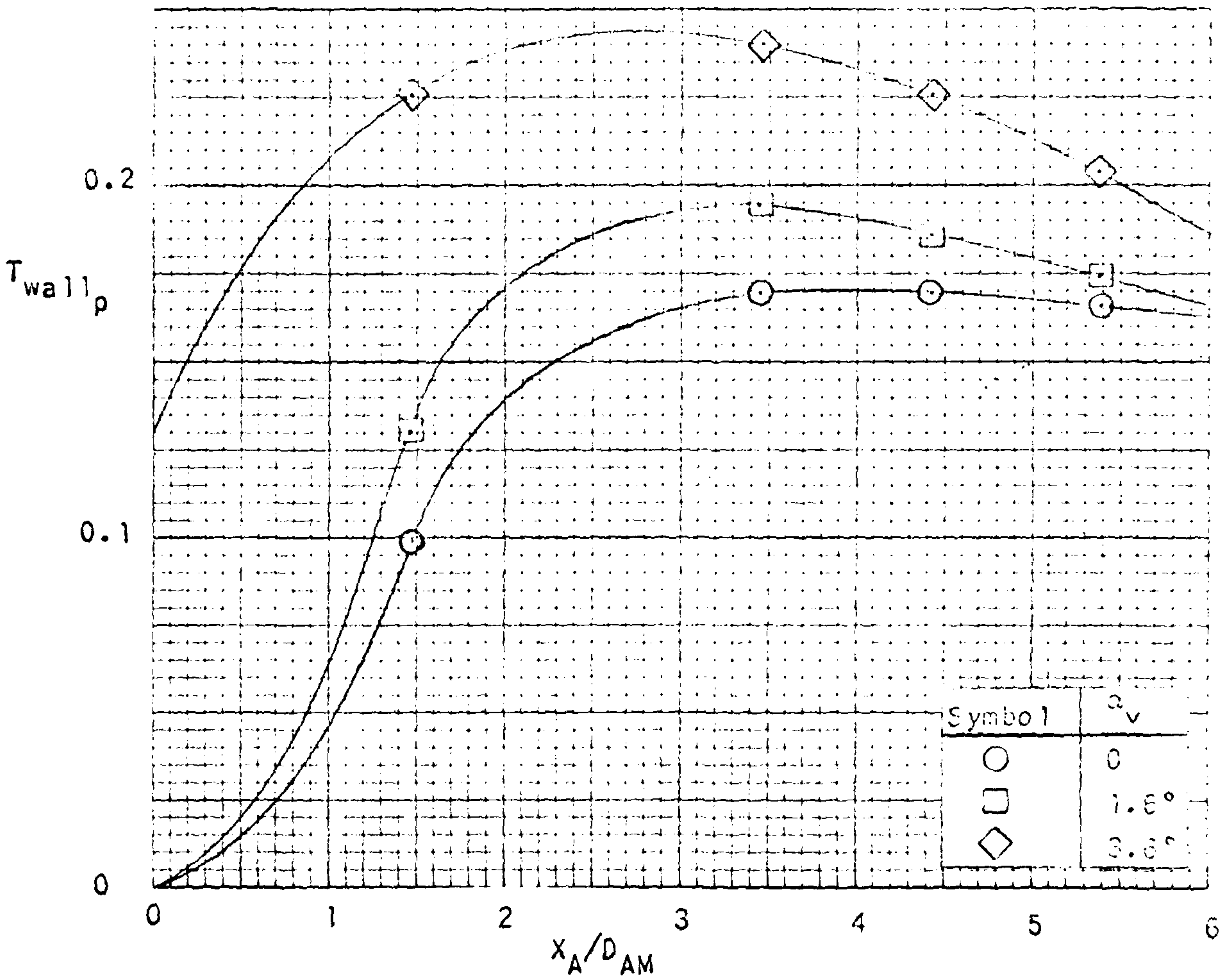

FIGURE 7.4-2. LONGITUDINAL BOTTOM WALL TEMPERATURE DISTRIBUTION VERSUS JET NOZZLE VERTICAL DEFLECTION FOR THE OBROUND AUGMENTER.
(A_A/A_{NT}=25, X_N/D_{NT}=1.6, L_A/D_{AM}=6, T_{T_N}/T_{amb}=4.6, λ_N=2.0, position a, Y_p=1.0)

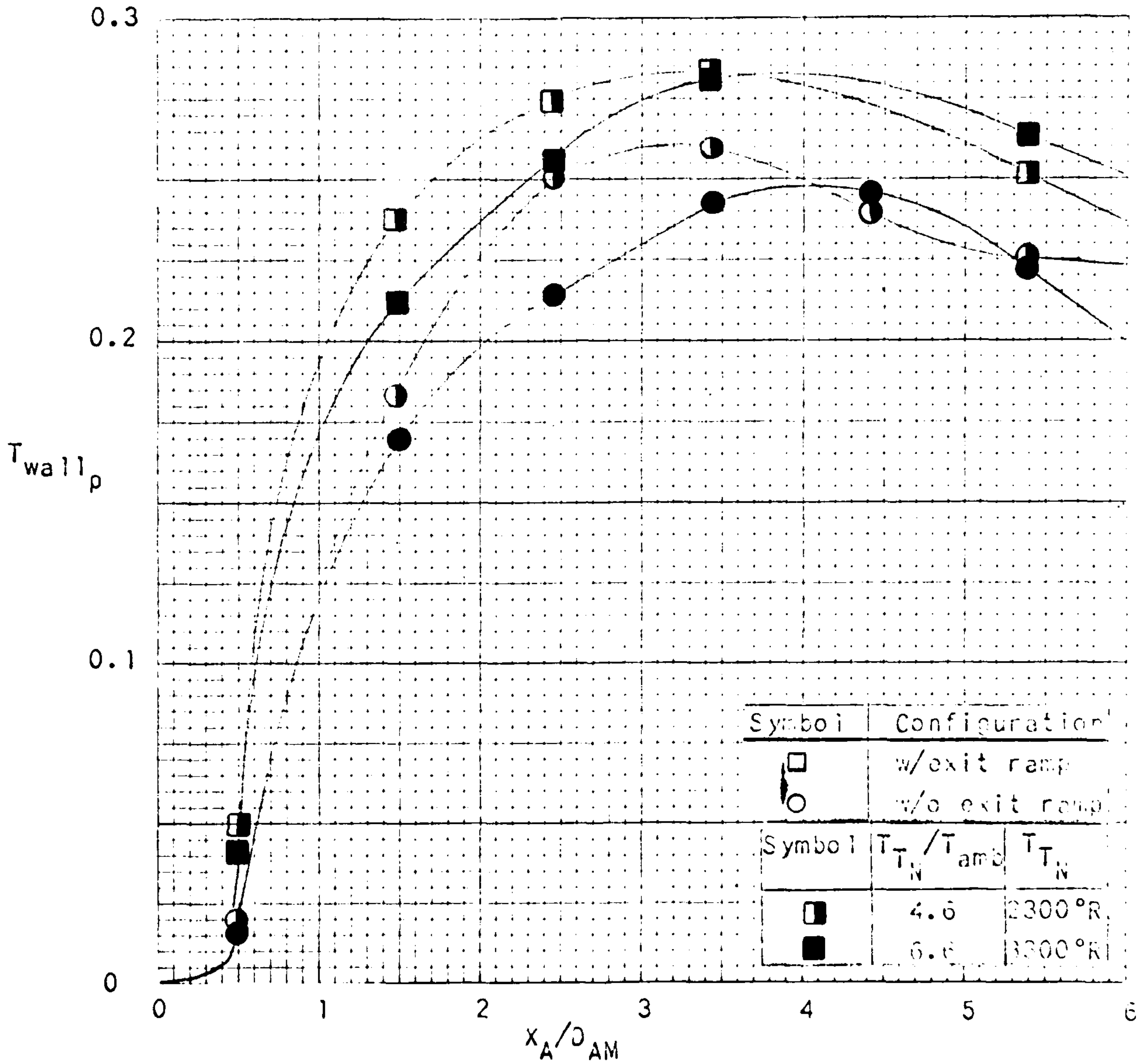

FIGURE 7.4-3. LONGITUDINAL SIDEWALL TEMPERATURE DISTRIBUTION FOR THE OBROUND AUGMENTER WITH AND WITHOUT THE EXIT RAMP AND AT DIFFERENT JET NOZZLE TO AMBIENT TEMPERATURE RATIOS.

$(A_A/A_{NT}=25, X_N/D_{NT}=1.6, L_A/D_{AM}6, Y_p=0.45, \lambda_N=2.0)$

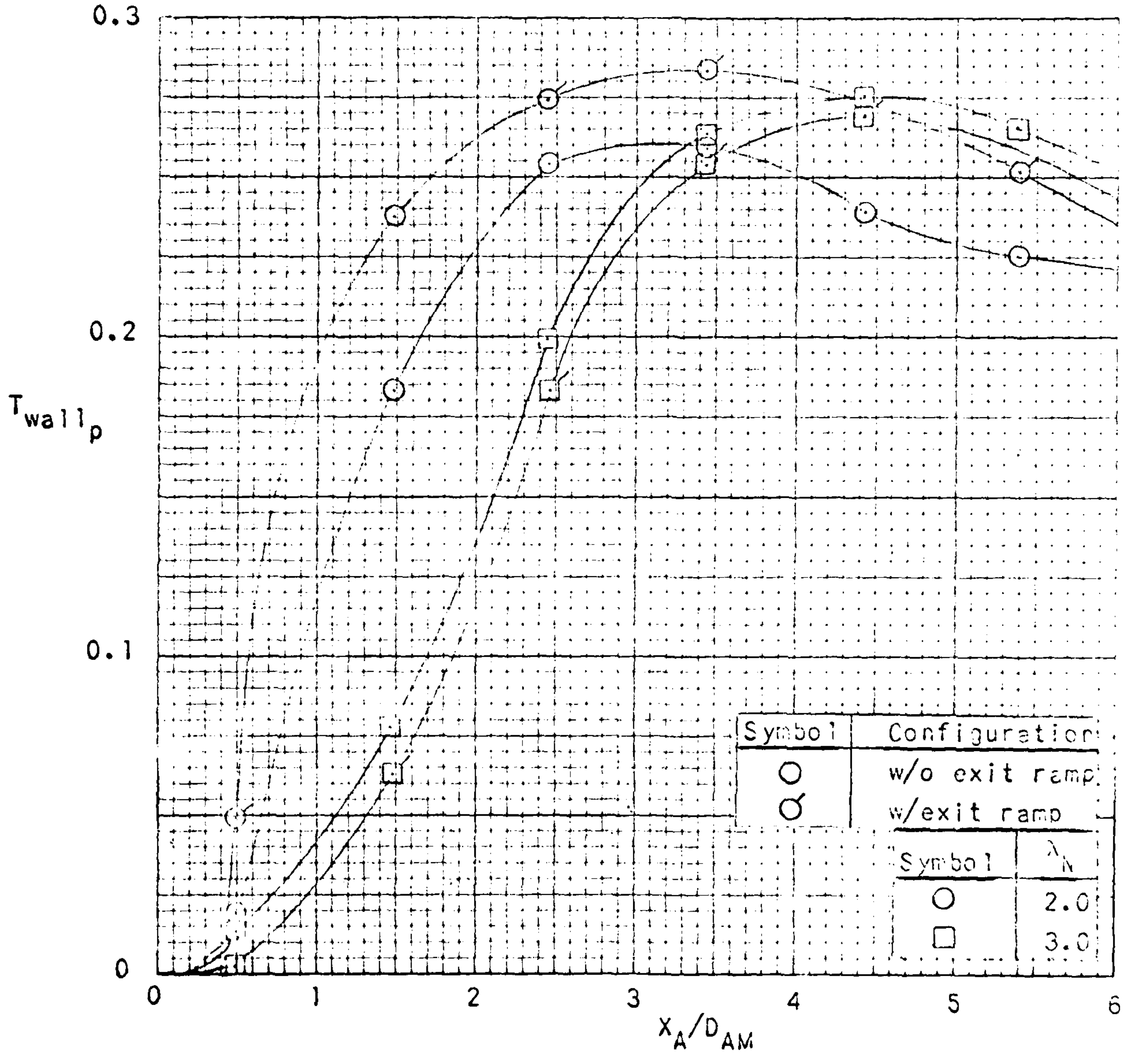

FIGURE 7.4-4. LONGITUDINAL SIDEWALL TEMPERATURE DISTRIBUTION FOR THE OBROUND AUGMENTER WITH AND WITHOUT THE EXIT RAMP FOR JET NOZZLE PRESSURE RATIOS OF 2.0 AND 3.0.
$(A_A/A_{NT}=25, X_N/D_{NT}=1.6, L_A/D_{AM}=6, Y_p=0.45, T_{T_N}/T_{amb}=4.6)$

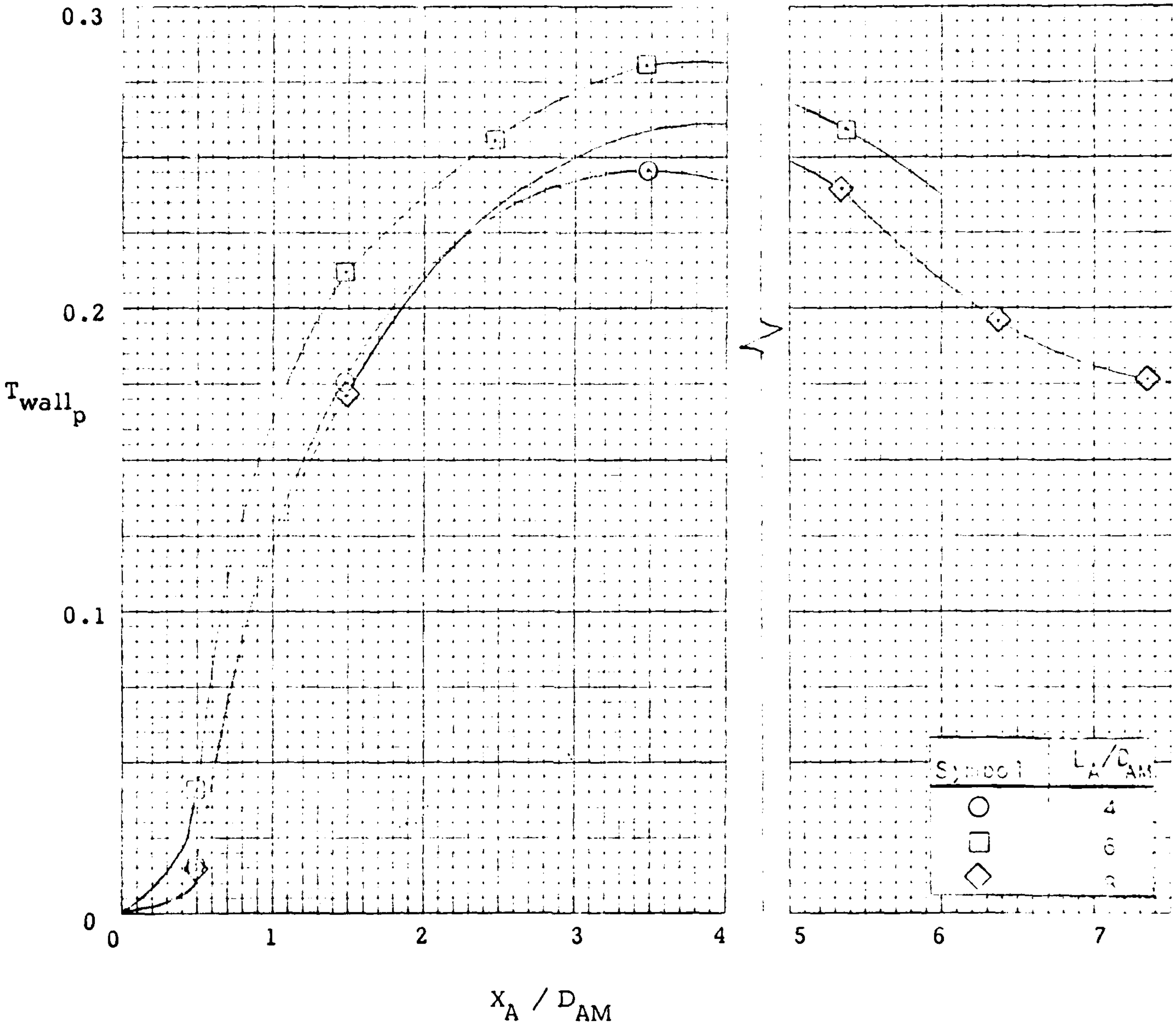

FIGURE 7.4-5 LONGITUDINAL SIDEWALL TEMPERATURE DISTRIBUTION FOR THE OBROUND AUGMENTER AND EXIT RAMP FOR VARYING AUGMENTER LENGTH-DIAMETER RATIOS.

$(A_A/A_{NT} = 25, X_N/D_{NT}=1.6, Y_p=0.45, T_{T_N}/T_{amb}=6.6, \lambda_N=2.0)$

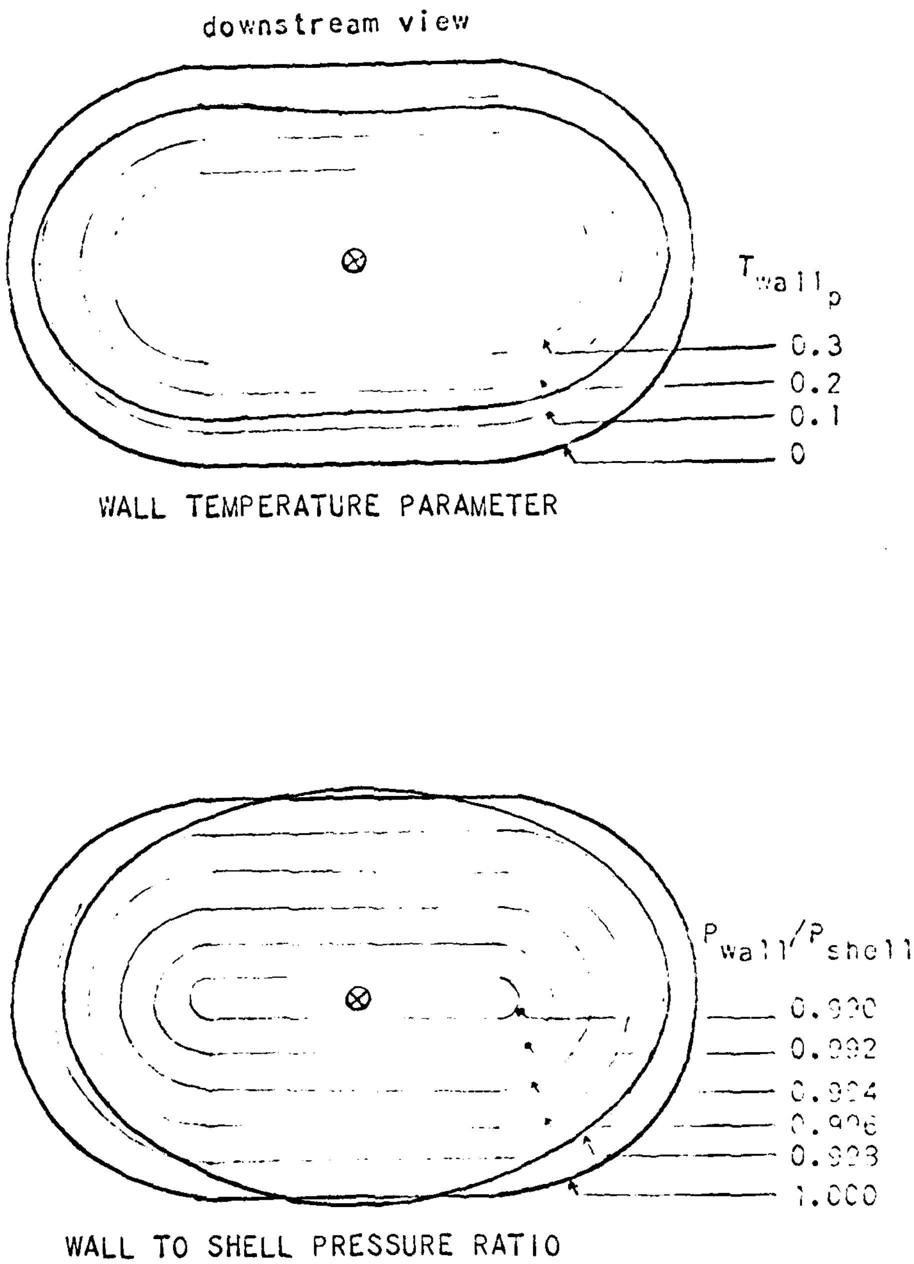

FIGURE 7.4-6. WALL PRESSURE AND TEMPERATURE VARIATION AROUND THE PERIMETER OF THE OBROUND AUGMENTER AT THE 42 IN. STATION WITH THE JET CENTERED (POSITION a, Y_p = 1.0) AND UNDEFLECTED.

downstream view

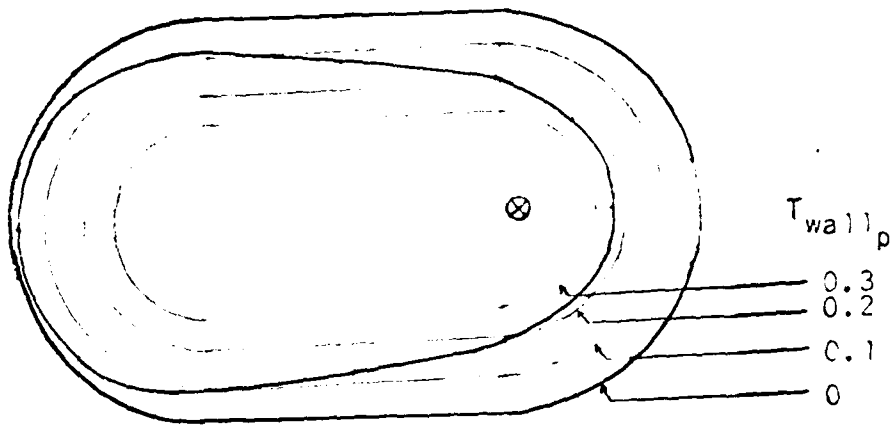

WALL TEMPERATURE PARAMETER

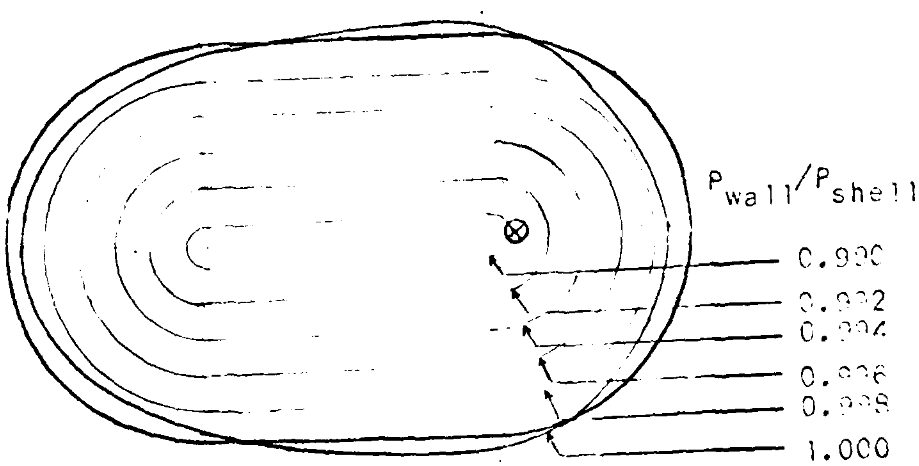

WALL TO SHELL PRESSURE RATIO

FIGURE 7.4-7. WALL PRESSURE AND TEMPERATURE VARIATION AROUND THE PERIMETER OF THE OBROUND AUGMENTER AT THE 42 IN. STATION WITH THE JET IN THE F-14A LOCATION (POSITION b, Y_p = 0.45) AND UNDEFLECTED.

downstream view

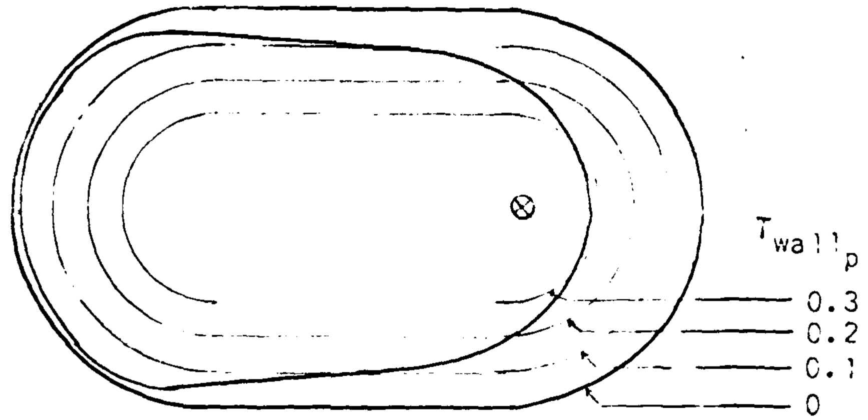

WALL TEMPERATURE PARAMETER

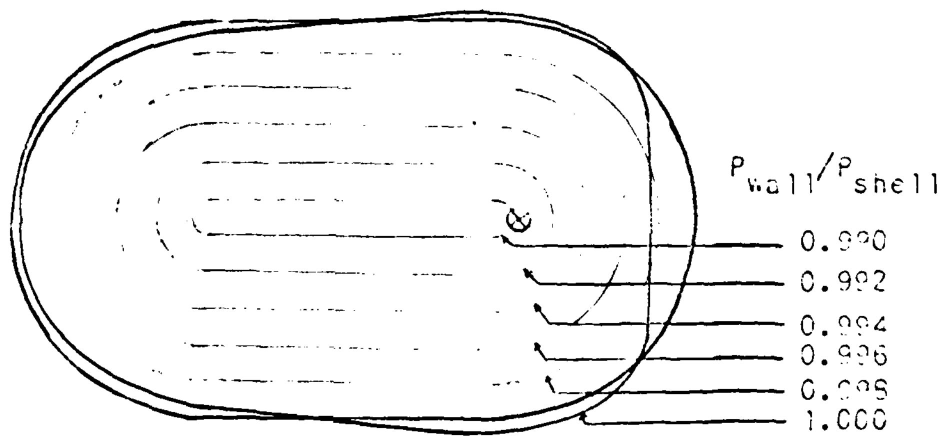

WALL TO SHELL PRESSURE RATIO

FIGURE 7.4-8. WALL PRESSURE AND TEMPERATURE VARIATION AROUND THE PERIMETER OF THE OBROUND AUGMENTER AT THE 42 IN. STATION WITH THE JET IN THE F14A LOCATION (POSITION b, $Y_p = 0.45$) AND DEFLECTED 3° LATERALLY TOWARD THE NEAR WALL OF THE AUGMENTER.

downstream view

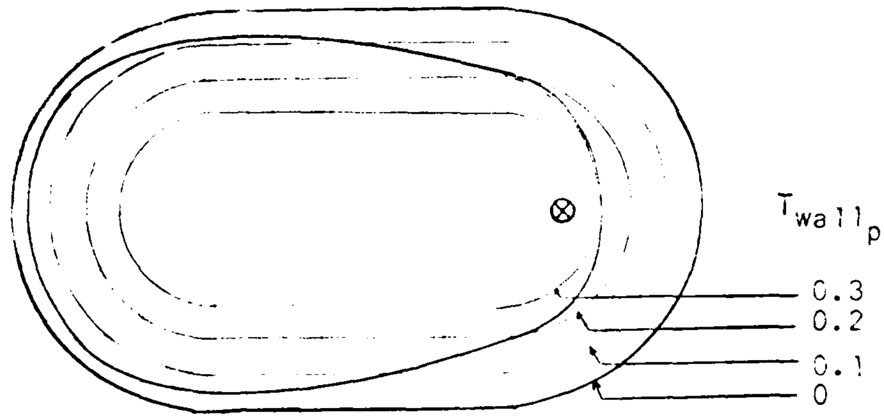

WALL TEMPERATURE PARAMETER

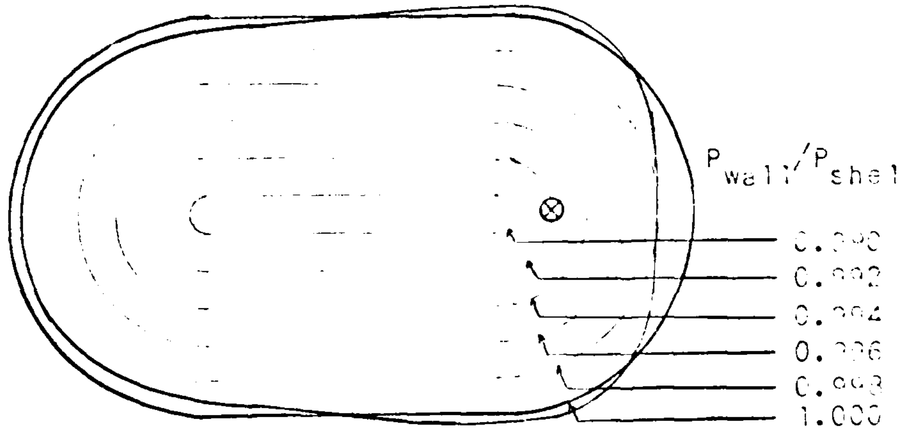

WALL TO SHELL PRESSURE RATIO

FIGURE 7.4-9. WALL PRESSURE AND TEMPERATURE VARIATION AROUND THE PERIMETER OF THE OBROUND AUGMENTER AT THE 42 IN. STATION WITH THE JET IN POSITION c (Y_p = 0.29) AND UNDEFLECTED.

downstream view

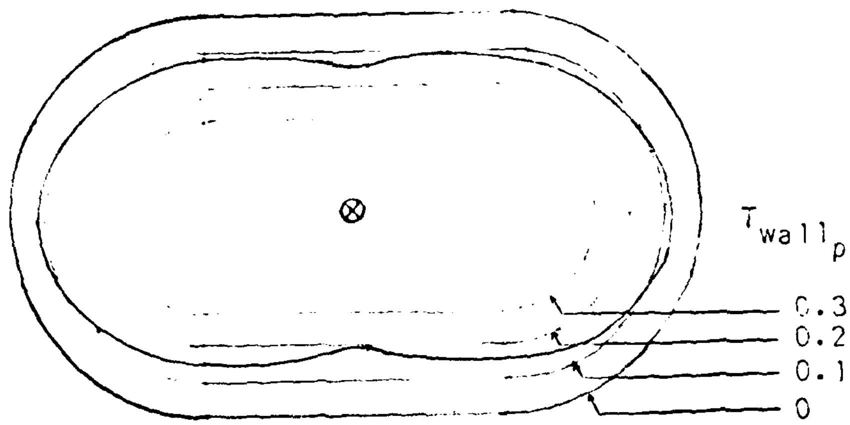

WALL TEMPERATURE PARAMETER

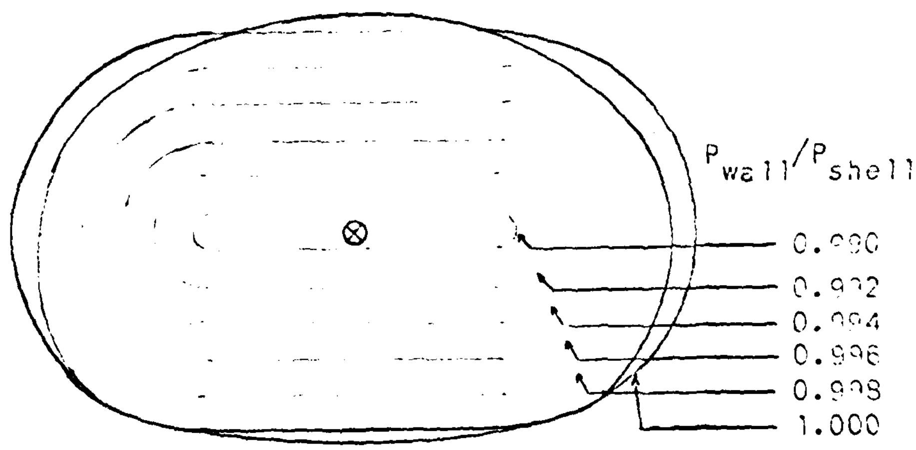

WALL TO SHELL PRESSURE RATIO

FIGURE 7.4-10. WALL PRESSURE AND TEMPERATURE VARIATION AROUND THE PERIMETER OF THE OBROUND AUGMENTER AT THE 42 IN. STATION WITH THE JET CENTERED (POSITION a, Y_p = 1.0) AND DEFLECTED DOWNWARD 1.6°.

downstream view

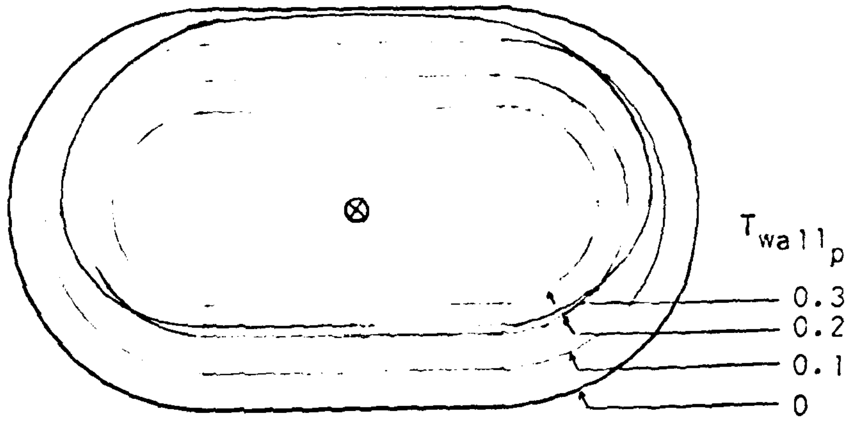

WALL TEMPERATURE PARAMETER

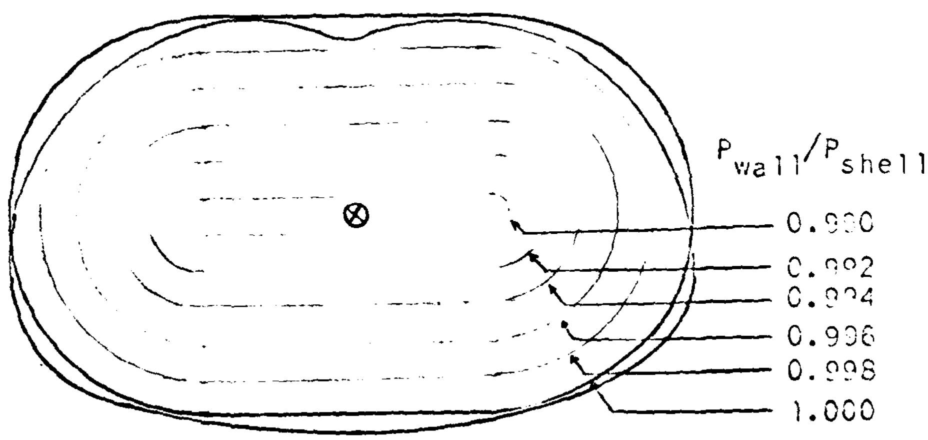

WALL TO SHELL PRESSURE RATIO

FIGURE 7.4-11. WALL PRESSURE AND TEMPERATURE VARIATION AROUND THE PERIMETER OF THE OBROUND AUGMENTER AT THE 42 IN. STATION WITH THE JET CENTERED (POSITION a, Y_p = 1.0) AND DEFLECTED DOWNWARD 3.6°.

The effects of jet nozzle pressure ratio on the sidewall temperature parameter with the offset jet ($Y_p = 0.45$, $\alpha_s = 0°$) appear in Figure 7.4-4. Operation at $\lambda_N = 3.0$ rather than 2.0 greatly reduces the extent of jet impingement on the augmenter sidewall. This is to be expected on the basis of the augmenter cross-section survey results (Figure 7.3-11) wherein the higher pressure ratio offset jet was not carried closer to the sidewall.

Figure 7.4-5 contains wall temperature parameter data for different augmenter length-diameter ratios. These data indicate that, within the accuracy obtainable, augmenter length-diameter ratio has little effect on the longitudinal wall temperature distribution.

Figures7.4-6, -7, -8, -9, -10 and -11 represent a different way of presenting the affect of impingement on wall temperature. At each of the instrumented axial stations, there were several thermocouples and wall pressure taps located around the augmenter liner perimeter. For the figures presented herein, the instrumentation at the 42" station has been selected to portray the influence of jet impingement on the distribution of wall temperature and pressure around the liner perimeter. Figure 7.4-6 shows the pressure and temperature distribution for a centered, undeflected jet nozzle. The temperatures and pressures must be symmetrical with respect to both the vertical and horizontal axes. Figures 7.4-7, -8 and -9 show the effects of varying amounts of lateral jet centerline offset and deflection. Similarly, Figures 7.4-10 and -11 present the data taken with different amounts of vertical nozzle centerline deflection.

7.5 Jet Nozzle Base Pressure

A single jet nozzle base pressure tap was installed on the nozzle boattail about 1/4 inch upstream of the nozzle exit. Measurements of nozzle base pressure were taken for all test points to make possible a determination of how the base pressure is affected by the Hush House environment. Because of the peculiar boattail configuration, the base pressure was significantly below ambient pressure even for the jet survey tests and corresponded to

$$\frac{P_{NB}}{P_{amb}} = .996 \quad \text{for all } \lambda_N \text{ and } T_{T_N} \text{ conditions .}$$

A base pressure parameter, P_{NB_p}, was defined to show how the base pressure pump-down with the jet inside of a Hush House would compare to the pump-down during out-of-doors (free field) operation.

$$P_{NB_p} = \frac{(P_{NB} - P_{interior})_{Hush\ House} - (P_{NB} - P_{amb})_{free\ field}}{P_{amb}}$$

$$= \frac{(P_{NB} - P_{BE})_{with\ augmenter} - (P_{NB} - P_{EE})_{jet\ survey}}{P_{EE}}$$

When an aircraft is placed in a Hush House, the Hush House interior pressure becomes, in effect, a different reference ambient pressure. A base pressure parameter of -0.005, for example, would imply that the nozzle base pressure in the Hush House environment is 2" H_2O lower, relative to this new reference ambient pressure than the free field base pressure is relative to barometric pressure. Figure 7.5-1 presents the base pressure parameter plotted versus jet nozzle to ambient temperature ratio for a variety of test configurations with a nozzle exit to augmenter entrance spacing typical of the expected F-14A installation. The data shows little excess nozzle base pump-down for most configurations when the jet nozzle to ambient temperature ratio, T_{T_N}/T_{amb}, corresponds to military or afterburning power. The pump-down increases with the increased pumped flow associated with the addition of a subsonic diffuser. A very small pump-down is apparent with the obround augmenter which implies that the nozzle base pressure with Hush House operation will bear the same relationship to the Hush House interior pressure as the free field operation base pressure does to barometric pressure.

Figure 7.5-2 shows the influence of nozzle exit to augmenter spacing on base pressure parameter. As the jet nozzle exit is moved very close to the augmenter entrance, the base pressure is influenced more and more by reduced static pressures in the pumped flow entering the augmenter and the base pressure parameter becomes more and more negative. At large spacings between the nozzle exit and augmenter entrance, on the other hand, the situation at the nozzle base approaches the free field situation and $P_{NB_P} = 0$ within the measurement accuracy.

Since the base pressure parameter shows little excess pump-down for configurations typical of Hush House installation with normal engine operating conditions, the nozzle base pressure effects will not be given further consideration.

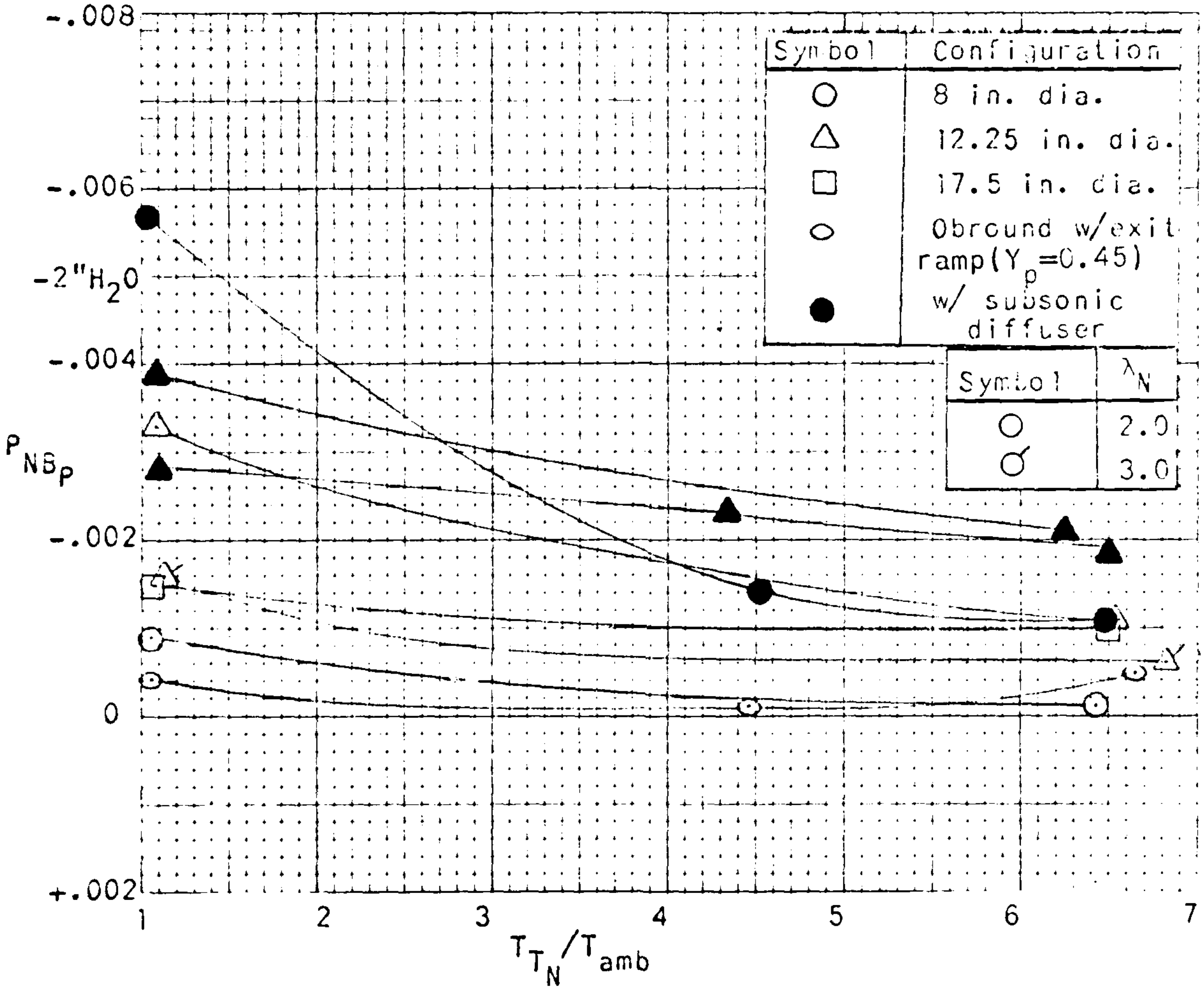

FIGURE 7.5-1. NOZZLE BASE PRESSURE PARAMETER VERSUS JET NOZZLE TO AMBIENT TEMPERATURE RATIO FOR VARIOUS AUGMENTER CONFIGURATIONS.

$X_N/D_{NT}=1.6, L_A/D_{AM}=6$

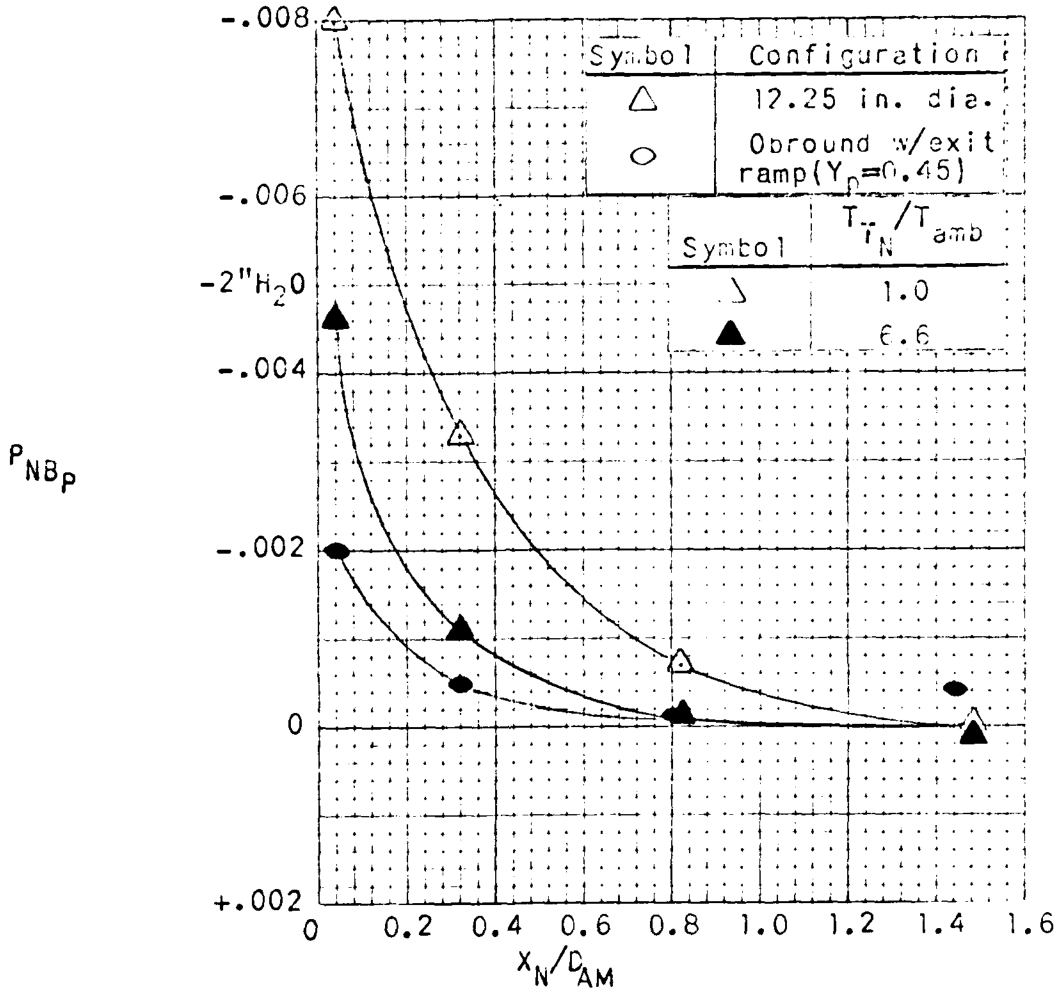

FIGURE 7.5-2. NOZZLE BASE PRESSURE PARAMETER VERSUS JET NOZZLE EXIT TO AUGMENTER ENTRANCE SPACING PARAMETER. ($A_A/A_{NT}=25, L_A/D_{AM}=6, \lambda_N=2.0$)

7.6 Acoustic Test Results

7.6.1 Jet survey

The purpose of the jet survey was to obtain baseline data on the PWL spectra of the undisturbed (not surrounded by an augmenter tube) jets used in the model study. The 2.75-in.-diameter convergent-divergent nozzle, as described in detail in Sec. 4.1, was run at pressure ratios λ_N of 2 and 3 and at jet nozzle temperatures T_{T_N} of 520°R, 2300°R, and 3300°R. Table 7.6.1 summarizes the characteristic acoustic parameters of the various model jets.

TABLE 7.6.1 CHARACTERISTIC ACOUSTIC PARAMETERS OF THE MODEL JETS*

Jet Total Temperature		Pressure Ratio	Jet Exit Velocity	Jet Mach Number	
T_{T_N} in °R	T_j in °R	λ_N	fps		ρ_{EXIT}/ρ_{AMB}†
520	426.4	2	1056	1.04	1.17
	380	3	1302	1.36	1.31
2300	1886	2	2221	1.04	0.264
	1680	3	2737	1.36	0.298
3300	2706	2	2660	1.04	0.184
	2410	3	3278	1.36	0.208

*This information was supplied by Fluidyne and is based on the assumption that the jet was expanded isentropically to P_{AMB} for each of the above conditions.

†Ratio of density of jet exhaust gas at exit plane to density of ambient temperature air.

Measured Data

Figure 7.6.1 shows the measured 1/3-octave band PWL spectra (in dB re 10^{-12} W) for $\lambda_N = 2$ with T_{T_N} as parameter. Figure 7.6.2 presents the same information, but for $\lambda_N = 3$. As expected, both figures show an increase in PWL with increasing jet temperature. The ratio of increase corresponds roughly to the square of the ratio of the absolute temperatures.

At $\lambda_N = 3$ and at room temperature (i.e., $T_{T_N} = 520°R$), the jet nozzle was not correctly expanded ($\rho_{EXIT} \neq \rho_{AMB}$) and jet screech was observed [*A-3, A-4*]. Screech is a phenomenon that involves an acoustic feedback from the shock region to the nozzle; it manifests itself in strong harmonically related pure-tone components in the PWL spectrum. In Fig. 7.6.2, one can see strong pure-tone components in the 2-kHz and 4-kHz center frequency 1/3-octave bands. Observations indicate [*A-3*] that the process is nonstationary and that the amplitude of the tones can vary strongly with even the slightest changes in the geometry of the reflecting surfaces in the vicinity of the nozzle. In addition to screech, the improperly expanded jet generates excess broadband noise due to the interaction of convected vortices with shock waves.

Since shock noise and screech occurred only at runs with ambient temperature and a pressure ratio of 3, neither of which condition corresponds to jet-engine operation, and since shock and screech noise are poorly documented and understood at present, the interpretation of this specific condition was not pursued. It should be noted only that screech often can be eliminated by adding on the nozzle lip a small projection that

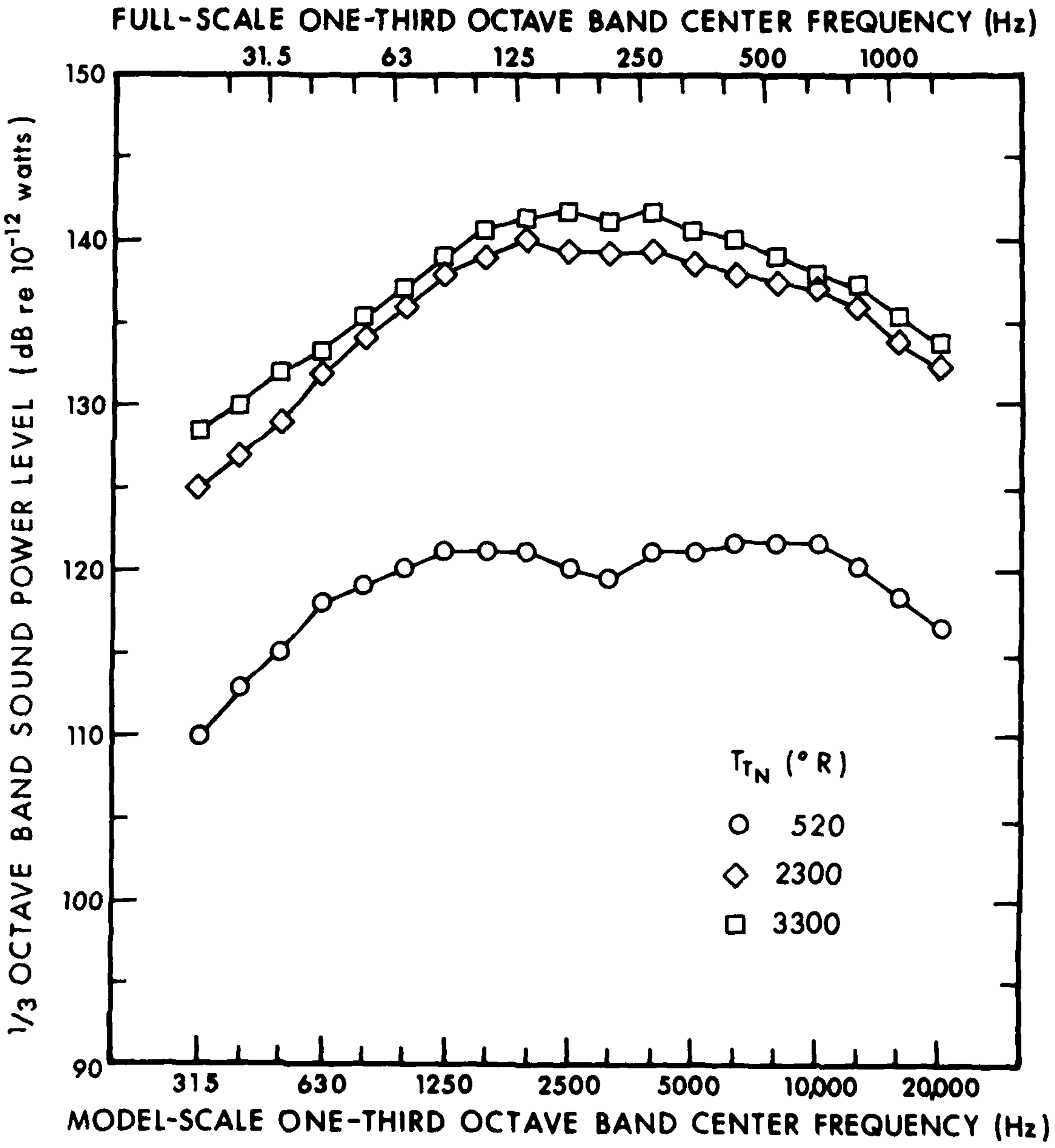

FIG. 7.6.1. MEASURED 1/3-OCTAVE BAND PWL SPECTRA FOR λ_N = 2.

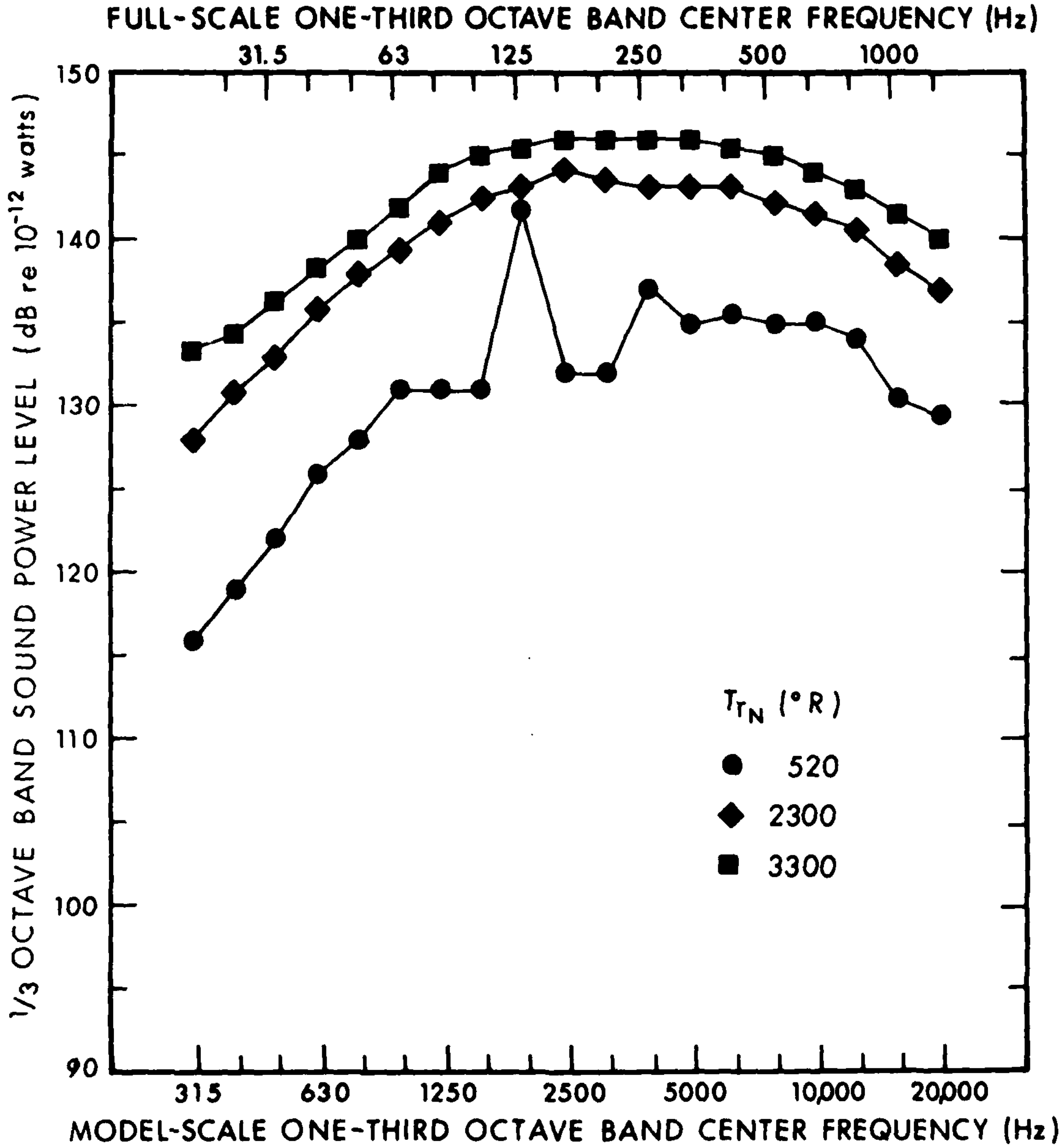

FIG. 7.6.2. MEASURED 1/3-OCTAVE BAND PWL FOR $\lambda_N = 3$.

is sufficient to disturb the correlation of the vortex shedding along the lip and thereby destroy the feedback mechanism [*A-3*].

Normalization of the Measured Data

The measured model data yield a satisfactory collapse into a single curve if the measured 1/3-octave band PWL data are normalized according to the empirical relationship given by

$$PWL_{NM} = PWL_M - 20 \log (T_{T_N}/520) - 30 \log \lambda_N \quad , \tag{7.6.1}$$

where PWL_M is the measured 1/3-octave band PWL in dB re 10^{-12} W of the model.

Figure 7.6.3 shows the model jet data of Figs. 7.6.1 and 7.6.2 normalized according to Eq. 7.6.1. Except for the ambient temperature run near the peak of the spectrum, the data collapse is quite satisfactory. Thus, at least in the pressure ratio and temperature ranges of interest, *the sound power at each frequency band increases with the square of the ratio of the absolute temperatures and with the third power of the pressure ratio.*

A common method for collapsing data is to plot them against the Strouhal frequency S defined as

$$S = \frac{fD_N}{U_j} \quad , \tag{7.6.2}$$

where f is the frequency, D_N is the diameter of the nozzle, and U_j is the jet flow exit velocity. This method gives good data collapse for cold subsonic jets, but did not work at all in our case of a hot supersonic jet. However, a Strouhal frequency

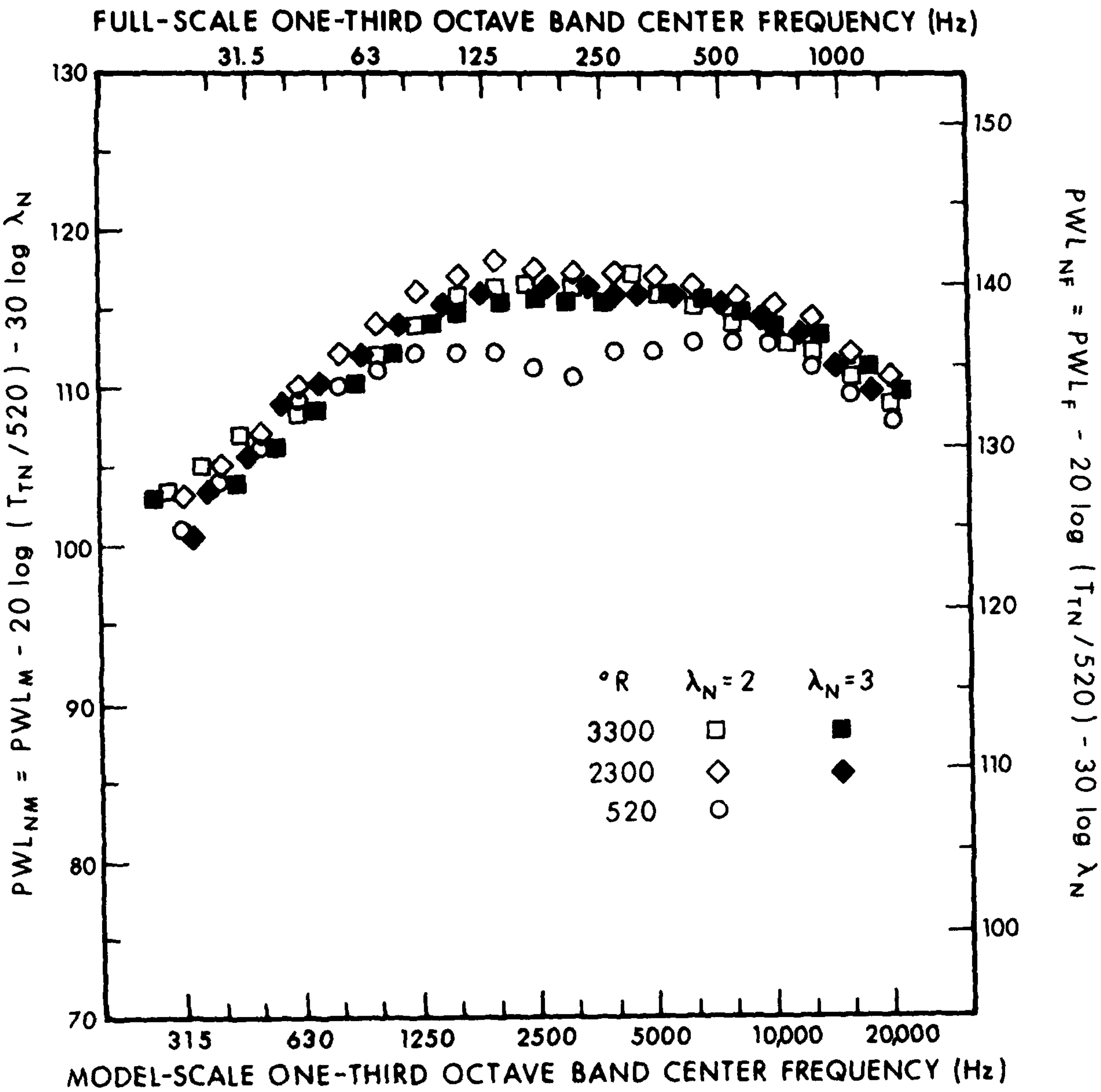

FIG. 7.6.3. NORMALIZED 1/3-OCTAVE BAND PWL SPECTRA OF THE JET SURVEY SERIES.

based on the speed of sound in the surrounding air rather than on the jet flow exit velocity yielded satisfactory data collapse.

Extrapolation to Full Scale

Keeping the same pressure ratio and temperature and increasing the diameter of the nozzle manifests itself in (1) an increase of the sound power output which is proportional to the square of the ratio of the diameters and (2) a shift of the model-scale spectrum toward the lower frequencies corresponding to the ratio of the diameters of the model-scale and full-scale nozzles (i.e., $f_F = f_M \, D_{NM}/D_{NF}$). Applying this procedure to Eq. 7.6.1, one can use the normalized sound power spectra PWL_{NM} obtained for scale-model data at model frequency f_M to predict the spectral level of the noise at full-scale frequencies f_F as follows:

$$PWL(f_F) = PWL_{NM}(f_M) + 20 \log (T_{T_N}/520) + 30 \log \lambda_N + 20 \log D_N/2.75 \quad , \tag{7.6.3}$$

where $PWL_{NM}(f_M)$ is the octave-band PWL spectrum of the 1:15 scale-model data (given in Fig. 7.6.4 and normalized according to Eq. 7.6.1) and $PWL(f_F)$ is the predicted octave-band PWL spectrum at full scale. An example of using this scaling procedure is given in Sec. 2.3.1.

7.6.2 Aeroacoustic tests

The primary purpose of the aeroacoustic tests run with various hard-walled augmenter configurations was the generation of aerodynamic data regarding pumping performance. Acoustic data were taken for every run, but very little variation was

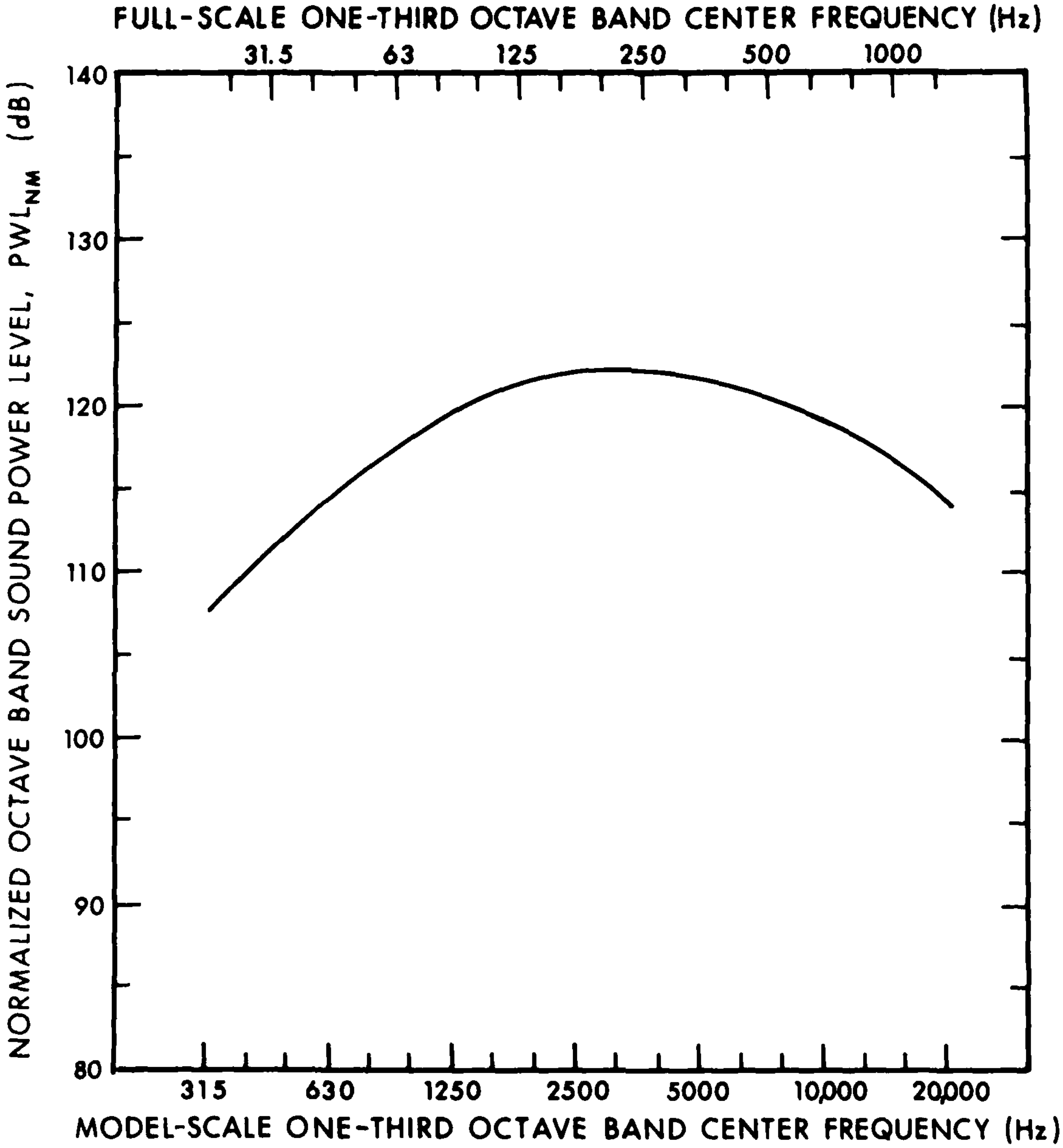

FIG. 7.6.4. OCTAVE-BAND PWL SPECTRUM NORMALIZED TO $\lambda_N = 1$, $T_{T_N} = 520°R$, AND $D_N = 2.75$ in.

observed; thus, the test results can be summarized by a few graphs that illustrate characteristic trends.

Effect of Nozzle Distance

Depending on the distance between the nozzle exit plane and the augmenter inlet, the distribution of sound power between the burner room and the exhaust room varies. Figure 7.6.5 shows the PWL spectra measured at 3300°R and a pressure ratio of 2 for a 72-in.-long, 12.5-in.-diameter, hard-wall augmenter tube when the nozzle was located 10.5 in. upstream of the augmenter exit plane. For this specific case, the jet PWL is very nearly evenly distributed between the two rooms.

The low-frequency portion of the spectrum, which is generated far downstream of the nozzle well inside the augmenter tube, propagates mostly into the exhaust room. The high-frequency part of the spectrum, which is generated near the nozzle, radiates primarily into the burner room. Except for a slight difference at high frequencies, the sum of the PWL spectra of the burner and the exhaust rooms closely corresponds to the total sound power of the free jet as measured previously in the jet survey series. This slight difference in sound power at high frequencies is most likely the result of a slight decrease in velocity gradient in the shear layer due to the more concentrated secondary flow pumped by the jet and a very small but finite attenuation of sound in the hard augmenter tube.

Figure 7.6.6 shows the characteristic changes in the PWL spectrum in the exhaust room, and Fig. 7.6.7 shows the corresponding change in the PWL spectrum in the burner room, with changing

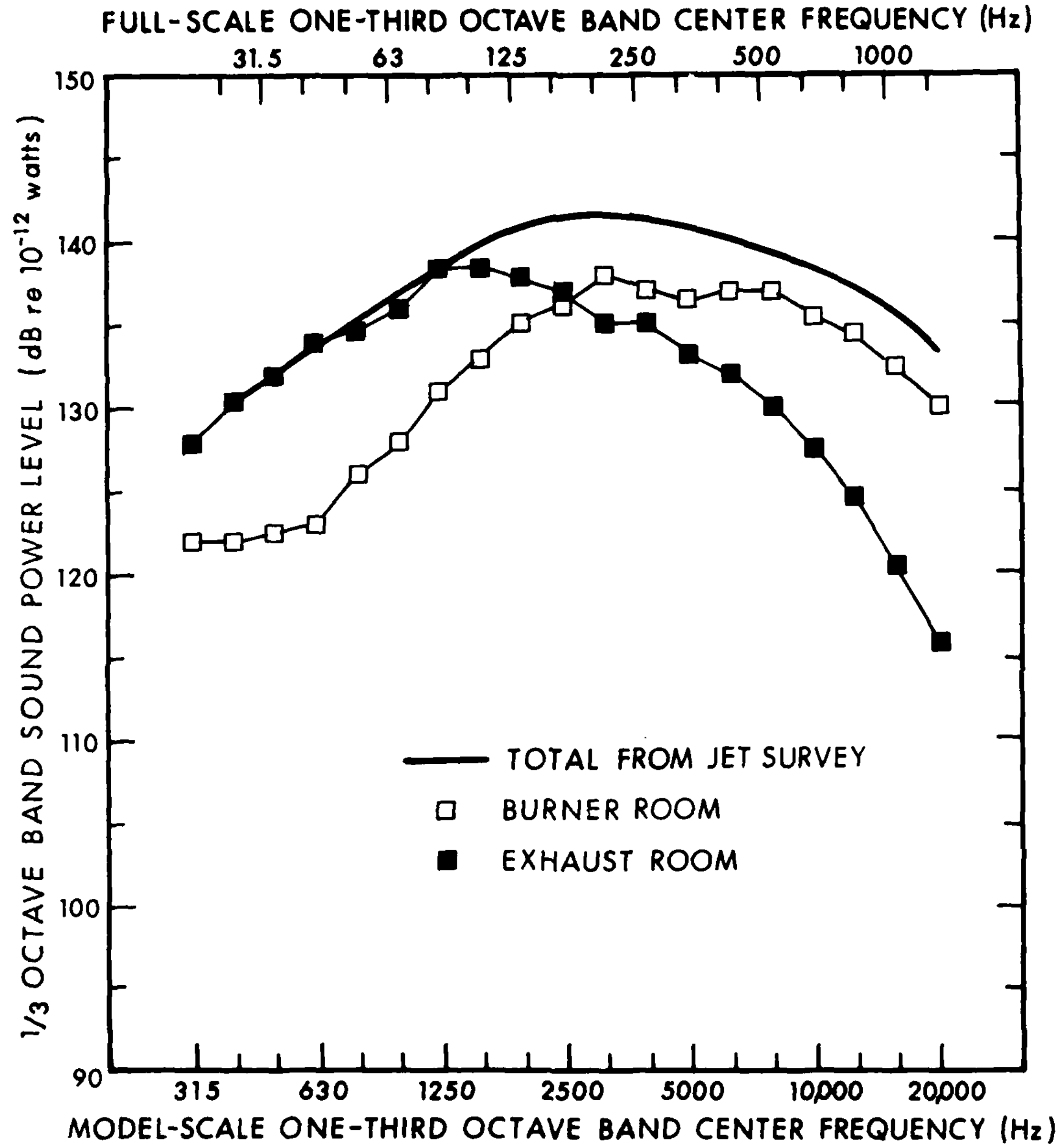

FIG. 7.6.5. DISTRIBUTION OF SOUND POWER BETWEEN BURNER ROOM AND EXHAUST ROOM AT 3300°R, $\lambda_N = 2$, $D_A = 12.5$ in., $L_A = 72$ in.

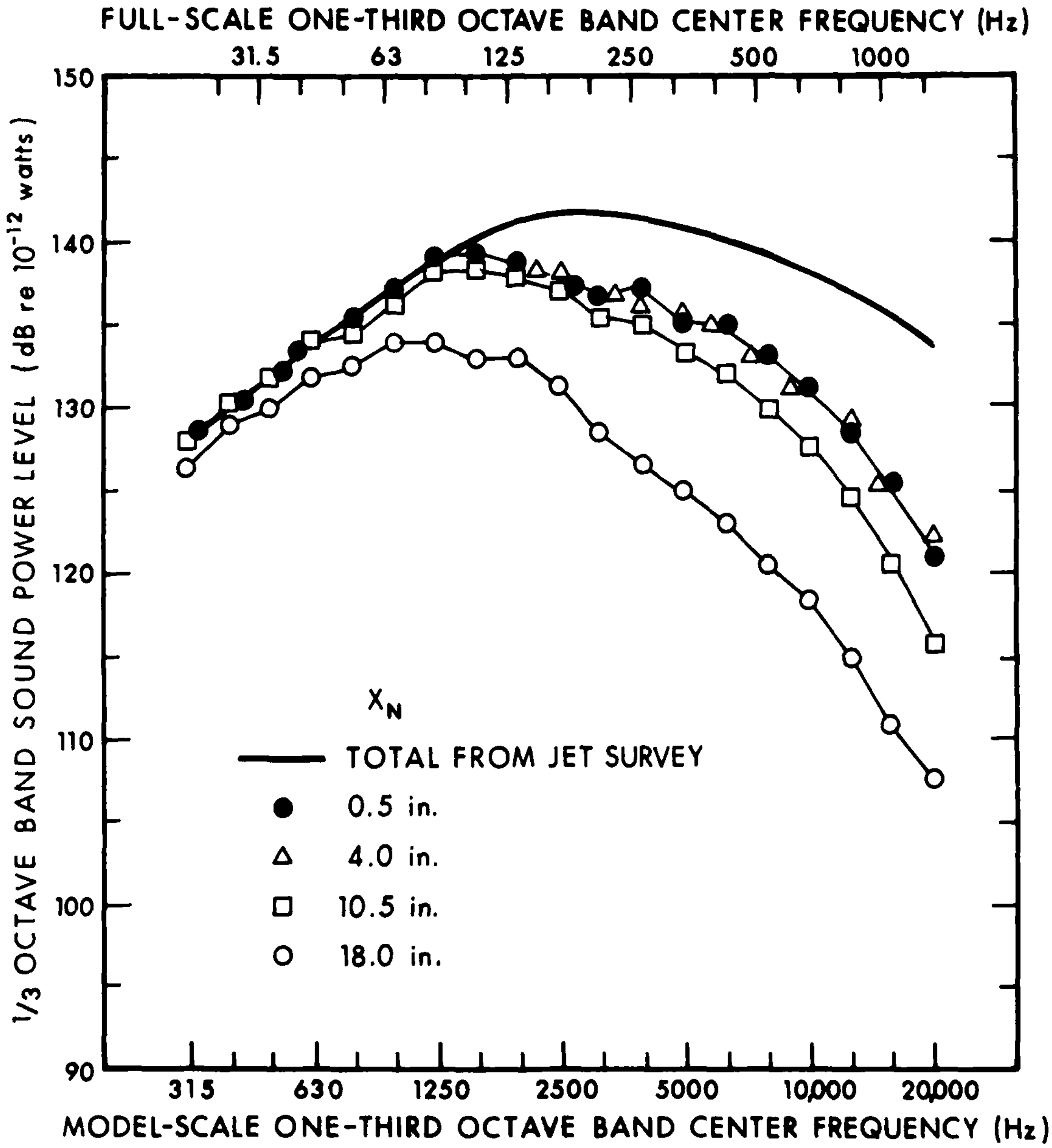

FIG. 7.6.6. EFFECT OF AXIAL DISTANCE ON THE SOUND POWER RADIATED INTO THE EXHAUST ROOM AT 3300°R, λ_N = 2, D_A = 12.5 in., L_A = 72 in.

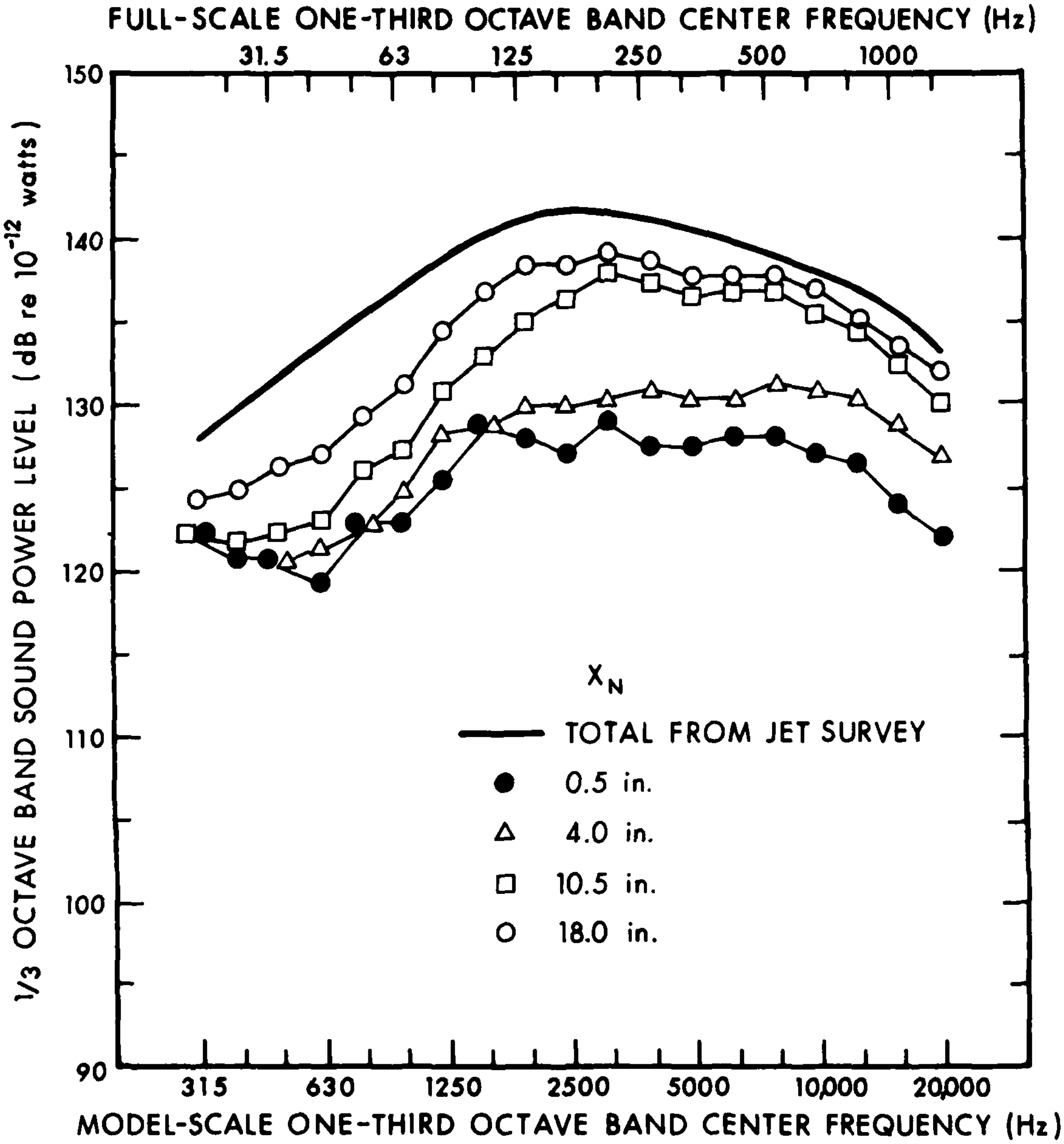

FIG. 7.6.7. EFFECT OF AXIAL DISTANCE ON THE SOUND POWER RADIATED INTO THE BURNER ROOM AT 3300°R, $\lambda_N = 2$, $D_A = 12.5$ in., $L_A = 72$ in.

axial distance X_N of the nozzle from the augmenter inlet. These data indicate that in Hush House designs *the axial distance X_N should be less than twice the diameter of the nozzle to reduce that portion of the high-frequency sound energy which enters the Hush House proper and produces noise levels in the vicinity of the aircraft in excess of the free-field levels.* Sound levels in excess of the free field values are undesirable, because they increase the noise exposure of service personnel and may lead to fatigue of fuselage or failure of certain instrument packages. Of course, as X_N decreases, more of the jet noise goes into the exhaust room.

Effect of Augmenter Tube Length

The length of the hard-walled augmenter tube has practically no influence on burner-room PWL spectra. Exhaust-room PWL spectra decrease slightly with increasing augmenter tube length, indicating a very small but finite sound attenuation in the hard augmenter tube. The data plotted in Fig. 7.6.8 illustrate this behavior, which is typical of other hard-walled augmenter configurations.

Effect of a Subsonic Diffuser

Except for a very slight decrease of high-frequency sound in the burner room, adding a subsonic diffuser to a hard augmenter tube to increase pumping performance has practically no effect on the efficiency of the noise-generation process.

Effect of Inlet Throttle

The throttling device used to effect small changes in the secondary cooling air volume pumped by the primary jet had no effect on either burner-room or exhaust-room noise levels.

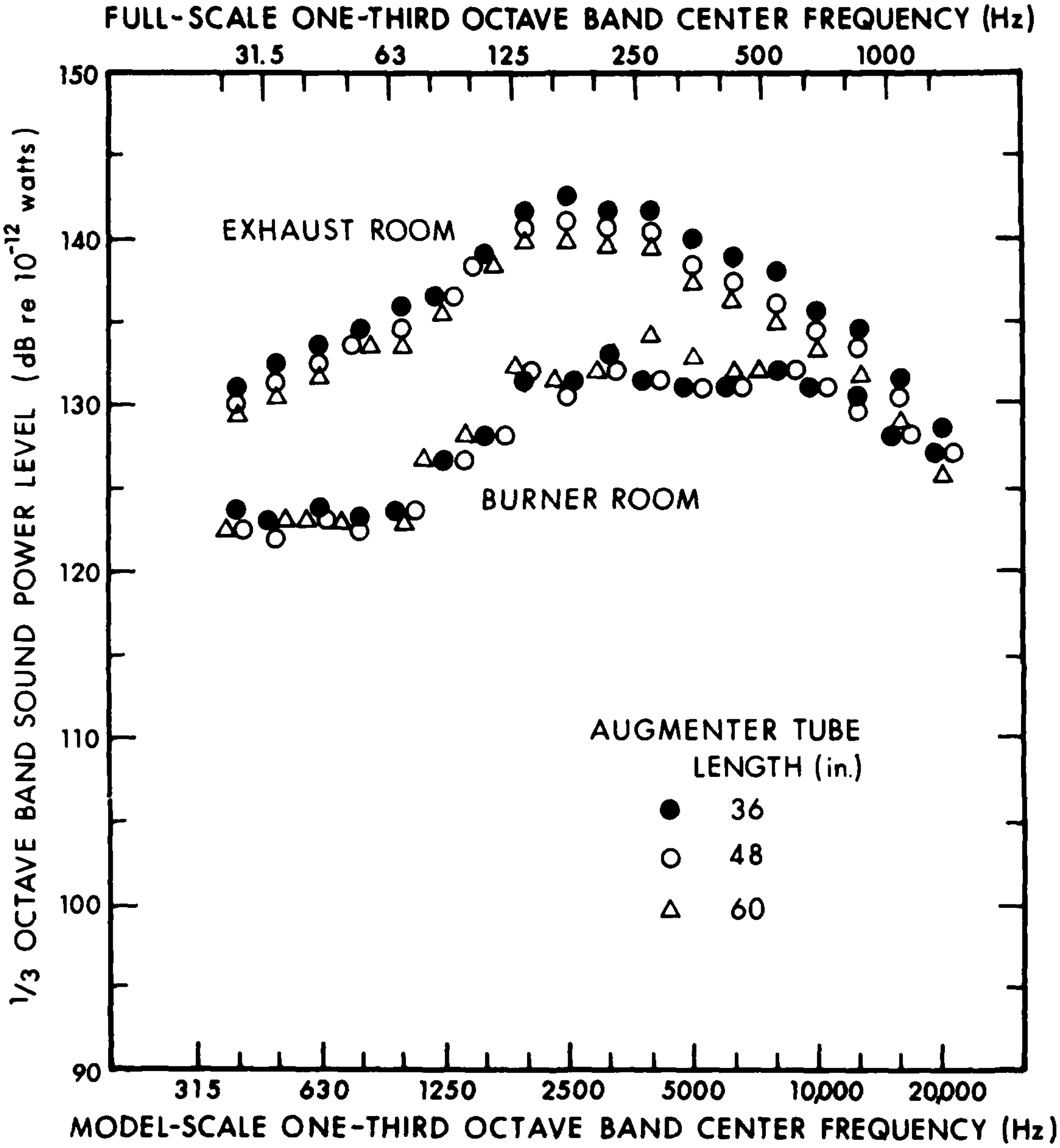

FIG. 7.6.8. EFFECT OF LENGTH OF HARD-WALLED AUGMENTER TUBE ON PWL AT 3300°R, λ_N = 2, D_A = 8 in., X_N = 4 in.

Effect of Augmenter Inlet Geometry

Round and conical bellmouths produce about the same sound power in both the burner and the exhaust rooms. A sharp-edged bellmouth was found to decrease sound levels in the burner room by about 2 dB at all but the lowest frequencies, but it had no significant effect on exhaust-room levels. Because most of the sound power entering the Hush House proper is due to reflection of highly directional sound radiating from the shear layer just downstream of the nozzle, the wall surfaces in the vicinity of the augmenter intake as well as of the augmenter bellmouth should have a highly effective sound-absorbing treatment or a geometry such that the jet noise reflected from these surfaces will either enter the augmenter tube or be directed toward other highly absorptive surfaces.

7.6.3 Aerothermal tests

The main purpose of the aerothermal tests was to provide design information regarding wall temperatures and velocity profiles in the obround lined augmenter tube modeling the Miramar installation.

Effect of Nozzle Position

The radial position of the nozzle with respect to the center of the augmenter tube affects the intensity of the exhaust noise exiting from a lined augmenter tube. The measured data plotted in Fig. 7.6.9 illustrate this effect. The lowest levels are generated when the nozzle is centered. Shifting the nozzle to the F-14 position increases the exhaust noise by 3 dB at frequencies where the radial dimension of the augmenter becomes large compared with the wavelength of sound. A further shift toward the lined wall

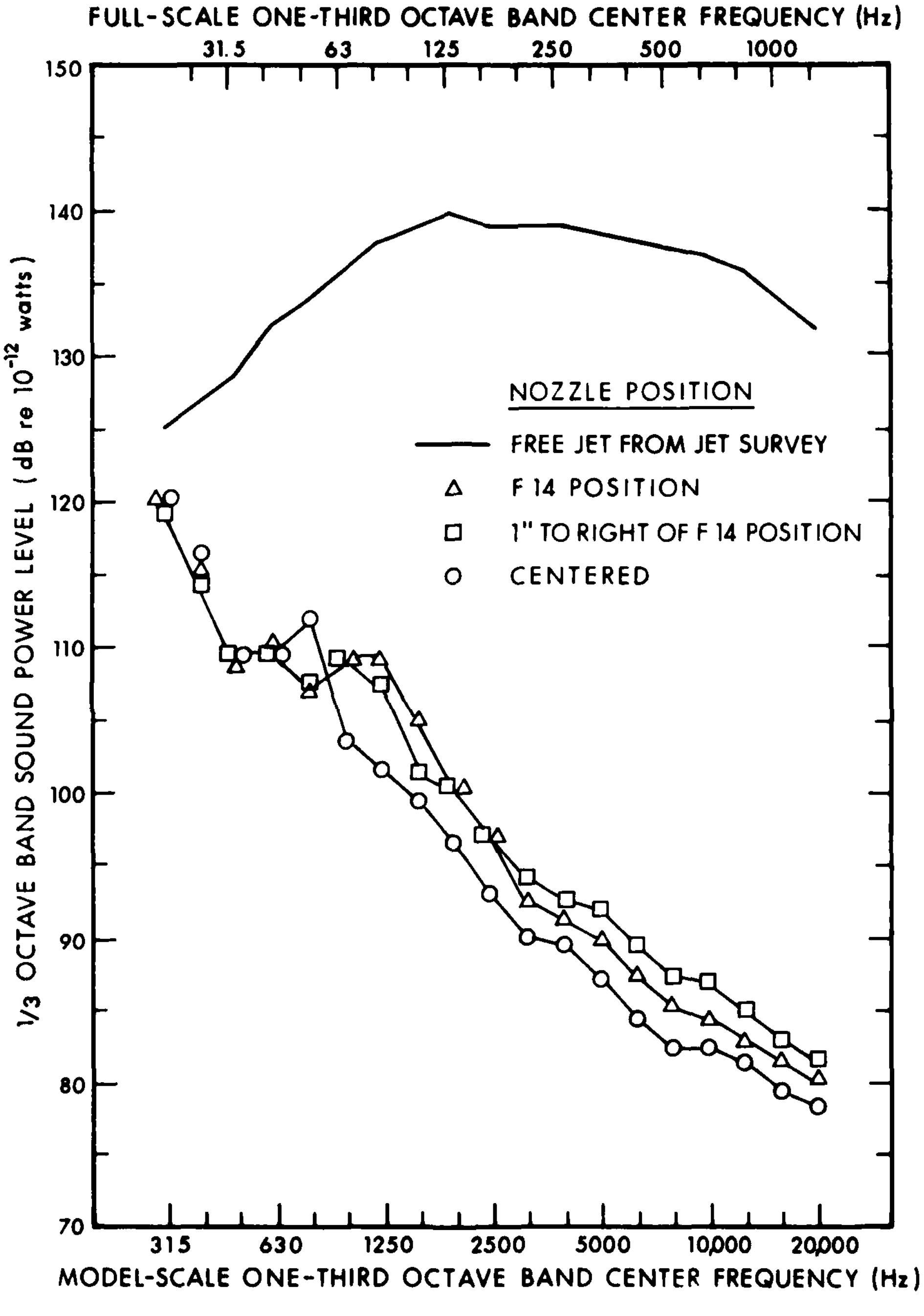

FIG. 7.6.9. EFFECT OF RADIAL POSITION OF NOZZLE ON EXHAUST ROOM NOISE: 72-in. BBN AUGMENTER, NO RAMP, T_{T_N} = 2300°R, λ_N = 2, X_N = 4 in.

results in a slight additional increase of the exhaust noise at high frequencies. The reason for this increase is most probably due to the fact that moving the jet from the center position shifts one half of the sound field nearer to and the other half further away from a sound-absorbing wall. The net result of this shift is always a reduced sound attenuation. In addition, the unsymmetric geometry results in higher peak exit velocities and in a higher degree of inhomogeneity of the flow, both of which conditions tend to increase self-noise levels.

Effect of Angular Misalignment

An angular misalignment of the nozzle from the augmenter tube axis results in higher exhaust room noise levels. As shown in Fig. 7.6.10, the acoustical effect of such angular misalignment is similar in nature to the effect observed for off-center positioning of an otherwise axially oriented nozzle (see Fig. 7.6.9 for comparison). Note that the effects of off-center spacing and angular misalignment are additive.

Burner-room noise levels remain practically unaffected by small angular misalignments, say less than 3°.

Effect of Rakes

During many aerothermal tests, rakes were deployed to measure the velocity and temperature profiles at axial locations X_A in the augmenter tube. Turbulent wakes and periodic vortex shedding from these rakes generated considerable noise; in certain frequency ranges, this noise exceeded the intensity of the jet noise attenuated by the lined augmenter tube. Except for Fig. 7.6.11, all acoustical data presented in this report were measured with no rakes in the lined augmenter.

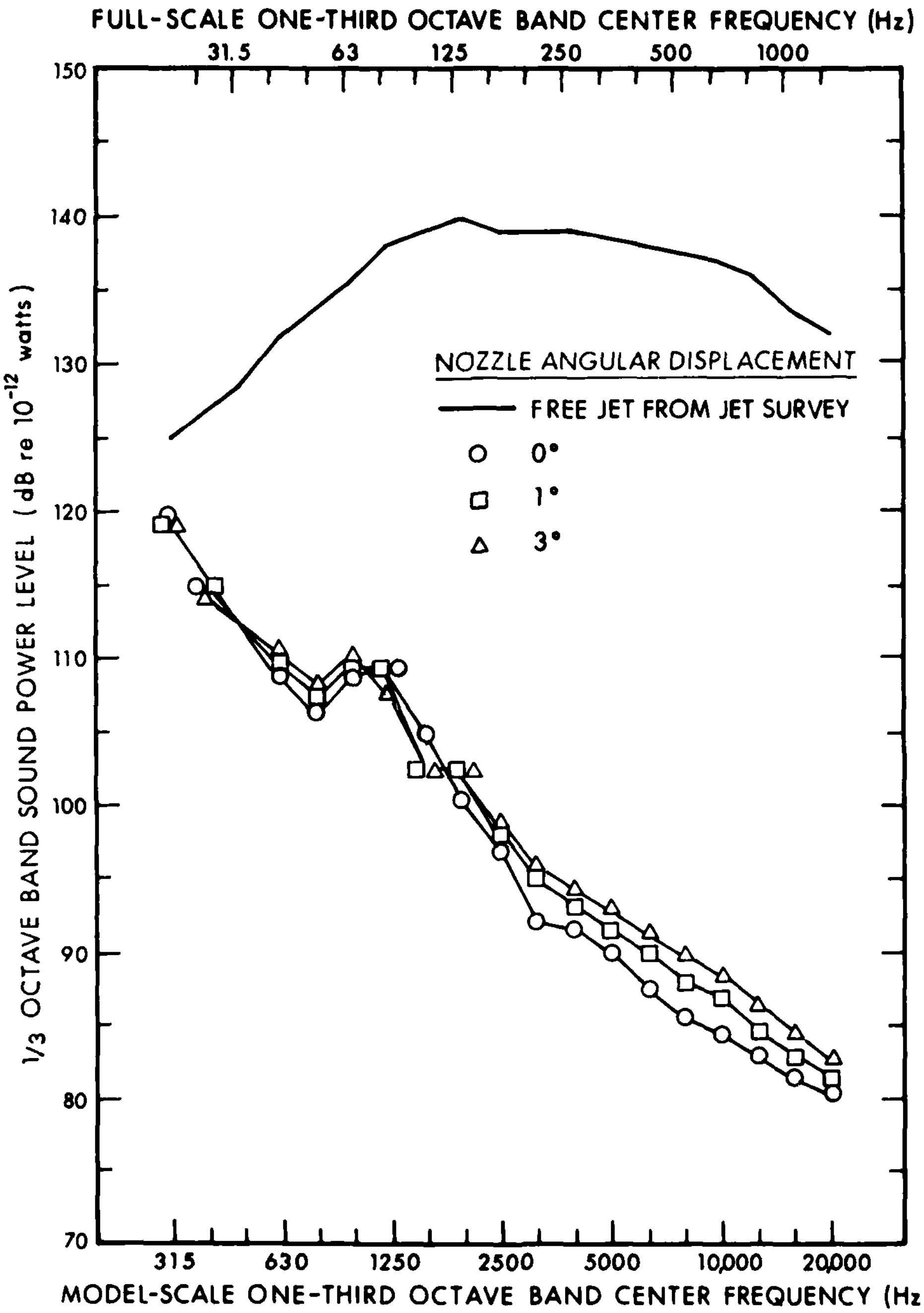

FIG. 7.6.10. EFFECT OF ANGULAR MISALIGNMENT ON EXHAUST ROOM NOISE: 72-in. BBN AUGMENTER, NO RAMP, F-14 POSITION, T_{T_N} = 2300°R, λ_N = 2, X_N = 4 in.

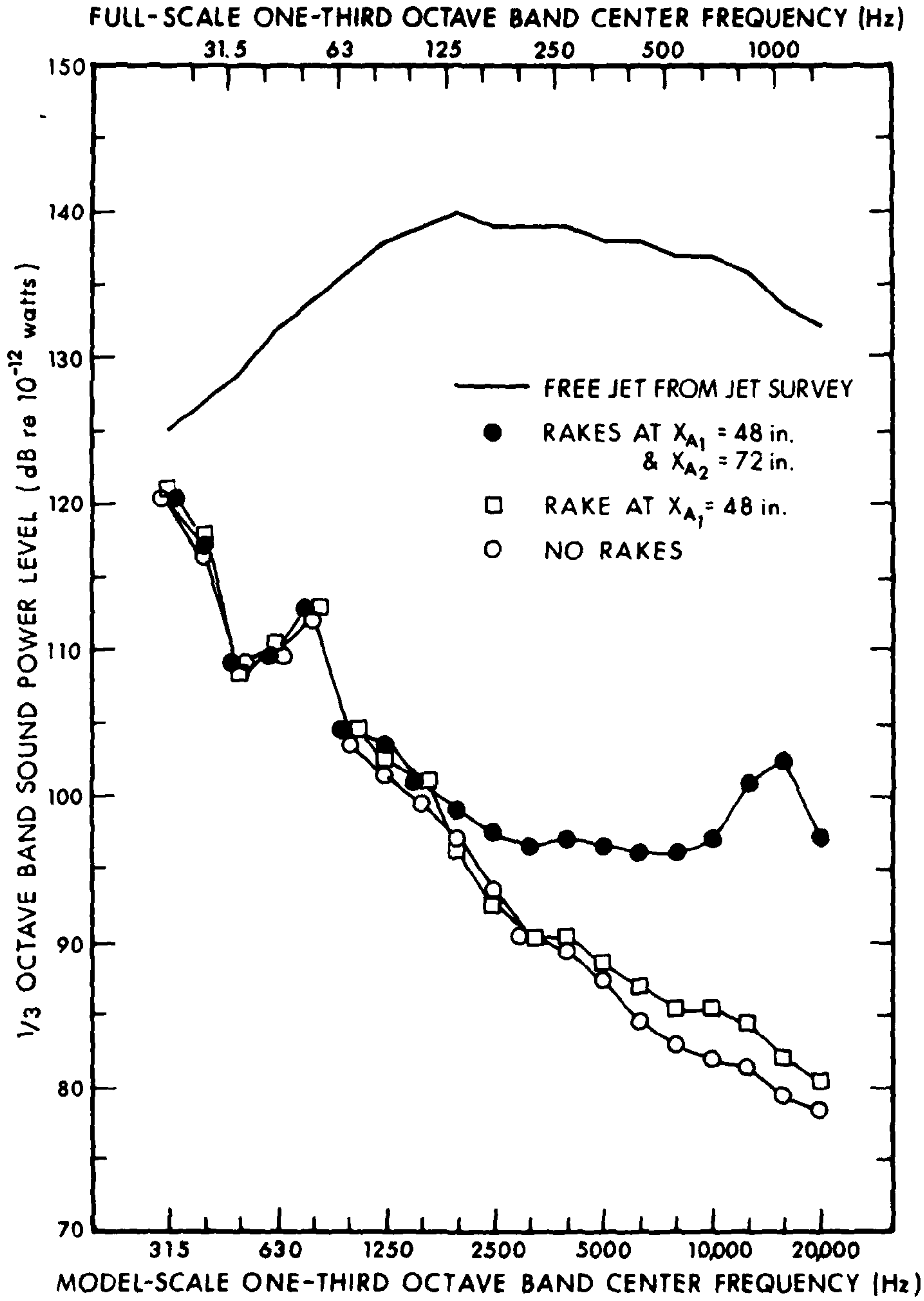

FIG. 7.6.11. EFFECT OF RAKES ON EXHAUST ROOM NOISE: 72-in. BBN AUGMENTER, NO RAMP, T_{T_N} = 2300°R, λ_N = 2, X_N = 4 in.

Figure 7.6.11 shows the effect of the rakes on the sound power entering the exhaust room through a lined augmenter tube, indicating that the presence of solid structures in the flow can considerably increase the exhaust noise. As expected, the increase is the highest for axial location X_{A_2} (i.e., at the end of the lined augmenter tube), where this is no lining downstream to absorb the sound generated at this location. Note also the strong peak in the exhaust room sound power spectrum at 16 kHz, which corresponds to the frequency of periodic vortex shedding from the small-diameter pitot tubes of the rake. Even when placed at X_{A_1} = 48 in. (i.e., one-third of the way upstream from the augmenter tube exit), the rake generated enough noise to control the intensity of the exhaust noise at high frequencies. These findings lead to the conclusion that *no such structures should be in the flow path when the acoustical performance of the full-scale Miramar Hush House is tested.*

7.6.4 Acoustic tests

The purpose of the acoustic tests was to determine the reduction in sound power provided by various lined augmenter configurations and by the stack with sound absorbing baffles. The reduction in sound power output ΔPWL is defined as the difference in the sound power level of the free jet and the sound power level of the noise reaching the exhaust room. We also measured the sound power level in the burner room to provide information for estimating sound pressure levels in the Hush House proper. The following exhaust configurations were tested:

- A model of the e.haust system of the Miramar Hush House
- A lined model augmenter tube designed by BBN

- A series combination of a hard-walled augmenter tube, hard subsonic diffuser, hard turning vanes, and a lined stack with sound absorbing parallel baffles.
- A variety of combinations of lined and hard augmenter sections and porous sound absorbing ramp.

The measured data were to yield information for (1) predicting the acoustical performance of the full-scale Miramar Hush House, (2) comparing the acoustical performance of the Miramar augmenter with that designed by BBN, and (3) use in the design of the lined exhaust systems of future Hush Houses.

The acoustical data measured for the various jet temperatures, pressure ratios, and exhaust configurations were the space-time-averaged sound pressure levels in both the exhaust and the burner rooms. Using these recorded data, one could calculate the 1/3-octave band PWL of the noise entering these rooms.

Variables Influencing Acoustical Performance

The acoustical performance of an exhaust silencer system (i.e., reduction in sound power level it provides) is influenced in a complex manner by a variety of parameters. Although all of these parameters were modeled so that the test results would reflect the expected performance of the full-scale system, we discuss these parameters in a qualitative manner at this point to help the reader in understanding and interpreting the data presented in the following sections.

As shown schematically in Fig. 7.6.12a, the exhaust sound power PWL_{EXH} is the sum of the attenuated jet sound power and the self-generated sound power of the flow exiting from the exhaust

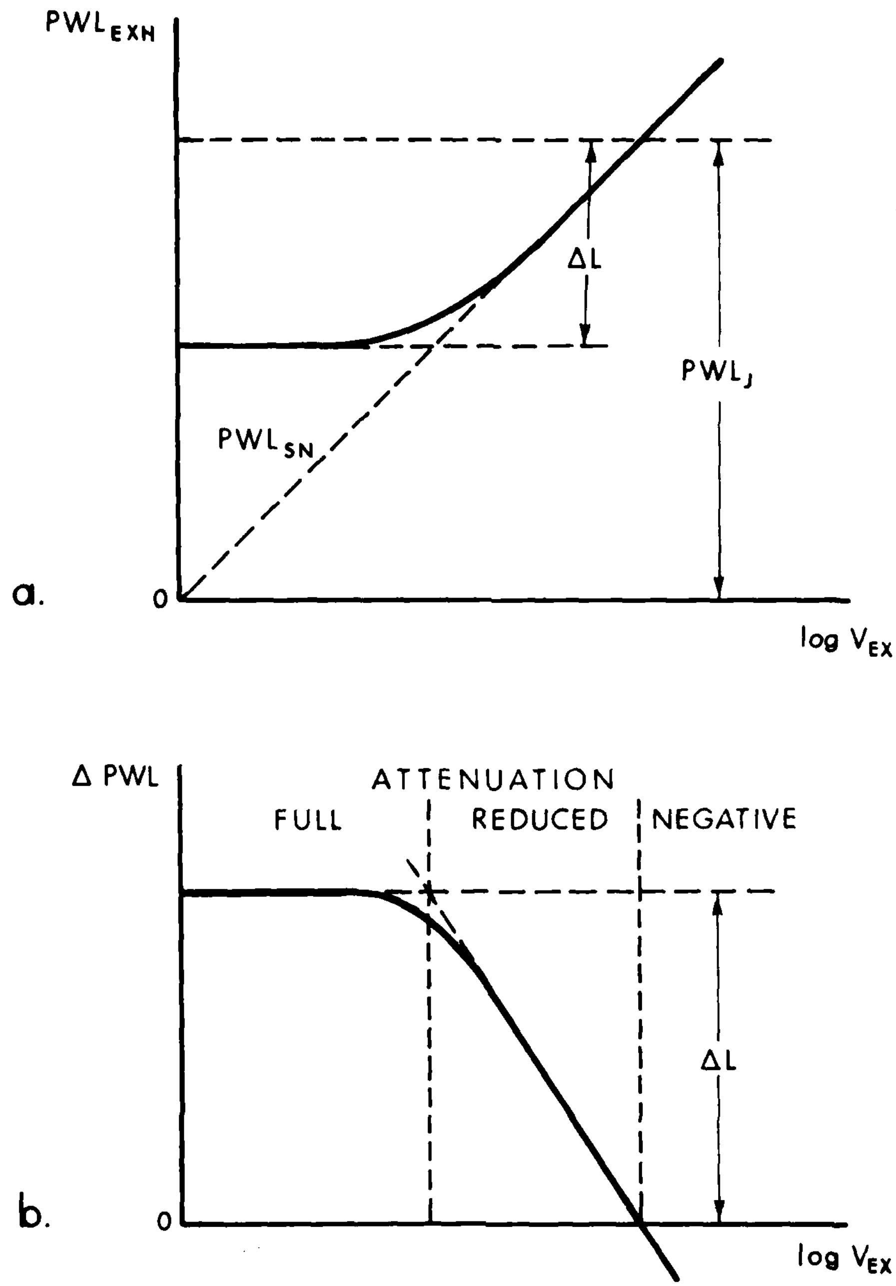

FIG. 7.6.12. EFFECT OF EXIT SPEED-GENERATED SELF-NOISE.
a. EXHAUST SOUND POWER, PWL_{EXH}
b. POWER LEVEL REDUCTION ΔPWL

end of the system PWL_{SN}. ΔL is the sound attenuation provided by the silencer, which is strongly affected by the temperature and by temperature and flow gradients. It increases with increasing silencer length, decreases with increasing cross-sectional area, and usually decreases somewhat with increasing flow speed. Silencer attenuation also depends in a very complex manner on the wall impedance of the lining, which changes with frequency.

For a given exit speed, self-generated noise sets an upper limit to the reduction of sound power ΔPWL; i.e., the silencer provides a measurable reduction ΔL of the sound power radiated by the jet exhaust. However, self-noise may control the level of PWL_{EXH} and therefore of ΔPWL. The effect of self-generated noise on ΔPWL is shown schematically in Fig. 7.6.12b. At low exit speeds, where self-generated noise is low, ΔPWL = ΔL and full advantage is taken of the silencer installation. If the exit speed is high enough that the level of the self-generated noise becomes comparable to, or is higher than, the level of source noise attenuated by the silencer, the reduction in source sound power level achieved will be smaller than the attenuation provided by the silencer (i.e., ΔPWL < ΔL). If the level of the self-generated noise is larger than the source sound power level (i.e., $PWL_{SN} > PWL_J$) ΔPWL becomes negative, indicating that more sound power exits from the silencer than is injected into it by the source. Such amplification may actually occur in cases where obstructions in the exit stack generate periodic vortex shedding, which interacts with the acoustical resonances of the stack.

In the case of the Miramar Hush House and the other model configurations tested, no such amplifications occur; however, in certain limited frequency ranges, the potential performance of the lined exhaust system may be slightly compromised by self-noise. This result is unavoidable unless facility size and cost is not an important consideration.

The sound power of the self-generated noise, PWL_{SN}, increases very strongly with the exit speed V_{EX}. If the exit noise is controlled by the noise generated by the mixing of the exiting flow with the surrounding stationary air, the exit flow can be considered as subsonic jet, and, in this case, the sound power of the self-noise increases with the eighth power of the exit velocity. If the noise generation is controlled by the interaction of the turbulent exit flow with solid objects, such as rakes, duct walls, and the lip of the exit duct, the sound power of the self-noise increases with the sixth power of the exit velocity. Since the maximum velocity of the mixed exhaust flow at the augmenter exit plane $V_{mix\ max}$* increases with decreasing augmenter length (though the mass flow remains nearly constant), the exhaust room PWLs measured for the 48-in., 72-in., and 96-in. long lined BBN augmenter tubes provide an opportunity to check whether or not the self-noise controls the exhaust sound power.

The octave-band sound power level of the exhaust noise, plotted as a function of $V_{mix\ max}$ in Fig. 7.6.13, shows that the level increases with increasing velocity. This increase is attributable to both the shorter lined augmenter length, resulting in a lower attenuation of the jet noise, and higher self-generated noise.

If the exhaust noise is entirely controlled by the self-noise, one would expect that the exhaust PWL would increase as $60 \log V_{mix\ max}$. The curves in Fig. 7.6.13 indicate that this result may occur only in the 8000-Hz center frequency octave band.

*$V_{mix\ max}$ represents the maximum velocity of the mixed exhaust flow.

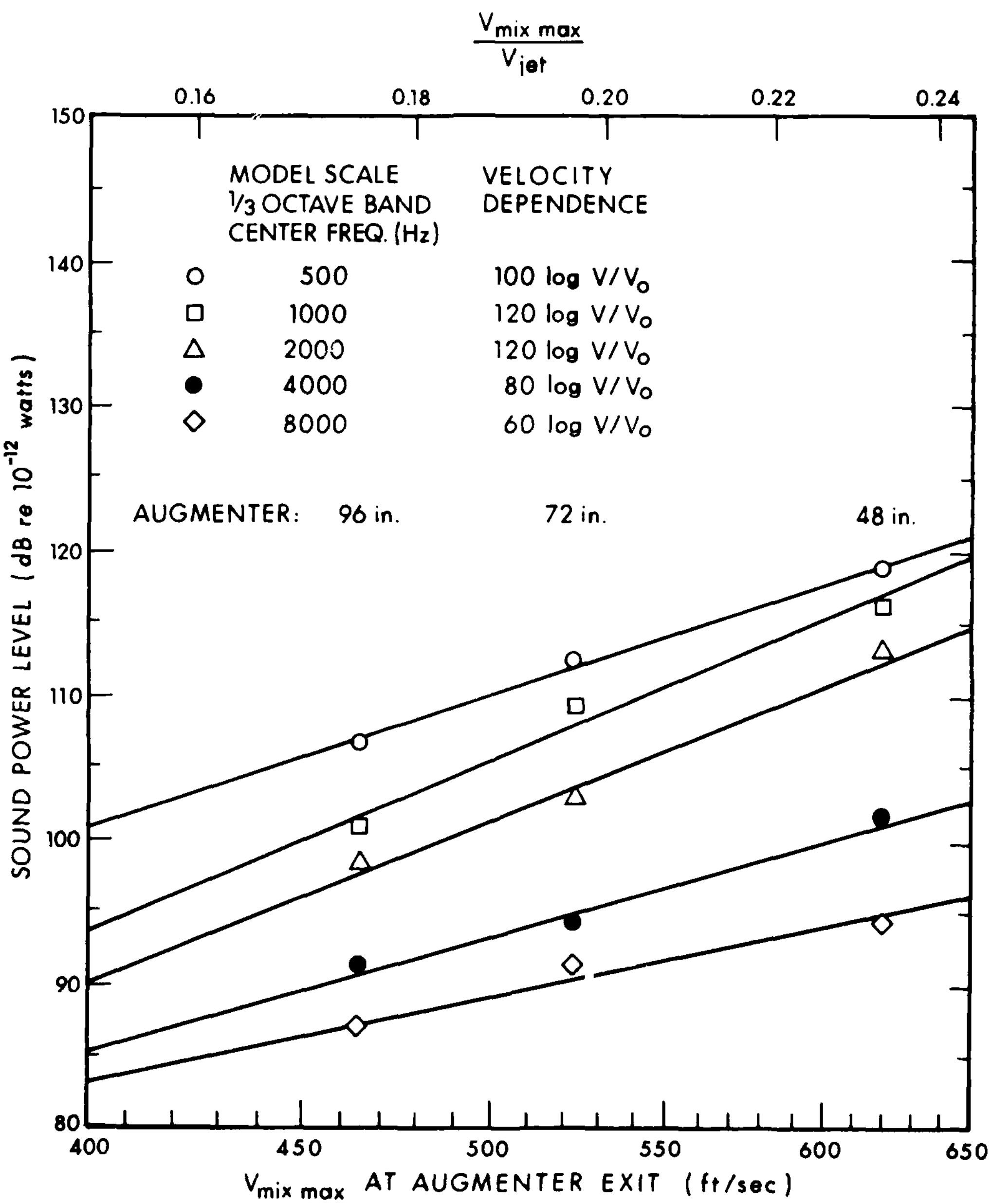

FIG. 7.6.13. DEPENDENCE OF EXHAUST ROOM PWL ON VELOCITY OF AIR EXITING FROM FULLY LINED BBN AUGMENTERS OF DIFFERENT LENGTHS: 45° RAMP, T_{T_N} = 3300°R, λ_N = 2, X_N = 4 in.

Self-generated noise is an unavoidable integral part of both the model and the full-scale systems, and it is properly included in all of our data and predictions. Although some attempts will be made to identify it in a qualitative manner, its separation from the attenuated source noise is not possible without more detailed information (i.e., the turbulence intensity spectrum). Should there be a need in the future for Hush Houses accommodating aircraft with a higher sound power output than the F-14, or should Hush Houses be required to meet noise criteria stricter than the present 85 dBA at 250 ft, *self-generated noise will certainly be a limiting factor and further studies must be undertaken to determine how to keep self-noise just low enough without an inordinate increase in facility size.*

Burner-Room Data

In a manner similar to that used during the aerothermal tests, we measured the 1/3-octave band burner-room PWL spectra for all runs. The analysis of the data provides the following conclusions:

1. Effect of Nozzle Position: The data plotted in Fig. 7.6.14 show the effect of nozzle distance, X_N, on the sound power spectra. The sound power reaching the burner room decreases strongly with decreasing axial distance. Comparing Figs. 7.6.14 and 7.6.7 shows that with the lined augmenter one can obtain substantially lower noise levels in the burner room than with a hard augmenter.

2. Effect of Inlet Throttle: Similar to the case of hard augmenter tubes, the inlet throttle has no appreciable effect on either burner-room or exhaust-room levels.

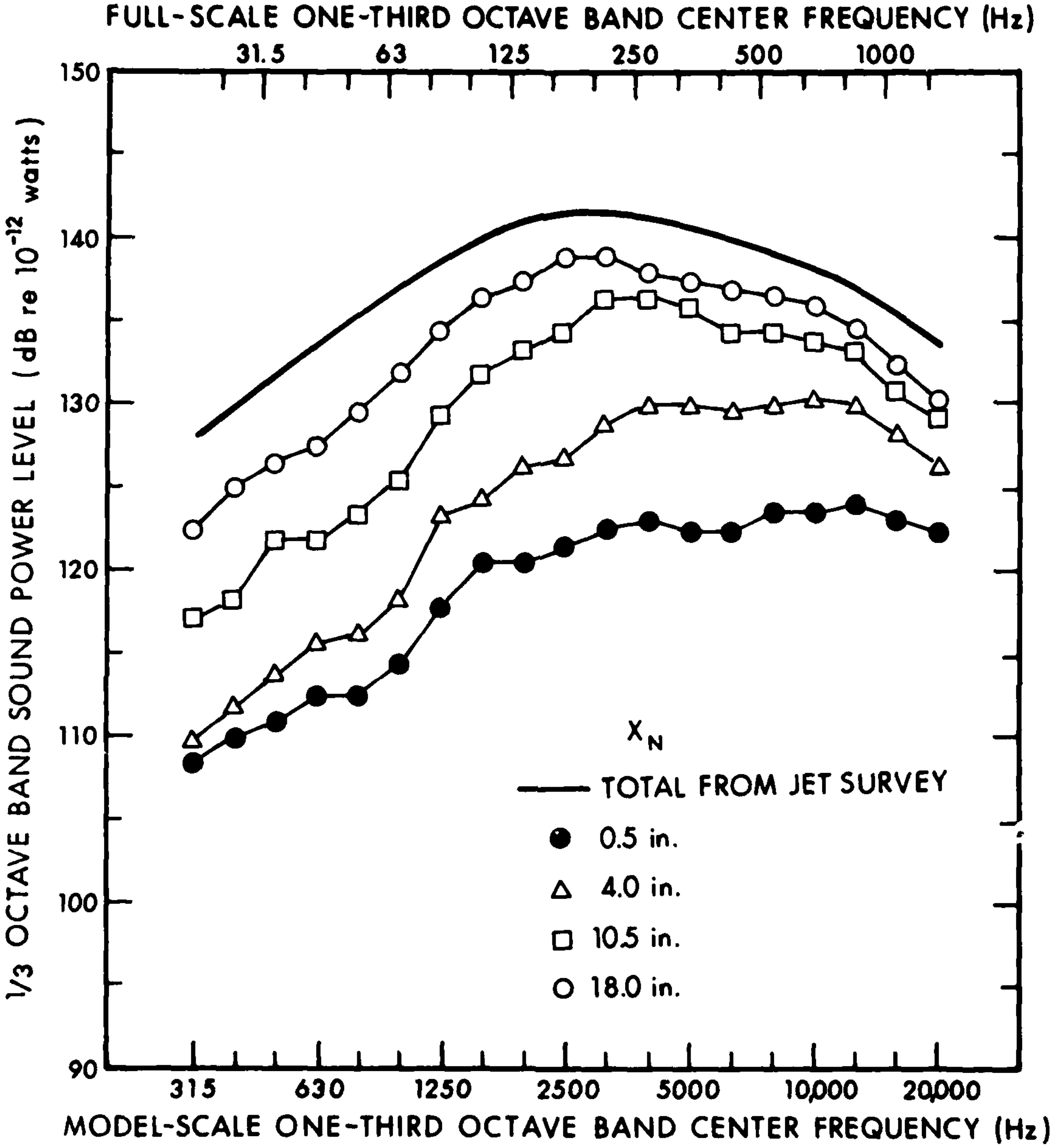

FIG. 7.6.14. EFFECT OF AXIAL DISTANCE X_N ON THE SOUND POWER RADIATED INTO THE BURNER ROOM: 72-in. BBN AUGMENTER, T_{T_N} = 3300°R, λ_N = 2.

3. Effect of Angular Misalignment: Angular misalignment of 1° to 3° results in slight (1 dB to 2 dB) increases in burner-room noise levels.

4. Effect of Augmenter Tube Length: The length of the lined augmenter tube in the range from 48 in. to 96 in. has no effect on the sound power radiated into the burner room.

5. Effect of the Ramp: Adding the ramp to a long lined augmenter does not affect burner-room noise levels. However, for a 12-in.-long lined augmenter section added to a 60-in.-long hard augmenter, the addition of a lined 45° ramp decreases the burner-room noise levels slightly at low frequencies, indicating that the ramp is effective in reducing the intensity of the sound reflected from the end of the augmenter tube back into the burner room.

6. Effect of Axial Position of 12-in.-long Lined Section: Sound power level in the burner room is determined mostly by the acoustic lining of the first 12 to 24 in. (model scale) of the upstream end of the augmenter. With the 12-in.-long lined section at the upstream end, burner-room PWL was nearly the same as with the fully lined augmenter, except at low frequencies where PWL was only 2 to 3 dB greater than for the fully lined augmenter. Placing the 12-in. section anywhere else in the augmenter resulted in poorer performance (PWL averaging 3 to 4 dB greater).

7. Effect of Exhaust Treatment: The choice of sound-attenuating treatment in the exhaust system influences the sound power entering the burner room, especially at low frequencies. Figure 7.6.15 illustrates this effect. Low burner-room levels can be obtained only if the augmenter tube has a lining which effectively absorbs the jet noise generated within its passage.

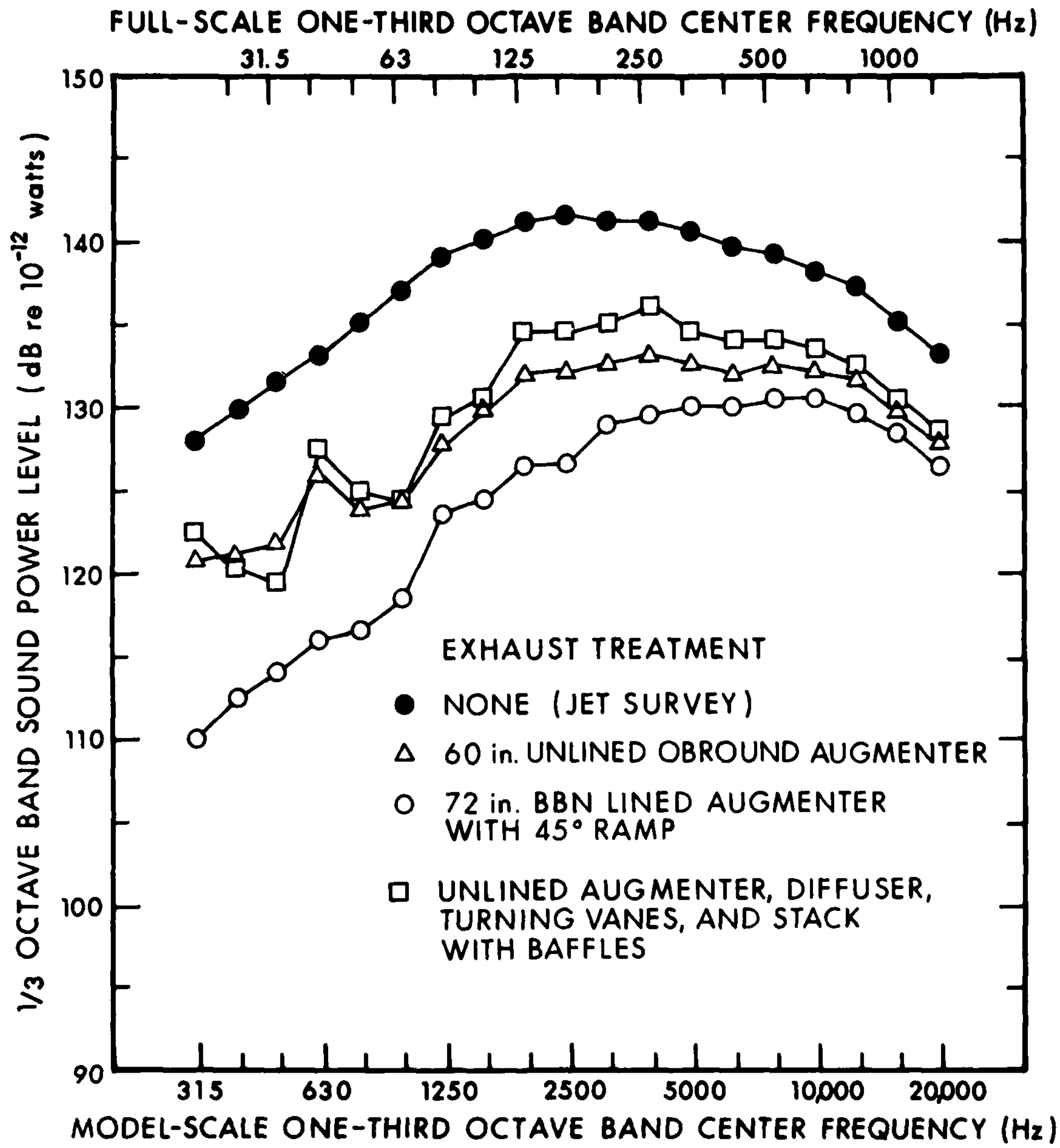

FIG. 7.6.15. EFFECT OF DIFFERENT EXHAUST TREATMENTS ON SOUND POWER LEVEL IN THE BURNER ROOM: T_{T_N} = 3300°R, λ_N = 2, X_N = 4 in.

Note that with respect to burner-room noise levels the stack-and-baffle exhaust treatment is practically equivalent to the unlined augmenter tube alone. This result is not surprising since both configurations have a long unlined augmenter, and sound energy can be reflected back into the burner room from the end of the unlined section.

8. Miramar and BBN Augmenters vs Stack with Baffles: With regard to burner-room noise levels, the two lined augmenters are equivalent. However, for the stack-and-baffle configuration, burner-room noise is considerably higher at low frequencies than that measured for the two configurations using the lined augmenter tube (see Fig. 7.6.15). This result is partly due to the lack of attenuation of the parallel baffles at low frequencies and to the absence of any attenuation between the location where low-frequency noise is generated and the augmenter inlet.

Exhaust-Room Data

In a manner similar to that used in the burner room, we measured the 1/3-octave band PWL spectra in the exhaust room for all runs and calculated the difference between the free jet PWL (obtained from the jet survey) and the exhaust room PWL. This difference in sound power level (ΔPWL), which characterizes the acoustic performance of the exhaust configurations tested, is discussed below:

1. BBN Augmenter with Ramp: The ΔPWL achieved with the 72-in.-long BBN augmenter in combination with a 45° ramp having a solid backing is plotted in Fig. 7.6.16 for $\lambda_N = 2$, F-14 position, and nozzle distance $X_N = 4$ in. as a function of frequency with the temperature as parameter. (The solid-backed ramp was a model of the Miramar full-scale ramp; the solid backplate was used in all runs with the ramp except those discussed in paragraph 2 below.) Generally, ΔPWL increases

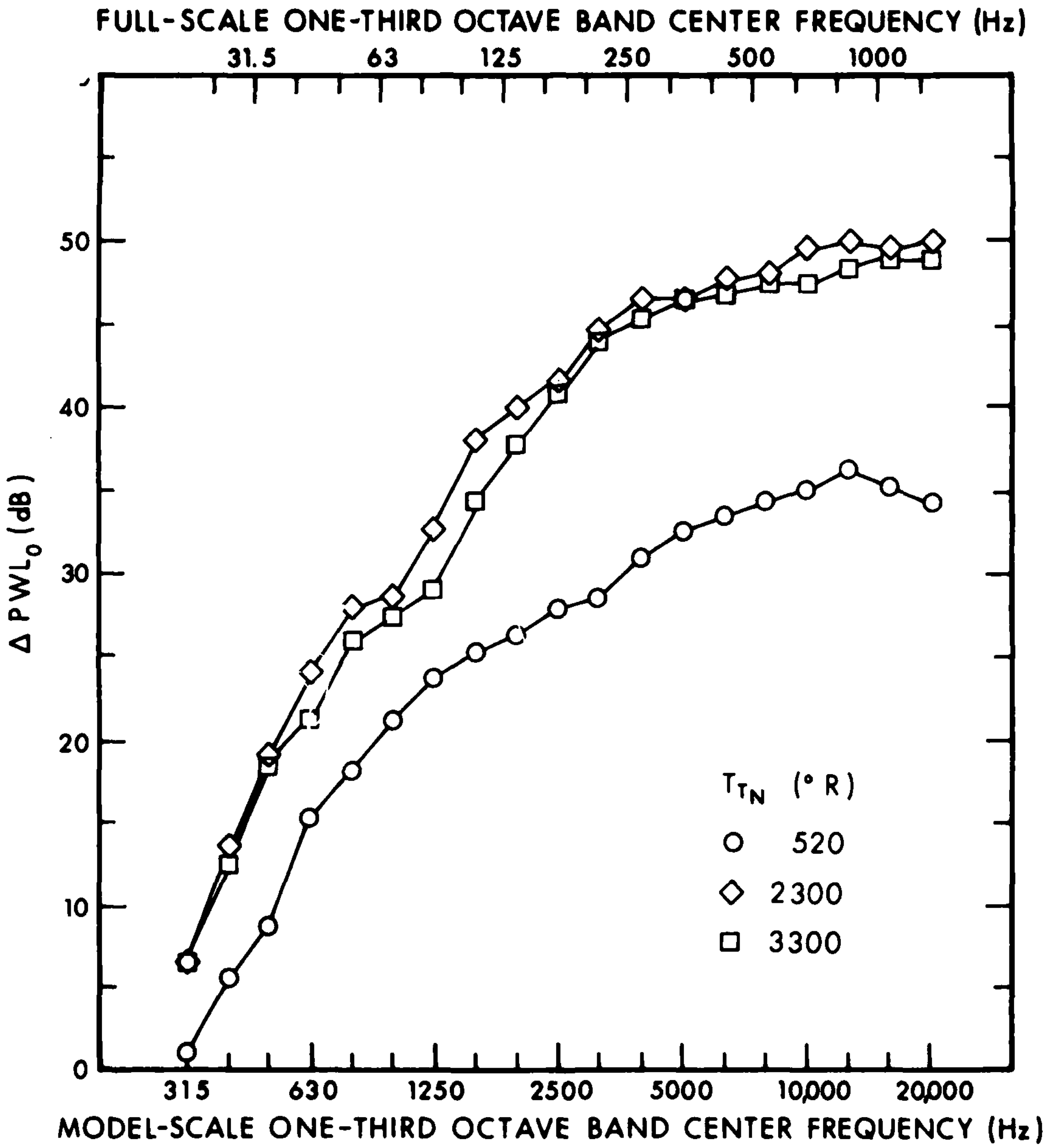

FIG. 7.6.16. ΔPWL FOR 72-in. BBN AUGMENTER WITH 45° RAMP, F-14 POSITION, λ_N = 2, X_N = 4 in.

with increasing frequency up to 10 kHz after which it tends to level off. The high-temperature runs provide substantially higher ΔPWL than the run at ambient temperature, because beneficial temperature gradients in the augmenter tube passage bend the originally axially oriented sound waves toward the sound absorbing wall lining. The two high-temperature runs (2300°R and 3300°R) yield almost the same ΔPWL. The ΔPWL-vs-frequency curves obtained for the $\lambda_N = 3$ runs with an exhaust configuration identical to the above are plotted in Fig. 7.6.17. For this higher pressure ratio, the ΔPWLs measured for ambient and high-temperature runs show little variation. We do not have a satisfactory explanation for this behavior at present. Comparing Fig. 7.6.17 with Fig. 7.6.16 shows that the ΔPWL is somewhat lower for the $\lambda_N = 3$ runs than for the $\lambda_N = 2$ runs, except for the ambient temperature run where the higher jet velocity may create higher flow velocity gradients, which provide an increased degree of beneficial refraction of sound toward the lining.

2. BBN Augmenter with Porous-Backed Ramp: To evaluate whether or not the acoustical performance of the exhaust system can be improved by making the air cavity behind the ramp acoustically useful, we removed the solid backing of the 45° ramp and repeated the $\lambda_N = 2$ runs. Figure 7.6.18 gives the results of these runs. Comparing Fig. 7.6.18 to Fig. 7.6.16 shows that the porous ramp provides 1-dB to 3-dB higher ΔPWL at low and mid frequencies than the ramp with solid backing.

3. BBN Augmenter Without Ramp: The ΔPWL obtained with the 72-in. BBN augmenter without the ramp for $\lambda_N = 2$ is plotted in Fig. 7.6.19. Figure 7.6.20 compares the data of Figs. 7.6.16 and 7.6.19. Note that for the high-temperature runs the presence of the ramp increases the ΔPWL in the frequency range from 600 Hz

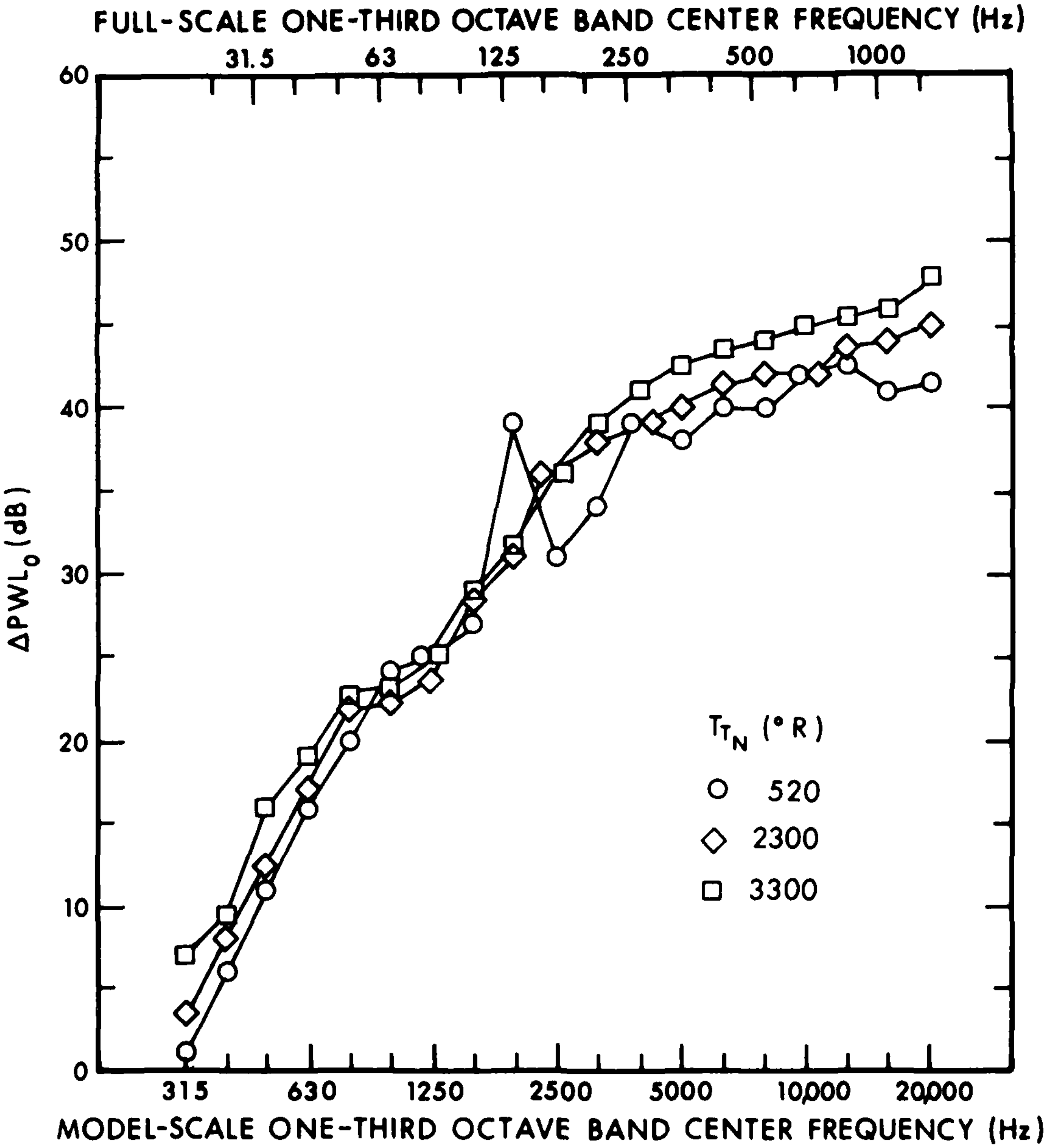

FIG. 7.6.17. ΔPWL FOR 72-in. BBN AUGMENTER WITH 45° RAMP: F-14 POSITION, $\lambda_N = 3$, $X_N = 4$ in.

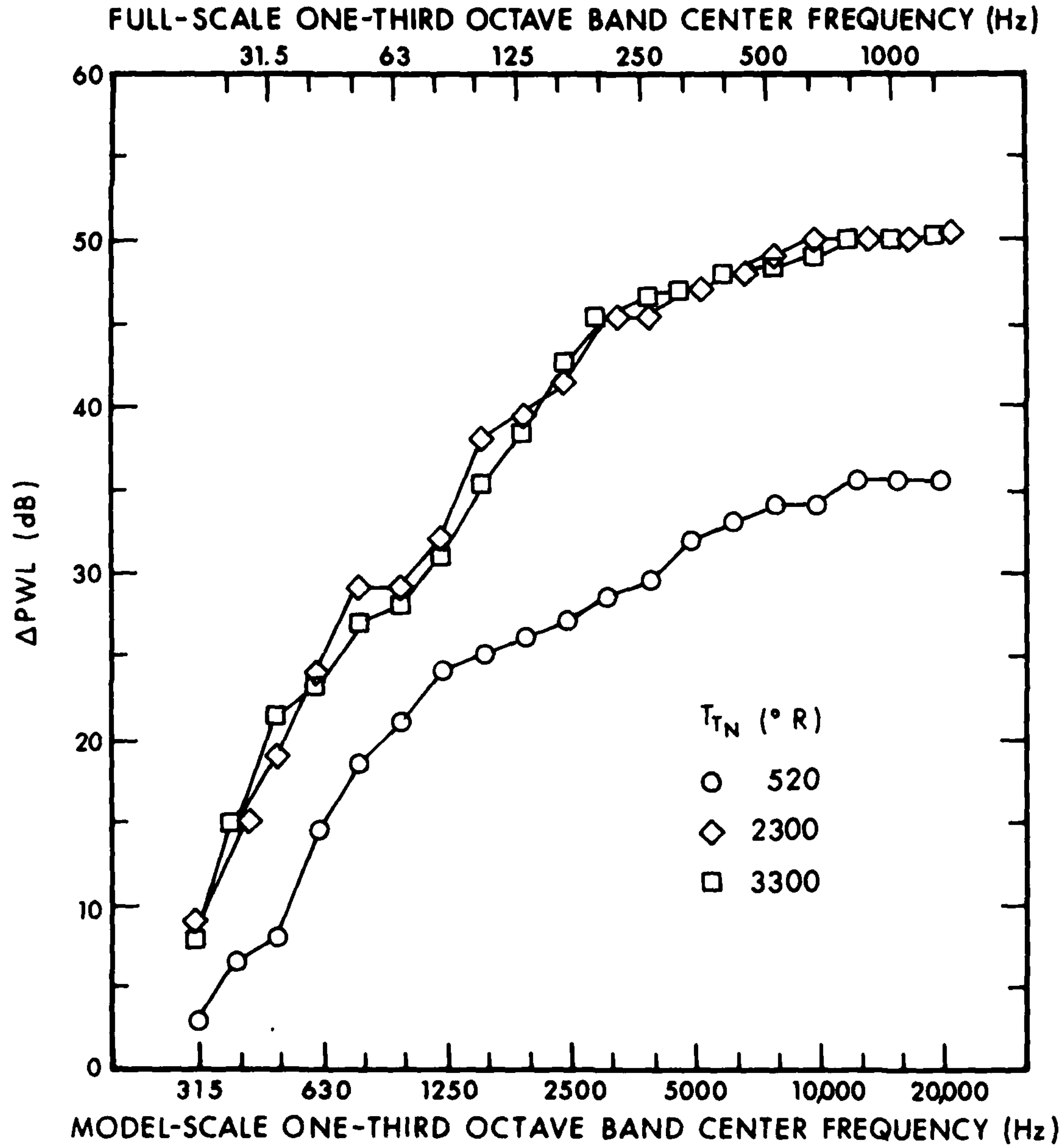

FIG. 7.6.18. ΔPWL FOR 72-in. BBN AUGMENTER WITH 45° POROUS-BACKED RAMP: F-14 POSITION, $\lambda_N = 2$, $X_N = 4$ in.

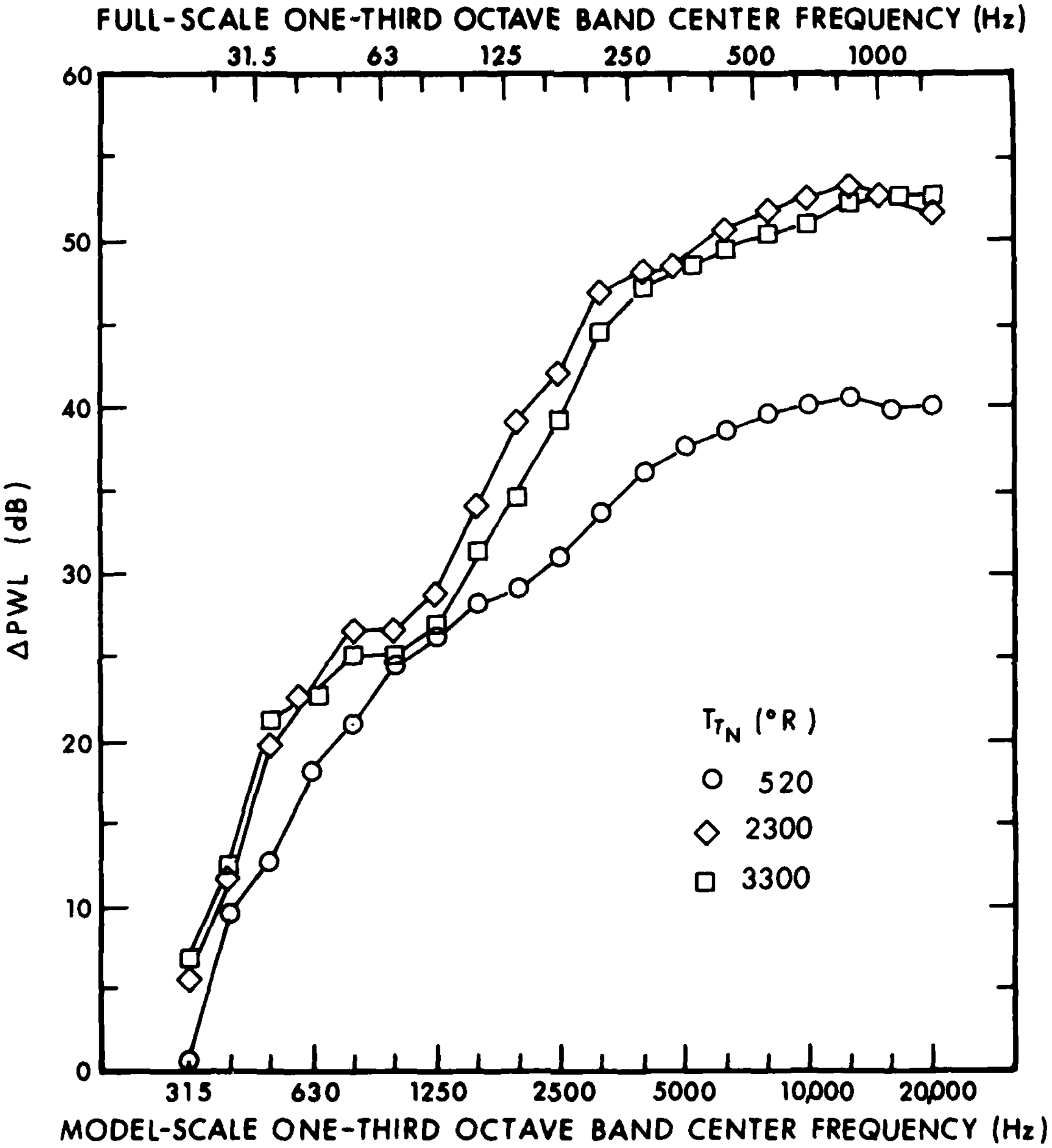

FIG. 7.6.19. ΔPWL FOR 72-in. BBN AUGMENTER WITHOUT 45° RAMP: F-14 POSITION, $\lambda_N = 2$, $X_N = 4$ in.

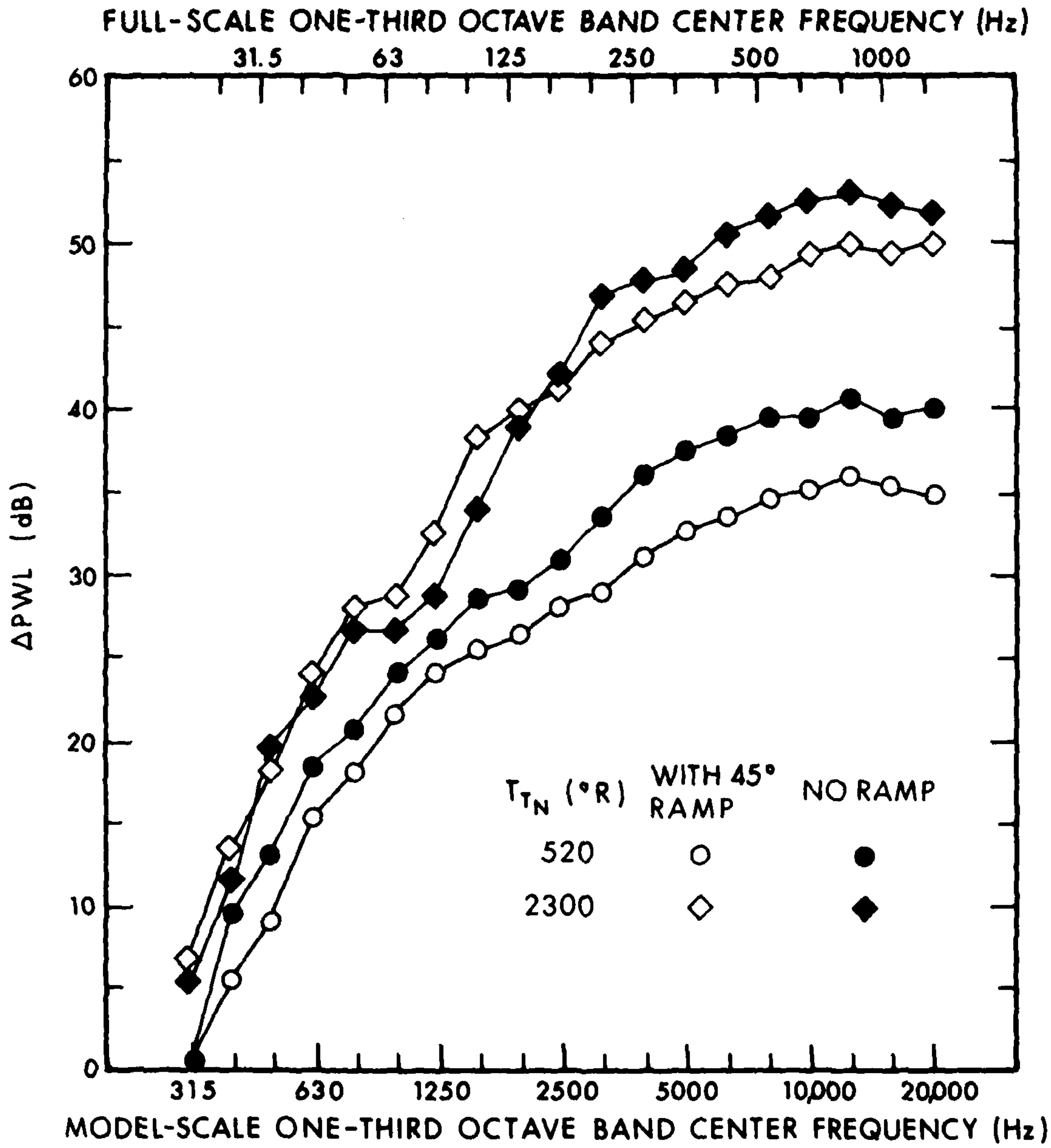

FIG. 7.6.20. ΔPWL FOR 72-in. BBN AUGMENTER WITH AND WITHOUT 45° RAMP: F-14 POSITION, $\lambda_N = 2$, $X_N = 4$ in.

to 3000 Hz and decreases it above 3000 Hz. This decrease of ΔPWL at high frequencies is probably caused by an increase in self-generated noise due to the distortion of the flow profile by the ramp. For ambient temperature runs, the presence of the ramp decreases ΔPWL in the entire frequency region. For these runs at high mass flow rate, ΔPWL is evidently controlled by self-noise.

4. Effect of Nozzle Radial Position: Figure 7.6.21 shows the effect of the radial position of the nozzle on ΔPWL for the 72-in.-long BBN augmenter without the exit ramp. It is expected that the relative differences would be approximately the same with the ramp installed. The measured data indicate that, except for the very low frequencies, the shift from the center to the F-14 position decreases ΔPWL on the average of 3 dB. This decrease is due to a less beneficial refraction pattern for the sound energy radiating toward the far wall which is not compensated for fully by the gain due to decreased distance to the near wall. In addition, the increase in the peak velocity of the flow exiting the augmenter tube because of the asymmetry of nozzle position may also increase the self-noise. One cannot determine from the data which of these mechanisms is the controlling one.

5. Effect of Nozzle Axial Position: Figure 7.6.22 shows the effect of changing X_N, the axial position of the nozzle, on the ΔPWL of the 72-in. BBN lined augmenter with 45° exit ramp. ΔPWL increases with increasing X_N because less acoustic energy enters the augmenter; instead, the energy enters the burner room (see Fig. 7.6.14).

6. BBN vs Miramar Lining: Figure 7.6.23 compares ΔPWL of the 72-in. BBN augmenter with that of the 72-in. Miramar augmenter. Both augmenters were tested in combination with a 45° hard-backed

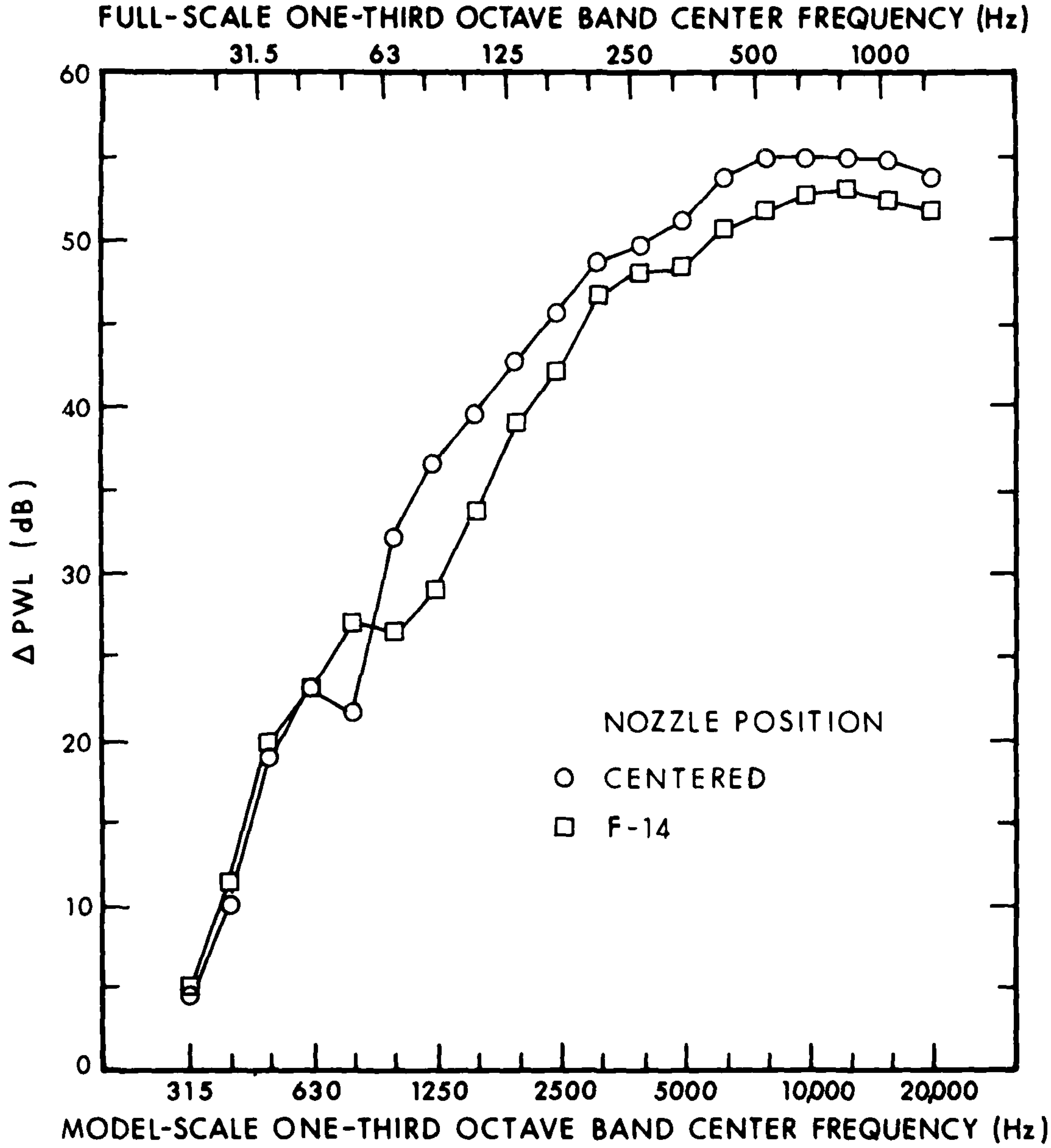

FIG. 7.6.21. ΔPWL FOR DIFFERENT RADIAL POSITION OF THE NOZZLE: 72-in. BBN AUGMENTER WITHOUT 45° RAMP, T_{T_N} = 2300°R, λ_N = 2, X_N = 4 in.

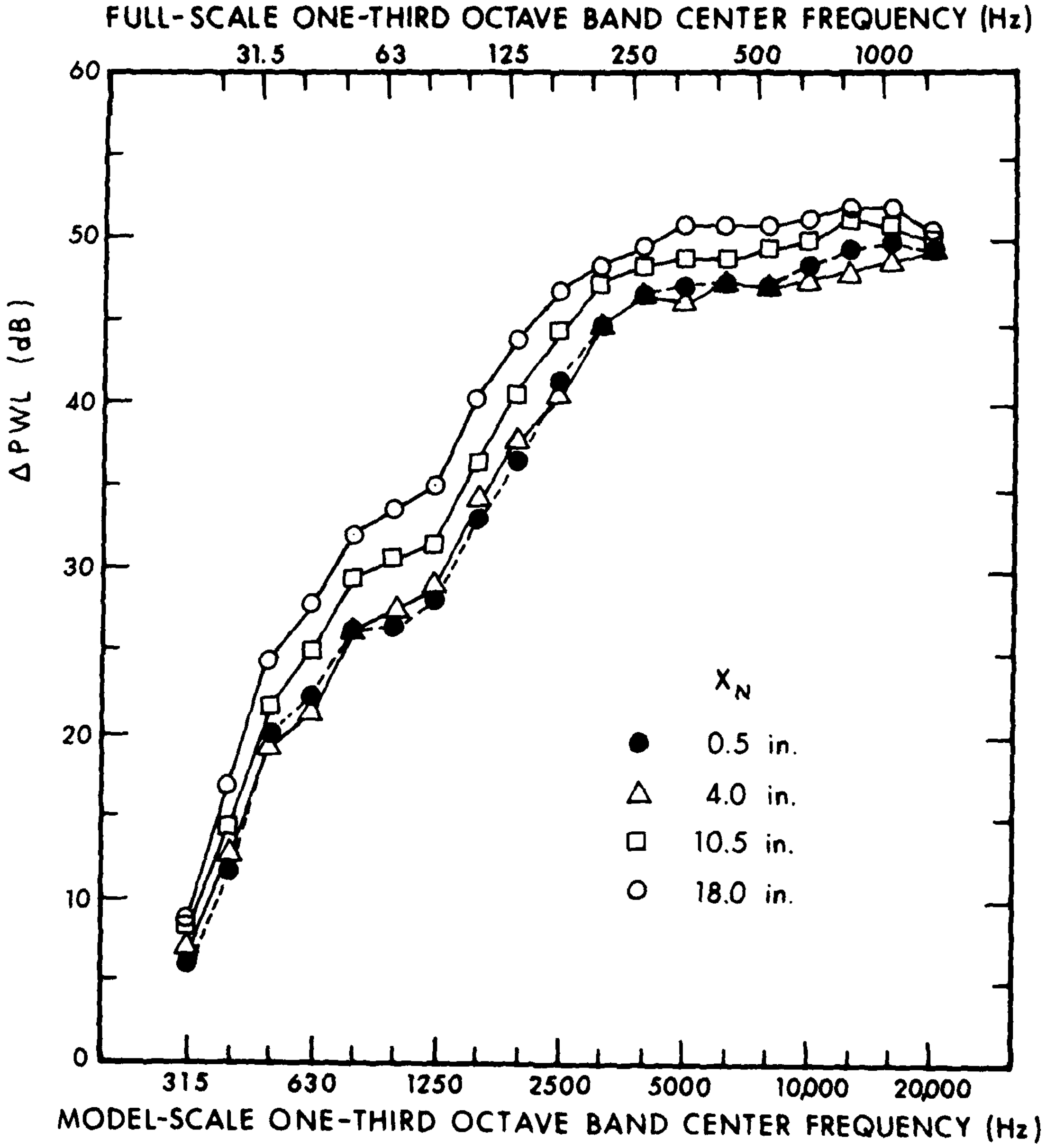

FIG. 7.6.22. ΔPWL FOR DIFFERENT AXIAL POSITIONS OF THE NOZZLE: 72-in. BBN AUGMENTER WITH 45° RAMP, F-14 POSITION, T_{T_N} = 3300°R, λ_N = 2.

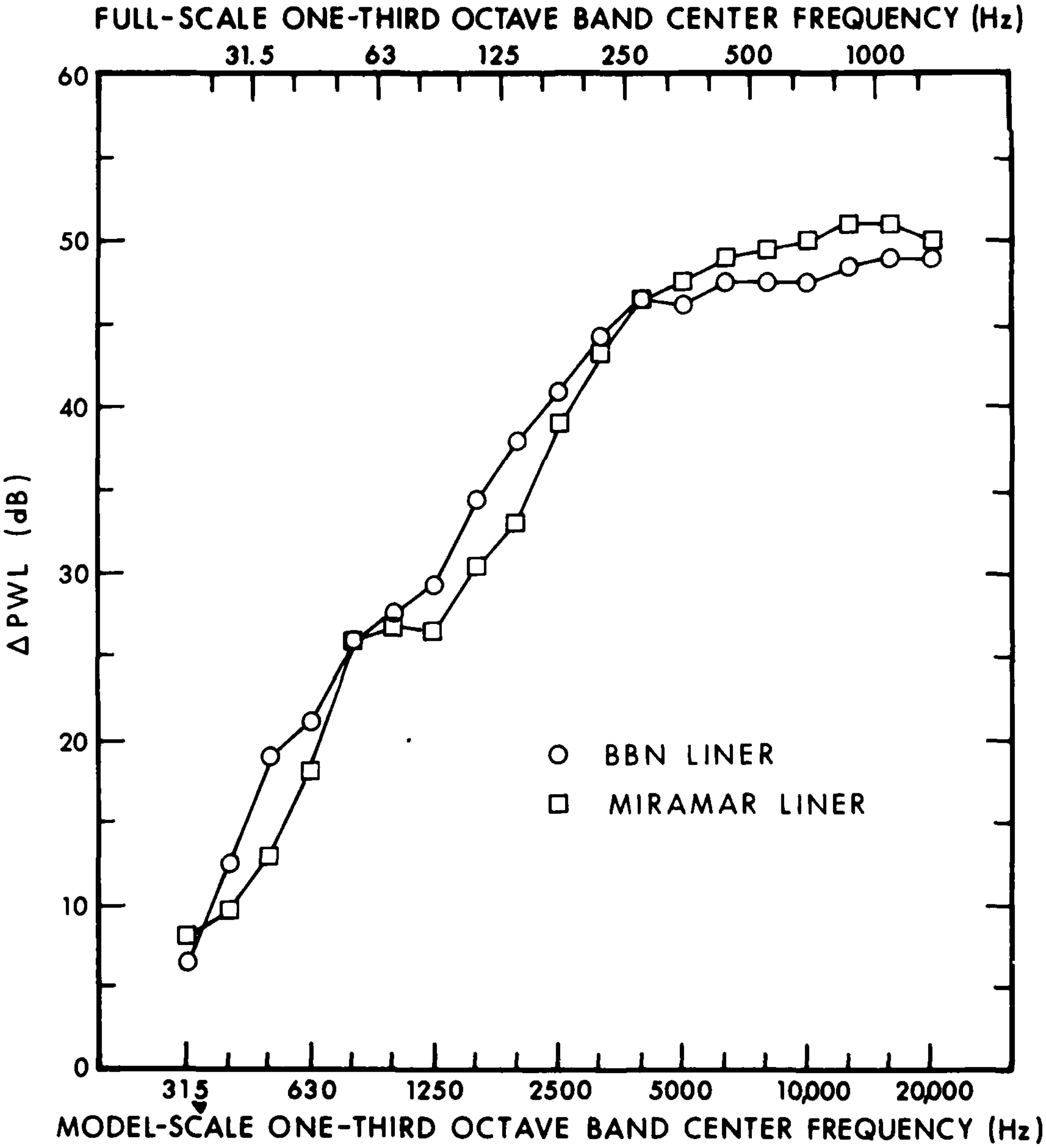

FIG. 7.6.23. ΔPWL FOR TWO 72-in. LINED AUGMENTERS WITH 45° RAMP: F-14 POSITION, T_{T_N} = 3300°R, λ_N = 2, X_N = 4 in.

exit ramp. The nozzle was, in both cases, at the F-14 position at an axial distance of 4 in. and operated at pressure ratio of 2 at 3300°R. The BBN augmenter provided higher attenuation at frequencies up to 4 kHz than the Miramar augmenter, because of lower total flow resistance of the BBN lining. Above 4 kHz, the Miramar augmenter provided a slightly higher ΔPWL. The slightly lower performance of the BBN augmenter at high frequencies is most likely due to the difference in alignment between the 12-in.-long augmenter sections. While the Miramar augmenter was hardly used, the BBN augmenter had been exposed to a large number of high-temperature runs, many of them with axial and radial misalignment, prior to these comparison tests. This exposure to a hostile environment caused some buckling of the protective surface resulting in misalignment between the sections and thereby may have caused increased self-noise at high frequencies.

7. Effect of the Liner's Axial Position on ΔPWL: To obtain information about the optimal location of lined sections within a long hard-walled augmenter tube, the ΔPWL was determined for a single 12-in.-long lined augmenter section of BBN design, positioned at various distances from the entrance of the hard augmenter tube which terminated into a 45° exit ramp. The total length of the augmenter tube was always 72 in. (i.e., 12-in. lined and 60-in. hard). Figure 7.6.24 shows the ΔPWL-vs-frequency curves obtained from these tests. As expected, the positions near the augmenter intake are most effective in attenuating high-frequency jet noise, which is generated near this location, but least effective in attenuating low frequencies, which are generated at locations further downstream. The lined section placed far downstream of the augmenter intake is effective in attenuating low frequencies but less effective in dealing with

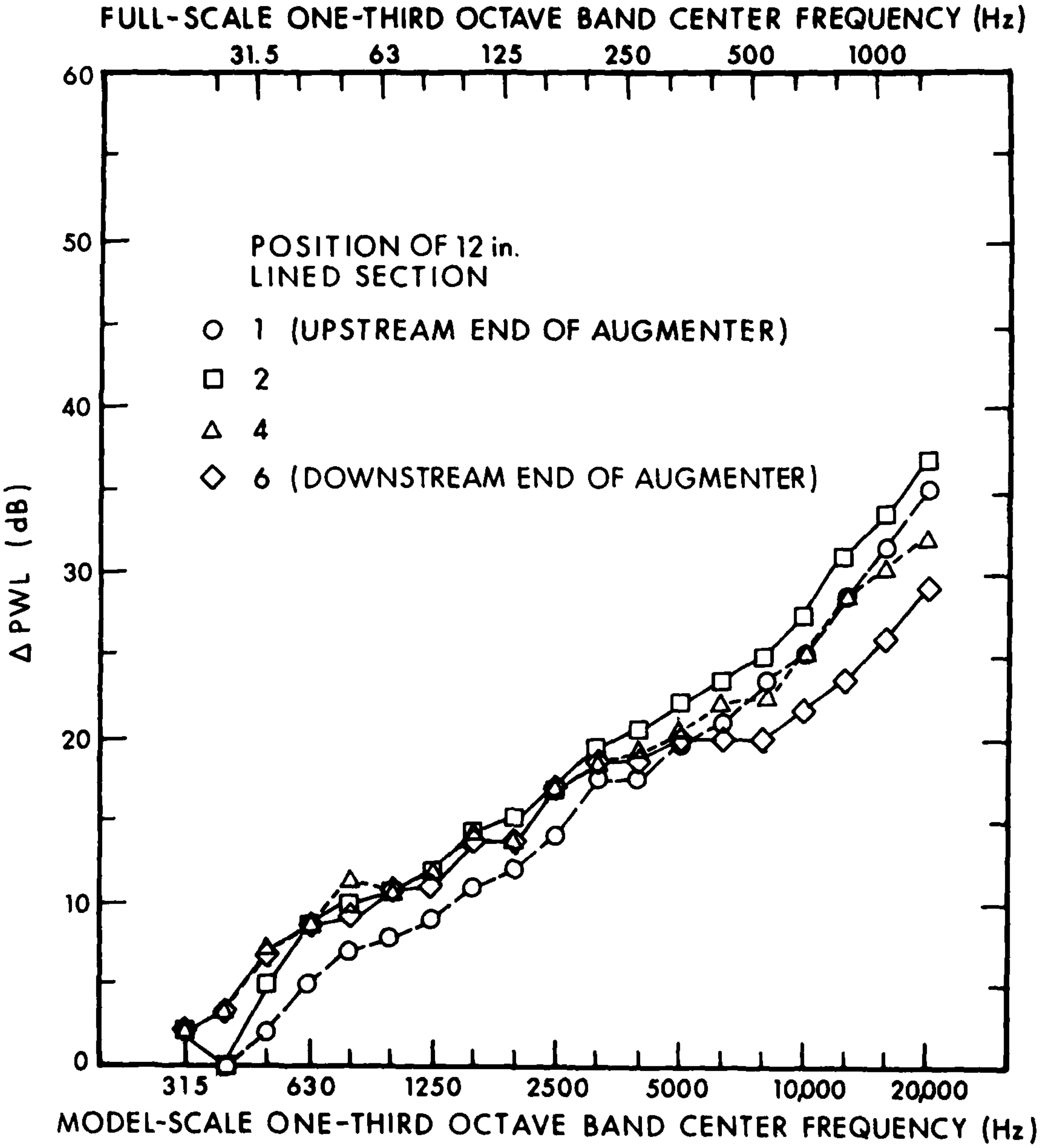

FIG. 7.6.24. ΔPWL FOR 12-in. SECTION OF AUGMENTER WITH BBN LINER AT VARIOUS POSITION IN THE 60-in. HARD-WALLED AUGMENTER WITH 45° RAMP: F-14 POSITION, T_{T_N} = 3300°R, λ_N = 2, X_N = 4 in.

high frequencies. The best balance between attenuation at high and low frequencies was obtained by positioning the center of the lined section 18 in. downstream of the augmenter intake. This distance is approximately seven nozzle diameters from the exit of the nozzle.

8. Effect of Lined Augmenter Tube Length: To evaluate the effect of the length of the lined augmenter tube on ΔPWL, we tested three different lengths, all with a 45° exit ramp, with the nozzle at the F-14 radial position and at an axial distance of 4 in. upstream of the augmenter intake, with a pressure ratio of 2, and at 3300°R. Figure 7.6.25 shows the measured ΔPWL values as a function of frequency for these three tube lengths. At low frequencies (below 1250 Hz 1/3-octave band), where the wavelength of sound is large compared with the cross-sectional dimension of the passage, the attenuation in dB increases roughly linearly with augmenter tube length. At 1280 Hz, the low-frequency attenuation is expected to reach its peak value because the average depth of the airspace behind the lining roughly corresponds to one-quarter of the wavelength. In this frequency region, the attenuation per unit length corresponding to half the height of the open passage (0.4 ft in our case) is approximately 2 dB. Accordingly, we would expect to achieve attenuation values of 20 dB, 30 dB, and 40 dB for the 4-ft, 6-ft, and 8-ft long augmenter tubes, respectively. Figure 7.6.25, at 1250 Hz, shows 20-dB, 29-dB, and 37.5-dB attenuations, which correspond reasonably well to the expected values.

9. Stack with Baffles: As an alternative to the lined augmenter tube and exit ramp, we tested a model configuration consisting of a 60-in.-long hard-walled augmenter tube followed by a subsonic diffuser, hard turning vanes, and a rectangular stack

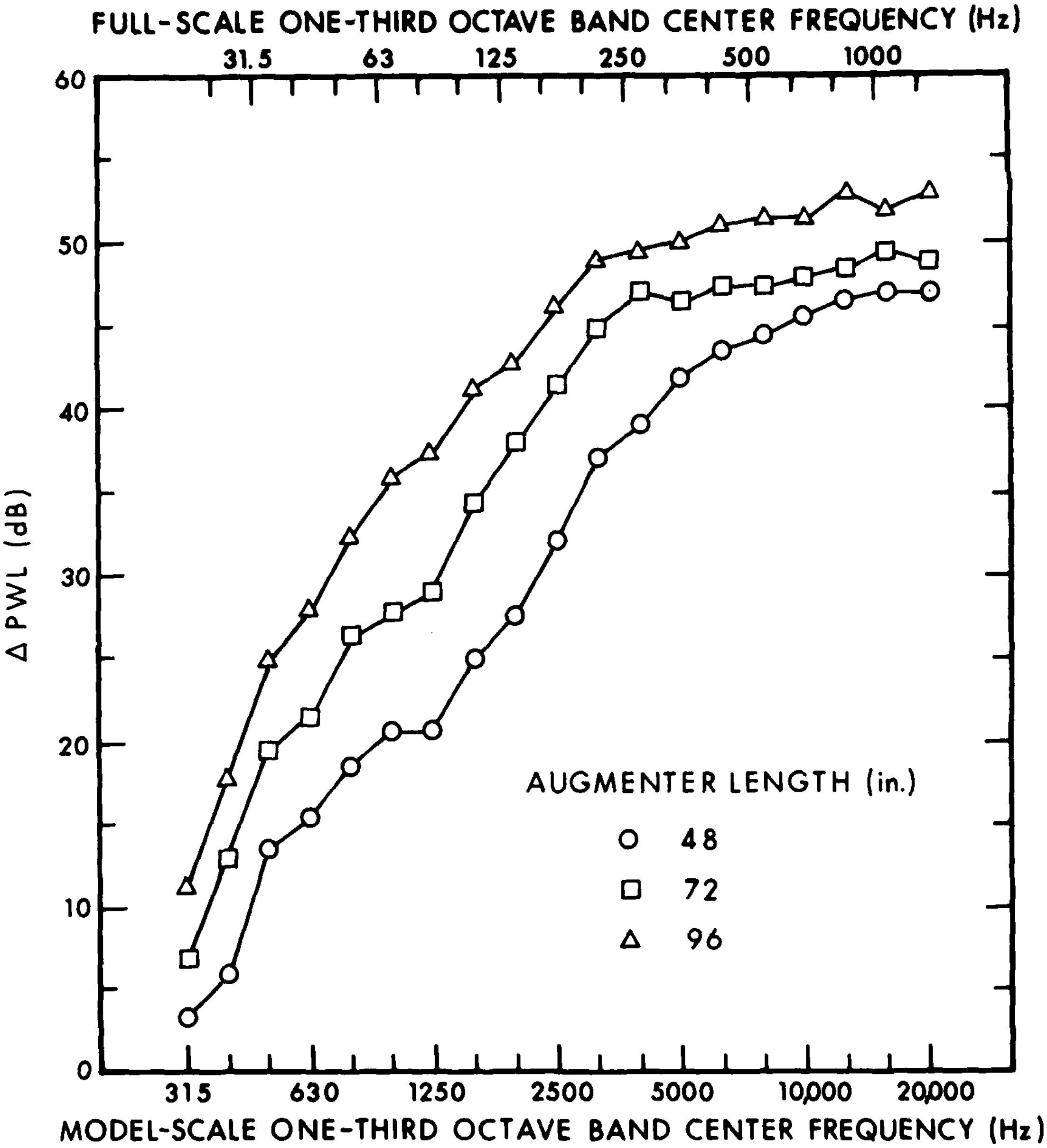

FIG. 7.6.25. ΔPWL FOR THREE DIFFERENT LENGTHS OF LINED BBN AUGMENTER WITH 45° RAMP: T_{T_N} = 3300°R, λ_N = 2, X_N = 4 in.

with parallel baffles. The configuration is shown in Figs. 4.4.1 and 4.4.2. The baffles were designed to simulate a full-scale installation that would yield approximately 85 dBA at 250 ft for one engine of an F-14A aircraft operating in the afterburning mode. Accordingly, this configuration would be useful for comparing the performance and cost of various alternative exhaust-silencing configurations. The stack-and-baffle configuration was evaluated at $\lambda_N = 2$ for three different temperatures. The ΔPWL obtained is shown in Fig. 7.6.26; it is lowest for the ambient temperature run which had the largest mass flow and highest for the 3300°R run which had the smallest mass flow. The protective fiber metal surface was observed to buckle when exposed to high temperature; this buckling reduced the effective width of the passage between the baffles and may thereby have increased the sound attenuation of the silencer. This effect may be partly responsible for the higher ΔPWL at high temperatures. The higher ΔPWL obtained with high-temperature runs may also be due to the favorable temperature gradients, the increased flow resistance of the porous material in the lining, and the increased end reflection. Comparing Fig. 7.6.26 with Fig. 7.6.16 shows that the ΔPWL obtained with the stack-and-baffle configuration is substantially less than that achieved with the lined augmenter tube configuration at all except high frequencies, where the two configurations yield comparable results.

7.6.5 No-flow tests

Tests of the attenuation of the lined augmenter without air flow were conducted for all acoustically treated augmenter configurations. Measurements were made by placing a loudspeaker close against the upstream end of the augmenter, with the speaker

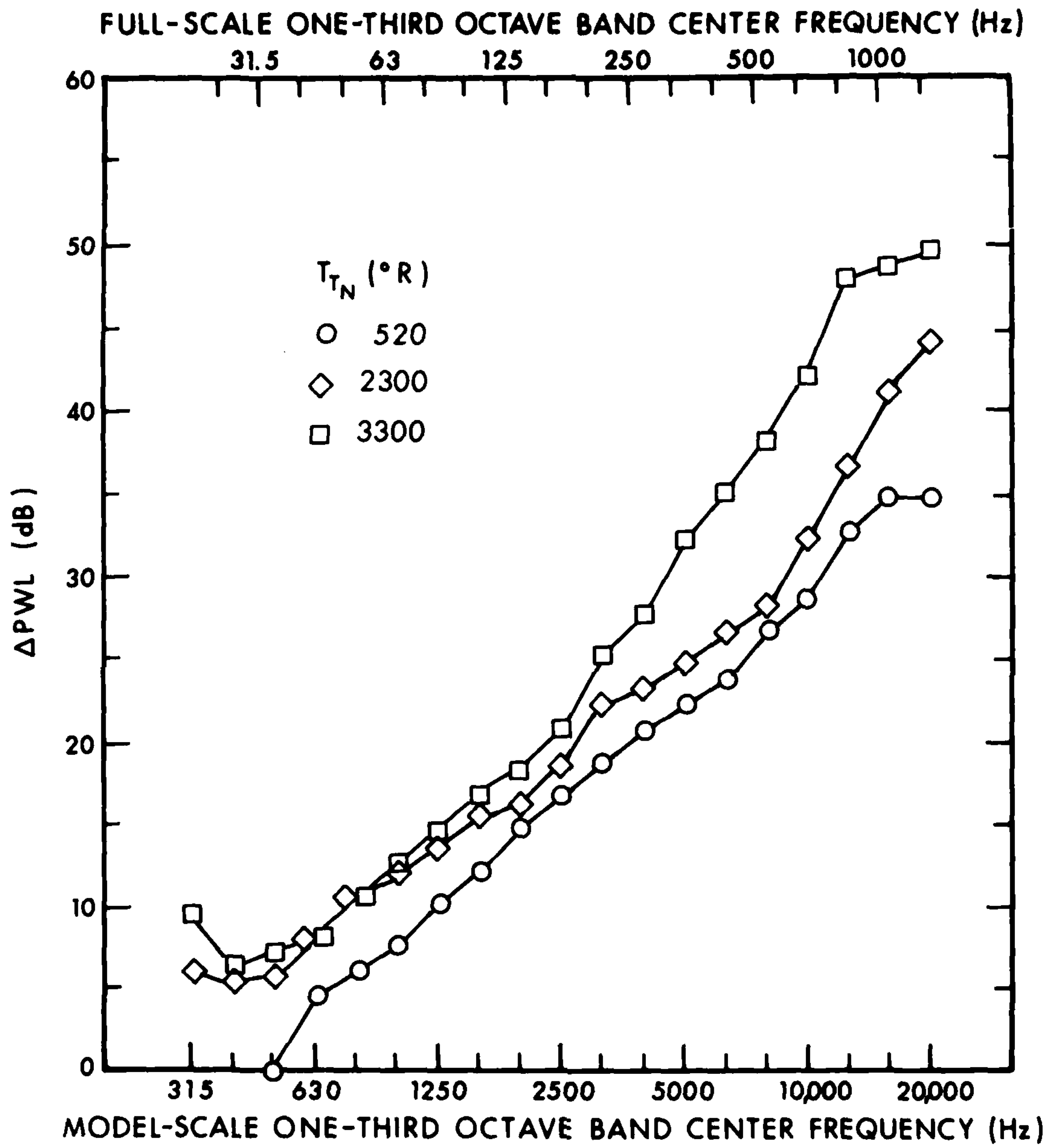

FIG. 7.6.26. ΔPWL FOR 60-in. HARD-WALLED AUGMENTER, SUBSONIC DIFFUSER, TURNING VANES, STACK WITH BAFFLES: F-14 POSITION, λ_N = 2, X_N = 4 in.

faced directly down the augmenter axis, and measuring the room-average sound pressure level $\overline{SPL}$ in the exhaust room, using the same instrumentation as was used during the jet runs (excluding the tape-recording system). Immediately after this measurement, an ILG was run in the exhaust room, and the $\overline{SPL}$ was again measured; this allowed correcting the $\overline{SPL}$ measured with the loudspeaker for for effects of temperature and humidity. One run was made with a 60-in.-long unlined obround augmenter, and the data were used as the baseline from which attenuation of the lined ducts was calculated; i.e., no-flow attenuation $\Delta L_{NF} = \overline{SPL}$ (60-in. unlined augmenter) - $\overline{SPL}$ (lined augmenter). Results are shown in Figs. 7.6.27 through 7.6.30.

Figure 7.6.27 shows attenuation of 4-ft, 6-ft, and 8-ft long fully lined BBN augmenters without the 45° exit ramp. Attenuation at high frequencies approaches the value given by

$$\Delta L_{NF} = 10 \log \frac{L_A}{D_A(1.5-\alpha)} \quad .$$

In the absence of the refraction caused by hot air flow, the no-flow attenuation at high frequencies is significantly less than the ΔPWL measured for jet noise. At low frequencies, the no-flow attenuation is greater than ΔPWL. The reasons for this are not known precisely, but they are probably related to the differences in wavelength, effective flow resistance, acoustic source size, location, and directivity.

Figure 7.6.28 shows attenuation for the same augmenters as for Fig. 7.6.27, but with the addition of the 45° exit ramp. Attenuation for the 6-ft and 8-ft long augmenters is essentially unaffected by addition of the ramp for frequencies of 1250 Hz

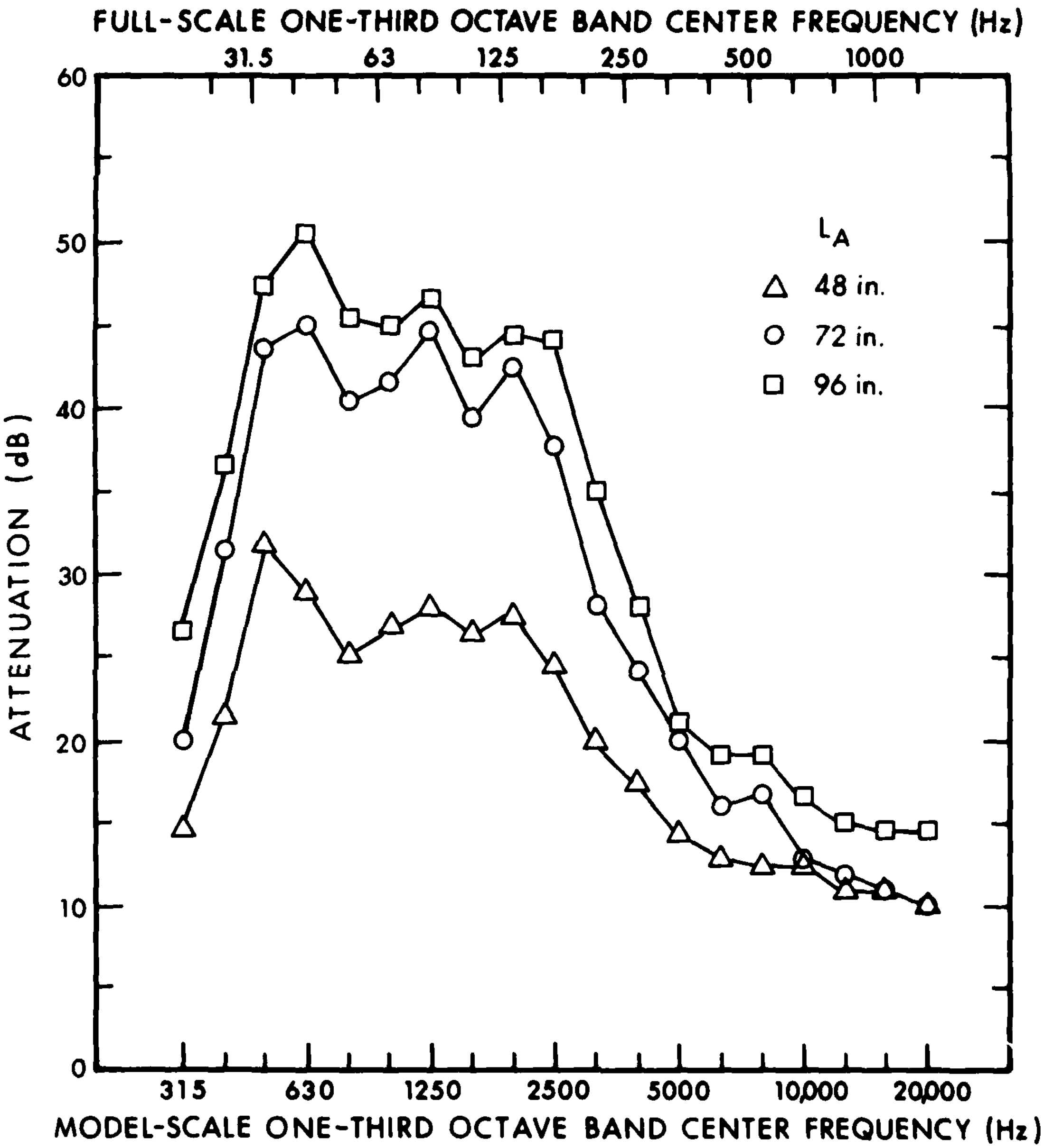

FIG. 7.6.27. NO-FLOW ATTENUATION OF FULLY LINED BBN AUGMENTERS OF THREE DIFFERENT LENGTHS WITHOUT 45° RAMP.

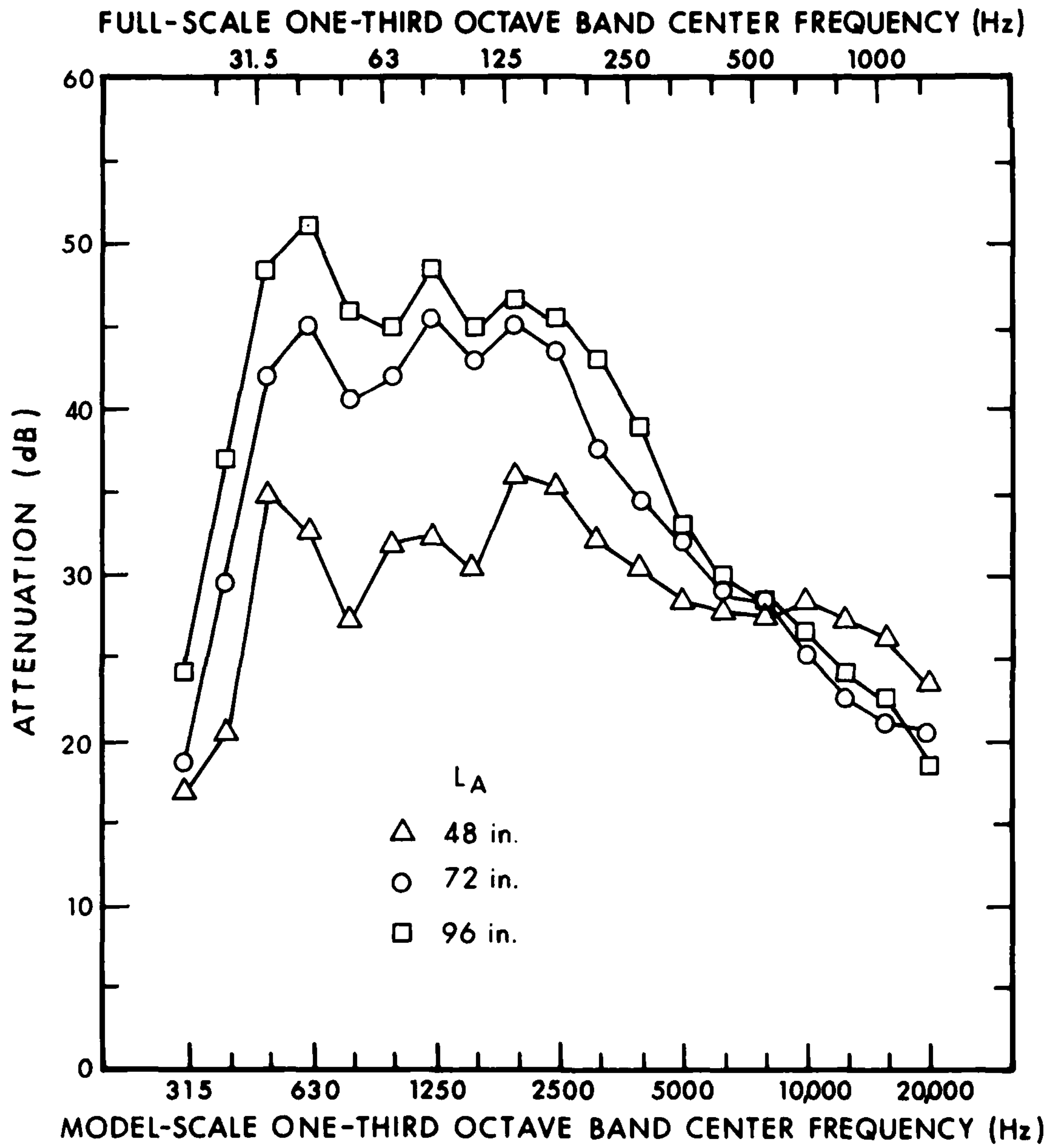

FIG. 7.6.28. NO-FLOW ATTENUATION OF FULLY LINED BBN AUGMENTERS OF THREE DIFFERENT LENGTHS WITH 45° RAMP.

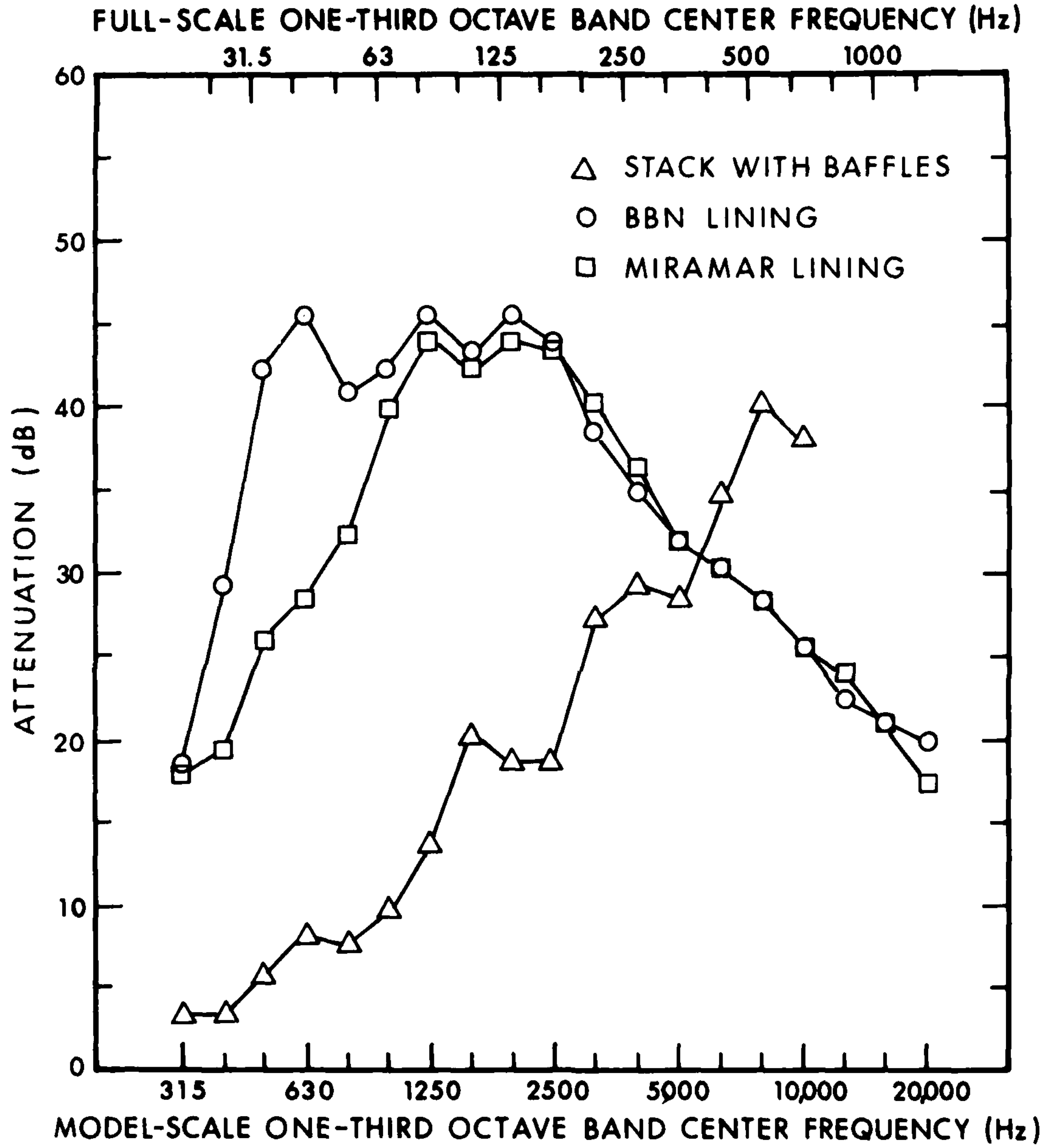

FIG. 7.6.29. NO-FLOW ATTENUATION OF FULLY LINED 72-in. BBN AND MIRAMAR AUGMENTERS WITH 45° RAMP AND STACK-AND-BAFFLE CONFIGURATION.

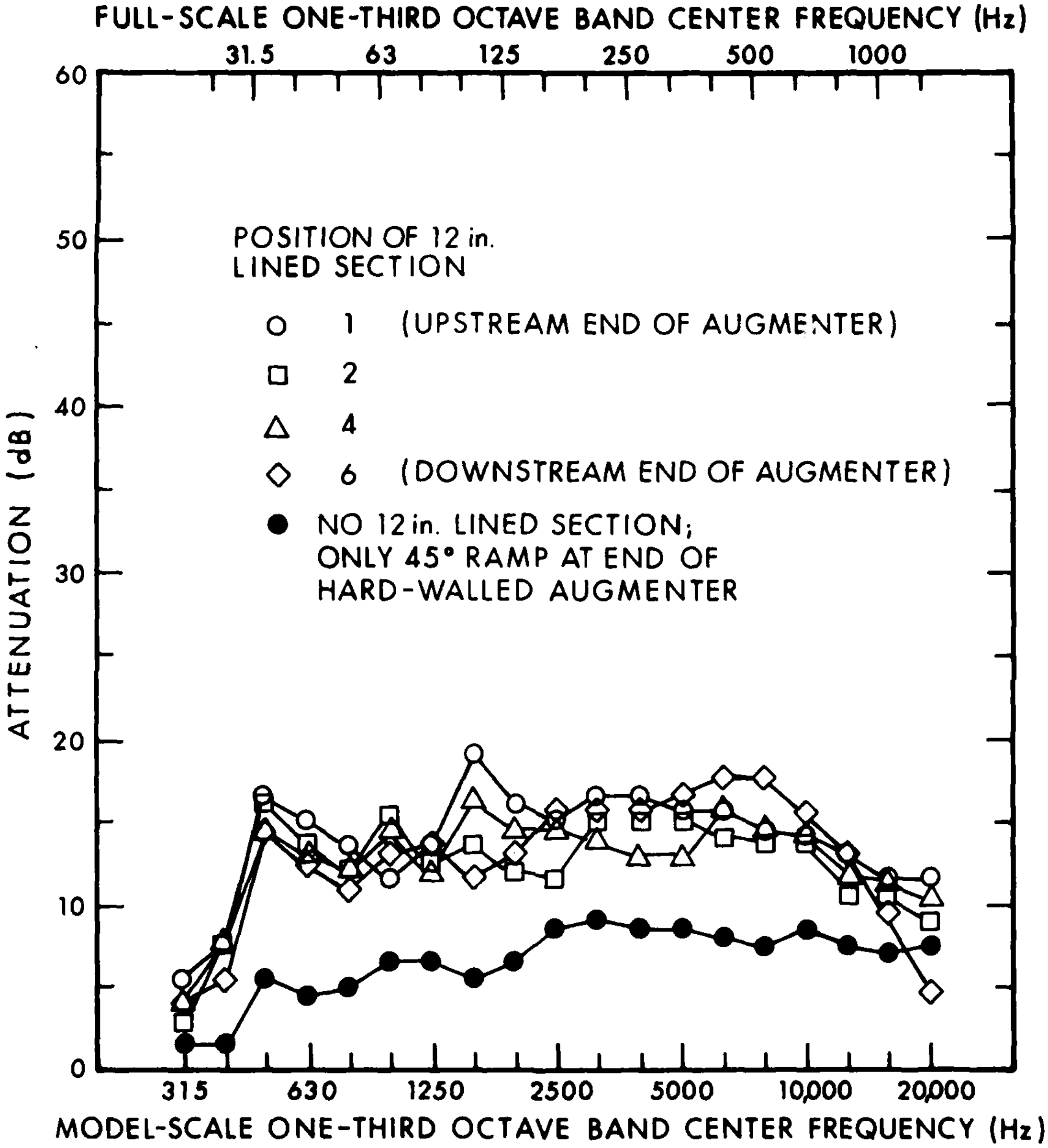

FIG. 7.6.30. NO-FLOW ATTENUATIONS OF 12-in. SECTION OF BBN LINER AT VARIOUS POSITIONS IN 60-in. HARD-WALLED AUGMENTER WITH 45° RAMP.

and below. The ramp increases attenuation by approximately 10 dB at high frequencies.

Figure 7.6.29 compares attenuation of the 6-ft BBN and Miramar lined augmenters and the stack with baffles. At frequencies between 400 and 1000 Hz, the BBN liner provides significantly greater attenuation than the Miramar liner; these two are approximately the same at higher frequencies. Both the BBN and Miramar liners have better no-flow attenuation than the stack with baffles at low frequencies and worse attenuation at frequencies of 6300 Hz and greater.

Figure 7.6.30 shows no-flow attenuation for the 12-in.-long BBN lined augmenter section placed at different axial positions in the 60-in. hard-walled augmenter with 45° exit ramp; also plotted is attenuation for the 60-in. hard-walled augmenter with ramp but without the 12-in. lined section. The attenuation is nearly independent of frequency between 500 and 16,000 Hz. Attenuation is best for position 1 (closest position to the loudspeaker) at lower frequencies, probably because of nearfield effects close to the speaker face. Excluding position 1, there is not apparent preferable location for the augmenter lining in the absence of refraction induced by the hot flow.

7.7 Conclusions

7.7.1 Conclusions from Aerodynamic-Thermodynamic Data

1. With an adequately large augmenter cross-section to jet nozzle throat area ratio, A_A/A_{NT}, sufficient cooling air can be pumped even without a subsonic diffuser.

2. Addition of a subsonic diffuser increases cooling air pumping by about 50% when ${}^{T}T_N/T_{amb} = 6.6$.

3. The test data show a consistent drop in augmentation ratio parameter with increased jet nozzle to ambient temperature ratio, ${}^{T}T_N/T_{amb}$, related to heat exchange from the jet to the pumped flow.

4. Pumping performance at ${}^{T}T_N/T_{amb} = 6.6$ varied no more than 10% over the tested range of augmenter length-diameter ratio from 4 to 8.

5. Augmenter inlet throttling devices and changes to the augmenter inlet configuration had a relatively small influence on augmenter pumping performance.

6. Increasing jet nozzle pressure ratio, λ_N, from 2.0 to 3.0 had no measurable influence on augmentation ratio parameter, other things remaining constant. Also, the augmentation ratio parameter remains relatively constant, even down to jet nozzle pressure ratios corresponding to idling.

7. The augmenter pumping performance was slightly higher with the rounded and conical augmenter entrance configurations, than with the sharp-edged configuration.

8. At a nominal augmenter cross-section to jet nozzle throat area ratio, A_A/A_{NT}, of 25, changing from a round to an aspect ratio

1.7 obround cross-section decreased pumping 10%. Part of this decrease resulted from the change from a hard-wall to a porous sound-absorbing wall.

9. With the obround augmenter, moving the jet nozzle centerline laterally off-center or deflecting it laterally toward the augmenter wall resulted in decreased pumping, high wall temperatures and increased maximum augmenter exit velocity. At an orientation corresponding to the F-14A configuration ($Y_p = 0.45$, $\alpha_s = 1°$), the pumping ratio parameter was 15% lower than for the centered, undeflected jet orientation and the maximum sidewall temperature parameter was over 100% higher.

10. At a jet nozzle pressure ratio of $\lambda_N = 2.0$, a laterally offset jet tended to be carried closer to the augmenter sidewall, while at $\lambda_N = 3.0$, the jet remained on the nozzle axis with a corresponding reduction in jet impingement.

11. The addition of an exit ramp to the obround augmenter caused a slight back-pressuring of the augmenter and a corresponding reduction in pumping performance.

12. With the augmenter plus stack-and-baffles configuration increasing the jet nozzle to ambient temperature ratio from 1.0 to 6.6 resulted in a 45% decrease in augmentation ratio parameter, which is greater than the corresponding decrease which occurred with the augmenter alone.

13. For typical jet aircraft being run up inside of a Hush House, the jet nozzle base pressure will bear essentially the same relationship to Hush House interior pressure as it would bear to barometric pressure during out-of-doors operation; that is, there will be no excess pump-down of the nozzle base pressure.

7.7.2 Conclusions from acoustical tests

1. Exhaust noise from the F-14A operating in the afterburning mode in the Miramar Hush House is expected to meet the 85-dBA criterion on the 250-ft radius, except possibly in a narrow range of directions downstream of the jet.

2. The measured data indicate that one can predict the full-scale sound power spectra of a jet, if jet total temperature, nozzle pressure ratio, and nozzle diameter are known.

3. The BBN-designed model augmenter lining provided slightly greater attenuation than the Miramar model lining; both lined augmenters were acoustically superior to the vertical stack with parallel baffles.

4. Hush House interior noise levels due to jet exhaust increase significantly as the axial distance of the jet nozzle from the augmenter inlet increases, while the exterior exhaust noise levels decrease as this distance increases.

5. Significant reduction in Hush House interior noise due to jet exhaust can be achieved by acoustical lining in the upstream end of the augmenter.

6. Optimum positions for installing acoustic lining in the augmenter to reduce exterior exhaust noise levels extend from approximately 5 to 25 nozzle diameters downstream from the nozzle exit plane.

7. Aeroacoustic tests showed that an unlined augmenter causes a slight decrease in jet sound power levels at high frequencies but no change at low frequencies. The acoustic energy of the free jet was distributed between two rooms corresponding

to the Hush House interior and exterior; most of the high-frequency energy remained in the interior and the sound energy at mid and low frequencies was transmitted to the exterior. The particular distribution of energy depends strongly on the axial distance between the nozzle exit and the augmenter tube entry plane.

8.0 FULL-SCALE TESTS AT NAS MIRAMAR

The following two subsections cover the recommended aerodynamic/thermodynamic and acoustical tests on the full-scale NAS Miramar Hush House with an F-14A installed. The purpose of these tests is to verify the general operating acceptability of the enclosure and to provide a correllating check on the design calculations for the full-scale Hush House and on the model scale data presented in this report. For such tests, it is recommended that the following engine operating conditions be run and data recorded for each condition:

Test	Port engine	Starboard engine
1	idle	idle
2	idle	max. non A/B
3	idle	intermediate (analyze data before proceeding) A/B
4	idle	max. A/B
5	max. non A/B	max. non A/B
6	max. A/B	idle

Runups will have to be made with and without augmenter rakes so that acoustical data can be obtained which is free of rake noise.

8.1 Pressure, Temperature and Flow Measurements

Measurement of outside atmospheric conditions corresponding to each test point are basic to the full-scale Hush House test program. These measurements should include:

a. barometric pressure P_{amb}

b. air temperature T_{amb}

c. relative humidity (for use in reducing the acoustical data)

d. wind velocity (also useful in interpreting acoustical data)

e. wind direction

Enough measurements should be made on the Hush House itself to determine total Hush House airflow, Hush House interior flow conditions, Hush House interior pressure, augmenter wall pressure and temperature, jet mixing progress at axial locations corresponding with the model test rake locations, ramp surface temperatures, ramp exit total pressures and aircraft nozzle base pressure (which should also be obtained free field). The following list represents the minimum number of measurements required to make the required determinations.

1. Inlet baffle surface static pressure, P_{inlet} (3)
2. Hush House interior static pressure, $P_{interior}$ (2)
3. Hush House interior total pressure survey, $P_{T_{flow}}$ (3)
4. Augmenter wall static pressure, P_{wall} (4)
5. Augmenter cross-section total pressure, total temperature surveys

   60 ft. station (10 P_T, 10 T_T total)
   90 ft. station (10 P_T, 10 T_T total run only at max. A/B condition)
6. Augmenter wall temperature, P_{wall} (9)
7. Ramp surface temperature, T_{ramp} (2)
8. Ramp exit total pressure survey, $P_{T_{ramp}}$ (4)
9. Aircraft nozzle base pressure, P_{NB} (1)

All pressures can be read using either a multi-tube water manometer referenced to barometric pressure or an accurate guage. Temperatures can be determined using iron-constantan or chromel-alumel thermocouple junctions and the required support equipment. The location of the measurement points is shown on Figures 8.1-1 and 8.1-2.

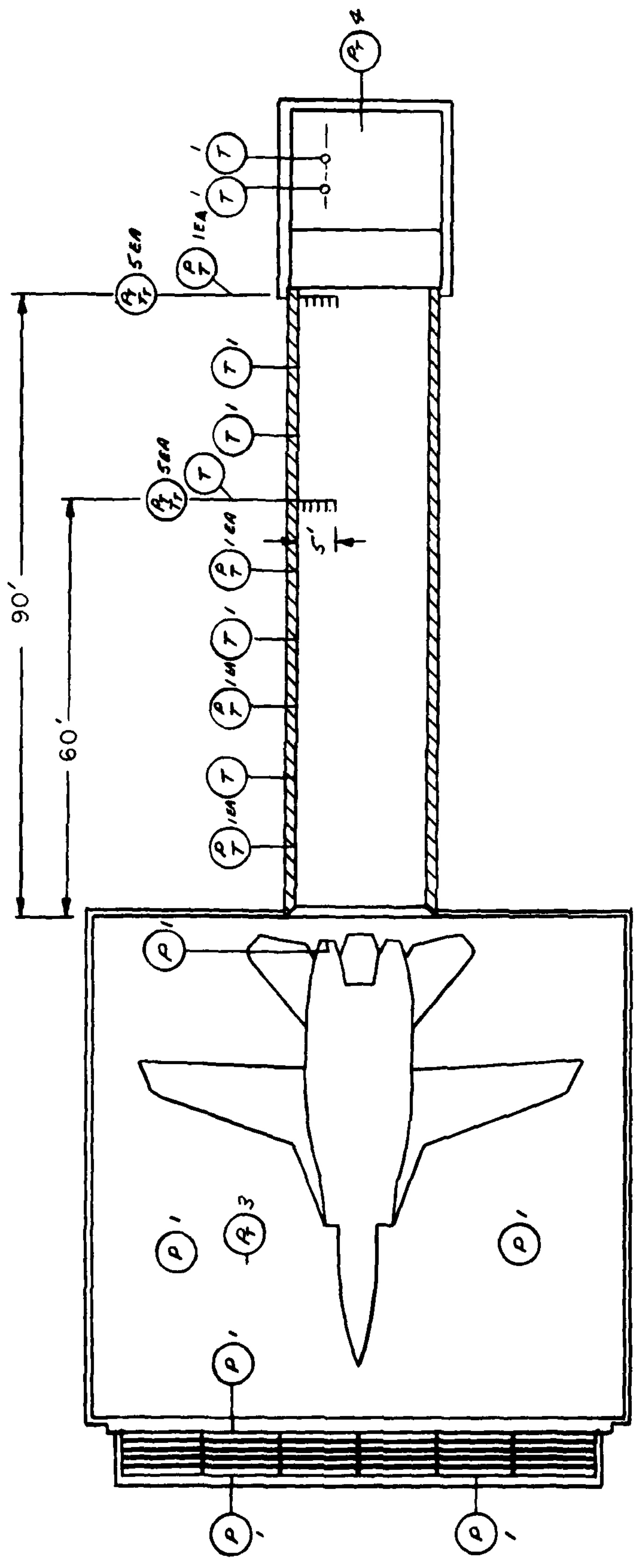

FIGURE 8.1-1. PLAN VIEW OF NAS MIRAMAR HUSH HOUSE SHOWING INSTRUMENTATION LOCATIONS FOR CHECKOUT

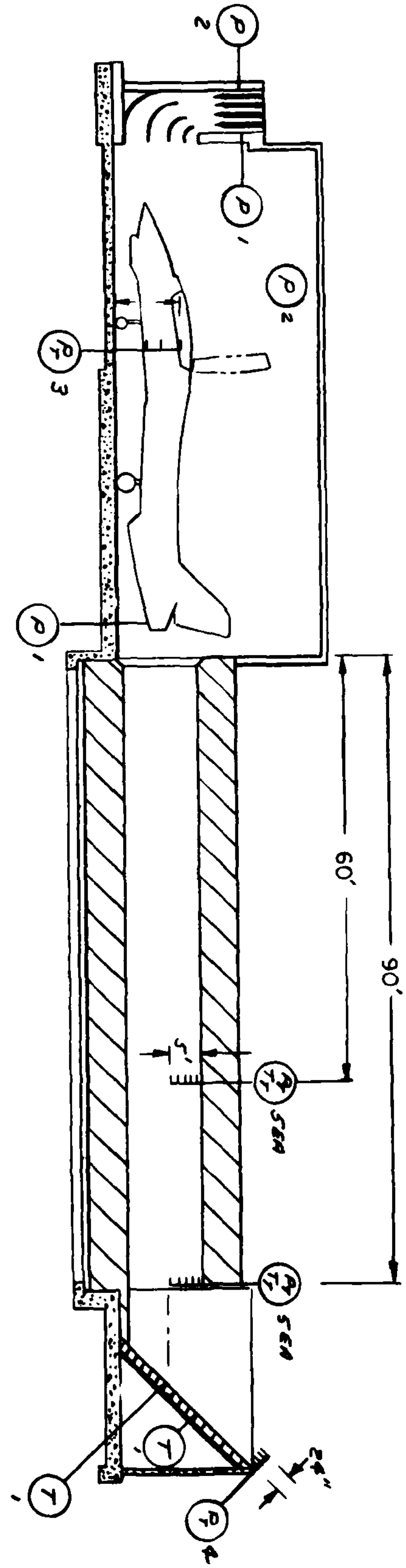

FIGURE 8.1-2. ELEVATION VIEW OF NAS MIRAMAR HUSH HOUSE SHOWING INSTRUMENTATION LOCATION FOR CHECKOUT

After reducing the raw data to absolute pressures and temperatures, the following additional calculations must be made so that the data can be checked with the design calculations and with the model scale test results.

Total Hush House Air Flow

$$\dot{W}_{inlet} = \rho_{inlet} \times g \times A_{inlet\ effective} \times V_{inlet}$$

$$q_{inlet} = P_{amb} - P_{inlet}$$

$$= \frac{1}{2} \times \frac{\rho_{inlet} \times g}{g} \times V_{inlet}^{2}$$

$$V_{inlet} = \sqrt{\frac{2g \times (P_{amb} - P_{inlet})}{\rho_{inlet} \times g}}$$

$$\dot{W}_{inlet} = \sqrt{2 \times \rho_{inlet} \times g^2 \times (P_{amb} - P_{inlet})} \times A_{inlet\ effective}$$

$$\rho_{inlet} = .00238 \times \frac{P_{inlet}}{P_{amb.\ std.}} \times \frac{T_{amb.\ std.}}{T_{amb.}}$$

Augmenter Pumping Performance

$$ARP = \frac{\dot{W}_{pumped}}{\dot{W}_{aircraft}} \times \sqrt{\frac{T_{amb}}{T_{T_N}} \times \frac{mw_N}{mw_{air}}}$$

Assume for every condition that $\dot{W}_{aircraft}$, T_{T_N}, mw_N are either known engine performance data for the aircraft, or can be readily obtainable by correcting standard day engine data.

$$\dot{W}_{pumped} = \dot{W}_{inlet} - \dot{W}_{aircraft}$$

so

$$ARP = \left(\frac{W_{inlet}}{W_{aircraft}} - 1\right) \times \sqrt{\frac{T_{amb}}{T_{T_N}} \times \frac{mw_N}{mw_{air}}}$$

Hush House Interior Flow Velocity

Using the Hush House interior pressure, $P_{interior}$, and the total pressure in the flow approaching the aircraft, $P_{T_{flow}}$, calculate the Hush House interior flow velocity, V_{flow}

$$V_{flow} = \sqrt{\frac{2g \times (P_{T_{flow}} - P_{interior})}{\rho_{amb} \times g}}$$

Check to see if V_{flow} is less than 50 fps and $P_{amb} - P_{interior}$ no greater than 2" H_2O .

Augmenter Wall Static Pressure

Reduce wall pressures to $\frac{P_{wall}}{P_{amb}}$ and plot versus $\frac{X_A}{D_{AM}}$ to compare with model scale results.

Augmenter Cross-Section Total Pressures and Total Temperatures

Reduce total pressures to P_T/P_{amb} and total temperatures to

$$T_{T_p} = \frac{T_T - T_{amb}}{T_{T_N} - T_{amb}}$$

and compare applicable points with model scale data.

Augmenter Wall Temperatures

Reduce wall temperatures to

$$T_{wall_p} = \frac{T_{wall} - T_{amb}}{T_{T_N} - T_{amb}}$$

and plot versus $\frac{X_A}{D_{AM}}$ for comparison with model scale data. Also, determine T_{mix_p} from calculated ARP and known T_{T_N}/T_{amb} and, using the maximum wall temperature, calculate

$$\frac{T_{wall\ max_p}}{T_{mix_p}} \quad .$$

Calculate Y_{param} for the test conditions and plot $\frac{T_{wall\ max\ p}}{T_{mix_p}}$ versus Y_{param} for comparison with model test results and to predict excessive wall temperature at max A/B before this condition is run.

Ramp Surface Temperature

Reduce to $T_{ramp_p} = \frac{T_{ramp} - T_{amb}}{T_{T_N} - T_{amb}}$, determine if T_{ramp} is acceptable and compare T_{ramp_p} with $T_{wall\ max_p}$ in the augmenter.

Ramp Exit Total Pressure Survey

Reduce to $P_{T_{ramp}}/P_{amb}$ and compare with model test results.

Nozzle Base Pressure

Reduce nozzle base pressure data as follows:

$$P_{NB_p} = \left(\frac{P_{NB}}{P_{amb}}\right)_{\substack{\text{Hush}\\ \text{House}}} - \left(\frac{P_{NB}}{P_{amb}}\right)_{\substack{\text{Free}\\ \text{Field}}} - \left(\frac{P_{interior}}{P_{amb}} - 1\right)$$

Check for acceptability and compare with model scale results.

Note: Checkout testing of the Hush House at NAS Miramar, using an F-14A along with other aircraft, was completed while this test report was being prepared. Augmenter pumping performance augmenter wall temperatures, etc. corresponded closely to the model test results. A copy of the memo summarizing the full-scale aerodynamic/thermal test data is bound with this report.

8.2 Acoustical Evaluation of the Miramar Full-Scale Exhaust Silencer

Since completion of the Full-Scale Miramar Hush House [A-5], BBN has carried out a detailed test program to evaluate the acoustical performance of the full-scale exhaust system. The objectives of this program were to:

1. provide a data base to compare the acoustical performance of the full-scale exhaust system with that predicted on the basis of the scale-model study, and

2. provide information regarding the directivity of the sound radiation from the exhaust plane.

8.2.1 Measurement set-up

Measurements of sound pressure levels in 1/3-octave bands from 25 Hz to 10,000 Hz and of A-weighted sound levels were made at each of 20 microphone positions around the jet exit ramp, as shown in Fig. 8.2.1. These positions were close enough to the exhaust exit that the measured levels were not likely to be affected by other noise sources. However, the 40-ft measurement positions were in the far field of the source and could be used to extrapolate the sound levels to positions on the 250-ft radius, thus enabling a determination of whether the exhaust noise was dominant at these positions. Measurement points 5, 10, 15, and 20 at the perimeter of the exhaust box provided information about the source location of the exhaust noise. All measurements were made with one engine of the F-14A aircraft operating at maximum afterburner power and the other engine at idle. No obstructions, such as pressure-temperature rakes, were in the augmenter tube or on the exit ramp during acoustic measurements.

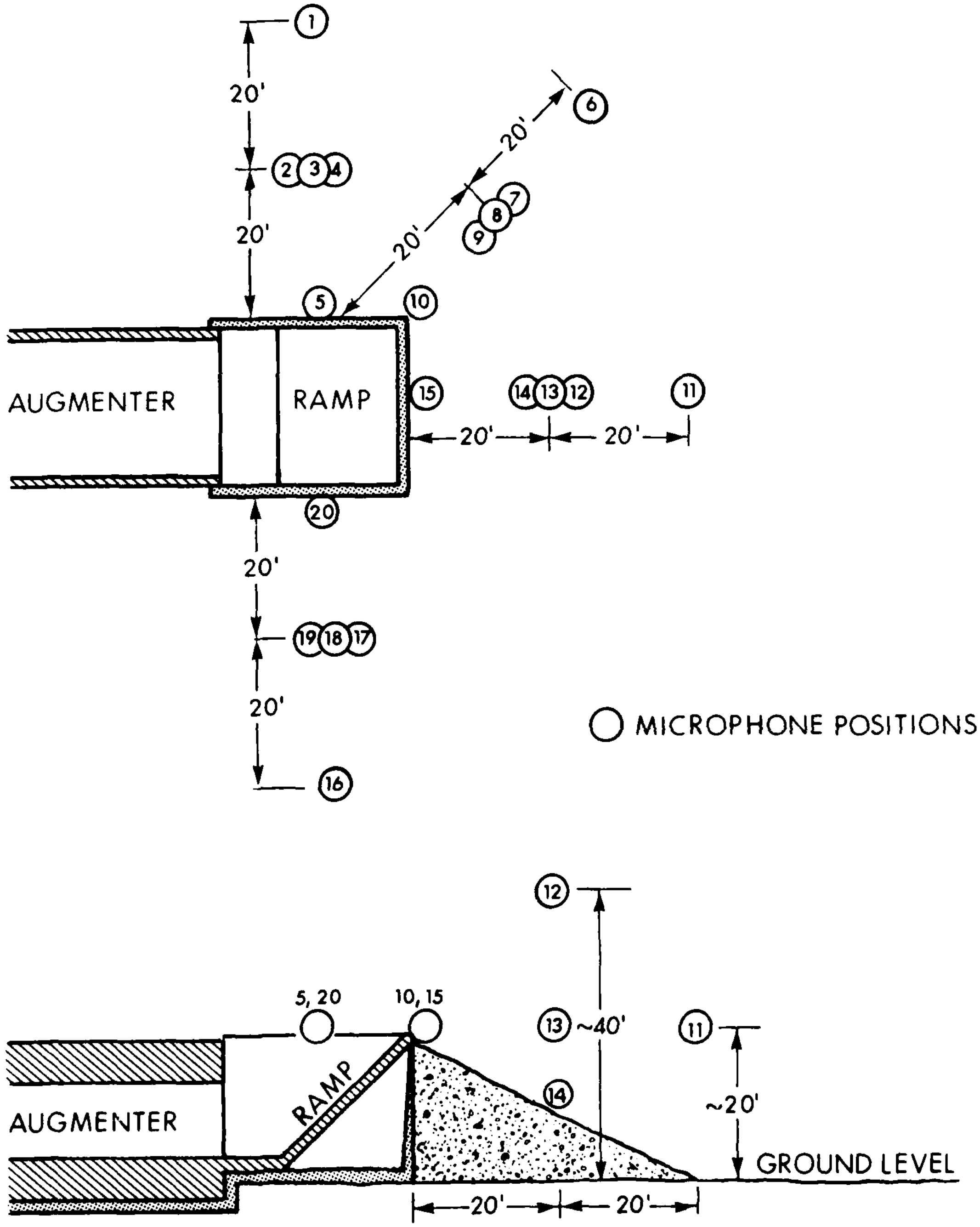

FIG. 8.2.1. MICROPHONE POSITIONS FOR THE ACOUSTIC EVALUATION OF THE MIRAMAR EXHAUST SILENCER.

A block diagram of the data-acquisition and data-reduction system used is shown in Fig. 8.2.2. Simultaneous recording of seven data channels permitted us to accomplish the data acquisition with a minimum of running time. All measurements were made between the hours of 4:00 a.m. and [illegible]:00 a.m., when there were no noisy activities at the Miramar Naval Air Station. Periodic recording of the ambient noise levels assured that the recorded data were not contaminated by background noise or by the electronic noise floor of the instrumentation. Pre-shaping of the microphone signal, which de-emphasized the low-frequency part of the spectrum, made it possible to avoid signal-to-noise ratio problems resulting from the limited dynamic range inherent in the tape-recording system.

8.2.2 Measured data

Figure 8.2.3 shows the octave-band spectrum of the exhaust noise measured 140 ft downstream of the exhaust box centerline (i.e., [illegible]50 ft from the engine exhaust) of the F-14A aircraft operating with one engine in maximum afterburner and the other at idle. This spectrum corresponds to a sound level of [illegible]4 dBA. For comparison, we have also plotted in the same figure the octave-band spectrum we predicted previously (see line [illegible] in Table 8.4.2) on the basis of the results of our scale-model study. The sound level which corresponds to this predicted spectrum is 83 dBA.

Using the sound pressure levels measured at different distances and at different angles from the exhaust box, we calculated the octave-band spectrum of the sound power exiting from the exhaust box. This spectrum is plotted as a solid line in Fig. 8.2.4, where, for comparison, we have also plotted the octave-band sound power spectrum predicted from our model study.

AD-A109 848 FLUIDYNE ENGINEERING CORP MINNEAPOLIS MINN F/G 14/2
AERODYNAMIC AND ACOUSTIC TESTS OF A 1/15 SCALE MODEL DRY COOLED--ETC(U)
OCT 75 J L GRUNNET, I L VER, G GETTER N62467-74-C-0490

UNCLASSIFIED NL

4 OF 4
AD A
109848

END
DATE
FILMED
02-82
DTIC

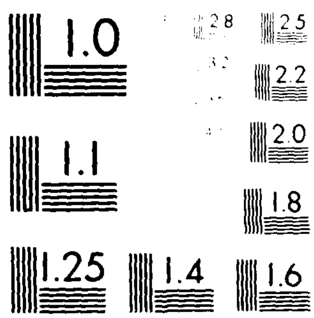
1.0
2.8
2.5
2.2
2.0
1.1
1.8
1.25
1.4
1.6

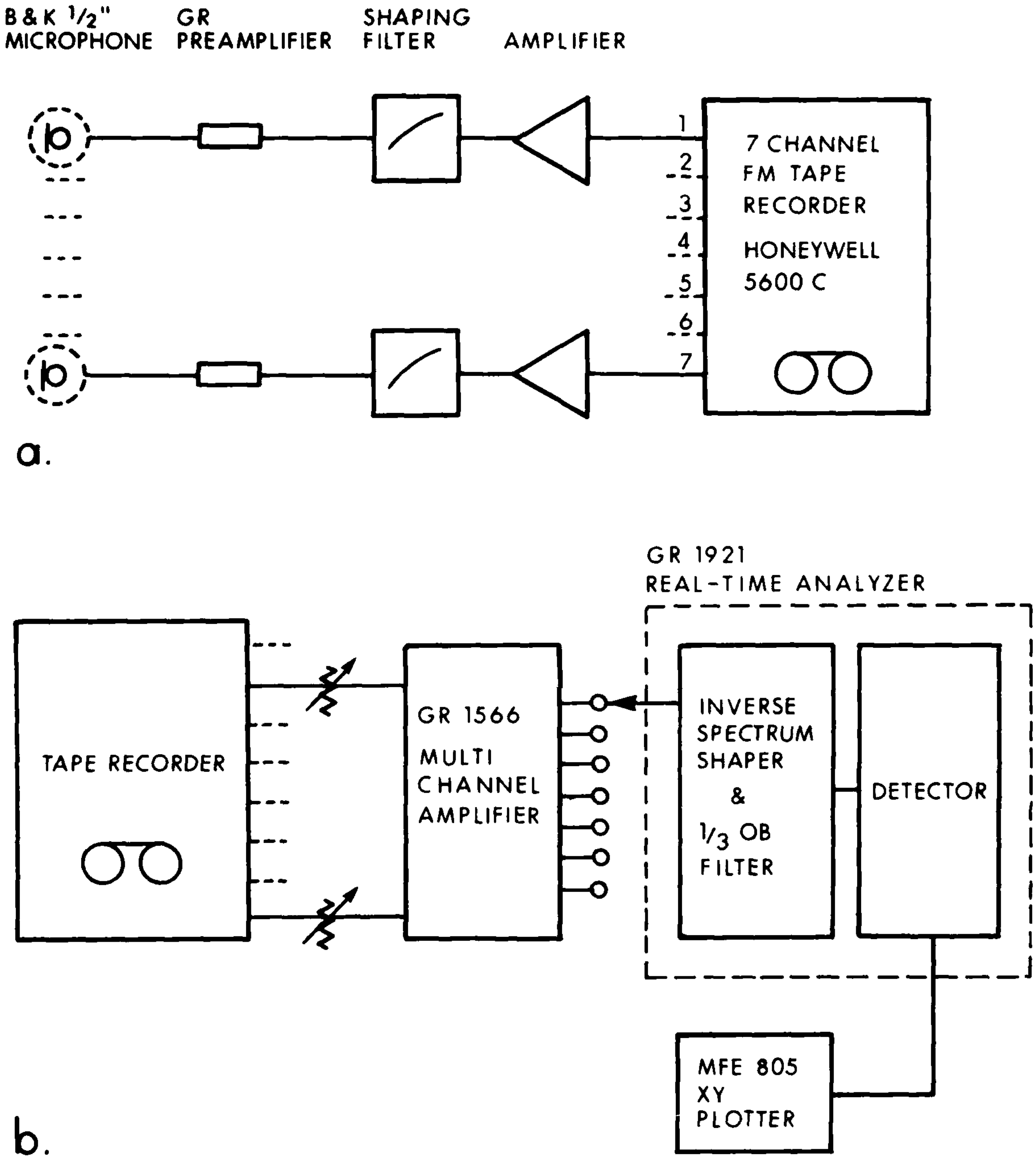

FIG. 8.2.2. BLOCK DIAGRAM OF THE DATA ACQUISITION (a) AND DATA ANALYSIS (b) SYSTEMS USED IN THE FULL-SCALE MEASUREMENTS.

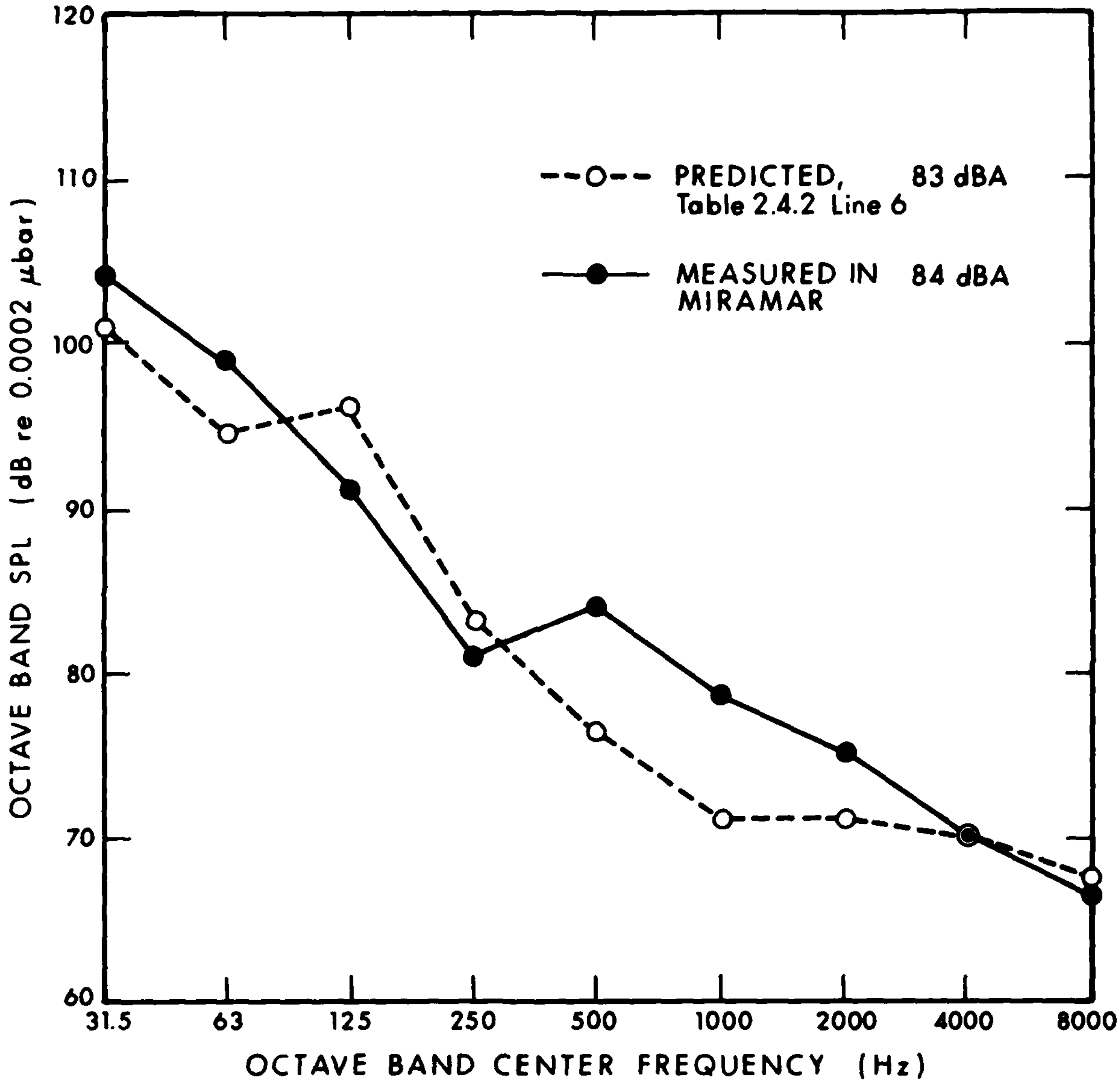

FIG. 8.2.3. MEASURED AND PREDICTED SPL AT 140 ft DOWNSTREAM OF THE EXHAUST BOX: F-14A; ONE ENGINE MAX AB, OTHER IDLE.

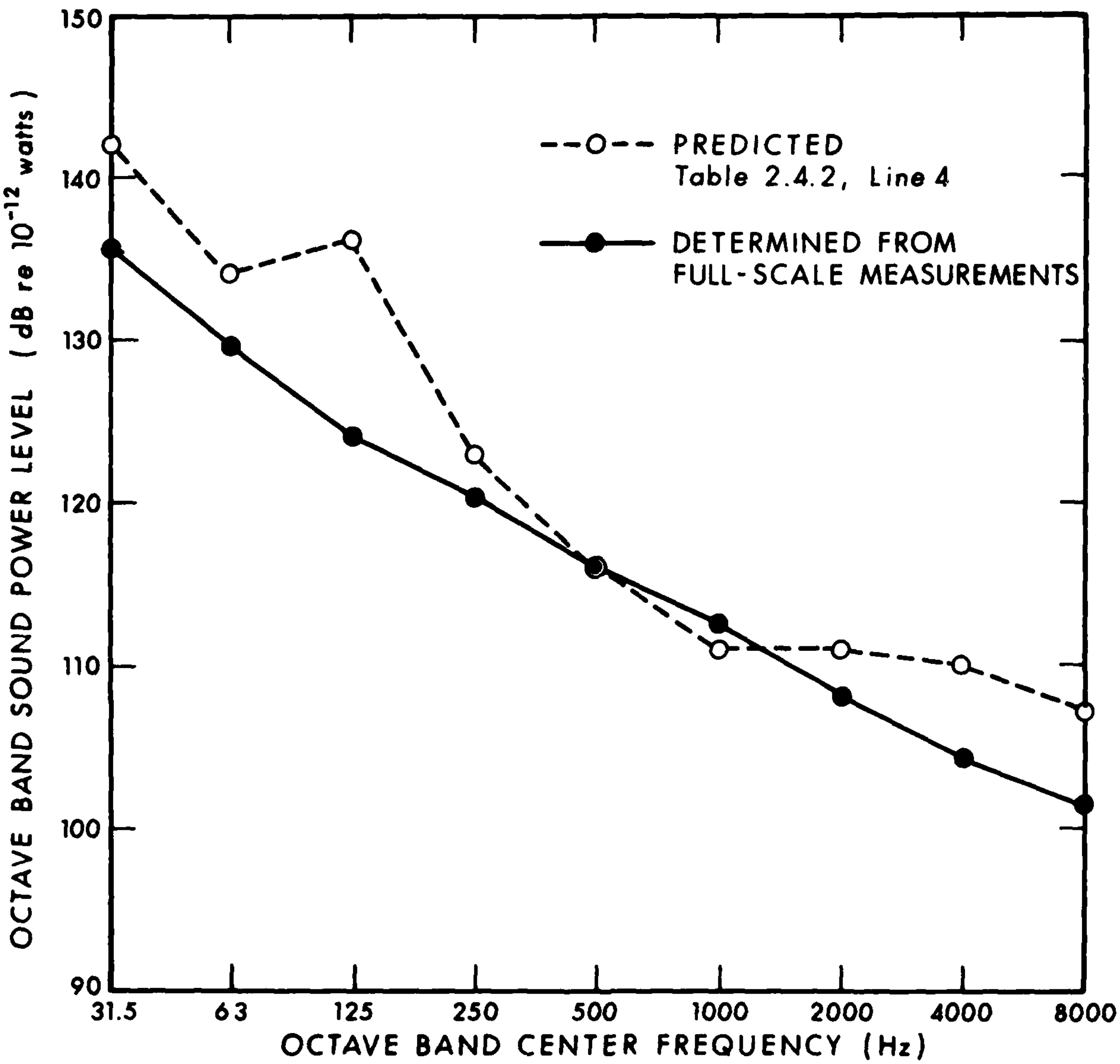

FIG. 8.2.4. PREDICTED AND MEASURED PWL OF THE EXHAUST NOISE FOR THE MIRAMAR HUSH HOUSE.

Agreement between the measured and predicted spectra is satisfactory.

The sound pressure levels measured at different angles around the exhaust box were also used to calculate the directivity index of the exhaust noise for the F-14A with one engine running at maximum afterburner. The results were presented in Table 2.3.3 and are repeated in Table 8.2.1. The angle, ϕ, is defined as being 0° in the downstream direction and increases toward the side of the exhaust box corresponding to the engine which is running in maximum afterburner. Thus the angle, ϕ, increases clockwise (looking down) if the port engine is running and counterclockwise if the starboard engine is running.

TABLE 8.2.1. DIRECTIVITY OF THE MIRAMAR EXHAUST FOR F-14A WITH ONE ENGINE IN MAXIMUM AFTERBURNER.

Direction	OCTAVE BAND CENTER FREQUENCY (Hz)									
	31	63	125	250	500	1000	2000	4000	8000	
ϕ = 0°	0	1	2	2	3	2	3	2	3	DI(ϕ), dB
ϕ = 45°	1	1	2	3	4	3	4	3	4	
ϕ = 90°	-1	-1	-1	1	1	1	2	1	1	
ϕ = 270°	-1	-4	-3	-3	-3	-3	-2	-3	-2	
ϕ = 315°	-1	-1	-1	-1	0	-1	-1	-2	-2	

In addition to the BBN measurements, NAEC-Lakehurst measured sound pressure levels at 14 points on the 250-ft-radius circle. The A-weighted sound levels that they measured in the downstream half-circle for the port engine running are presented in Fig. 8.2.5.

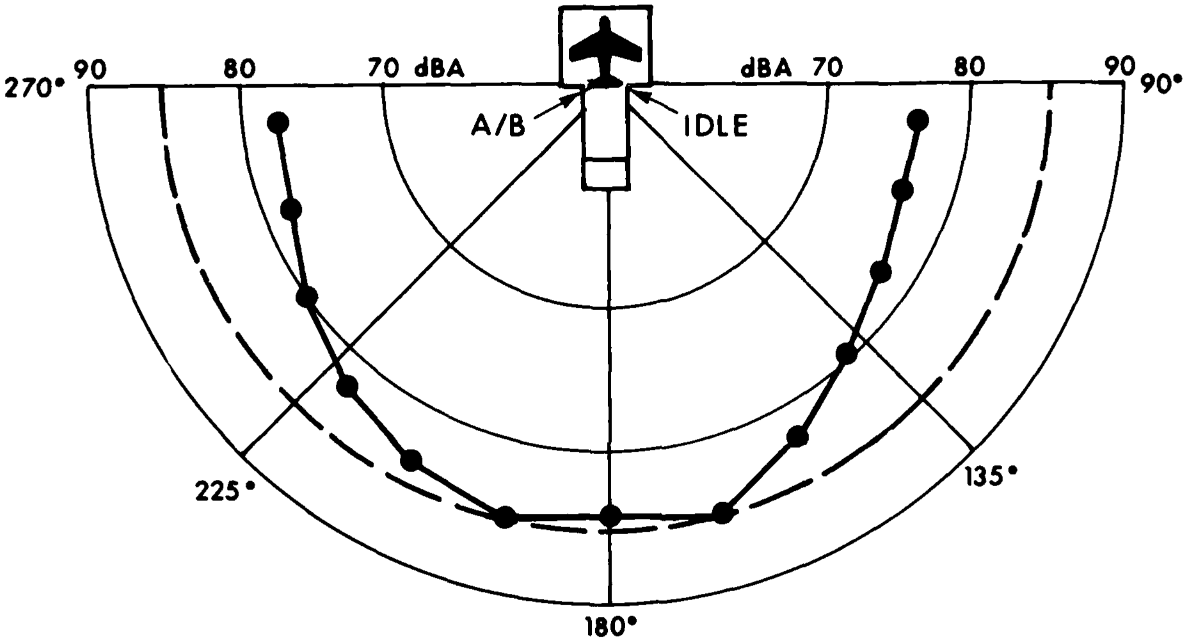

FIG. 8.2.5. A-WEIGHTED SOUND LEVELS MEASURED ON A 250-ft RADIUS: F-14A, PORT ENGINE IN ZONE 5 AFTERBURNER STARBOARD ENGINE IDLE. (SOURCE: NAEC-LAKEHURST.)

With the starboard engine running, the levels would appear as the mirror image of those plotted in Fig. 8.2.5.

The analysis of the sound pressure levels measured at different distances around the stack of the full-scale Miramar Hush House indicates that the noise emanating from the exit plane generally controls the noise levels measured in the downstream quarter-circle at 250 ft. However, at frequencies below 100 Hz the spectral levels measured at 250 ft are higher than would be expected on the basis of data obtained at 40 ft, assuming hemispherical spreading. This result implies that at frequencies below 100 Hz there is another yet unidentified source controlling the noise levels at both the 40-ft and the 140-ft locations. Since, in this case, the spectral levels at these low frequencies do not influence the A-weighted sound, this effect is of no consequence. However, if the noise criterion is stated in another form that puts more emphasis on low frequencies than the A-weighted sound level does, the contribution of this source may prove to be of interest.

The analysis of the data recorded near the edge of the exhaust box shows that the highest nearfield sound pressures were measured on the side that corresponds to the afterburning engine of the aircraft under test, the maximum being measured at the top edge of the ramp. This location of the measured maximum nearfield pressures corresponds to the location of the maximum local exit velocity, which is the likely location of the source of the self-generated noise.

The exit flow from the augmenter tube is deflected upwards by the 45° ramp. The exhaust flow along this ramp resembles a wall jet which, when it reaches the top of the ramp, creates trailing-edge aerodynamic noise. The microphone measures the sum of the aerodynamically generated trailing-edge noise and the engine noise attenuated by the lined augmenter, and there is no easy way to separate their relative contributions to the farfield noise. However, there are some limited data available for the prediction of the aerodynamically generated trailing-edge noise [*A-6*] of a wall jet in the characteristic decay region, if the flow speed and the boundary layer thickness are known. Although we cannot assume that the degree of turbulence and the pressure gradients in the wall jet experiments of Ref. A-6 are fully representative of the conditions of the ramp exit flow of the full-scale Miramar Hush House, it is still useful to attempt a prediction of the self-noise on the basis of these idealized conditions.

Since the aerodynamically generated trailing-edge noise increases with the sixth power of the flow velocity, the peak exit velocity is weighted heavily against the average. Accordingly, if one assumes an "effective" ramp flow velocity of U_{eff} = 400 ft/sec and a boundary layer thickness of δ = 1.25 ft, the prediction scheme of Ref. A-6 yields, for a location 140 ft downstream of the exhaust stack, the predicted self-noise spectrum shown in Fig. 8.2.6. For comparison, we also show the octave-band spectra of the sound pressure levels measured at the same location for the full-scale Miramar Hush House.

Although the choice of 400 ft/sec "effective" flow velocity is somewhat arbitrary and the noise prediction scheme strictly applies only to a wall jet on a flat plate, this exercise again points out that level of the aerodynamically generated noise, although not dominant, may be only slightly below the level of the attenuated aircraft noise. Because of the sixth-power dependence of the aerodynamic noise on the local flow velocity, in

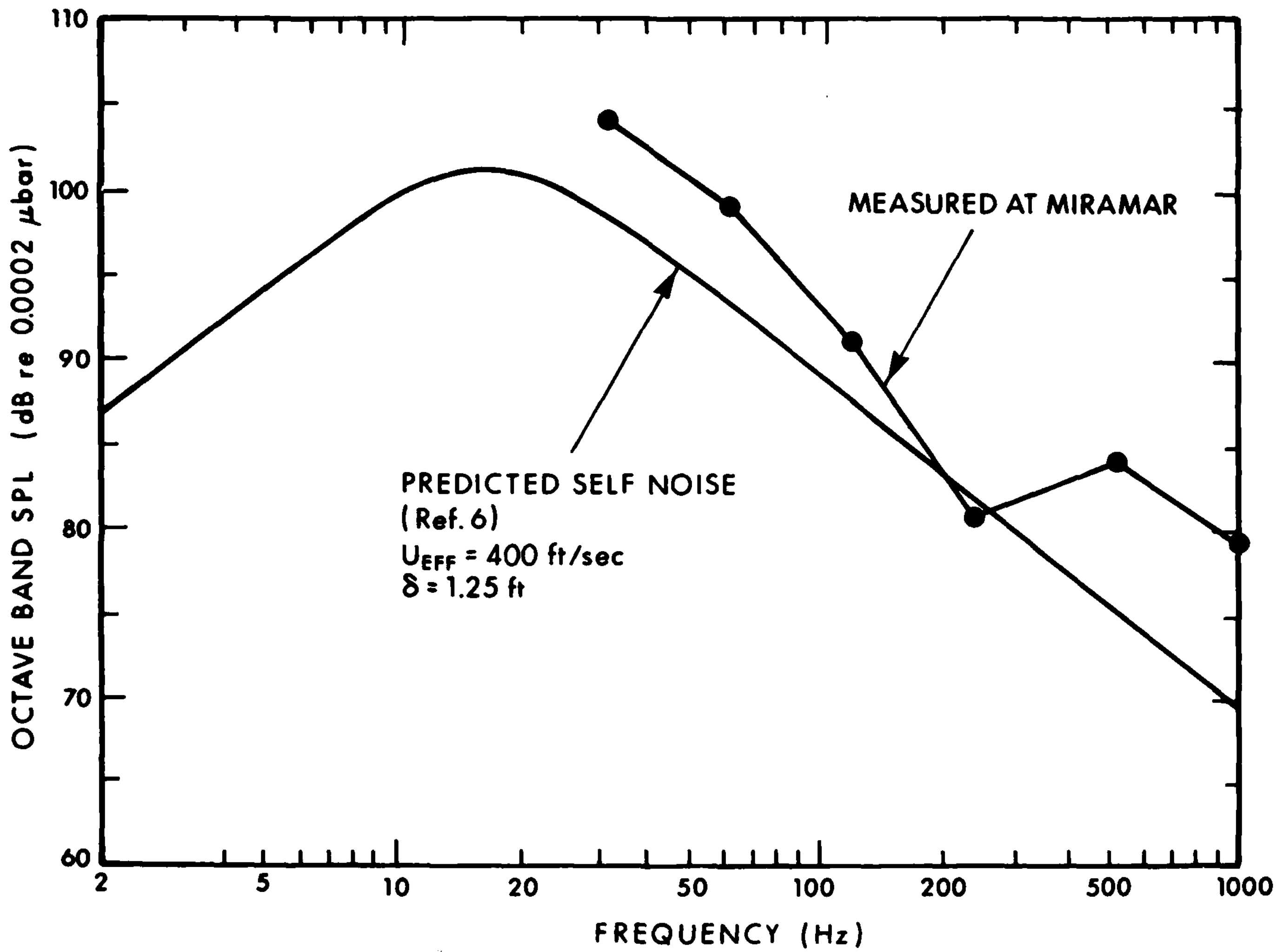

FIG. 8.2.6. COMPARISON OF THE MEASURED EXHAUST NOISE AT 250 ft WITH PREDICTED SELF-NOISE.

situations where higher exit velocities are called for or stricter noise criteria must be met, the self-noise may be a controlling factor. Our knowledge of the self-noise is very limited at present; it is therefore recommended that systematic self-noise investigations be conducted.

9.0 LIST OF REFERENCES

9.1 Aerodynamic/Thermodynamic References

A/T-1. Veneklassen, P. S., Noise Control for Ground Operation of the F-89 Airplane, " J. Acoustical Society of America, May 1953, pp. 417-422.

A/T-2. Pulcher, E. T., "In-Airframe Ground Runup Noise Suppressor Program," U.S. Navy, NAEC-GSED-78, March 1974.

A/T-3. Gustav Getter Associates, "Aircraft Noise Suppression Study," U. S. Navy Contract N62467-73-C-0503.

A/T-4. Lemmerman, R. D., and Lockwood, H. J., "Test Cell Augmenter Design," Aeronautical Engineering Review, Volume 14, Number 3, May 1955, pp. 37-43.

A/T-5. Morse, B. E., "Influence of Noise Control Components and Structures on Turbojet Engine Testing and Aircraft Ground Operation," Aerospace Medical Division, Wright Patterson AFB, Ohio, Report Number AMRL-TDR-62-134, December 1962.

A/T-6. Deleo, R. V. and Wood, R. D., "The Use of a Hot Gas Ejector for Boundary Layer Control," WADC TR52-128, April 1952.

A/T-7. Bailey, D C., Tower, P. W. and Fuhs, A. E., "Pollution Control of Airport Engine Test Facilities," AGARD C.P. 125, Paper Number 14, 1973.

LIST OF ACOUSTICAL REFERENCES

A.1 Aerospace Medical Research Laboratory, Wright-Patterson AFB, Ohio, Test 73-016-001, Run 03 (30 July 1973).

A.2 ANSI Standard S1.21-1972.

A.3 M.J. Fisher *et al.*, "Jet Noise," *J. Sound Vib.* 28(3):563-585 (1973).

A.4 A. Powell, "On the Noise Emanating from a Two-Dimensional Jet Above Critical Pressure," *Aeronautical Quarterly* 4: 103-122 (1953).

A.5 Gustav Getter Associates, "Aircraft Noise Suppression Study," U.S. Navy Contract N62467-73-C-0503 (July 1973).

A.6 R.E. Hayden, Y. Kadman, and S. Africk, "An Approach to Detailed Diagnostic Calculations of Airframe Noise," BBN Report No. 2791 (March 1974).

FLUIDYNE

ENGINEERING CORPORATION
5900 Olson Memorial Highway
Minneapolis, Minnesota 55422

IN REPLY REFER TO

29 October 1975

From: FluiDyne Engineering Corporation
5900 Olson Memorial Highway
Minneapolis, Minnesota 55422
(Attention: Owen P. Lamb)

To: Mr. R. B. Foster Code 403F
Southern Division
Naval Facilities Engineering Command
Post Office Box 10068
Charleston, S. C. 29411

Mr. E. Ference Code 0452
Naval Facilities Engineering Command
200 Stovall Street
Alexandria, Virginia

Mr. M. Lepor Code 40
Naval Undersea Center
San Diego, California 92132

Mr. D. D. Croce Code SE-422
Naval Air Engineering Center
Philadelphia, Pennsylvania 19112

Mr. Denny O'Dell Code 53431B
Naval Air Systems Command Headquarters
Washington, D. C. 20361

Subject: Contract N62467-74-C-0490 Model Study of a Dry Jet Engine Noise Suppression System - Summary of Full-Scale Aerodynamic and Thermal Data from the NAS Miramar Hush House Checkout Tests

This memo summarizes the aerodynamic and thermal data from the checkout testing of the full-scale NAS Miramar F-14 Hush House and relates the test results to the Hush House design calculations and to the results of the 1/15 scale model tests. The full-scale acoustical data are included in the portion of the model study report provided by Bolt, Beranek and Newman, Incorporated and they will not appear separately.

29 October 1975
Page two

Table 1 presents the raw basic data taken during the initial checkout tests in early August, 1975. In the cases of Hush House inlet pressure and interior pressure, the values presented represent the average of pressures taken at more than one location.

TABLE 1. RAW BASIC DATA FROM INITIAL NAS MIRAMAR HUSH HOUSE TESTS

Aircr.	Power Setting	Baro. "hg abs	Air Temp. °F	Hush Hs Inter. Press. " H_2O gage	Hush Hs Inlet Press. " H_2O gage	Veloc. Probe Total Press. " Hg abs	Max. Augm. Wall Temp.	Max. Ramp Temp.	Run Date
A-4	MIL	29.48	80	-0.75	-1.30	29.46	149	162	(7-31-75)
F-8	MIL	29.51	71	-0.70	-1.30	29.49	164	168	(8-1-75)
F-8	A/B	29.51	71	-0.80	-1.45	29.49	394	373	(8-1-75)
F-4	(1)MIL	29.47	74	-0.75	-1.20	29.47	201	195	(8-2-75)
F-4	(1)A/B	29.47	74	-0.80	-1.30	29.45	471	420	(8-2-75)
F-4	(2)MIL	29.47	74	-1.40	-2.53	29.42	215	237	(8-2-75)
F-14A	(1)MIL	29.34	85	-0.85	-1.40	29.31	215	204	(8-6-75)
F-14A	(1)A/B	29.34	85	-0.90	-1.30	29.31	970	660	(8-6-75)
F-14A	(2)MIL	29.45	70	-1.75	-3.00	29.39	---	202	(8-1-75)

The barometric pressures listed above do not correspond to the published data, in some instances, because the published barometric pressure didn't appear to correlate properly with some of the other absolute pressures. Table 2 presents augmenter axial wall temperature data taken during the intial tests and both wall temperatures and pressures taken during later tests (9-23-75) with the F-14A having one engine in afterburning power setting.

TABLE 2. AUGMENTER AXIAL SIDE WALL TEMPERATURES AND PRESSURES FROM NAS MIRAMAR HUSH HOUSE CHECKOUT TESTS WITH THE F-14A HAVING ONE ENGINE IN A/B POWER SETTING

Axial Station	Axial Location X_A/D_{AM}	Wall Pressure " H_2O gage (9-23-75 data) Baro 29.46 T_{amb} 77°F	Wall Temperature °F (9-23-75)	(8-6-75 data) T_{amb} 82°F
1	0.67	-4.7	248	
2	1.33	-4.2	560	
3	2.00	-3.4	735	950
4	2.67	-2.2	823	970
5	3.33	-1.7	723	965
6	4.00			947
8	5.33	-0.6	748	

Figure 1 shows the location of maximum total temperature and maximum total pressure in the Miramar augmenter exit cross-section with the F-14A obtained during the 9-23-75 test, using a P_T, T_T rake.

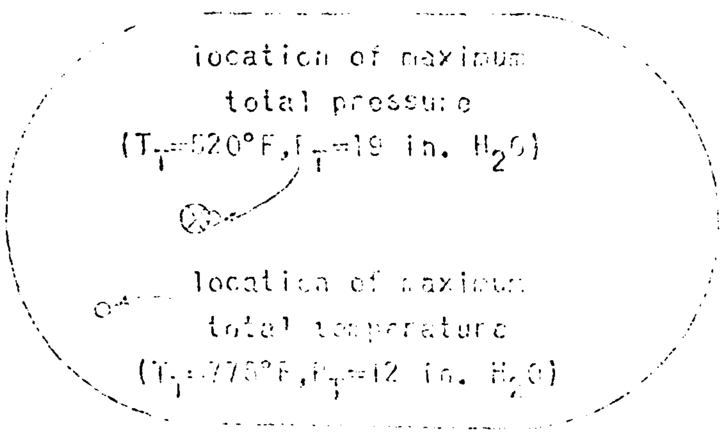

FIGURE 1. MAXIMUM TOTAL PRESSURE AND TOTAL TEMPERATURE IN THE MIRAMAR AUGMENTER EXIT CROSS-SECTION WITH THE F-14A HAVING ONE ENGINE IN A/B POWER SETTING.

The aerodynamic/thermodynamic data taken during the [illegible] Hush House checkout tests corresponded to the recommendations in Section 8.1 of the model test report with two exceptions: the air-craft nozzle base pressure was not measured and there was no [illegible] exit total pressure rake. The data which were taken will [illegible] analyzed to relate it to the Hush House design and to the [illegible] model test results.

Hush House Interior Pressure

The Miramar Hush House air inlet was sized so that the Hush House interior pressure depression would not exceed 2 "H_2O for operation with the F-14B having both engines in maximum non-afterburning (MIL) power setting. Since the F-14B aircraft is not in service, the Hush House was checked out using the F-14A. With both engines in military power setting, the Hush House interior pressure was -[illegible] "H_2O gage, which indicates reasonable agreement with the design criteria.

Total Hush House Inlet Air Flow Rate

In order to check the effective area of the Hush House air inlet and verify the pumping performance data from the 1/15 scale model test program, the total Hush House inlet air flow rate was calculated using three independent methods and the results compared.

For method one, the air flow rate was calculated by applying the 1/15 scale model test results presented in Section 2.1 of the model test report, in conjunction with the aircraft data and the full-scale augmenter cross-sectional area of A_A = 183 sq. ft.

$$\dot{W}_{inlet} = \dot{W}_N + \dot{W}_{pumped} = \dot{W}_N + \dot{W}_N \times ARP \times \sqrt{\frac{T_{T_N}}{T_{amb}} \times \frac{mw_{amb}}{mw_N}}$$

The results of this calculation, along with pertinent information used in making the calculations, is presented in Table 3.

TABLE 3. [illegible]

Aircr.	Power Setting	$\dot{W}_N$ pps	A_{NT} sq. ft.	A_A/A_{NT}	T_{T_N} °R	mw_N	$P_{T_{sec}}/P_{T_{exit}}$	[illegible]	[illegible]
A-4	MIL	160	1.79	102	1600	27	.999	[illegible]	[illegible]
F-5	MIL	170	2.77	66	1600	27	.999	[illegible]	[illegible]
F-8	A/B	170	4.62	40	3700	24	.999	[illegible]	[illegible]
F-4	(1)MIL	180	2.52	73	1600	27	.999	[illegible]	[illegible]
	(1)A/B	180	4.20	44	3700	24	.999	[illegible]	[illegible]
	(2)MIL	360	5.04	36	1600	27	.998	3.18	[illegible]
F-14A	(1)MIL	250	3.56	51	1400	28	.999	3.61	[illegible]
	(1)A/B	250	7.50	24	3700	24	.999	1.94	1652
	(2)MIL	500	7.12	26	1400	26	.998	2.53	[illegible]
								AVG.	1799

also assumed for these calculations:

T_{amb} = 75°F (535°R)

mw_{air} = 29

In some cases, the estimate required a considerable extrapolation of the model test data (the A-4 with A_A/A_{NT} = 102, for instance).

The second mass flow rate estimate was made using the 285 sq. ft. effective inlet area (335 sq. ft. geometric) assumed for the Hush House inlet design, along with the static pressure measured at this area during the Miramar checkout tests. Using typical ambient conditions of 29.5 Hg_{abs} (400 "H_2O abs) barometric pressure and 75°F temperature, one projects an air density of 0.0731 lb/cu. ft. and a speed of sound in air of 1140 ft. per second. The mass flow rate through the air inlet can then be calculated as follows.

$$W_{inlet} = \rho g \times A_{\substack{inlet \\ effective}} \times V_{inlet}$$

$$= 0.0731 \times 285 \times 1140 \times M_{inlet}$$

$$= 23750 \times M_{inlet}$$

where M_{inlet} is the inlet Mach number corresponding to the inlet static pressure measurements:

$$\frac{P}{P_{T}}_{inlet} = \frac{400 + P_{inlet\,"H_2O}}{400}$$

Table 4 contains the results of these calculations for the four aircraft run during the checkout tests.

TABLE 4. HUSH HOUSE INLET AIR FLOW RATE CALCULATED FROM THE INLET STATIC PRESSURE

Aircr.	Power Setting	Inlet Static Pressure "H_2O	P/P_{T} inlet	M_{inlet}	$\dot{W}_{inlet}$ [illegible]
A-4	MIL	-1.30	.9968	.068	1615
F-8	MIL	-1.30	.9968	.068	1615
F-8	A/B	-1.45	.9964	.072	1710
F-4	(1)MIL	-1.20	.9970	.066	1568
F-4	(1)A/B	-1.30	.9968	.068	1615
F-4	(2)MIL	-2.58	.9936	.096	2280
F-14A	(1)MIL	-1.40	.9965	.071	1686
F-14A	(1)A/B	-1.30	.9968	.068	1615
F-14A	(2)MIL	-3.00	.9925	.104	2470
					1797

The third and final inlet mass flow rate estimate was made on the basis of conditions at the outlet of the Hush House doors by assuming that the total pressure there was between barometric pressure and the measured Hush House interior survey rake total pressure and that the static pressure was equal to the Hush House interior pressure. The effective flow area of the door outlet was based upon the results of a rough survey of separated flow regions at the door exit applied to the geometric outlet area of 738 sq. ft. and resulted in an estimated effective area of 412 sq. ft. This effective area is considerably less than that assumed for the Hush House inlet design and implies more flow separation from the vanes, etc. The resulting relation for inlet mass flow rate is:

$$W_{inlet} = \rho g \times A_{outlet\ effective} \times V_{outlet}$$

$$= 0.0731 \times 412 \times [illegible] \times M_{outlet}$$

$$= 34337 \times M_{outlet}$$

Table 5 presents the calculated results.

TABLE 5. [illegible]
([illegible])

Aircr.	Power Setting	Door Outlet Total Pressure "H_2O abs	Hush Ho. Interior Pressure "H_2O [illegible]	$P/P_{T_{outlet}}$	M_{outlet}	[illegible]
A-4	MIL	399.9	-0.75	.9984	.048	164[illegible]
F-8	MIL	399.9	-0.70	.9985	.046	1579
F-8	A/B	399.9	-0.80	.9982	.050	1717
F-4	(1)MIL	399.9	-0.75	.9984	.048	1648
F-4	(1)A/B	399.9	-0.80	.9982	.050	1717
F-4	(2)MIL	399.75	-1.40	.9971	.064	2197
F-14A	(1)MIL	399.9	-0.85	.9981	.052	1785
F-14A	(1)A/B	399.9	-0.90	.9980	.053	1820
F-14A	(2)MIL	399.75	-1.75	.9962	.074	2541
					AVG.	1850

A comparison of the three mass flow predictions reveals that in each case, the different prediction methods yield results that are usually within 7% of the mean. Furthermore, the averages of all of the cases for the different prediction methods are within 2% of their mean. This agreement suggests that:

1. the ratio of effective to geometric inlet area assumed during the design of the Hush House air inlet is correct; and

2. the pumping performance obtained from the model scale tests agrees fairly well with the full-scale performance.

Hush House Interior Flow Velocity

Total and static pressure probes were located within the Hush House in the vicinity of the aircraft during the early checkout tests. Since the static pressures were essentially equal to Hush House interior pressure, the interior pressure was used for this analysis. The measured values and the results of the calculations appear in Table 6.

TABLE 6. HUSH HOUSE INTERIOR FLOW VELOCITY AT THE AIRCRAFT LOCATION

Aircr.	Power Setting	Baro.	Hush Hs. Interior Press. "H_2O gage	Velocity Probe Total Press. "Hg abs	P/P_t	$M_{interior}$	$V_{interior}$ fps
A-4	MIL	29.48	-0.75	29.46	0.9988	0.041	46.7
F-8	MIL	29.51	-0.70	29.49	[illegible]	0.040	[illegible]
F-8	A/B	29.51	-0.80	29.49	0.9937	0.043	49.0
F-4	(1)MIL	29.47	-0.75	29.47	0.9981	0.052	59.3
F-4	(1)A/B	29.47	-0.80	29.45	0.9987	0.043	49.0
F-4	(2)MIL	29.47	-1.40	29.42	0.9982	0.051	58.1
F-14A	(1)MIL	29.34	-0.85	29.31	0.9989	0.040	45.6
F-14A	(1)A/B	29.34	-0.90	29.31	0.9987	0.043	49.0
F-14A	(2)MIL	29.45	-1.75	29.39	0.9975	0.060	68.4

With the exception of one questionably high estimated velocity, the resulting velocities correspond properly with the estimated Hush House air flow rates listed in Tables 3, 4 or 5. The Miramar Hush House air inlet was designed to limit the Hush House interior flow velocity to 50 feet per second with an F-14B having both of its engines in maximum military power setting. The resulting 68.4 feet per second with the F-14A in that power setting indicates more flow separation from the inlet turning vanes and door dividing panels than was assumed during design. While this higher than desirable velocity doesn't pose any serious operating problems, an attempt will be made to lower this velocity in subsequent Hush House designs.

Augmenter Axial Pressure Distribution

The augmenter wall pressures listed in Table 2 were reduced to P/P_{amb} and plotted with the model test results on model test report Figure 7.2-9. The full-scale and model test results correspond satisfactorily.

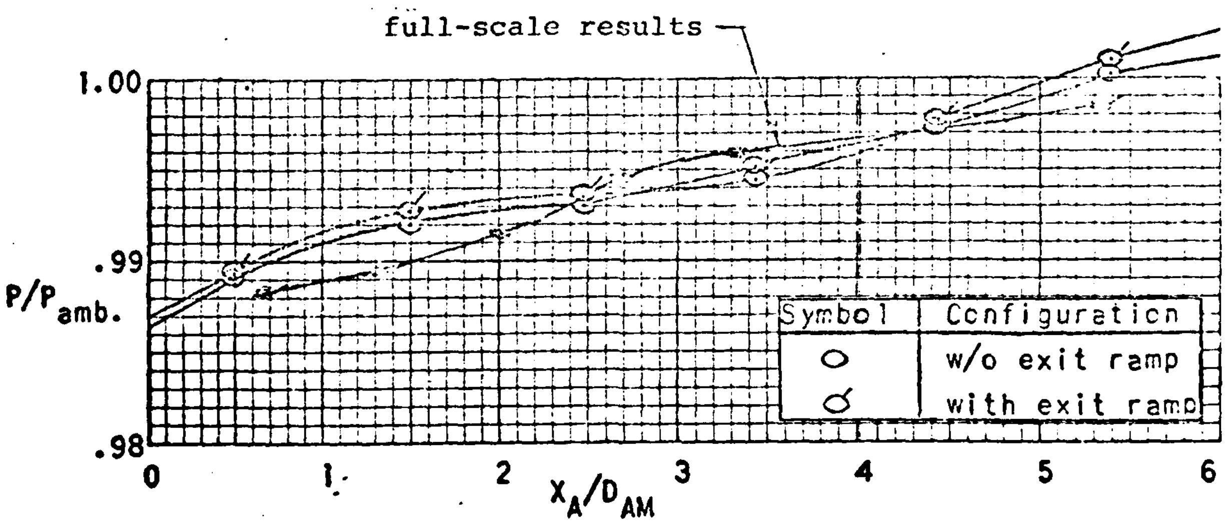

FIGURE 7.2-9. LONGITUDINAL SHELL PRESSURE DISTRIBUTION FOR THE OBROUND AUGMENTER WITH AND WITHOUT EXIT RAMP. (A_A/A_{NT}=25, X_N/D_{NT}=1.6, L_A/D_{AM}=6, T_{T_N}/T_{amb}=6.6, λ_N=2.0, Y_p= 0.45)

Augmenter Axial Sidewall Temperature Distribution

The augmenter sidewall temperatures listed in Table 2 were reduced to T_{wall_p} and plotted with the model test results on model test report Figure 7.4-1. The full-scale test results taken on 8-6-75 correspond closely to the model results over the limited length of augmenter that the data were taken. A greater length of augmenter was covered for the test of 9-23-75. The variation of T_{wall_p} over the augmenter length has the same general character as the model test results, but the values are lower. This could be due to either aircraft misalignment or a failure to allow sufficient time for temperatures to stabilize before recording the data.

Augmenter Exit Cross-Section Total Pressure and Total Temperature

The locations of maximum total pressure and total temperature in the full-scale [illegible] augmenter exit cross-section and the corresponding values of total pressure and total temperature were presented in Figure 1. Figure 2 shows the augmenter exit cross-section with isolines of T_p and P_T/P_{amb} from the model test data for the [illegible] configuration.

Isoline	P_T/P_{amb}	T_p
1	1.0[illegible]	0.[illegible]
2	1.03	[illegible]
3	1.0[illegible]	0.2[illegible]
4	1.0[illegible]	0.2[illegible]

Note: $T_p = \frac{T - T_{amb}}{T_{T_{p}} - T_{amb}}$

FIGURE 2. CROSS-SECTION TOTAL PRESSURE AND TEMPERATURE CONTOURS FOR THE [illegible] CONFIGURATION FROM THE MODEL TEST RESULTS.

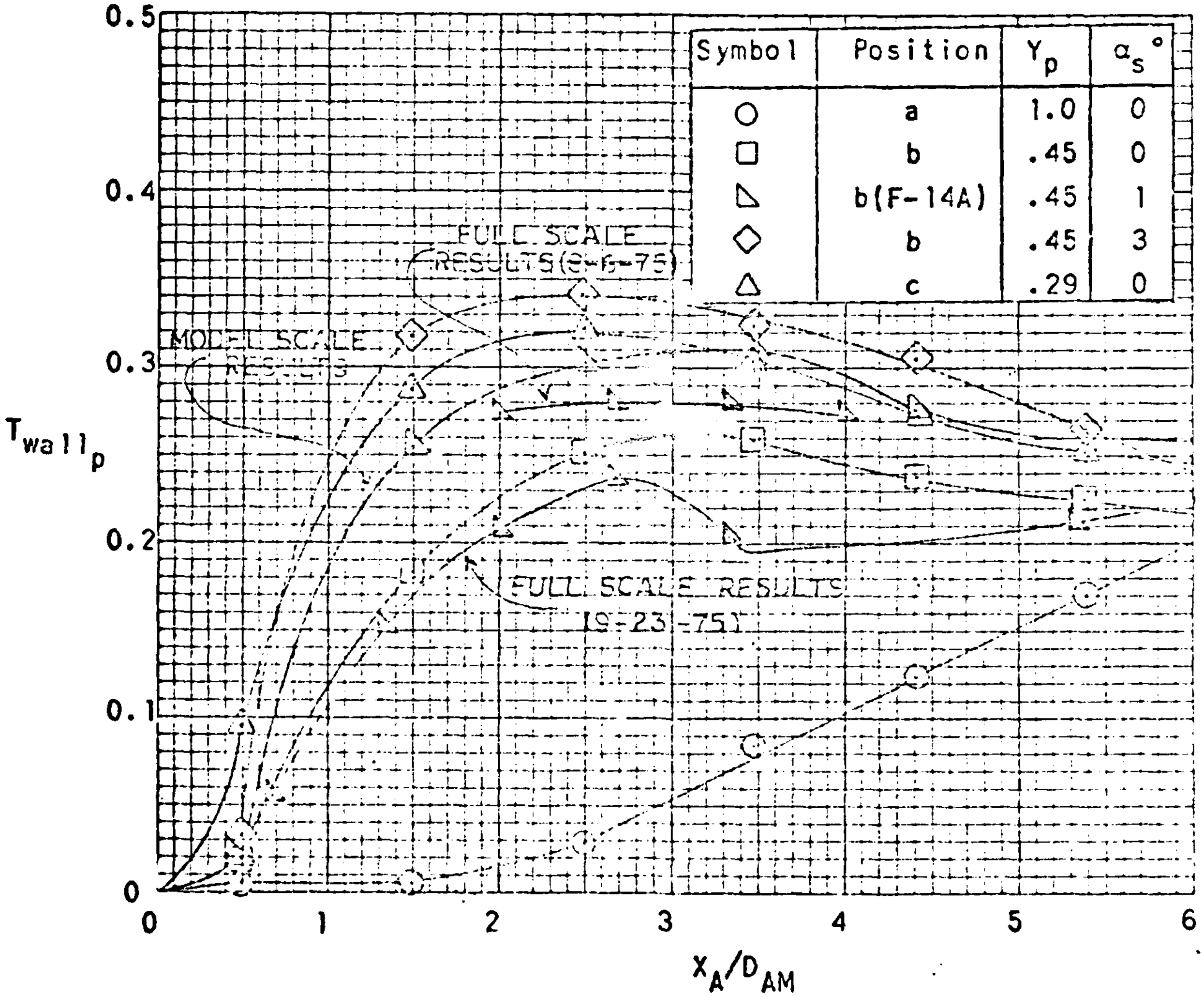

FIGURE 7.4-1. LONGITUDINAL SIDEWALL TEMPERATURE DISTRIBUTION VERSUS JET NOZZLE LATERAL POSITION AND DEFLECTION FOR THE OBROUND AUGMENTER.
(A_A/A_{NT}=25, X_N/D_{NT}=1.6, L_A/D_{AM}=6, T_{T_N}/T_{amb}=4.6, λ_N=2.0)

The full-scale total pressure and total temperature values were reduced to P_T/P_{amb} and T_P, respectively, and the results are compared to the model scale projections for each location in Table 7.

TABLE 7. COMPARISON OF FULL-SCALE AUGMENTER CROSS-SECTION TOTAL PRESSURE AND TOTAL TEMPERATURE WITH MODEL SCALE TEST RESULTS

Full-scale location	Full-scale results P_T/P_{amb}	Full-scale results T_P	Model scale results P_T/P_{amb}	Model scale results T_P
max P_T	1.048	0.15	1.065	0.235
max T_T	1.030	0.22	1.050	0.235

The full-scale results show lower total pressures and total temperatures than the model scale results. They correspond to a lower augmenter exit velocity than would be projected from the model scale results.

$V_{exit\ max,\ full\text{-}scale}$ = 39[illegible] ft./sec.

$V_{exit\ max,\ model\ scale\ proj.}$ = 545 ft./sec.

Memo Prepared By
James L. Grunnet

Submitted By

Owen P. Lamb
Vice President